Model-based Temperature Control of a Diesel Oxidation Catalyst

Olivier Lepreux

▶ **To cite this version:**

Olivier Lepreux. Model-based Temperature Control of a Diesel Oxidation Catalyst . Mathematics [math]. École Nationale Supérieure des Mines de Paris, 2009. English. ⟨NNT : 2009ENMP1670⟩. ⟨pastel-00005857⟩

HAL Id: pastel-00005857

https://pastel.hal.science/pastel-00005857v1

Submitted on 9 Mar 2010

HAL is a multi-disciplinary open access archive for the deposit and dissemination of scientific research documents, whether they are published or not. The documents may come from teaching and research institutions in France or abroad, or from public or private research centers.

L'archive ouverte pluridisciplinaire **HAL**, est destinée au dépôt et à la diffusion de documents scientifiques de niveau recherche, publiés ou non, émanant des établissements d'enseignement et de recherche français ou étrangers, des laboratoires publics ou privés.

HAL Authorization

ED n°431 : ICMS - Information, Communication, Modélisation et Simulation

T H E S E

pour obtenir le grade de

DOCTEUR DE L'ECOLE NATIONALE SUPERIEURE DES MINES DE PARIS

Spécialité "Mathématique et Automatique"

présentée et soutenue publiquement par
Olivier LEPREUX

le 9 octobre 2009

Modélisation et commande de la température pour un catalyseur d'oxydation diesel

Model-based Temperature Control of a Diesel Oxidation Catalyst

Directeur de thèse : M. Nicolas PETIT

Jury

M. Yann LE GORREC	Président
M. Jean-Pierre CORRIOU	Rapporteur
M. Michiel J. VAN NIEUWSTADT	Rapporteur
M. Denis DOCHAIN	Examinateur
M. Yann CREFF	Examinateur
M. Nicolas PETIT	Examinateur

THÈSE

pour obtenir le grade de

DOCTEUR DE L'ÉCOLE NATIONALE SUPÉRIEURE DES MINES DE PARIS

Spécialité

MATHÉMATIQUE ET AUTOMATIQUE

présentée par

Olivier LEPREUX

Modélisation et commande de la température pour un catalyseur d'oxydation diesel

Model-based Temperature Control of a Diesel Oxidation Catalyst

Soutenue le 9 octobre 2009 devant le jury composé de

M. Yann LE GORREC	ENSMM, FEMTO-ST / AS2M	Président et Examinateur
M. Jean-Pierre CORRIOU	LSGC-CNRS-ENSIC	Rapporteur
M. Michiel J. VAN NIEUWSTADT	Ford Motor Company	Rapporteur
M. Denis DOCHAIN	Université Catholique de Louvain	Examinateur
M. Yann CREFF	IFP Lyon	Examinateur
M. Nicolas PETIT	MINES ParisTech	Directeur

Résumé

Le problème étudié dans cette thèse est la commande d'un système DOC (Diesel Oxidation Catalyst) tel qu'utilisé dans les systèmes de dépollution des gaz d'échappement des moteurs Diesel automobiles.

Ce système est par nature un système à paramètres répartis en raison de sa géométrie allongée parcourue par un flux gazeux en contact avec un catalyseur réparti. Après avoir étudié expérimentalement ce système, nous avons décidé de prendre en compte cette nature répartie, qui comme on le montre, se retrouve également dans les autres systèmes de dépollution (filtres à particules, pièges à NOx, SCR).

Une première contribution du manuscrit consiste en un modèle du système DOC. Celui-ci est obtenu par des simplifications successives, justifiées expérimentalement (observations, estimations des ordres de grandeurs) ou par analyse des équations régissant la dynamique du système (développements asymptotiques, changements de variables). Ce modèle permet de rendre compte de la complexité de la réponse de la température de sortie du DOC à des variations des grandeurs d'entrée. En particulier, les effets de réponses inverses et de retards sont bien représentés.

Une seconde contribution est un ensemble d'algorithmes de commande (précompensation, rétroaction, et synchronisation) permettant de maîtriser les phénomènes thermiques dans le DOC.

Ces deux contributions ont été testées expérimentalement et validées. En conclusion, les performances obtenues sont évaluées. En résumé, en utilisant l'approche présentée dans ce manuscrit, il est possible de commander, *en conditions réelles*, la température de sortie du DOC à $\pm 15°$C.

Summary

The problem studied in this thesis is the control of a DOC (Diesel Oxidation Catalyst) as used in aftertreatment systems of diesel vehicles.

This system is inherently a distributed parameter system due to its elongated geometry where a gas stream is in contact with a distributed catalyst. After having studied this system experimentally, we decided to take into account its distributed nature, which as shown, is also found in other aftertreatment devices (particulate filters, NOx traps, SCR).

A first contribution of the thesis is a model for the DOC system. It is obtained by successive simplifications justified either experimentally (from observations, estimates of orders of magnitudes) or by an analysis of governing equations (through asymptotic developments, change of variables). This model can account for the complexity of the temperature response of DOC output to changes in input variables. In particular, the effects of inverse responses and delays are well represented.

A second contribution is a combination of algorithms (feedback, feedforward, and synchronization) to control the thermal phenomena in the DOC.

Both contributions have been tested and validated experimentally. In conclusion, the outcomes are evaluated. In summary, using the approach presented in this manuscript, it is possible to control, *in real conditions*, the outlet temperature of the DOC within $\pm 15^{\circ}$C.

Remerciements

La grande majorité de cette thèse a été effectuée à l'IFP Lyon. Je remercie en premier lieu Monsieur Yann Creff qui est l'initiateur de cette thèse. Son intérêt et son implication, ainsi que son expertise scientifique et technique ont été une contribution inestimable à la qualité et à l'aboutissement de mes travaux. Le soutien et la confiance qu'il m'a accordés m'ont permis de donner à cette thèse la portée que j'en attendais.

Mes remerciements vont tout particulièrement à mon directeur de thèse, Monsieur Nicolas Petit, pour ses conseils scientifiques, son soutien, sa disponibilité et sa grande réactivité. Sa vision sur mon travail, toujours pertinente, et ses conseils efficients, ont été déterminants dans l'avancement des travaux.

J'exprime ma gratitude à Messieurs Jean-Pierre Corriou et Michiel Van Nieuwstadt, rapporteurs de ma thèse, pour l'intérêt qu'ils ont montré pour mes travaux et pour leurs commentaires avisés sur mon mémoire. Je remercie Messieurs Yann Le Gorrec et Denis Dochain, examinateurs, de m'avoir fait l'honneur d'évaluer mes travaux.

J'adresse également mes sincères remerciements à tous les collègues de R103, R105 et R11 qui ont contribué à la mise en œuvre et à la réussite de ce projet. Merci notamment à Luc Voise, Stéphane Zinola, Nicolas Deport, et Eric Peurière, pour la réussite des essais à Solaize et à Olivier Grondin, Frédéric Lippens, Régis Cantais, Christophe Dufresnes, et Eric Watel pour le succès des essais à Rueil. Merci à l'équipe de simulation et aux stagiaires qui ont participé de près ou de loin à l'avancement des travaux.

Merci aux collègues que j'ai côtoyés quotidiennement et qui ont contribué à rendre ce travail convivial. Merci aux doctorants de la direction, et notamment à Eugênio, Sébastien, Matthieu, et Rachid.

Enfin, merci à tous les proches qui m'ont encouragé dans ce travail. Je remercie Julie pour sa patience, sa compréhension et son soutien inconditionnel.

Contents

Nomenclature

A_{cell} cell cross-sectional area, 38

A_j pre-exponential factor in rate equations, 39

α_i power-law on species in rate equations, 39

β_k power-law on species in rate equations, 39

C_s species mass concentration, 39

$\overline{C}_g$ gas molar concentration, 37

Cp gas constant pressure specific heat, 38

Cp_s specific heat of monolith, 38

$\overline{C}_s$ surface molar concentration, 38

C_u control HC concentration, 46

δ synchronization delay, 76

ΔH^a adsorption heats in Langmuir-Hinshelwood reaction rate inhibition terms, 39

ΔH_u heat of combustion of control HC, 45

δ_{L_u} characteristic propagation delay of control HC, 94

E total internal energy of gas, 37

E_a activation energy in rate equations, 39

ε void ratio, 38

η control HC conversion efficiency, 43

ΔH_{dis} heat of combustion of disturbance reductants, 113

η_{dis} disturbance reductants conversion efficiency, 113

F gas mass flow rate, 38

F_{dis} "disturbance reductants" flow rate, 41

G_a geometric surface area-to-volume ratio, 38

Γ surface site density, 39

G_{ca} catalytic surface area-to-volume ratio, 38

G_{dis} steady-state gain from disturbance reductants flow rate F_{dis} (input) to DOC outlet temperature (output), 113

G_{dis}^{dyn} "Dynamic" gain for F_{dis}, 117

G_u steady-state gain from control HC flow rate u (input) to DOC outlet temperature (output), 46

H total enthalpy of gas, 37

h_g convective heat transfer coefficient between gas and solid, 38

h_j enthalpy of chemical species j, 38

K pre-exponential factor in Langmuir-Hinshelwood reaction rate inhibition terms, 39

k_g thermal conductivity of gas, 38

$k_{m,j}$ mass transfer coefficient of species j, 38

L DOC length, 49

L_c reactive length, 49

L_u fictitious transport length, 64

n power-law term in Langmuir-Hinshelwood reaction rate inhibition terms, 39

N_M number of gaseous species, 37

N_S number of surface intermediate species, 39

p gas pressure, 37

ρ_g gas density, 37

ρ_s monolith density, 38

R_j rate of reaction of species j, 38

R_u universal gas constant, 39

S Generalized source term in Euler equations, 37

s Laplace variable, 51

$\dot{s}_m$ chemical species heterogeneous molar production rate of species m, 39

T gas temperature, 38

t time, 37

$T^{in}_{eq,dis}$ Boundary input equivalent to F_{dis}, 115

T^{in}_{eq} Boundary input equivalent to u, 65

Θ_m coverage fraction of surface intermediate species m, 39

T^{in} DOC inlet gas temperature variations (disturbance variable), 41

T^{out} DOC outlet gas temperature variations (output variable), 41

T_s monolith temperature, 38

T^{sp} DOC outlet temperature setpoint, 95

u control HC flow rate (control variable), 41

Υ Heaviside function, 50

v gas velocity in the channel (disturbance variable), 37

z coordinate along the flow axis, 37

Chapitre 1

Introduction

Dans ce chapitre, on présente différentes technologies de systèmes de post-traitement diesel, et on souligne quelques unes de leurs particularités. L'accent est mis sur leur nature spatialement répartie. L'organisation de la thèse est présentée à la fin de ce chapitre.

1.1 Panorama des systèmes de post-traitement diesel : piège à NOx, SCR, FAP et DOC

Ces dernières décennies, les moteurs diesels ont été de plus en plus utilisés dans le domaine de l'automobile en Europe. Ceci est lié à leur rendement important. En 1990, moins de 15% des nouveaux véhicules à usage particulier étaient des véhicules diesels - la partie restante étant pour les véhicules à essence. En 2008, plus de 50% étaient des diesels[1] (ACEA 2009). En parallèle, les normes sur les émissions polluantes sont devenues de plus en plus strictes (Ecopoint Inc. 2008). Afin de satisfaire ces normes, un effort important de recherche et développement a été mis en place dans l'industrie automobile.

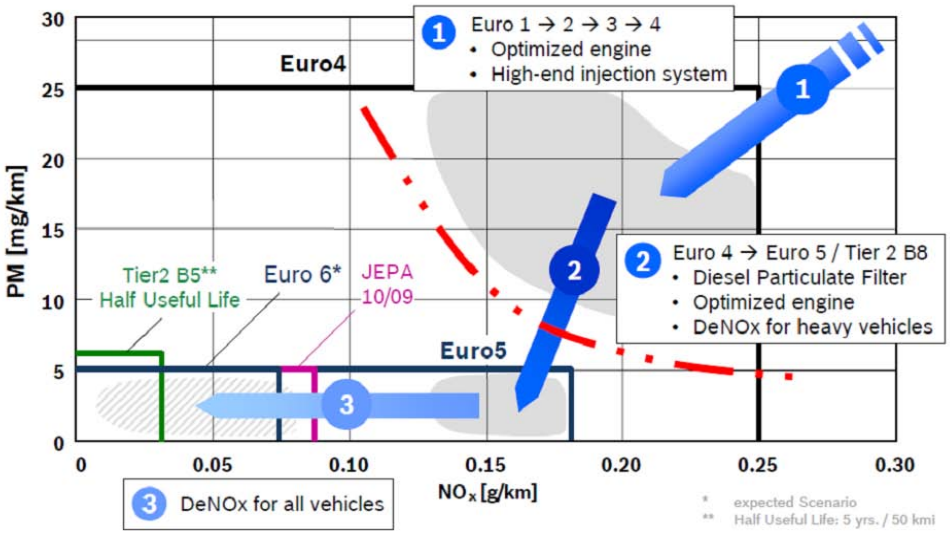

FIGURE 1.1 – Evolution des principales normes passées et attendues concernant les NOx et les particules (PM) pour les véhicules diesels légers (Source : Bosch, MinNOx 2007)

[1] 100% des véhicules poids lourds sont des diesels

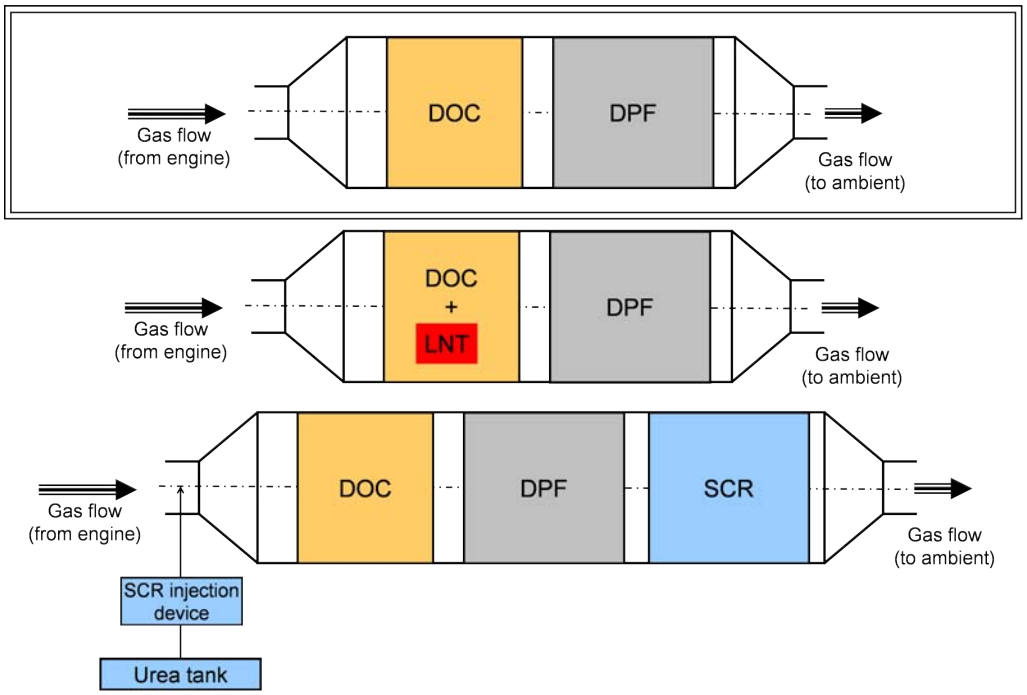

FIGURE 1.2 – Différentes configurations possibles de systèmes de post-traitement dans la ligne d'échappement

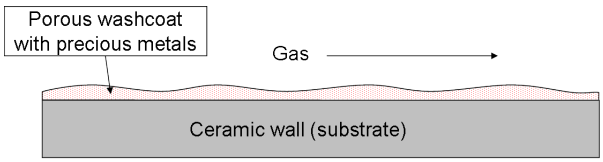

FIGURE 1.3 – Les couches constitutives d'un convertisseur catalytique

Quatre polluants sont actuellement réglementés : les hydrocarbures (HC), le monoxyde de carbone (CO), les oxydes d'azote (NOx), et les particules (PM). Malgré les avancées importantes dans la technologie des moteurs à combustion interne, ces normes ne pourront sans doute pas être satisfaites sans l'utilisation extensive de *systèmes de post-traitement*. L'évolution des normes de NOx et de PM est présentée en Fig. 1.1 pour les véhicules légers diesels (les besoins nécessaires pour les atteindre sont également décrits dans la figure).

Les NOx et les PM sont les polluants les plus problématiques pour les systèmes de post-traitement diesels. Ces polluants sont, d'un point de vue simpliste, le résultat d'un compromis lors de l'optimisation du moteur. Ceci est lié à leurs conditions respectives de formation. Pour cette raison, deux stratégies consensuelles ont émergé. D'abord, la norme Euro 5 (2009) nécessite l'utilisation d'un système de traitement des particules pour les véhicules diesels légers. Ensuite, la norme Euro 6 (2014) nécessitera sans doute l'utilisation d'un système de post-traitement pour les NOx. Une brève présentation des systèmes de post-traitement est réalisée dans ce chapitre.[2] D'abord, dans le § 1.1.1, les systèmes de post-traitement pour les NOx sont présentés. A l'heure actuelle, deux technologies sont utilisées : les pièges à NOx (PàNOx) et la réduction catalytique sélective (SCR) par l'urée (Urea-SCR). Ensuite, dans § 1.1.2, les filtres à particules (FAP) (utilisés pour traiter les particules) sont

[2]Des informations détaillées sur ce sujet sont largement diffusées, cf. par exemple AECC (2007), Auto-innovations EURL (2007) ou Ecopoint Inc. (2008).

présentés. Dans une dernière partie, on abordera les catalyseurs d'oxydation (DOC).

Le DOC est le sujet de cette thèse. Il est utilisé pour traiter HC et CO. Des exemples d'architectures de systèmes de post-traitement dans la ligne d'échappement sont donnés sur la Fig. 1.2. Les différents systèmes impliqués (DOC, FAP, SCR) ont des géométries similaires. Ce sont des réacteurs monolithiques (dans la plupart des cas en céramique) constitués de nombreux canaux fins permettant l'écoulement gazeux. Cette géométrie a pour but de maximiser les échanges entre gaz et solide, tout en limitant l'espace occupé par le système. Ces systèmes (excepté certains cas de FAP) incluent un catalyseur (métal précieux dans la plupart des cas). Ce catalyseur est habituellement logé sur un support en alumine, comme schématisé sur la Fig. 1.3. Le support est poreux et les polluants ont ainsi accès au métal précieux. Il faut noter que le support peut aussi avoir une influence dans le processus réactionnel.

1.1.1 Les systèmes de post-traitement pour les NOx

La norme Euro 5 pour véhicules diesels légers peut être satisfaite sans l'utilisation de système de post-traitement pour les NOx. Toutefois, la limite attendue pour Euro 6 impliquera leur utilisation. Nous présentons ici deux technologies, le piège à NOx (PàNOx) et la réduction catalytique sélective par l'urée (Urea-SCR).

Piège à NOx (PàNOx)

Un PàNOx est un réacteur monolithique recouvert par un support en alumine sur lequel on trouve un « piège » à base de baryum et un catalyseur à base de platine et de rhodium. Ce système nécessite que les gaz d'échappement passent dans des conditions riches[3] quelques secondes toutes les quelques minutes. L'environnement riche est, dans plupart des cas, créé à l'aide d'une injection tardive dans le cylindre. Inévitablement, ceci génère des problèmes de dilution d'huile et de surconsommation de carburant. Dans la ligne d'échappement, la fonction PàNOx peut être supportée par le même monolithe que le DOC, ou bien par un élément distinct.

Afin de simplifier la description du processus de conversion, il est possible de considérer que les NOx sont piégés dans des sites catalytiques disponibles pendant les phases pauvres. Pendant les phases riches, les NOx sont relargués et réagissent pour former du dihydrogène et du dioxyde de carbone. Cette phase est également appelée « purge riche ». Le processus de réaction est détaillé sur la Fig. 1.4. Il peut être décrit comme suit. Pendant les phases pauvres, le rapport NO_2 sur NOx augmente, dû à la catalyse sur le platine. Le NO_2 réagit avec le baryum pour former le composé stable de $Ba(NO_3)_2$. Pendant les phases riches, le composé est « dissocié » et des NOx sont relargués. Ensuite, les NOx réagissent sur le rhodium pour former du dihydrogène et du dioxyde carbone.

De plus, les PàNOx peuvent être empoisonnés par les composés soufrés. Ils doivent être périodiquement désulfatés dans un environnement riche et à haute température. Ces phases sont appelées « désulfatations ».

Le lecteur intéressé pourra se reporter à Olsson et al. (2005) pour plus de détails.

[3] Les conditions sont dites *riches* lorsque le rapport air/fuel est inférieur aux conditions stoechiométriques et *pauvres* lorsque ce rapport est supérieur aux conditions stoechiométriques.

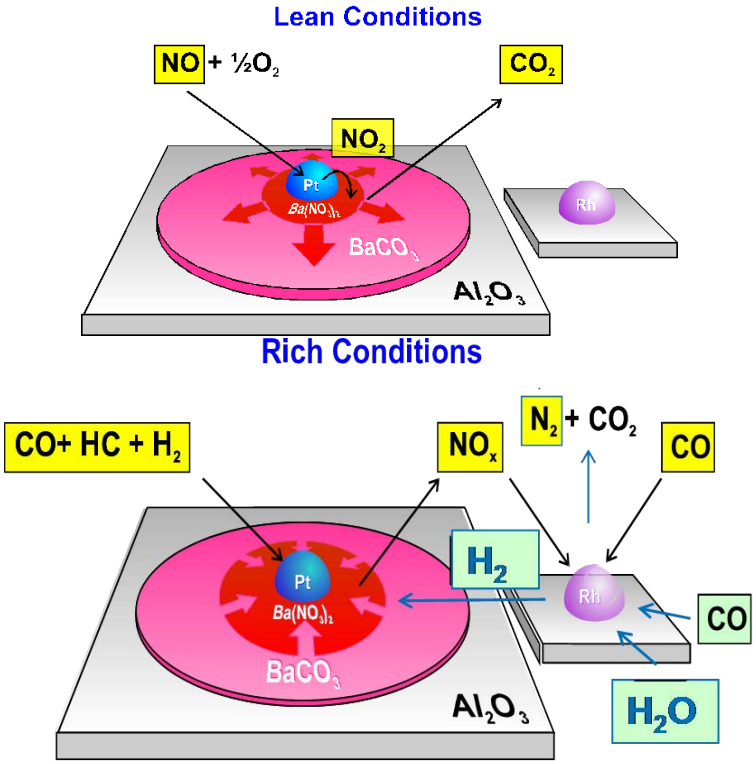

FIGURE 1.4 – Fonctionnement du PàNOx. En conditions pauvres, le NO est oxydé, et le NO_2 est stocké. En conditions riches, des NOx sont reformés et réduits à l'aide du rhodium. Source : IFP.

La réduction catalytique sélective par l'urée (Urea-SCR)

La technologie SCR est déjà très répandue dans les applications poids lourds. Elle est en train d'être adaptée pour les véhicules particuliers en vue de satisfaire la norme Euro 6, particulièrement exigeante en ce qui concerne les NOx. La technologie SCR a des rendements très élevés mais a un coût additionnel dans le véhicule et nécessite un entretien spécifique.

Un système Urea-SCR est composé d'un réservoir spécifique contenant de l'urée, qui est injectée dans la ligne d'échappement à l'aide d'un circuit dédié. L'urée se décompose en ammoniac (NH_3) qui réagit avec les NOx sur le catalyseur SCR (lequel peut être par exemple TiO_2, V_2O_5, Fe-Ze, Cu-Ze, ...).

Dans la ligne d'échappement, le système SCR est habituellement placé en aval du DOC et du FAP, tel qu'illustré dans la Fig. 1.2.

Les principales réactions SCR sont brièvement décrites. D'abord, les principales voies de réductions des NOx sont

- $2\,NH_3 + 2\,NO + \frac{1}{2}\,O_2 \rightarrow 2\,N_2 + 3\,H_2O$ (Réaction « Standard SCR »)
- $2\,NH_3 + NO + NO_2 \rightarrow 2\,N_2 + 3\,H_2O$ (Réaction « Fast SCR »)
- $8\,NH_3 + 6\,NO_2 \rightarrow 7\,N_2 + 12\,H_2O$ (Réaction NO_2 SCR)

De plus, le stockage NH_3 est un paramètre clé en commande de système SCR. Si l'on note Σ un site catalytique libre et NH_3* la forme adsorbée de NH_3, un schéma simplifié (typé contrôle-commande) de stockage d'ammoniac peut s'écrire

- $NH_3 + \Sigma \rightarrow NH_3*$ (Adsorption de l'ammoniac)
- $NH_3* \rightarrow \Sigma + NH_3$ (Désorption de ammoniac)

Notons que dans certains cas, différentes formes adsorbées de NH_3 doivent être considérées (Grossale et al. 2008) (Frobert, Creff, Raux, Charial, Audouin & Gagnepain 2009). Aussi, l'oxydation directe de l'ammoniac est importante puisque le débit d'ammoniac constitue la variable de commande pour le système SCR, et la proportion qui n'est pas utilisée dans l'oxydation des HC doit être connue avec précision :

- $2\ NH_3 + \frac{3}{2}\ O_2 \rightarrow N_2 + 3\ H_2O$ (Oxydation de l'ammoniac)

Finalement, l'oxydation du NO/réduction du NO_2 doit être considérée puisque le ratio NO/NO_2 est un autre paramètre clé dans la commande des systèmes SCR :

- $NO + \frac{1}{2}\ O_2 \leftrightarrow NO_2$

1.1.2 Le filtre à particules (FAP)

Sur la plupart des nouveaux véhicules diesels, les exigences à l'égard des particules (Ecopoint Inc. 2008) sont satisfaites par l'utilisation d'un filtre à particules (FAP). La norme Euro 5 réduit d'un facteur cinq (comparé à Euro 4) la limite sur les émissions de particules. Le filtre, placé dans la ligne d'échappement du véhicule, accumule les particules, qui sont ensuite brûlées dans un processus de régénération active (Achour 2001).

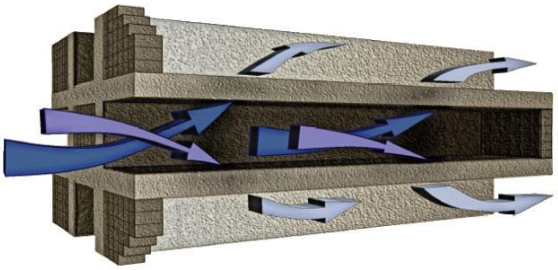

FIGURE 1.5 – Schéma des canaux d'un FAP. Le gaz chargé en particules, en bleu foncé, est filtré lorsqu'il traverse les parois poreuses. Le gaz traité, en bleu clair, sort par les canaux adjacents. Figure source : www.cd-adpco.com.

Le FAP est un réacteur en céramique (le plus souvent en cordiérite ou carbure de silicium) composé de nombreux canaux. Ces canaux sont bouchés alternativement d'un côté ou de l'autre. Ils sont reliés aux canaux adjacents par des parois poreuses. Les gaz sont donc forcés de traverser ces parois, qui agissent comme des filtres pour les particules. Ce processus est schématisé en Fig. 1.5. Tous les 500 km environ, le filtre doit être nettoyé. Ceci est réalisé en élevant sa température (entre $450°C$ et $600°C$ suivant les supports) en présence d'oxygène (i.e. dans un environnement pauvre). Ce processus est appelé régénération active du FAP.

1.1.3 Le catalyseur d'oxydation diesel (DOC)

Historiquement, les catalyseurs d'oxydation ont été les premiers systèmes de post-traitement utilisés dans l'industrie automobile. Ils ont été largement développés depuis le milieu des années 70s pour les moteurs à essence à cause de leurs émissions importantes en HC et CO.

(a) DOC utilisé sur le modèle Peugeot 407 HDi FAP 2.0-L. 1.22-L / Ø 5.63 x 3 in / densité de canaux : 400 cpsi

(b) DOC utilisé sur le modèle Renault M9R 2.0-L. 2.21-L / Ø 5.67 x 5.5 in / densité de canaux : 400 cpsi

FIGURE 1.6 – Exemples de DOC trouvés sur véhicules. Les deux DOC sont composés d'environ 900 canaux. Photographies : IFP

Les catalyseurs d'oxydation utilisés pour les moteurs diesels (i.e. DOC) sont apparus plus tard. Ceci est lié à leurs émissions relativement faibles en HC et CO, comparées à celles des moteurs à essence. Ces espèces sont dans la plupart des cas traitées par un catalyseur à base de platine. De plus, le DOC permet de réduire la masse des particules. Ceci explique pourquoi le DOC est systématiquement utilisé dans les systèmes de post-traitement diesels.

Les oxydations de HC et CO sont fortement exothermiques. C'est pourquoi le DOC est aussi utilisé pour contrôler la température dans la ligne d'échappement. En particulier, il est utilisé pour générer la température nécessaire pour le processus de *régénération active du FAP* (Van Nieuwstadt & Tennison 2006). Pour augmenter la température en amont du FAP, des réducteurs sont oxydés dans le DOC, ce qui provoque l'augmentation de sa température de sortie. C'est pourquoi, dans la plupart des architectures de systèmes de post-traitement, un DOC est placé en amont du FAP dans la ligne d'échappement (voir Fig. 1.2).

1.2 Nature répartie des systèmes de post-traitement et perspectives de commande

Tel qu'on l'a déjà présenté, les systèmes de post-traitement sont des réacteurs monolithiques conçus pour maximiser le transfert de matière à la surface catalytique. Pour cela, les canaux du monolithe sont étroits et nombreux (un ordre de grandeur typique est de 400 cpsi[4]). Cette configuration géométrique conduit aussi à des transferts de chaleur très efficaces entre gaz et solide. C'est pourquoi la phase solide (i.e. le monolithe) agit comme un réservoir réparti d'énergie et de matière. Le phénomène de propagation qui en résulte conduit à des réponses fortement retardées. Cet aspect sera illustré à plusieurs occasions dans ce manuscrit.

Les modèles pour ces systèmes sont basés sur des équations monodimensionnelles à paramètres répartis, assez similaires à celles qui seront présentées dans le Chapitre 2 (les équations du FAP sont légèrement différentes). Par la suite, on soulignera que les aspects monodimensionnels doivent être

[4] cells per square inch (cellules par pouces carrés) .

inclus dans la modélisation, et qui plus est, qu'ils doivent être pris en compte dans les stratégies de contrôle-commande.

Un exemple de nature répartie monodimensionnel pour la matière : SCR

Un modèle de commande pour la SCR peut s'écrire de la manière suivante

$$\begin{cases} \dfrac{\partial X}{\partial t} + v\,\dfrac{\partial X}{\partial z} = -a\,X\,(1-\theta) + d\,\theta \\ \dfrac{\partial Y}{\partial t} + v\,\dfrac{\partial Y}{\partial z} = -c\,\theta\,Y \\ \Omega\dfrac{\partial \theta}{\partial t} = a\,X(1-\theta) - d\,\theta - c\,\theta\,Y \end{cases} \tag{1.1}$$

où

- X est la concentration molaire de NH_3 ;
- Y est la concentration molaire de NOx ;
- Ω est la capacité totale des sites catalytiques ;
- θ est la proportion de sites catalytiques disponibles ;
- a est une fonction d'adsorption du NH_3. Elle dépend en particulier de la température ;
- d est une fonction de désorption du NH_3. Elle dépend en particulier de la température ;
- c est une fonction de consommation des NOx. Elle dépend en particulier de la température. c inclut toutes les réactions de consommation des NOx décrites dans § 1.1.1 ;
- v est la vitesse des gaz dans les canaux.

Ce modèle minimal, arrive à décrire les expériences basiques. L'une d'elles est détaillée par la suite. La Fig. 1.7 reproduit une expérience sur un catalyseur SCR (Fe-ZSM5), pour un point de fonctionnement du moteur correspondant à une température relativement basse (213°C en entrée du catalyseur) et à un débit de gaz faible (34 kg/h) (Frobert, Creff, Raux, Charial, Audouin & Gagnepain 2009). Au temps $t = 0$, l'urée est injectée. Son débit est ajusté pour maintenir le rapport molaire NH_3 sur NOx égal à 1. L'efficacité, i.e. le pourcentage des NOx traités sur le catalyseur, est tracée. L'efficacité croît lentement jusqu'à ce que l'injection d'urée soit coupée à $t = 3600$s. L'origine de cette augmentation lente n'est pas commentée ici. On veut se focaliser sur la forme de la courbe lors de la coupure de l'injection d'urée. Cette coupure se produit ensuite lorsque l'ammoniac stocké sur le catalyseur est consommé, ce qui explique que l'efficacité ne chute pas de manière brutale à 0. Quoi qu'il en soit, si le stockage est modélisé par un modèle 0D, on devrait observer une décroissance se rapprochant d'un comportement exponentiel. On décrit les choses de la manière suivante :

- le NH_3 stocké le long du catalyseur est progressivement relargué pour réduire les NOx, depuis l'entrée jusqu'à la sortie, ce qui explique la chute d'efficacité ;
- lorsqu'il ne reste presque plus de NH_3 stocké, l'efficacité chute brutalement.

Ce comportement ne peut donc pas être décrit sans utiliser un modèle qui prend en compte la distribution inhomogène du NH_3 dans le pain catalytique. Ceci souligne le besoin de modèle monodimensionnel, tel que celui présenté ci-dessus, pour prendre en compte le stockage NH_3 et améliorer la commande du système SCR. De nombreuses améliorations de ce modèle sont évidemment possibles, mais ceci est le sujet d'autres travaux.

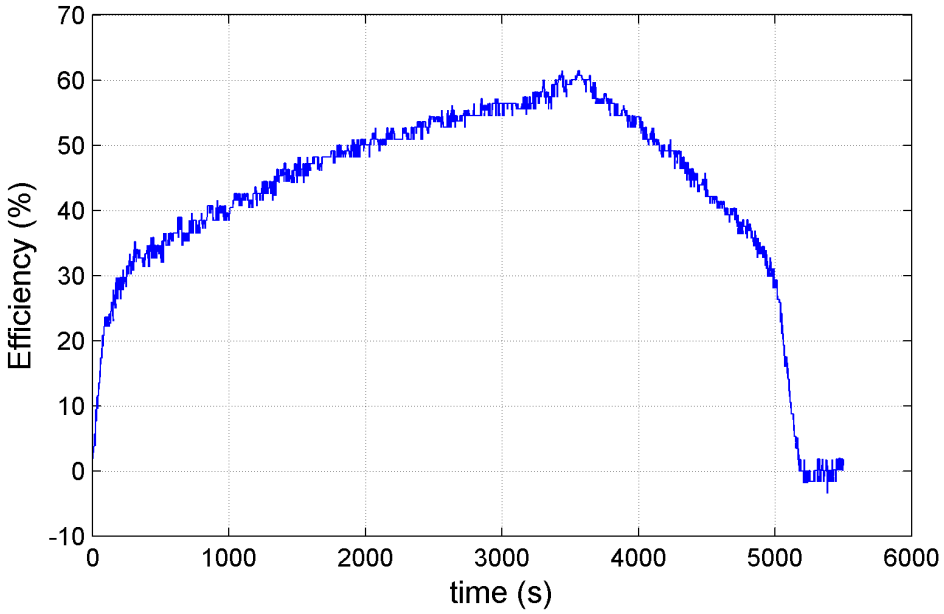

FIGURE 1.7 – Exemple d'efficacité de conversion des NOx suite à des changements type échelons de débit de NH_3. Au temps $t = 0$, l'urée est injectée. Au temps $t = 3600$s l'injection d'urée est coupée. Données expérimentales.

Un exemple de nature répartie monodimensionnel pour la thermique : DOC-FAP

Un modèle de référence pour le FAP est présenté dans Bisset (1984). Pendant le processus de régénération, le FAP se comporte comme un réacteur potentiellement instable (Achour 2001), et sa température doit être commandée avec précaution afin d'éviter tout risque d'emballement. La loi de commande ne peut être basée uniquement sur une rétroaction de la température en aval du FAP. Cela est dû aux phénomènes monodimensionnels dans le FAP et aux retards induits : l'élévation de température liée à l'oxydation des particules en entrée ou au centre du réacteur est fortement retardée à la sortie. La commande de cet élément s'effectue en boucle ouverte par la température des gaz entrants. En fait, le FAP peut être vu comme un élément passif. Pour mener à bien le processus de régénération, un profil de température doit être défini en prenant en compte le type de particules et le chargement. Toutefois, en pratique, ce profil est souvent réduit à une consigne constante. Un exemple de tel profil peut être trouvé dans Mercuri (2007). Il est reproduit dans la Fig. 1.8.

Comme expliqué précédemment, le DOC peut être utilisé pour commander la température de la ligne d'échappement. En particulier, il est utilisé pour les régénérations actives du FAP.

Le DOC est aussi décrit par des équations monodimensionnelles (qui seront présentées dans le Chapitre 2). On peut faire la constation basique suivante, soulignant cet aspect monodimensionnel : le temps de réponse thermique global est important (environ 10 à 100 secondes), alors que le temps de résidence du gaz est très court (typiquement une fraction de seconde). En fait, le DOC agit comme un réservoir localisé pour la chaleur. D'un point de vue de système dynamique, la température en sortie de DOC peut être commandée par un débit spécifique de HC (variable de contrôle). Comme pour le FAP, la commande de la température DOC ne peut être uniquement basée sur l'information du capteur de température en sortie du DOC (rétroaction). Ceci est dû aux temps de réponse importants causés par la nature répartie du système et à la fréquence et l'importance des perturbations auxquelles le système est soumis. Ces perturbations sont principalement la température d'entrée, le débit de gaz,

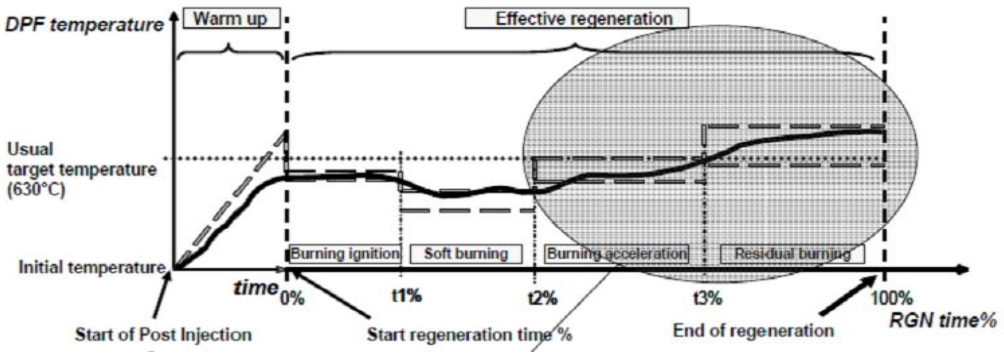

FIGURE 1.8 – Exemple de profil de température à suivre lors de la régénération du FAP (Source : Mercuri (2007)).

et la composition non désirée du gaz en entrée (HC, CO, . . . , résultants d'une combustion incomplète dans les cylindres).

Le DOC est un sujet d'intérêt particulier dans les systèmes de post-traitement. Une meilleure stratégie de commande peut réduire significativement les temps d'élaboration et de réglage du contrôleur. Elle peut en outre améliorer la maîtrise de la température et ainsi réduire le risque d'emballement du filtre à particules. Si les fluctuations de température sont réduites, il est alors possible de décaler la valeur de consigne vers la limite d'emballement et, en conséquence, réduire le temps nécessaire à la régénération. Ceci a aussi des effets bénéfiques en terme de surconsommation de carburant et de dilution d'huile. Enfin, on peut souligner un autre aspect bénéfique indirect. Du point de vue de la conception, une meilleure maîtrise de la température DOC peut permettre d'utiliser des monolithes plus longs (plus le monolithe est long, plus sa commande est difficile). Ce sont les raisons qui motivent le travail de recherche présenté dans cette thèse.

1.3 Aperçu de la thèse

Comme discuté précédemment, les systèmes de post-traitement sont de plus en plus fréquemment incorporés dans les nouveaux véhicules. La réduction des coûts, et l'allongement de la durée de vie de ces réacteurs chimiques peuvent être obtenus par des algorithmes de commande performants. Pour être réaliste, leur effort de calibration doit être restreint.

Après avoir souligné certains aspects liés à la nature répartie (1D) de différents systèmes de post-traitement dans cette introduction, nous allons maintenant nous focaliser sur le problème de commande de la température DOC pour la régénération active du FAP. C'est le sujet de cette thèse, qui est organisée comme suit. Dans le chapitre 2, nous présentons un modèle détaillé pour le DOC, issu de la littérature, et qui s'est complexifié au cours du temps. Dans le chapitre 3, ce modèle est réduit au minimum nécessaire à la description des réponses thermiques. Un modèle agrégeant les réactions chimiques dans un terme « source » réparti sert de base pour notre loi de commande.

Dans le chapitre 4, il est montré que ce terme source réparti peut être approximé par une condition au bord. Enfin, on présente un modèle paramétré basé sur l'équation advection-diffusion. Cette approximation représente le comportement du système lorsque ses principaux paramètres varient. Cependant, d'autres effets doivent être considérés en vue d'une application réelle. Ils sont détaillés, avec les possibilités de précompensation, dans le chapitre 5. Dans le chapitre 6, on développe une loi de commande par précompensation de la température d'entrée (perturbation), basée sur le modèle proposé. De plus, une action de précompensation est proposée pour atténuer les effets des variations

de débit de gaz (perturbation). Le modèle de commande proposé permet aussi d'adapter l'évolution des paramètres dans la loi de rétroaction dans des conditions variables de débit de gaz. Finalement, pour souligner la pertinence de la stratégie proposée, des résultats expérimentaux sont présentés dans le chapitre 7.

Concernant l'implémentation pratique On pourra se reporter au chapitre 7 pour une présentation détaillée de la loi de commande proposée et des résultats expérimentaux.

Remarque importante Dans le corps du manuscrit, une perturbation est intentionnellement omise afin de clarifier la présentation. Les adaptations de la stratégie proposée sont faites en Annexe A pour le traiter le « cas réel ». Dans l'Annexe C, un contrôleur utilisant des stratégies de commande classiques est développé en tant que référence. Les paramètres d'un modèle de premier ordre avec retard sont calculés à l'aide des valeurs physiques du DOC, ce qui permet un effort de calibration restreint et une synthèse directe de contrôleur. Malheureusement, cette voie classique ne donne pas de résultats complètement satisfaisants. L'étude présentée dans l'Annexe D a pour but d'accélérer la réponse thermique du DOC. Bien qu'elle ne soit pas utilisée directement dans la stratégie de commande, cette stratégie donne des indications intéressantes qui sont utilisées dans le corps du texte. L'Annexe E rassemble les calculs dont les résultats sont présentés dans le texte principal. L'Annexe F présente le banc d'essai utilisé pour les expériences. En Annexe G, les problèmes de commande relatifs à l'environnement du contrôleur de température DOC (boucle d'air, boucle de carburant, estimation des émissions) ayant conduits aux résultats expérimentaux sont présentés.

Remarque. Tous les résultats expérimentaux présentés dans ce manuscrit ont été obtenus lors d'expériences menées au cours de la thèse.

Introduction

In this chapter, we present the various technologies found in diesel aftertreatment systems and stress some of their particularities. A particular emphasis is put on the spatially distributed nature which is a common factor between them. At the end of the chapter, we present the organization of this thesis.

1.4 A panorama of diesel aftertreatment systems: NOx trap, SCR, DPF and DOC

Due to their high efficiency, the use of diesel engines in automotive has been in constant growth over the last decades in Europe. In 1990, less than 15% of new European passenger car registrations were diesel engines (CI) (the remaining part being for Spark Ignited (SI) engines). In 2008, more than 50% were for CI[5] (ACEA 2009). In the meantime, the automotive emissions standards have steadily become more stringent (Ecopoint Inc. 2008). Satisfying these emissions requirements has needed much research and development work for the automotive industry.

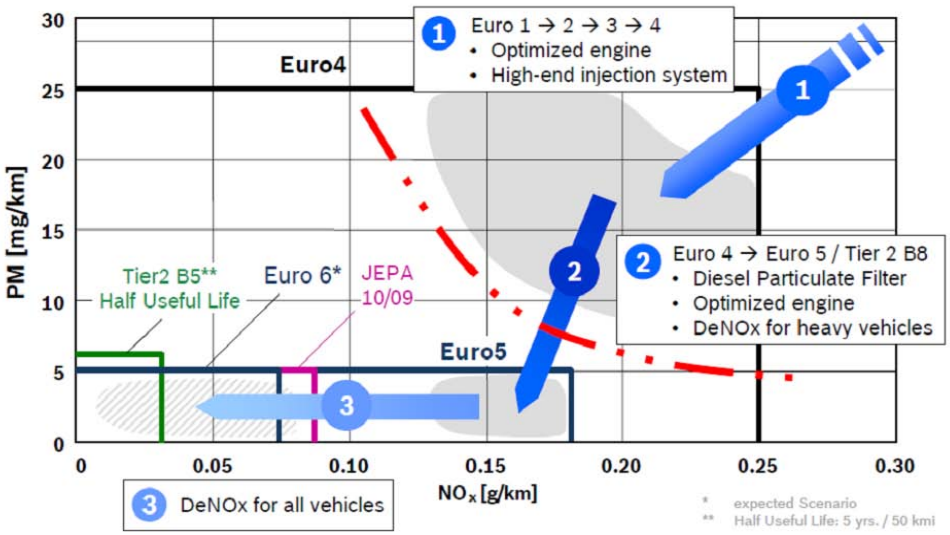

Figure 1.9: Main NOx and PM standards evolution for light-duty diesel vehicles and expected required aftertreatment systems (Source: Bosch, MinNOx 2007)

Four pollutants are regulated by current standards: hydrocarbons (HC), carbon monoxide (CO), nitrogen oxides (NOx), and particulate matter (PM). In spite of striking advances in engine technologies, it is likely that emissions constraints will not be satisfied without extensive use of *exhaust*

[5] the ratio CI-DI is also 0%-100% for trucks

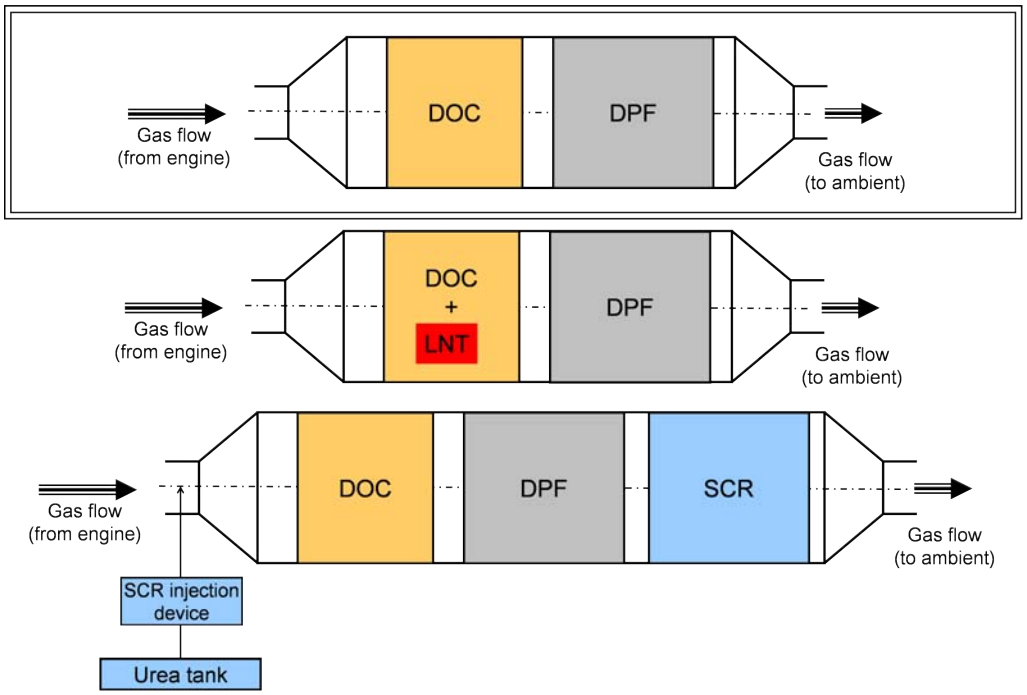

Figure 1.10: Different possible configurations of aftertreatment devices in the exhaust line

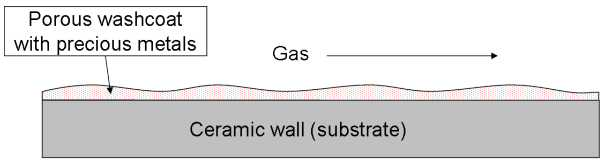

Figure 1.11: Layers of aftertreatment catalytic converters

aftertreatment systems. The evolution of the standards is presented in Fig. 1.9 for NOx and PM for diesel light-duty vehicles (corresponding needs to reach these levels are also described in the figure).

NOx and PM are the most problematic issues for diesel aftertreatment. They are, from a simplistic viewpoint, contradictory objectives in engine optimization. This is due to their respective conditions of formation. For this reason, two consensus-based strategies have emerged in European standards. First, Euro 5 (2009) requires the use of a PM aftertreatment device for most light-duty vehicles. Then, Euro 6 (2014) will require the use of a NOx aftertreatment device. A brief presentation of aftertreatment systems is made in this chapter.[6] First, in § 1.4.1, NOx aftertreatment systems are presented. Two main technologies are currently in use: lean NOx trap (LNT) and urea selective catalytic reduction (SCR). Then, in § 1.4.2, diesel particulate filters (DPF), which are used to treat PM, are presented. Finally, diesel oxidation catalysts (DOC) are introduced.

The DOC is the subject of this thesis. It is used to treat HC and CO. Examples of configurations of aftertreatment devices in the exhaust line are pictured in Fig. 1.10. The various systems involved (DOC, DPF, SCR) have similar geometries. They are monolithic reactors (in most cases made of ceramics) composed of numerous thin channels conveying the gas flow. This geometry is designed to maximize gas exchange with solid surface while limiting the room occupied by the system. These systems (except in some specific cases of DPFs) include a solid catalyst (precious metals in most

[6]Comprehensive information on the subject can be found e.g. in AECC (2007), Auto-innovations EURL (2007) or Ecopoint Inc. (2008).

cases). This catalyst is usually borne by an alumina washcoat as is pictured in Fig. 1.11. The washcoat is porous so that molecules have access to precious metals. Washcoat material have also an influence on the catalytic reaction.

1.4.1 NOx aftertreatment systems

In diesel engines, Euro 5 standard requirements on NOx can be met without aftertreatment system for light vehicles. However, the expected limit for Euro 6 does imply the use of a NOx aftertreatment system. We now present two such technologies, Lean NOx Trap (LNT) and Urea Selective Catalytic Reduction (Urea-SCR).

Lean NOx Trap (LNT)

A lean NOx trap is a monolith covered by an alumina washcoat bearing a barium-based trap and a platinum and rhodium based catalyst. This system requires the gases to switch to rich[7] conditions for a few seconds every few minutes. This rich environment is most often created by in-cylinder late post-injection. Unavoidably, this generates engine oil dilution and extra fuel consumption. In the exhaust line, the LNT can either be included in a separated monolith or included in the DOC or the DPF.

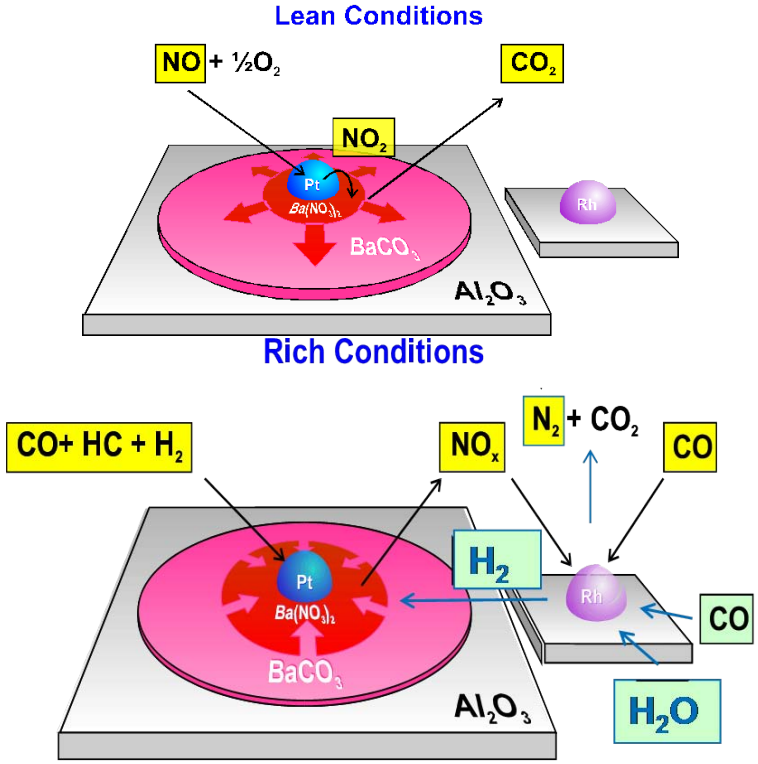

Figure 1.12: LNT process. Under lean conditions, NO is oxidized and NO_2 is stored. Under rich conditions, NOx is re-formed and is reduced over rhodium. Source: IFP.

To simplify the conversion process description, it is possible to consider that NOx is trapped in available sites during lean combustion phases. During rich phases, NOx is released from the sites and reacts to form nitrogen and carbon dioxide. This phase is also called “rich purge”. Detailed reaction

[7] Conditions are *rich* when the air to fuel ratio is below stoichiometry and *lean* when it is above stoichiometry.

process is pictured in Fig. 1.12 and described as follows. During the lean phases, the NO_2 to NOx ratio is increased by platinum-based catalysis. NO_2 reacts with barium to form a stable compound $Ba(NO_3)_2$. During the rich phases, the compound is "dissociated" and NOx is released. Then, NOx reacts over the rhodium to form nitrogen and carbon dioxide.

Besides, LNT get poisoned by sulfur compounds. It must be periodically desulfated under high temperatures and rich conditions. These phases are called "desulfations".

The interested reader can report to Olsson et al. (2005) for more details.

Urea Selective Catalytic Reduction (Urea-SCR)

The SCR technology is already widespread among heavy duty applications. It is currently being adapted to passenger cars because of the coming NOx-stringent Euro 6 emission requirements. SCR systems yield high NOx conversion rates but require costly additional in-vehicle hardware and specific servicing.

A Urea-SCR system is composed of a specific tank containing urea, which is injected into the exhaust line through a dedicated circuit. Then, it is decomposed into ammonia (NH_3) which reacts with NOx on the SCR catalyst (which can be e.g. TiO_2, V_2O_5, Fe-Ze, Cu-Ze ...).

In the exhaust line, the SCR system is usually located downstream of both the DOC and the DPF as shown in Fig. 1.10.

Main reactions with SCR systems are briefly introduced. First, main NOx reduction reactions are

- $2\ NH_3 + 2\ NO + \frac{1}{2}\ O_2 \rightarrow 2\ N_2 + 3\ H_2O$ (Standard SCR reaction)
- $2\ NH_3 + NO + NO_2 \rightarrow 2\ N_2 + 3\ H_2O$ (Fast SCR reaction)
- $8\ NH_3 + 6\ NO_2 \rightarrow 7\ N_2 + 12\ H_2O$ (NO_2 SCR reaction)

Besides, NH_3 storage is a key parameter in SCR control. Denoting Σ a free catalytic site and NH_3* an adsorbed form of NH_3, a simplified ammonia storage control-oriented scheme can be written as

- $NH_3 + \Sigma \rightarrow NH_3$* (Ammonia adsorption)
- NH_3* $\rightarrow \Sigma + NH_3$ (Ammonia desorption)

Note that, in some cases, different forms of adsorbed NH_3 must be considered (Grossale et al. 2008) (Frobert, Creff, Raux, Charial, Audouin & Gagnepain 2009). Further direct oxidation of ammonia is important because ammonia represents the control variable in SCR control, and it must be known when it is not used for NOx reduction.

- $2\ NH_3 + \frac{3}{2}\ O_2 \rightarrow N_2 + 3\ H_2O$ (Ammonia oxidation)

Finally, NO oxidation/ NO_2 reduction should be considered because the NO/NO_2 ratio is another key parameter in SCR control.

- $NO + \frac{1}{2}\ O_2 \leftrightarrow NO_2$

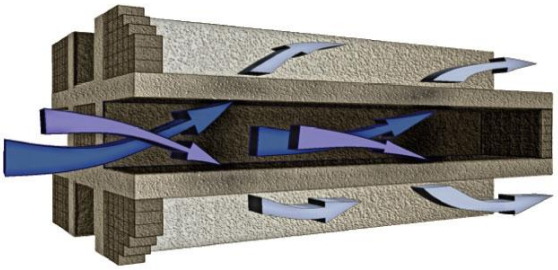

Figure 1.13: Schematic view of DPF channels. Gas loaded with PM, in dark blue, is filtered when flowing through porous walls. Clean flow, in light blue, exits to adjacent channels. Figure source: www.cd-adpco.com.

1.4.2 Diesel Particulate Filter (DPF)

On most modern diesel vehicles, the increasing requirements regarding particulate matter emissions (Ecopoint Inc. 2008) are satisfied using a diesel particulate filter (DPF). The Euro 5 standard has divided by five (compared to Euro 4) the maximum allowable value of particulate matter. This device is now widely spread among new vehicles. The filter, located in the vehicle exhaust line, stores particulate matter until it is burnt in an active regeneration process (Achour 2001).

In fact, the DPF is a reactor made of ceramic (mainly cordierite or silicon carbide) composed of numerous channels. These channels are blocked alternatively at one end or the other. They are related to adjacent channels by porous walls. Therefore, gases are forced to flow through the walls which act as filters for the particulate matter. This process is illustrated in Fig. 1.13. About every 500 km, the filter must be cleaned. This is achieved by raising the filter temperature (between $450°C$ and $600°C$ depending on the supports) in the presence of oxygen (i.e. in a lean environment). This process is called DPF active regeneration.

1.4.3 Diesel Oxidation Catalyst (DOC)

Historically, oxidation catalysts have been the first aftertreatment systems in automotive industry. They have been widely developed since the mid-70s for SI engine applications because of the high HC and CO emissions levels of these engines.

Catalysts used for diesel applications (i.e. DOC) have appeared later because of the relative lower values of HC and CO emissions found in CI engines compared against SI engines. These species are most often treated by a platinum-based catalyst. Further, DOC reduces PM mass. This explains why DOC is systematically used in diesel aftertreatment systems.

Because the HC and CO reactions are strongly exothermic, the DOC is also used to control the exhaust line temperature. In particular, it is used to generate the temperature required for the already mentioned *DPF active regeneration* (Van Nieuwstadt & Tennison 2006). To increase the DPF inlet temperature, reductants are oxidized in the DOC, which, in turn, increases its outlet temperature. This is why, in commonly observed aftertreatment architectures, a DOC is placed upstream of the DPF in the vehicle exhaust line (see Fig. 1.10).

(a) DOC used with a Peugeot 407 HDi DPF 2.0-L engine. 1.22-L / Ø 5.63 x 3 in / cell density: 400 cpsi

(b) DOC used with Renault M9R 2.0-L engine. 2.21-L / Ø 5.67 x 5.5 in / cell density: 400 cpsi

Figure 1.14: Examples of DOC found in commercial vehicles. Both the DOCs are composed of about 900 channels. Pictures: IFP

1.5 One-dimensional distributed nature of aftertreatment devices and control perspectives

As has been presented, aftertreatment systems use monolith converters which are designed to maximize the mass transfer to the catalytic surface. To this end, the channels of the monolith are narrow and numerous (a typical order of magnitude is 400 cpsi[8]). This geometric configuration also yields highly-efficient heat transfer between gas and solid. Hence, the solid phase (i.e. the monolith) acts as a spatially-distributed storage of energy and species. The induced propagation phenomenon leads to highly-delayed responses. This point will be illustrated at several occasions in the manuscript.

Models for these devices are based on one-dimensional distributed parameters equations similar to those presented in Chapter 2 (the DPF equations are slightly different). In the following it will be pointed out that one-dimensional effects must be included for in the modeling and further, that they should be accounted for in the control strategies.

An example of a 1D distributed parameter chemical model: SCR

A control-oriented model for the SCR can be written as

$$\begin{cases} \dfrac{\partial X}{\partial t} + v\,\dfrac{\partial X}{\partial z} = -a\,X\,(1-\theta) + d\,\theta \\ \dfrac{\partial Y}{\partial t} + v\,\dfrac{\partial Y}{\partial z} = -c\,\theta\,Y \\ \Omega\dfrac{\partial \theta}{\partial t} = a\,X(1-\theta) - d\,\theta - c\,\theta\,Y \end{cases} \tag{1.2}$$

where

- X is the molar concentration of NH_3;

[8] cells per square inch.

- Y is the molar concentration of NOx;
- Ω is the total capacity of catalytic sites;
- θ is the fraction of available catalytic sites;
- a is an adsorption function for NH_3. In particular, it depends on the temperature;
- d is a desorption function for NH_3. In particular, it depends on the temperature;
- c is a consumption function of NOx. In particular, it depends on the temperature. c encompasses all the NOx consumption reactions described in § 1.4.1;
- v is the gas velocity in channels.

This minimal model successfully describes basic experiments, one of which is illustrated in the following. Fig. 1.15 reproduces an experiment on a SCR catalyst (Fe-ZSM5), for an operating point corresponding to a low temperature (213°C at catalyst inlet) and a low gas flow rate (34 kg/h) (Frobert, Creff, Raux, Charial, Audouin & Gagnepain 2009). At time $t = 0$, urea is injected. Its flow rate is

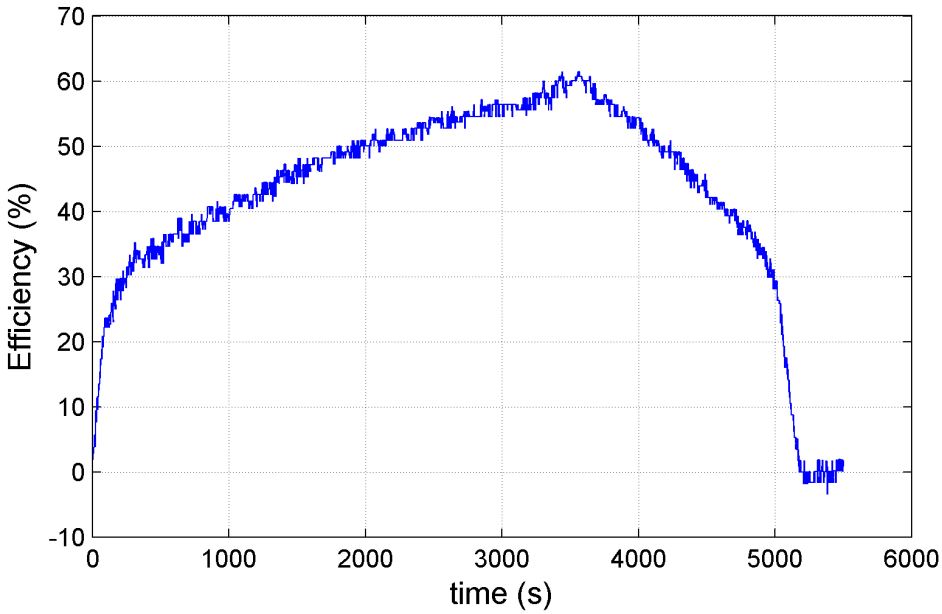

Figure 1.15: Example of NOx conversion efficiency during step changes in NH_3 supply. At time $t = 0$, urea is injected. At $t = 3600$s urea injection is cut. Experimental data.

adjusted such that the molar NH_3 to NOx ratio is equal to 1. The efficiency, i.e. the percentage of NOx that are treated on the catalyst, is plotted. The efficiency slowly rises until the urea injection is cut at $t = 3600$s. The origin of this slow rise is not commented here. We want to focus on the shape of the curve once the urea injection is cut. What happens then is a consumption of the ammonia stored in the catalyst, which explains why the efficiency does not immediately drops to 0. Anyway, if this storage were to be modeled by a 0-dimensional model, one should see a decrease merely looking like an exponential decrease. Here, what indeed happens is the following:

- NH_3 stored along the catalyst is progressively released to reduce NOx, from inlet to outlet, explaining the efficiency loss;

- when almost no NH_3 remains stored, efficiency quickly falls.

So, the observed behavior cannot be properly described, unless a model is used that accounts for an non-homogeneous spreading of NH_3 inside the catalyst. This underlines the need of a 1-dimensional model, such as the one presented above, to account for NH_3 storage and improve the SCR control. Many improvements of this model are obviously possible. This is the topic of other works.

An example of 1D thermal distributed dynamics: DOC-DPF

A reference model for DPF is presented in Bisset (1984). During the regeneration process, DPF behaves like a potentially unstable reactor (Achour 2001), and its temperature must be carefully controlled to prevent its runaway. This control cannot be only based on feedback information from a DPF downstream sensor. This is due to one-dimensional phenomena in the DPF and induced lag: temperature effects of PM oxidation taking place at the inlet or at the center of the reactor are highly delayed at the DPF outlet. Control of this element is achieved in open-loop by controlling its inlet gas flow temperature. In facts, a DPF is usually seen as passive element. To carry out the regeneration process efficiently, a DPF inlet gas flow temperature profile can be defined, taking into account the kind of PM and the PM loading. In practice, however, it is often restricted to a constant setpoint. An example of such a profile can be found in Mercuri (2007). It is reproduced in Fig. 1.16.

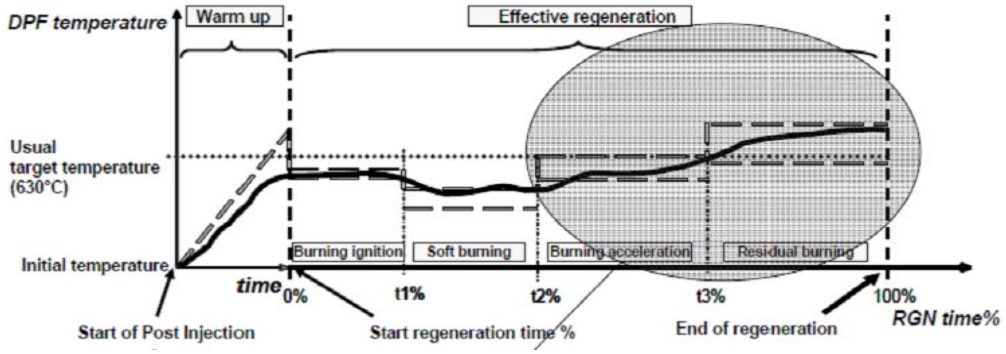

Figure 1.16: Example of strategy for DPF temperature profile for regeneration (Source: Mercuri (2007)).

As has been explained earlier, the DOC can be used to control the exhaust line temperature. In particular, it is used for DPF active regeneration.

DOC follows also 1D equations (that will be described in Chapter 2). One basic observation pointing out this one-dimensional nature is that, while the gas residence time is very short (typically a fraction of a second), the overall thermal response is important (about 10 to 100 seconds). In facts, a DOC acts as a distributed heat reservoir. From a dynamical system standpoint, the DOC outlet temperature can be controlled by a specific amount of injected HC (control variable). As for the DPF, DOC outlet temperature control strategies cannot be only based on feedback information from the DOC downstream sensor. This is because of the mentioned long response times due to 1D distributed nature of the system, and because of the large and frequent disturbances it is subject to. These are mostly inlet temperature, gas flow rate, and undesired upstream gas composition (HC, CO, ..., resulting from in-cylinder engine partial combustion).

DOC control is a topic of strong interest in aftertreatement systems. A better control can alleviate calibration effort and save time in the controller design and tuning. Further, improving the temperature control performance reduces the risk of filter runaway. When temperature fluctuations are reduced,

one can shift the setpoint closer to the runaway limit, and in turn decrease the required regeneration time. This also has some beneficial effects in terms of fuel consumption and engine oil dilution problems. Finally, there is another (indirect) beneficial aspect. From a design viewpoint, a better DOC temperature control allows the use of longer monoliths (the longer the monolith, the more difficult the control is).These are the reasons motivating the research work presented in this thesis.

1.6 Thesis outline

As discussed earlier, aftertreatment systems will tend to be systematically incorporated into modern vehicles. Reducing the costs and lengthening the life expectancy of these chemical reactors can be achieved thanks to improved control algorithms. To be realistic, one should keep their calibration effort low.

After having sketched some of the issues related to the distributed (1D) natures of various aftertreatment systems in this introduction, we will now focus on the problem of the DOC temperature control for the DPF active regeneration. This is the subject of this thesis which is organized as follows. In Chapter 2, we present a detailed model for the DOC using results from the literature, which has become richer and richer over the years. In Chapter 3, we reduce this model to a minimum required to describe the thermal responses properly. A model encompassing all the chemical reactions in a distributed "source" term serves as a basis for validation. In Chapter 4, it is shown that this distributed source term can be well-approximated by a boundary condition. Then, a parameterized model based on the advection-diffusion equation is considered. This approximation represents the behavior of the system when its main parameters are varying. Yet, some effects must be considered in view of real applications. They are detailed along with compensation possibilities in Chapter 5. In Chapter 6, a feedforward control based on the proposed model is developed for the inlet temperature (disturbance). Besides, a feedforward action is proposed to attenuate effects of the gas flow variations (disturbance). The proposed control scheme allows the evolution of parameters in the feedback law to be scheduled under varying gas flow conditions. To stress the relevance of the contribution, experimental control results are presented in Chapter 7.

For practical implementation Report to Chapter 7 for a detailed presentation of the proposed control solution and experimental results.

Important remark In the main body of the manuscript, a disturbance is intentionally omitted to clarify the presentation. Adaptations of the proposed control solution are made in Appendix A for the "real case". In Appendix C, a controller using classic control methods is developed as reference. The parameters of a first order plus delay model are calculated with physical parameters of the DOC, allowing a light calibration effort and straightforward controller design. Unfortunately, this classic path leads to not completely satisfying results. The study presented in Appendix D aims at speeding up DOC temperature response. Although not used in the control application, these insightful results are referred to in the main text. Appendix E gathers computation developments whose results are used in the main chapters. Appendix F presents the experimental setup used for experiments. In Appendix G, control problems related to the DOC temperature controller environment (air path, fuel path, emission estimation) having led to experimental results are presented. Management strategies for the actuators (and related difficulties) are presented.

Remark. All presented experimental data are the results of tests carried out during the Ph.D. term.

Chapter 2

DOC detailed modeling

In the field of diesel oxidation, catalytic phenomena are a topic of intense research. Models used by catalyst manufacturers and scientists to understand and optimize efficiency have steadily become more complex over the years. Early models essentially described simplified energy balances (Vardi & Biller 1968), and progressively, more detailed mass balances were added (at least two mass balances per considered species are now considered). Spatial inhomogeneity has been considered too, from a multi 0-dimensional model (Kuo et al. 1971) or a 1-dimensional model (Oh & Cavendish 1982), most recent automotive catalyst models lead to 2-dimensional or 3-dimensional simulation softwares ((Chen et al. 1988), (Tischer et al. 2001), (Shamim et al. 2002)). Obviously, they require heavy computational effort. Because of the geometric symmetry of the monolith which is mostly cylindrical, it is reasonable, as we do it in this thesis, to base our analysis on 1-dimensional models. As detailed in Depcik & Assanis (2005), and as will appear in the light of experimental results, this reveals to be a quite accurate approach and yields a substantial reduction of the mathematical difficulties.

In the approach of Depcik (2003), 1-dimensional models are based on the Euler equations of motion (mass, momentum, energy and molar species), which are often used for low viscosity 1-dimensional reacting flow in channels

$$\begin{cases} \dfrac{\partial \rho_g}{\partial t} + \dfrac{\partial (\rho_g\, v)}{\partial z} = S_{mass} \\ \dfrac{\partial (\rho_g\, v)}{\partial t} + \dfrac{\partial \left(\rho_g\, v^2 + p\right)}{\partial z} = S_{mom} \\ \dfrac{\partial (\rho_g\, E)}{\partial t} + \dfrac{\partial (\rho_g\, v\, H)}{\partial z} = S_{eng} \\ \dfrac{\partial \overline{C}_{g,j}}{\partial t} + \dfrac{\partial \left(u\, \overline{C}_{g,j}\right)}{\partial z} = S_j \quad j = 1, \ldots, N_M \end{cases} \tag{2.1}$$

where t is the time variable, z is the coordinate along the flow axis, ρ_g is the gas density, v stands for the gas velocity in the channel, p is the gas pressure, E is the total internal energy of gas, H is total enthalpy of gas, N_M is the number of considered species and, subscript j refers to the species j, $\overline{C}_g$ is gas molar concentration, and S terms are generalized source terms. One can refer to the work of Depcik & Assanis (2005) for comprehensive details.

These equations represent a generalization of a simpler set of equations proposed by various authors in earlier works such as those cited above. This general formulation has allowed relevance verification of explicit or implicit assumptions formulated in those earlier works: it is found that most of the representations were indeed relevant although results may differ in some specific cases. The main phenomena at stake are summarized in Fig. 2.1. Usually, corresponding models include

- one temperature equation for the gas phase

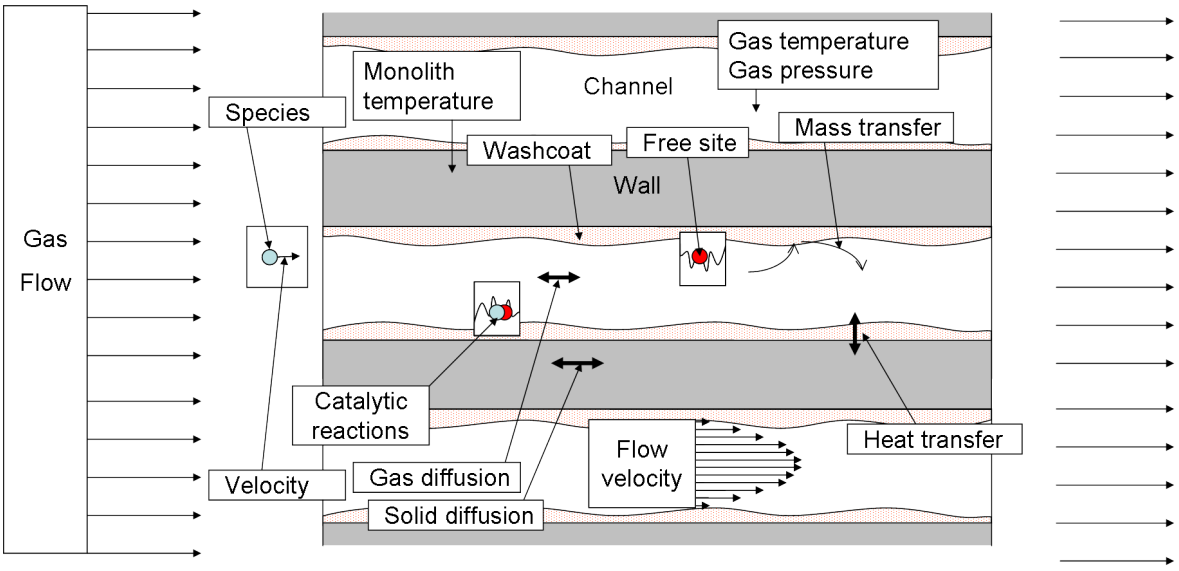

Figure 2.1: Phenomena involved in the numerous channels of the DOC. Reductant species in exhaust gas (in blue) are converted over the catalytic surface (in red).

- one temperature equation for the solid phase
- one balance equation per considered species in the gas phase
- one balance equation per considered species at the interface (surface)

These formulations include at least the following species: CO, O_2, H_2, two types of HC; and preferably NO, NO_2, CO_2, H_2O and other species.

In the following, we present a classic model based on the formulation of Oh & Cavendish (1982). It is a reference in terms of description of governing phenomena. The following symbols are used. T, $\overline{C}$ and ρ refer to the temperature, the molar concentration, and the density, respectively. Subscript s refers to monolith or surface. Where present, subscript g refers to gas. Cp is the specific gas heat, Cp_s is the specific heat of monolith, F is the gas mass flow rate, ε is the ratio of gas volume to total volume (void ratio), A_{cell} is the mean cell cross-sectional area (wall and channel), k_g is the thermal conductivity of gas, h_g is the convective heat transfer coefficient between gas and solid, G_a is the geometric surface area-to-volume ratio, G_{ca} is the catalytic surface area-to-volume ratio, R_j is the rate of reaction of species j, h_j is the enthalpy of chemical species j, $k_{m,j}$ is the mass transfer coefficient of species j. For more details on these variables, the reader can report to Depcik & Assanis (2005).

Balances equations are written as

- Gas temperature equation as

$$\underbrace{\varepsilon\,\rho_g\,Cp\,\frac{\partial T}{\partial t}}_{\text{Gas storage}} + \underbrace{\frac{F}{A_{cell}}Cp\frac{\partial T}{\partial z}}_{\text{Gas transport}} = \underbrace{\frac{\partial}{\partial z}\left(\varepsilon k_g \frac{\partial T}{\partial z}\right)}_{\text{Diffusion}} - \underbrace{h_g G_a (T - T_s)}_{\text{Exchange with monolith}} \tag{2.2}$$

- Monolith temperature equation as

$$\underbrace{(1-\varepsilon)\,\rho_s\,Cp_s\,\frac{\partial T_s}{\partial t}}_{\text{Monolith storage}} = \underbrace{\frac{\partial}{\partial z}\left((1-\varepsilon)k_s\frac{\partial T_s}{\partial z}\right)}_{\text{Solid diffusion}} + \underbrace{h_g G_a (T-T_s)}_{\text{Exchange with gas}} + \underbrace{G_{ca}\sum_{j=1}^{N_M} R_j h_j}_{\substack{\text{Enthalpy flow of}\\ \text{chemical reactions}}} \tag{2.3}$$

- Mass balance for gas species

$$\underbrace{\varepsilon\frac{\partial \overline{C}_{g,j}}{\partial t}}_{\text{Gas storage}} + \underbrace{\frac{F}{\rho_g A_{cell}}\frac{\partial \overline{C}_{g,j}}{\partial z}}_{\text{Gas transport}} = -\underbrace{k_{m,j} G_a(\overline{C}_{g,j}-\overline{C}_{s,j})}_{\text{Exchange with surface}} \quad j=1,\ldots,N_M \tag{2.4}$$

- Mass balance for surface gas species

$$\underbrace{(1-\varepsilon)\frac{\partial \overline{C}_{s,j}}{\partial t}}_{\text{Surface storage}} = \underbrace{k_{m,j} G_a(\overline{C}_{g,j}-\overline{C}_{s,j})}_{\text{Exchange with gas}} - \underbrace{G_{ca} R_j}_{\text{Chemical reaction}} \quad j=1,\ldots,N_M \tag{2.5}$$

where the reaction rate R_j is often fit to a Langmuir-Hinshelwood rate equation (see e.g. Olsson & Andersson (2004))

$$R_j = \frac{A_j\ \mathbf{e}^{-\frac{E_{a,j}}{R_u\,T_s}}\ C_{s,i}^{\alpha_i} C_{s,j}^{\beta_k}}{\left(1+K_i\ \mathbf{e}^{-\frac{\Delta H_i^a}{R_u\,T_s}}\ C_i + K_k\ \mathbf{e}^{-\frac{\Delta H_k^a}{R_u\,T_s}}\ C_k\right)^{n_i}\left(1+K_m\ \mathbf{e}^{-\frac{\Delta H_m^a}{R_u\,T_s}}\ C_m\right)^{n_m}} \tag{2.6}$$

where i,j,k and m refer to species index, A_j is the pre-exponential factors of species j, $E_{a,j}$ is activation energy of species j, $C_{s,j}$ are the species mass concentrations of species j, K are the pre-exponential factors of inhibition terms, ΔH^a are the adsorption heats in inhibition terms, n are power-law terms in reaction rate inhibition terms, α_i and β_k are power-law on species, and R_u is the universal gas constant. Alternatively, many different formulations can be considered for the reaction rate.

Note that most authors in the literature neglect the gas storage term $\frac{\partial \overline{C}_{s,j}}{\partial t}$ in the surface species balance (2.5). It is found in Depcik & Assanis (2005) that this approximation systematically leads yields little errors and is fully justified.

Although surface gas species storage is negligible, it must be noted that, in reality, washcoat plays an important role in the chemical reaction process (report to Herz & Sell (1985)). Taking into account detailed catalytic mechanisms requires another equation. This equation has been first introduced by Pattas et al. (1994) and later generalized by Windmann et al. (2003), Yamauchi et al. (2005), Depcik (2003). In its simplest form, it can be seen as an equation of availability of catalytic sites and is written as

$$\frac{d\Theta_m}{dt} = \frac{\dot{s}_m}{\Gamma} \quad j=1,\ldots,N_S \tag{2.7}$$

where N_S is the number of surface intermediate species, Θ_m is the coverage fraction of surface intermediate of species m, $\dot{s}_m$ is the chemical species heterogeneous molar production rate of species m, and Γ is the surface site density.

It turns useful to model formation of intermediate species and, in turn, describe mechanisms like oxygen storage over cerium or NO_2 storage over barium. Hence, it is particularly important when modeling three-way catalysts (catalyst used for SI engine and working in a close to stoichiometric environment) or LNT functions.

Finally, minimal catalyst formulations include 5 species as in Oh & Cavendish (1982) and, therefore, models includes at least 10 equations for the species. We will focus on the energy balances in the next chapter, gathering oxidation reactions in a single macroscopic source term.

Chapter 3

Reduced model

A DOC is a chemical system difficult to control because of the highly-varying delays and because of the large and frequent disturbances it is subjected to. As explained in Chapter 2, the natural complexity of this system has given birth to increasingly complex models over the years. Classic models are usually composed of at least a dozen of coupled partial differential equations ((2.2)-(2.5)). This large dimension makes difficult the development of model-based control laws. Later, simplified catalyst modeling approaches have been introduced (e.g. (Please et al. 1994), (Leighton & Chang 1995), (Ramanathan et al. 2004), (Keith et al. 2001)). Such approaches have provided insights into catalyst parameters optimization (void fraction, material, precious metal loading distribution, ...) or light-off prediction, but not on control design. In this thesis, our goal is to present a simplified model *dedicated to DOC outlet temperature control during DPF regeneration*. This will be accomplished in two steps. In this chapter, we first determine a distributed parameter model that takes the form of two 1-dimensional hyperbolic partial derivatives equations. In the following Chapter 4, we determine an approaching parabolic equation.

After an outline of modeling objectives corresponding to experimental observations that we wish the model to capture, simplifications are proposed and motivated, and, finally, a reduced model is extracted. As is demonstrated, it closely imitates the physical observations but does not directly lead to a control design. It is validated by experimental results.

3.1 Modeling objectives

We focus on the dynamics of the simple system pictured in Fig. 3.1, for which the steady-state effects are easily captured. The inputs are the control variable u (control HC flow rate), the disturbance variable T^{in} (inlet temperature), and the disturbance variable v (gas speed). *This latter disturbance is also referred to as gas flow rate F from now on*, since a straightforward relation relates gas flow rate and gas speed (given later by (3.18)).

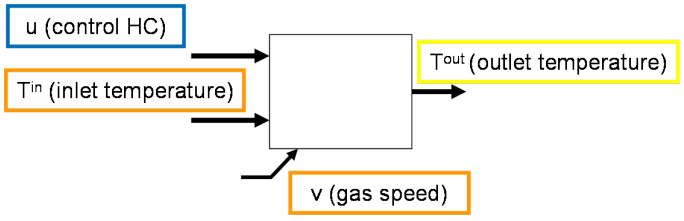

Figure 3.1: DOC reduced model

Certainly, the real picture of the DOC is more complicated, as it involves several other disturbances, among which is, in particular, the reductants flow (having effects similar to the control HC's). The reductants will be referred to as *disturbance reductants* (or variable F_{dis}) from now on. They will be mentioned and explained in some of the experimental results interpretations. Otherwise, *for sake of clarity, they will be voluntarily omitted*. Relevant extensions of the approach presented in the thesis are given in Appendix A.

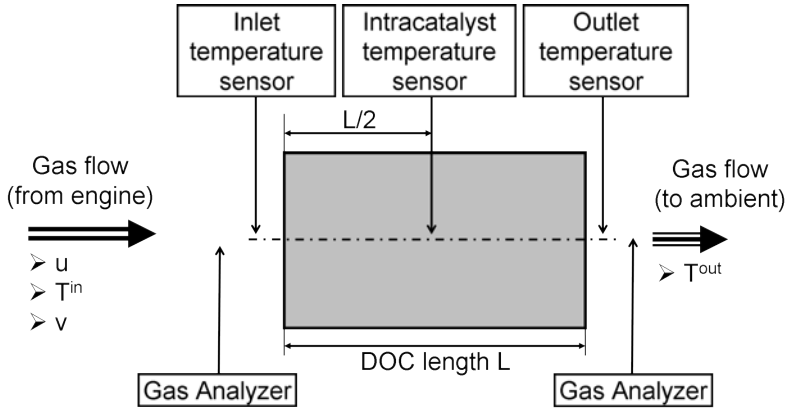

Figure 3.2: Simplified overview of the DOC experimental setup. See Appendix F for details.

A simplified overview of the DOC experimental setup used in the testbench modeling experiments is presented in Fig. 3.2. Gas temperatures are measured upstream and downstream of the DOC. Additionally, an intra-catalyst temperature sensor is located at the center of the DOC. Gas compositions can be measured upstream or downstream of the DOC. For a detailed description of the experimental setup, the reader can refer to Appendix F.

It is worth noticing that the input and output variables (u, T^{in}, T^{out}, v) are indeed available in embedded applications: u is the control variable related to the injector energizing time, T^{in} and T^{out} are provided by the DOC inlet and outlet temperature sensors (embedded sensors), and v can be evaluated from the mass air flow sensor, the inlet temperature sensor, and a pressure sensor (embedded sensors). On the other hand, intra-catalyst temperature (T^{intra}) as well as upstream and downstream gas compositions are *not* available in embedded applications. Further details are given in Appendix F.

Model requirements The description of the following phenomena is desired:

- response of T^{out} to control HC (u);
- response of T^{out} to inlet temperature (T^{in});
- influence of gas speed (v).

The above objectives can be divided into two subsets: steady-state values, and dynamic response matching. First, the steady-state effects of u and T^{in} are considered. It is shown that they can be easily described, under various constant gas speed (v) conditions. On the other hand, the dynamic effects of u and T^{in} are studied, first, under various constant gas speed v conditions, and then, the influence of the gas speed variations is considered. *For a sake of clarity, after their presentation, it will be assumed that the steady-state effects (§ 3.1.1) are known a priori and our focus will be on the dynamic responses (§ 3.1.2) in the rest of the thesis.*

3.1.1 Steady-state effects

First, we wish to relate the steady-state output temperature value to the input parameters (control HC flow rate, inlet temperature, and gas speed). The two inputs u and T^{in} have superimposing effects, that we describe one after the other.

3.1.1.1 u-to-T^{out} steady-state gain

We report here physical observations that suggest to write the steady-state gain of the DOC as the gain of an adiabatic reactor.

Main factor: gas flow rate For a given HC flow rate u, the output temperature T^{out} rise is strongly related to the gas flow rate F. In Fig. 3.3, the steady-state gain (i.e. the ratio of T^{out} rise to corresponding u variation) is reported. This figure shows a close to hyperbolic relationship of this ratio on the gas flow rate. Equivalently, one can consider that the inlet-to-outlet temperature difference is proportional to the inlet concentration (ratio of HC mass flow rate to gas mass flow rate). This point is supported by the data obtained with the gas analyzers that are reported in Fig. 3.4[1].

In more details, temperature rise is also impacted by the conversion efficiency, i.e. only the fraction of reductants that are actually oxidized in the catalyst contribute the temperature rise. As presented in Fig. 3.5, the conversion efficiency η mostly depends on the gas flow rate (or gas speed). At low gas flow rates, the efficiency is very high. It continuously decreases when gas flow rate increases. This can be easily taken into account by a look-up table.

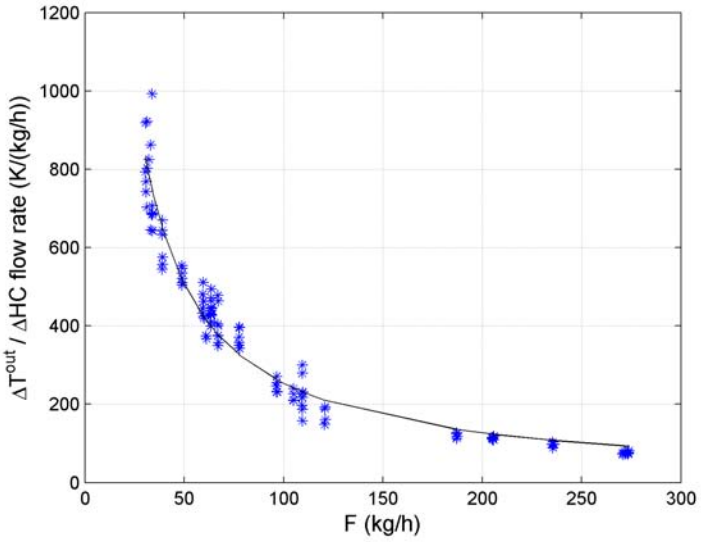

Figure 3.3: Steady-state gain versus gas flow rate F. Inlet temperature remains constant during HC flow rate variations. Experimental data.

[1] Disturbance reductants are accounted for in this figure

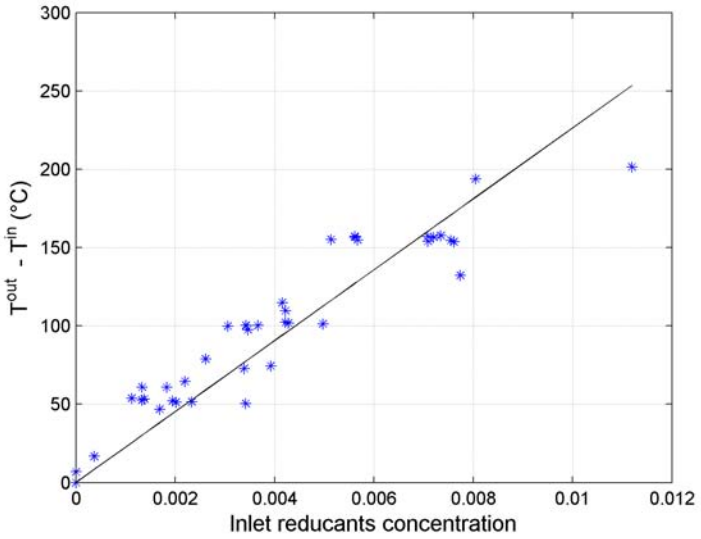

Figure 3.4: Inlet-to-outlet temperature rise versus inlet reductants concentration. Experimental data.

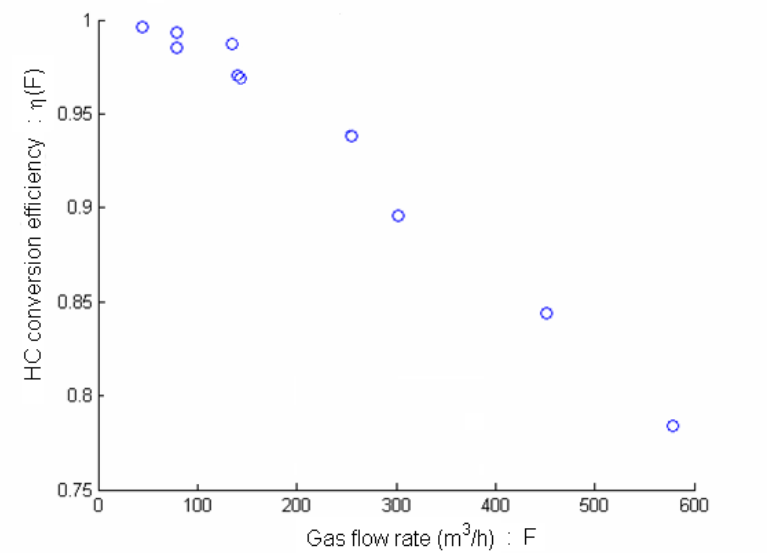

Figure 3.5: DOC conversion efficiency η versus gas volume flow rate. Experimental data.

About inlet reductants flow rate and inlet temperature To be consistent with real world regeneration scenarios of DOC usage, most of the results in the thesis are obtained at high temperatures and under lean conditions (i.e. in excess of oxygen). Under these conditions, oxidation reactions are fast. This corresponds to normal conditions for DPF regeneration. Absolute values of reductants flow rate (including u, other reductants are accounted for in Appendix A) and absolute inlet temperature are neglected in the steady-state gain considerations. The gain can be, as illustrated in Fig. 3.3, considered to be a function of the gas flow rate only.

About heat losses Because of the DOC geometry (it consists of a large number of channels), the adiabatic assumption for channels near the center line is common and relevant (see references in Chapter (2)). In Fig. 3.6, outlet-to-inlet temperature difference is compared to adiabatic theoretical value recalculated from gas analyses measurements for various gas flow rate, inlet temperature, and HC flow rate conditions. It is shown that DOC inlet-to-outlet thermal losses (in the flow center line) are almost independent of the operating point. In an attempt to model heat losses, the temperature difference between DOC and ambient would be the first factor of influence. During the regeneration process, because the outlet temperature is globally constant, this factor has a small impact. In embedded applications, heat losses may vary to some extent. They can be impacted by the ambient temperature, and the vehicle speed. However, it is assumed that they vary slowly enough so that they can be compensated by integral effects in the control law. Hence, this phenomenon will not be accounted for in our modeling.

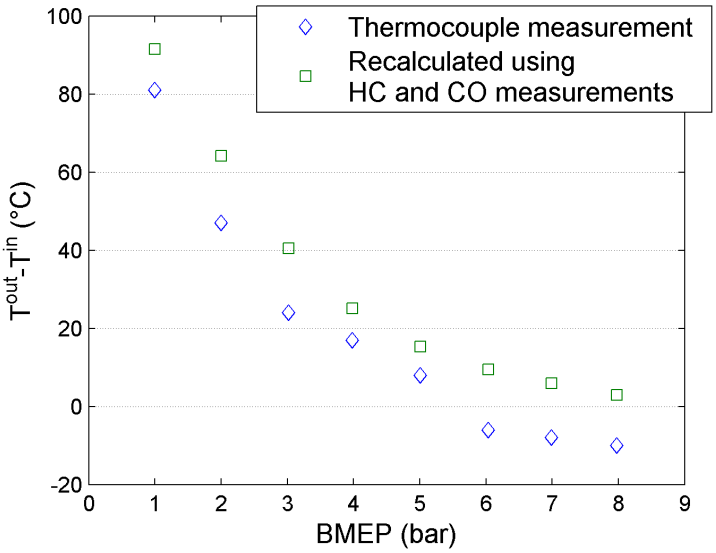

Figure 3.6: Outlet-to-inlet temperature difference in DOC from temperature sensors measurement compared against iso-thermal computation from gas analyzer measurement at various engine operating points (engine speed of 1500 rpm). Heat losses are independent of the operating point. Experimental data.

Steady-state gain Consider the DOC as an adiabatic system. Steady-state energy balance for the system is commonly written as (according to the previously defined notations)

$$F\ Cp\ T^{in} - F\ Cp\ T^{out} + \eta\ \Delta H_u\ u = 0 \tag{3.1}$$

where ΔH_u is the heat of combustion of the control HC. We get

$$T^{out} - T^{in} = \frac{\eta \, \Delta H_u}{F \, Cp} \, u \tag{3.2}$$

From this, inlet-to-outlet temperature rise varies as an hyperbolic function of the gas flow (scaled by η). From another viewpoint, temperature rise is simply proportional to the HC inlet concentration $C_u = u/F$ (scaled by η).

$$T^{out} - T^{in} = \eta \, \frac{\Delta H_u}{Cp} \, C_u$$

These results are in accordance with the previous experimental observations. From (3.2), the steady-state influence of control HC to outlet temperature can be easily determined. The steady state gain of the transfer function from the control HC flow rate to the outlet temperature is given by

$$G_u = \eta \frac{\Delta H_u}{F \, Cp} \tag{3.3}$$

3.1.1.2 T^{in}-to-T^{out} steady-state gain

According to previous conclusions about heat losses, the inlet-to-outlet temperature steady-state gain of the considered adiabatic system is equal to 1. We note

$$G_{T^{in}} = 1$$

3.1.2 Dynamic responses

We now briefly describe the dynamic effects that we wish our model to capture. These are: response under constant gas speed, and the (counter-intuitive) response to variation of gas speed. Eventually a model is proposed in § 3.2.

3.1.2.1 Outlet temperature response to control HC (u) and inlet temperature (T^{in}) at constant gas speed (v)

Temperature response to control HC (u) A main requirement for our modeling is to describe the dynamic response to control HC flow rate, which is the control variable. In Fig. 3.7, an example of experimental HC step responses is given for two different gas flow rates. One can see that response times and overall response shapes are significantly different between the two cases.

Temperature response to inlet temperature (T^{in}) Considering the experimental device presented in Appendix F, it is difficult to experimentally isolate the influence of inlet temperature variations from variations of the other disturbances. However, it can be observed that responses to inlet temperature are highly-delayed and highly-variable, in a similar way as responses to control HC.

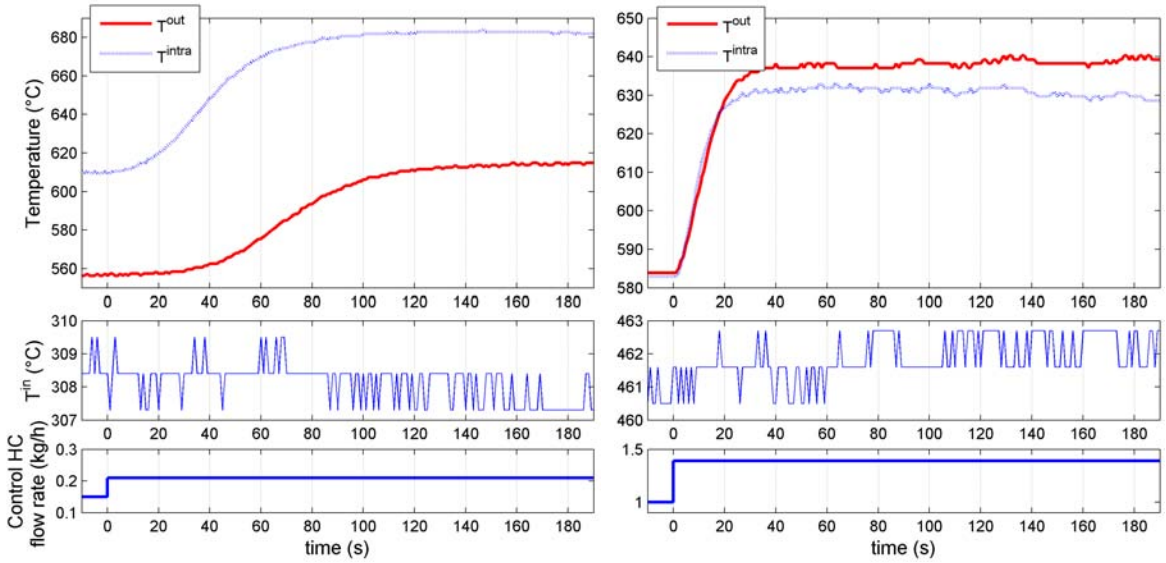

Figure 3.7: 3-inch long DOC thermal response to a step increase (at $t = 0$) in the control variable. Response times strongly depend on the gas flow rate (gas flow rate of 32 kg/h (left) vs. 190 kg/h (right)). Inlet temperature is kept constant during the tests. Experimental data.

3.1.2.2 Effects of gas speed variations (v) on the DOC outlet temperature ("overshoot and undershoot" phenomena)

Again, in view of the experimental device considered in this thesis, gas flow variations cannot be generated independently of inlet temperature variations, nor of the engine disturbance reductants (see Appendix A for more details). However, this does not prevent us from investigating the phenomena involved in the DOC during gas flow rate variations.

It can be noticed in Fig. 3.8 that a fall in the gas flow rate (it is illustrated in Fig. 3.5 that this fall is associated to an increase of conversion efficiency) together with an increase in HC concentration upstream of the DOC imply an increase in the intra-catalyst temperature. Despite this increase, the outlet temperature undershoots during a transient phase (see Fig. 3.8).

By contrast, an increase in gas flow rate (associated with a fall in efficiency) together with a fall in HC concentration imply a fall in intra-catalyst temperature. Despite this decrease, the outlet temperature is overshooting during a transient phase (see again Fig. 3.8).

Experimental results show that these two phenomena appear irrespective of whether the inlet temperature is rising or falling[2]. This is not surprising: because of the one-dimensional distributed state nature discussed in § 1.5, there is no direct transfer from the inlet temperature to the outlet temperature[3].

[2] See Fig. 5.6 for an example of a rising inlet temperature while the outlet temperature is undershooting.
[3] More details about inlet temperature response are given in § 3.5.1.

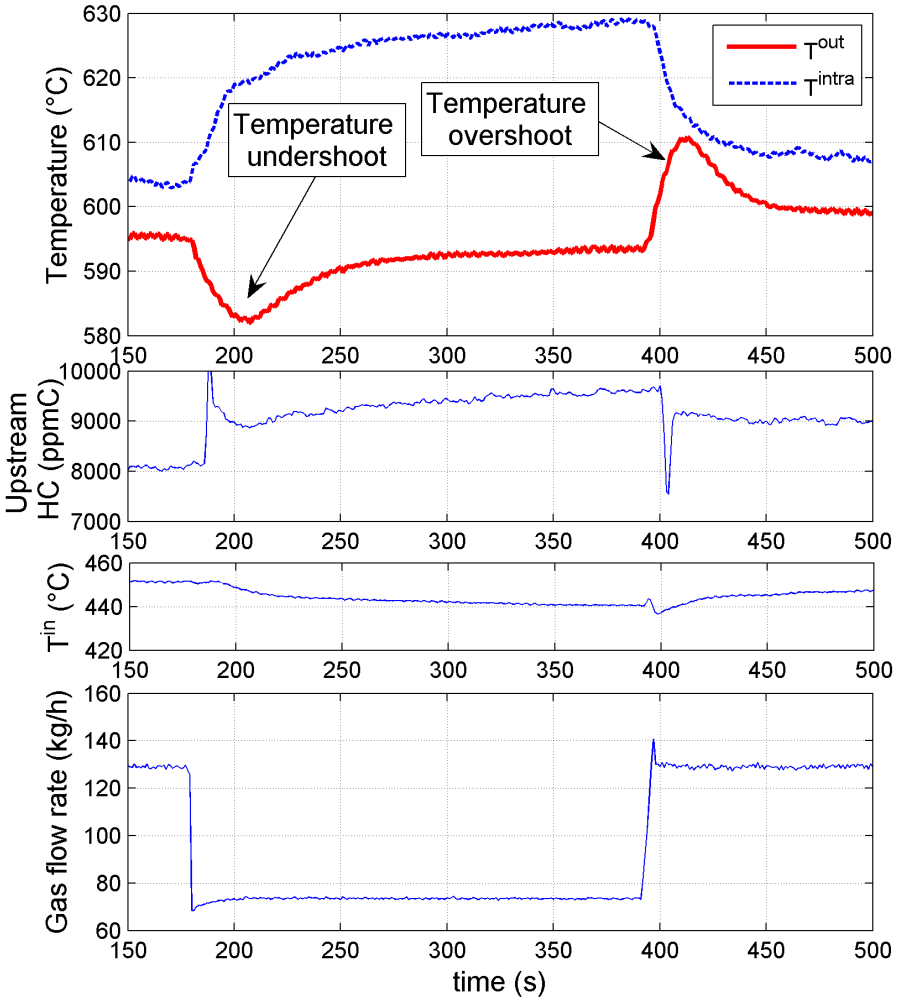

Figure 3.8: DOC outlet temperature undergoes counter-intuitive evolutions related to gas flow rate variations. Experimental data.

3.2 Proposed reduced model

In this section, an overview of the proposed reduced model, as well as its main properties, is given. Experimental validation results will be presented in § 3.3. Assumptions and justifications leading to the presented reduced model will be detailed in § 3.4.

The proposed reduced model is given by

$$\left\{\begin{array}{rcl} \dfrac{\partial T}{\partial t}(z,t) & + & v(t)\dfrac{\partial T}{\partial z}(z,t) = -k_1\left(T(z,t) - T_s(z,t)\right) \\ \dfrac{\partial T_s}{\partial t}(z,t) & = & k_2\left(T(z,t) - T_s(z,t)\right) + \Psi(z,u(t),v(t)) \end{array}\right. \tag{3.4}$$

where

- T is the gas temperature
- T_s is the solid phase temperature
- $T^{out}(t) \triangleq T(L,t)$ is the system output (outlet gas temperature) where L is the length of the DOC
- $T^{in}(t) \triangleq T(0,t)$ is a system disturbance (inlet gas temperature)
- v is a system disturbance (speed of the gas flowing through the DOC)
- Ψ is a distributed input variable related to the control variable u (called "source" term)
- k_1 and k_2 are constant parameters

Ψ is a distributed source term constant over some spatial interval

$$\left\{\begin{array}{ll} \Psi(z,u,v) = \psi(u,v), & 0 \leq z \leq L_c(v) \\ \Psi(z,u,v) = 0, & L_c(v) < z \leq L \end{array}\right. \tag{3.5}$$

where L_c is a piecewise affine function of the channel gas speed v,

$$L_c(v) = \min(L, \quad a \cdot v + b) \tag{3.6}$$

a and b being two positive constants. The source term ψ is depending on the length L_c, and the control HC flow rate u by the following relation

$$\psi(u,v) = \frac{1}{L_c(v)}\, G_u(v)\, \frac{k_2\, v}{k_1}\, u \tag{3.7}$$

Comments on the model

The model (3.4) is a linear infinite-dimensional (distributed parameter) model with distributed control (3.5) acting homogenously on a reduced spatial domain defined by (3.6) by the disturbance variable v. The gain of the control u is defined by the static model determined earlier in § 3.1.1 and expressed in (3.7). The model has been obtained by keeping the energy balances (2.2) and (2.3) of the detailed model, where the conduction effects have been neglected, and where the source term gathers the distributed reaction enthalpy presented above. Precisely, $\Psi(z,u,v)$ includes the sum of the enthalpies of the various reactions taking place inside the DOC. L_c is the length of the portion of the DOC where the heat is released (reactive length) as is pictured in Fig. 3.9.

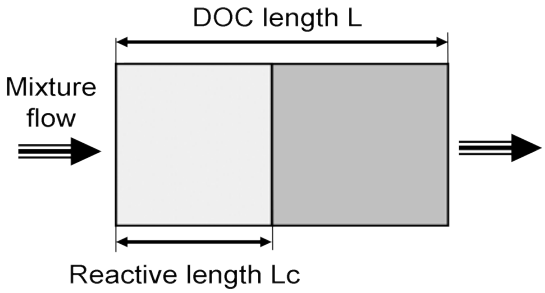

Figure 3.9: Reduced model reactive zone. Reductants are oxidized uniformly on the upstream part of the DOC.

About calibration Gas speed v can be easily computed using air flow rate measurements (see later (3.18)). The set of parameters (k_1, k_2) can either be deduced from (3.18) and from usual correlations (given for example in Osizik (1977)), or identified from experimental variations of the inlet temperature (an example is given in § 3.3.3). On the other hand, L_c can be readily identified from experimental HC step responses. However, it is not used directly in the controller, and the calibration is performed by another variable (see Chapter 7).

Considering temperature variations To study the proposed *linear* model (3.4)-(3.5)-(3.6)-(3.7), it can be assumed that the reactor is initially at steady state, i.e. $T(z,0)$ and $T_s(z,0)$ are equal and constant. It is then correct to assume that T and T_s represent the variations of temperature about steady state instead of the (absolute) temperatures themselves. Therefore, from now on, the initial conditions are

$$\begin{cases} T(z,0) = 0 \\ T_s(z,0) = 0. \end{cases} \tag{3.8}$$

3.3 Experimental validation

In this part, the reduced model is experimentally validated in terms of dynamic response to HC (input u) in § 3.3.1, under variable gas speed v conditions in § 3.3.2, and in terms of dynamic response to inlet temperature T^{in} (disturbance) in § 3.3.3.

3.3.1 Experimental validation by HC step responses at constant gas speed

In this part, to validate the previously proposed reduced model, we focus on the temperature response to control HC variation u. Detailed calculations yielding the following results can be found in Appendix E.1.

Transfer function Consider a step input of magnitude α, i.e.

$$\psi(u(t), v) = \alpha\, \Upsilon(t), \tag{3.9}$$

where Υ is the Heaviside function. In the Laplace domain, the response of the T variables to this input signal is

$$\hat{T}(z,s) = \hat{T}^{in} \exp\left(-\hat{A}z\right) - \frac{\hat{B}}{\hat{A}} \exp\left(-\hat{A}z\right) + \frac{\hat{B}}{\hat{A}} \exp\left(-\hat{A}(z - L_c)\right) \tag{3.10}$$

where

$$\begin{cases} \hat{A}(s) = \dfrac{1}{v}\left(s + k_1 - \dfrac{k_1 k_2}{s + k_2}\right) \\ \hat{B}(s) = \dfrac{k_1}{v}\dfrac{\alpha}{s(s + k_2)} \end{cases} \tag{3.11}$$

and where s is the Laplace variable, $\hat{x}$ is the Laplace transform of x (for every function $t \mapsto x(t)$).

Steady-state value The steady-state value of the temperature can be computed using (3.10), for every value of z. It is given by

$$\lim_{t\to\infty} T(z,t) = \overline{T^{in}} + \frac{k_1 \alpha L_c}{k_2 v} \tag{3.12}$$

where $\overline{T^{in}}$ is the steady-state inlet temperature value. In particular, when $\overline{T^{in}} = 0$, one has

$$\lim_{t\to\infty} T(z,t) = \frac{k_1 \alpha L_c}{k_2 v} \tag{3.13}$$

Variables α, L_c and G_u are related through by (3.7)

$$\alpha\, L_c = G_u\, \frac{k_2\, v}{k_1}\, u \tag{3.14}$$

HC step response In the time domain, the response to step input (3.9) is given by the inverse Laplace transform of (3.10)

$$\begin{aligned} T_h(z,t) &= \Upsilon\,(t - z/v) \exp\left(-\frac{k_1 z}{v}\right) M(z, t - z/v) \\ &- \Upsilon\,(t - z/v) \exp\left(-\frac{k_1 z}{v}\right) N(z, t - z/v) \\ &+ \Upsilon\,(t - z/v) \exp\left(-\frac{k_1 z}{v}\right) N(z - L_c, t - z/v) \end{aligned} \tag{3.15}$$

where

$$\begin{cases} M(z,t) &= T^{in}(t) + \displaystyle\int_0^t \exp\left(-k_2\tau\right)\sqrt{\frac{m(z)}{\tau}}\mathrm{I}_1(2\sqrt{m(z)\tau})T^{in}(t-\tau)d\tau \\ N(z,t) &= g(t) + \displaystyle\int_0^t \exp\left(-k_2\tau\right)\sqrt{\frac{m(z)}{\tau}}\mathrm{I}_1(2\sqrt{m(z)\tau})g(t-\tau)d\tau \\ g(t) &= \dfrac{k_1\alpha}{k_1+k_2}t - \dfrac{k_1\alpha}{(k_1+k_2)^2}\left(1 - \exp\left(-(k_1+k_2)t\right)\right) \\ m(z) &= k_1 k_2 z/v \end{cases}$$

with I_1 the modified Bessel function of the first kind (see Abramowitz & Stegun (1965)).

Experimental validation In Fig. 3.10, we present experimental HC step responses obtained under various operating conditions. Gas speed v remains constant during each of these tests, as well as the inlet temperature. It is shown that the analytic formula (3.15) fits experimental data well.

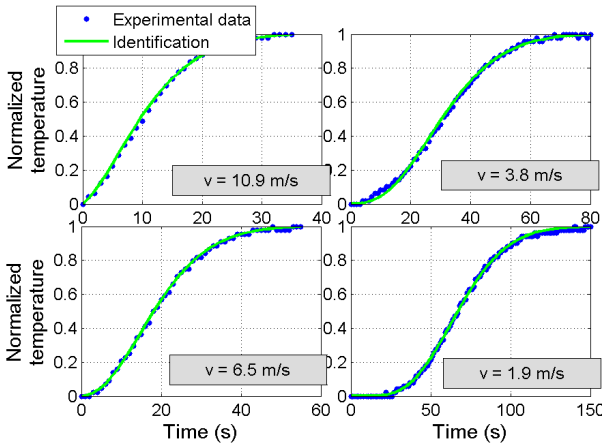

Figure 3.10: Experimental HC step response u in various operating conditions and at steady gas flow rate.

3.3.2 Experimental validation under variable gas speed conditions

In the proposed model, oxidation reactions starts at the DOC inlet. The value of the reactive length L_c depends on the gas speed v through (3.6). We wish to investigate the relevance of this assumption. The model is compared against experimental data in Fig. 3.11. Physical measurements (gas flow rate, inlet temperature, inlet HC[4]), related to the model inputs, are also plotted. It appears that the temperature variations are well represented by our model. In particular, the phenomena of "overshoot" and "undershoot" related to the gas flow rate increase at $t = 90$ s, and, decrease at $t = 275$ s are well reproduced. For comparisons, the simulation results in the case of a constant reactive length are also plotted. Clearly, the proposed model of varying reactive length (3.6) outperforms it. This stresses that relating the reactive length to the gas flow rate is a solution to reproduce the observed counter-intuitive overshoot and undershoot phenomena.

[4]Disturbance reductants are accounted for in this experiment.

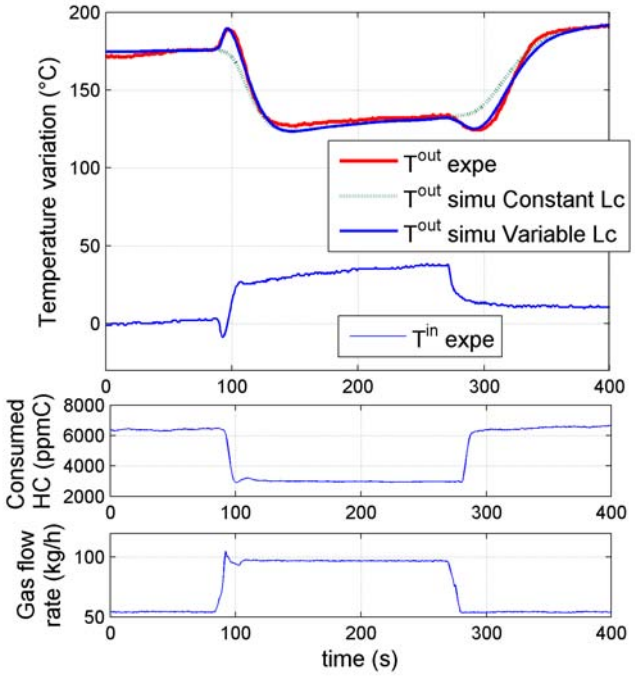

Figure 3.11: Model validation under variable gas flow conditions. Accounting for variable reactive length L_c reproduces the inverse response experimentally observed. The label "Temperature variations" refers to variations about a reference value (approximately 450°C for the experimental data).

3.3.3 Experimental validation by large inlet temperature variations

On the experimental setup considered in this thesis (see Appendix F), it is not possible to generate inlet temperature variations totally independently from other disturbances (gas flow rate, inlet HC[5]). Nevertheless, we present in Fig. 3.12 an experiment in which the catalyst undergoes mostly T^{in} variations.

In this experiment, the engine is initially working under low gas flow rate conditions, the temperature responses are slow, and, there exists a HC flow at the catalyst inlet due to engine partial combustion (see Appendix A). Then, the engine injection system is switched off. This makes the DOC inlet temperature plummet. Gas flow rate remains roughly constant, because an electric motor drives the engine at a constant speed. Injection cut-off (at $t \approx 500$ s) implies a HC variation. This impacts on the beginning of the response. Additionally to this variation, T^{in} is varying over a long period, such that, from $t \approx 600$ s, it can be assumed that outlet temperature variation is the consequence of T^{in} variation only. Interestingly, the response is well-represented by our model over the whole time range.

Moreover, in this test, the temperature variation range is large, and, interestingly, accuracy of the results stresses the validity of linearity assumption.

[5]Disturbance reductants are accounted for in this experiment (see Appendix A).

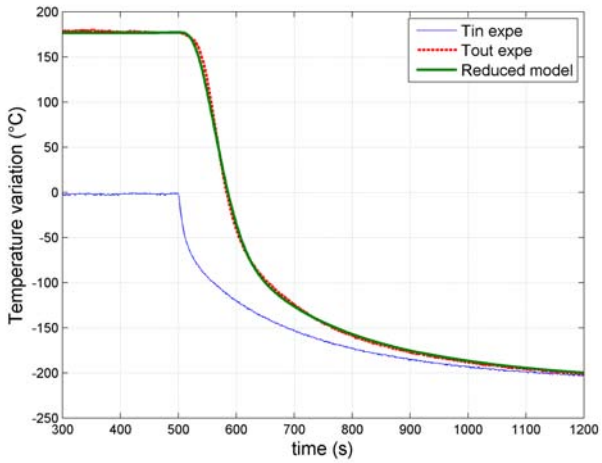

Figure 3.12: In this experiment, gas flow rate remains constant and response to inlet temperature variations is stressed. Experimental and simulation data.

3.4 Model assumptions & justifications

As discussed in Chapter 2, numerous models have been used and improved since the 1960s for oxidation catalysts. Following Depcik & Assanis (2005), several key simplifying assumptions are usually considered. As seen in Chapter 2, the channels are in large number and they are all similar. This geometry allows only one "average" channel to be considered in the modeling. It is supposed to represent them all. Further, because of its geometry, the DOC is thermally isolated and heat losses to the surroundings can be neglected. Axial diffusion in the fluid phase is negligible since the Peclet number (Osizik 1977) is large (Pe>50) while the axial conduction in the solid is not important[6]. Except under very high flow rate conditions, the entry length is a small fraction of the converter length. As a result, the Nusselt and Sherwood numbers (Osizik 1977) can be assumed equal to the fully-developed flow constant values. Neglecting dependencies corresponding to the previous assumptions, the following equations can be written from gas and solid energy balances (2.2) and (2.3)

$$\varepsilon\rho_g Cp\frac{\partial T}{\partial t}(z,t)+\frac{F(t)}{A_{cell}}Cp\frac{\partial T}{\partial z}(z,t)=-h_g G_a\left(T(z,t)-T_s(z,t)\right) \tag{3.16}$$

$$(1-\varepsilon)\rho_s Cp_s\frac{\partial T_s}{\partial t}(z,t)=h_g G_a\left(T(z,t)-T_s(z,t)\right)+G_{ca}\sum_{j=1}^{NM}R_j(t)\cdot h_j \tag{3.17}$$

[6]Authors of first catalyst models ((Vardi & Biller 1968), (Kuo et al. 1971), (Harned 1972), (Young & Finlayson 1974)) do not include axial diffusion in their calculation. However it is found that accurate results can be achieved. It has been first stated by Oh & Cavendish (1982) that conduction should be included in the calculations to properly model temperature propagation in the direction opposite to gas flow during light-off phase. Our model is dedicated to temperatures higher than light-off temperature. In these conditions, the "backward" propagation is no longer dominating. Moreover, our modeling aims at being used for control design. Diffusion phenomenon actually helps temperature control, because its tends to "smooth" temperature peaks. Then, as demonstrated in this thesis, even if diffusion is underestimated in the modeling, control strategies remain valid. We remark that neglecting solid diffusion does not mean that there is no global diffusion. Global diffusion is due to gas and solid exchanges as explained in § 4.2. Also, attention must be paid to numerical scheme used to solve 1D equations, as it has a strong influence on numerical diffusion effects.

Rewriting (3.16) and (3.17) with the following normalizing parameters

$$\begin{cases} k_1 & = & \dfrac{h_g G_a}{\varepsilon \rho_g C p} \\ k_2 & = & \dfrac{h_g G_a}{(1-\varepsilon)\rho_s C p_s} \\ v & = & \dfrac{F}{\varepsilon \rho_g A_{cell}} \\ \Psi(z,t) & = & \dfrac{G_{ca}}{(1-\varepsilon)\rho_s C p_s} \displaystyle\sum_{j=1}^{NM} R_j\left(z,t,T_s(z)\right) \cdot h_j\left(z,t,T_s(z)\right) \end{cases} \tag{3.18}$$

we get

$$\begin{cases} \dfrac{\partial T}{\partial t}(z,t) & + & v(t)\dfrac{\partial T}{\partial z}(z,t) = -k_1\left(T(z,t) - T_s(z,t)\right) \\ \dfrac{\partial T_s}{\partial t}(z,t) & = & k_2\left(T(z,t) - T_s(z,t)\right) + \Psi(z,t) \end{cases} \tag{3.19}$$

In the full-order modeling, the source term is determined by species balances (2.4) and (2.5). This approach requires the determination of chemical coefficients depending on the catalyst and on the fuel speciation. Referring to Benjamin & Roberts (2004), this approach leads to results that are significantly dependent on the catalyst formulation. As a result, most authors perform careful calibration of their kinetic constants. In practice, adjusting these coefficients is a tedious and difficult task requiring thorough experimental analyses and time-consuming optimization procedures. Hence, our viewpoint is to transfer this calibration effort to a simpler macroscopic source term. In the following, assumptions are made to reduce the source term calibration effort to its minimum.

3.4.1 Hypothesis underlying the definition of the "source" term

A main feature of the proposed model is that it involves a single but (uniformly) distributed source term to represent the effects of the chemical reactions. We now comment on this.

Encompassing exothermic reactions in a single source term During the regeneration process, the DOC is used at high temperatures, which ensures that the rate of conversion of reductants is high. Moreover, a large quantity of HC is injected to generate exothermicity. Consequently, the effect of these reductants is dominating over other species'. For this reason, we have proposed to encompass all the chemical reactions in a distributed "source term Ψ".

Accounting for disturbance reductants flow separately In a strict approach, the total reductants flow rate at the catalyst inlet is split into the control HC mass flow rate u and the "disturbance" reductants flow rate F_{dis} resulting from in-cylinder incomplete combustion and modifying undesirably the DOC inlet reductants flow rate. For sake of simplicity, the source term describes only the effects of u. Because of the linearity of model (3.4) with respect to Ψ, the same approach can be used for F_{dis}. It will be seen in Appendix A how, in an accurate description, F_{dis} can be taken into account in the model and the control laws.

Temperature independence As explained above, the catalyst is used at a temperature significantly higher than the light-off temperature. Experimental HC step responses are not really impacted by the temperature level. Implicitly, we consider that the inlet temperature does not influence the source term. Hence, $\Psi(z,t)$ is not a function of T_s.

Decoupling chemical and thermal dynamics By construction, a DOC is designed to yield large heat and mass transfer. These transfers are very effective, and the time scales implying the thermal phenomena are much higher than the ones implying chemical reactions. For the experiments presented in this thesis, gas residence time (typically a fraction of a second) is approximately 1000 times smaller than the outlet temperature response time. Because there is no HC storage effect at high temperature, and because experiments show high conversion rates, time constants of chemical reactions are at least one order of magnitude lower than thermal time constants. Hence, for a thermal model, chemical reactions establish very rapidly to the steady-state value of $\Psi(z, v(t), u(t))$. In other words, $\Psi(z, v(t), u(t))$ is not explicitly a function of t. This is why the source term Ψ, and in particular the reactive length L_c (see below § 3.4.2), is studied under steady-state conditions of v.

Uniform profile of $\Psi(z, v(t), u(t))$ As mentioned above, the temperature does not influence the chemical reaction process much, and because thermal and chemical dynamics have been decoupled, it can be assumed that, for a given value of $(v(t), u(t))$, a z-profile of Ψ can be considered. The uniform profile is presented here.

The heat transfer between the monolith and the gas is very efficient. Further, the conversion rate is high. This suggests that it can also be true for the mass transfer. The configuration of the monolith plays a particular role here. We assume that the rate of reaction is, at first order, *independent of the species concentration*. Formally, considering (2.4) and (2.5) with a constant rate of reaction over the DOC, the HC concentration profile decreases linearly until the zero concentration is reached, and the consumption profile is constant. Then, the heat release and therefore the source term Ψ are constant over the reactive spatial interval which is defined as the zone of non-zero concentration. Then, the following discontinuous function is considered

$$\begin{cases} \Psi(z, u(t), v(t)) = \psi\left(u(t), v(t)\right), & 0 \leq z \leq L_c(v(t)) \\ \Psi(z, u(t), v(t)) = 0, & L_c(v(t)) < z \leq L \end{cases} \tag{3.20}$$

Remark. In these conditions, consider a flow rate u_1 of control HC ($u = u_1$), reacting over the length L_c. The HC concentration decays linearly upon z and reaches zero at $z = L_c$. The value of Ψ is uniform over the length L_c and zero over the remaining length. Now, if the inlet HC flow rate is doubled ($u_2 = 2 \cdot u_1$), then the HC concentration decays linearly upon z (more rapidly than in the latter case), and reaches zero at $z = L_c$. Ψ is again uniform over L_c but higher than in the latter case (see (3.7)). This is illustrated in Fig. 3.13. Assuming that the reactive length is independent of the inlet HC concentration obviously has some limitations. In particular, this assumption is wrong when high concentrations of HC are reached. This phenomenon is well illustrated by the second part of § 5.2.2, and explained in particular in Fig. 5.8. However, we consider that, in normal cases, the reactive length is independent of the inlet concentration. On the contrary, considering that the reactive length depends, at first order, on the concentration would lead to significantly different response times for different inlet concentrations, which has not been observed in our experiments. Finally, it is important to note that a uniform profile of Ψ has been considered because it is the simplest form that describes experimental data well. The detailed description of the profile is not primordial here, because, in Chapter 4, the data are re-identified to another model.

In (3.20), the source term ψ is related to the length L_c, the gain G_u, and u the amount of control HC. We now detail this. Consider the system (3.4) under quasi-steady-state conditions

$$\begin{cases} v(t)\dfrac{\partial T}{\partial z}(z,t) &= -k_1\left(T(z,t) - T_s(z,t)\right) \\ 0 &= k_2\left(T(z,t) - T_s(z,t)\right) + \Psi(z, u(t), v(t)) \end{cases}$$

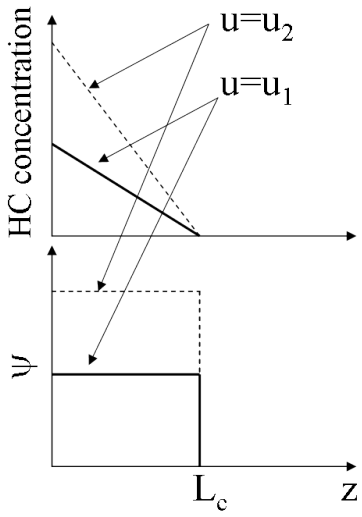

Figure 3.13: Schematic evolution of source term Ψ for different inlet HC concentrations and at constant gas flow rate v.

These equations lead to

$$\frac{\partial T}{\partial z}(z,t) = \frac{k_1}{k_2\, v}\Psi(z, u(t), v(t))$$

or, equivalently,

$$T(z,t) = \frac{k_1}{k_2\, v}\int_0^L \Psi(z, u(t), v(t))\, dz + K$$

where K is a constant. Boundary condition $T(0) = T^{in}$ yields, after an evaluation of the above integral

$$T - T^{in} = \frac{k_1}{k_2\, v}\, \psi\, L_c$$

Further, by invoking the steady-state gain G_u from § 3.1.1 we simply identify the following relation (3.7) (provided that T^{in} is constant)

$$\psi(u,v) = \frac{1}{L_c(v)}\, G_u(v)\, \frac{k_2\, v}{k_1}\, u$$

Finally, the dependence of L_c on $v(t)$ is detailed below in § 3.4.2. As a summary, for a given $v(t)$, the control $u(t)$ determines the input $\Psi(z, v(t), u(t))$ through the equation above and (3.20).

Other profiles of $\Psi(z, v(t), u(t))$ Additionally to the uniform profile, other profiles of Ψ have been considered (e.g. exponentially decaying, linearly decaying, freely optimized). They were tested through identification to experimental results. These possible candidates are presented in Appendix E.1. They do not improve the results of the uniform profile, and are therefore left unused in the following. More details about the process that have led us to select a uniform profile of Ψ rather than other profiles can be found in Appendix E.1.5.

3.4.2 Accounting for variable v: modeling of the reactive length L_c

It has been explained in § 3.4.1 that, in the proposed model, the chemical phenomena are encompassed in a simple source term distributed over a reactive zone. Now, we detail the nature of the

reactive zone which length is L_c. In § 3.4.2.1, the existence of the moving reactive zone is stressed, and in § 3.4.2.2 the parameter L_c is constrained to minimize the calibration effort and to respect our modeling objectives.

3.4.2.1 Moving reactive zone

Experimental data presented in Fig. 3.14 show that there exists a reactive zone moving inside the DOC. The outlet temperature roughly remains constant while the gas flow rate F (v is related to

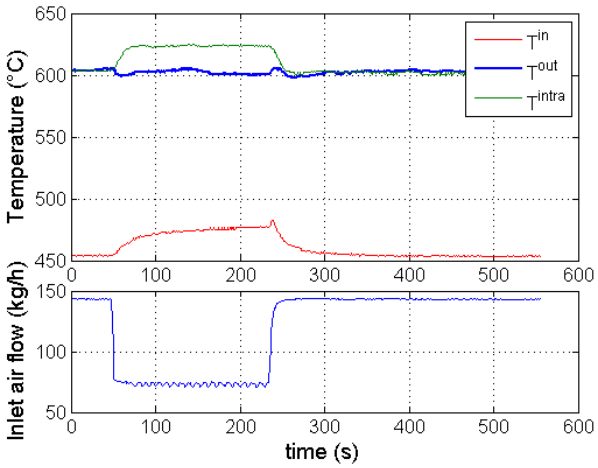

Figure 3.14: Variations of T^{intra} with gas flow while T^{out} remains constant is interpreted as a displacement of reactive zone. Experimental data.

F) is switched between 140 kg/h and 70 kg/h (u is adapted accordingly). At 140 kg/h, the inlet-to-outlet temperature difference is about 150°C; at 70 kg/h, it is about 125°C. Hence, in the second case, the inlet HC concentration (related to inlet-to-outlet temperature difference) is lower than in the first case. Smaller exotherm is generated in the second case. However, the intra-catalyst temperature is significantly higher in the second case than in the first one. This is because, in the second case, the reactive zone is smaller than in the first one (as pictured in Fig. 3.2 intra-catalyst temperature T^{intra} is measured at half the catalyst length). Then, the monolith temperature in the middle of the catalyst length is higher. This proves that the spatial distribution of the reaction has changed as v has.

Another way to stress the displacement of this reactive zone is to analyze the steady-state $T^{intra} - T^{out}$ difference for an increasing inlet HC concentration. It is shown in Fig. 3.15, that, at low gas flow rate, an increase in the inlet concentration implies an increase in the $T^{intra} - T^{out}$ difference. In other words, T^{intra} grows more rapidly than T^{out} does. This is because the reactive zone is small. Then, the vast majority of HC is oxidized upstream of the intra-catalyst temperature sensor.

On the contrary, under high gas flow rate conditions, an increase in the inlet concentration implies a decrease in the $T^{intra} - T^{out}$ difference. In other words, T^{out} grows more rapidly than T^{intra} does. Increasing the inlet concentration influences T^{out} more than it influences T^{intra}. This is because the reactive zone is longer. Then, a larger part of HC is oxidized downstream of the intra-catalyst temperature sensor.

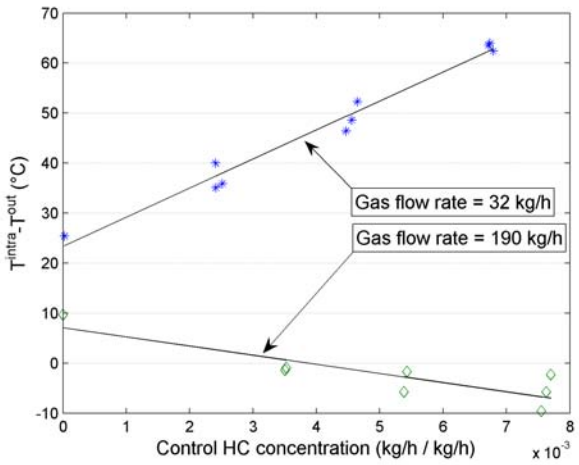

Figure 3.15: $T^{intra} - T^{out}$ versus concentration of control HC (exhaust injection in this case) for two different engine operating points. At low gas flow rate (up), the $T^{intra} - T^{out}$ difference increases when HC concentration increases. At high gas flow rate (down) trend is opposite. It shows that the length of reactive zone increases with gas flow rate. Experimental data.

3.4.2.2 Model description with variable reactive length

It has been considered previously that catalytic HC combustion takes place in the upstream zone of the DOC. The length L_c of this zone has not been specified. In fact, it depends on the nature of the catalyst and it is a priori unknown. Further, for a given catalyst, this length also depends on the operating point (as is evidenced in § 3.4.2.1). In this section, consequences of a change in the reactive length are detailed and a simple model to define L_c corresponding to experimental observations is proposed.

From our macroscopic viewpoint, we assume that heat is homogeneously released along the reactive length, and is zero on the downstream non-reactive length. Now, consider an increase in the reactive length as pictured in Fig. 3.16. During this transient, a part of the formerly non-reactive zone

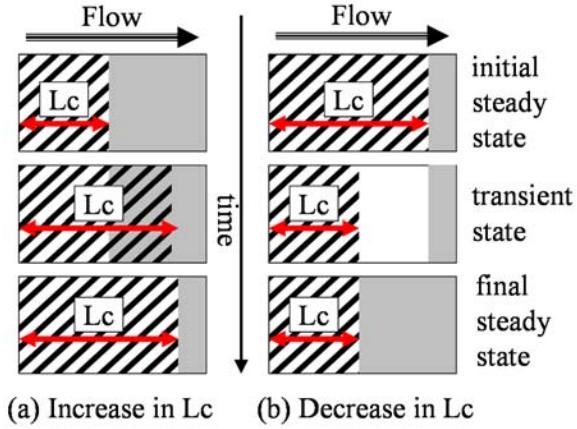

Figure 3.16: Simplistic scheme of phenomena involved during a variation of reactive length. In transient state, a zone is overheated (increase in L_c) or underheated (decrease in L_c).

is covered by the reactive zone, where HC heat is now released. Then, the new heat supply in this

covered zone is more than required by the final steady-state conditions, because it has already stored energy during the initial steady-state conditions. The heat propagates mostly in the flow direction and causes an outlet temperature increase until the final steady state is reached. Now, consider a decrease in the reactive length: there exists a zone which is not supplied with heat during the transient. This causes an outlet temperature decrease until steady state is reached. Contrary to the highly-delayed inlet temperature effects, the described phenomena are almost synchronous to the gas flow variations because they take place in the vicinity of the outlet of the DOC.

This approach is in accordance with preliminary observations of § 3.1.2.2. To take them into account, we propose here to detail the dependency of the reactive length L_c of model (3.4) upon gas flow rate. Residence time of reductants in the monolith determines how they reach the catalytic surface. As a first approximation, L_c is considered to be a piecewise affine function of the channel gas speed v,

$$L_c(v) = \min(a \cdot v + b, \quad L) \tag{3.21}$$

where a and b are positive constants, and L is the DOC length. This assumption is corroborated by identification results of L_c, obtained in § 3.3.1. Further, this model description is validated experimentally in § 3.3.2.

Remark. This proposed description is useful to simply describe the DOC behavior under normal DPF regeneration conditions. In fact, when the HC flow rate is high, a large HC fraction slips to the outlet, and, in this case, the length L_c is not a function of the gas speed only. However, these extreme special conditions should not happen in practice.

3.5 Disturbance rejection possibilities

In this section, compensation possibilities for inlet temperature and gas flow rate disturbances are explored. Further, disturbance reductants compensation is detailed in Appendix A.

3.5.1 Rejection possibilities of the inlet temperature disturbance

Inlet temperature variations T^{in} are a disturbance. In order to study possibilities to reject them, it is insightful to compare the T^{in} step response and the HC (input u) step response that we have already computed in Eq. (3.15). Experimental results reported in § 3.3, have shown that analytic formulas derived from model (3.4) are quite accurate regarding the T^{in} and HC flow rate inputs. In particular, the model (3.4) yields the T^{in} step response (see Appendix E.1.3 for calculation details), for $z = L$, as

$$T_h(z,t) = \Upsilon(t - \frac{z}{v}) \exp\left(-\frac{k_1 z}{v}\right) \times \left[1 + \int_0^{t-z/v} \exp\left(-k_2\tau\right) \sqrt{\frac{m(z)}{\tau}} \mathrm{I}_1(2\sqrt{m(z)\tau}) d\tau\right] \tag{3.22}$$

For efficient numeric evaluation of the above expression, the following (exact) power series expansion can be used (see Appendix E.1.3)

$$T_h(z,t) = \exp\left(-\frac{k_1 z}{v}\right) \Upsilon(t - z/v) \times \left[1 + \sum_{r=1}^{\infty} \frac{\Gamma_{\text{inc}}(k_2(t - z/v), r)}{r!(k_2/m(z))^r}\right] \tag{3.23}$$

Equivalently, in the Laplace domain, the transfer function from input $\hat{T}^{in}(s)$ to output $\hat{T}(z,s)$ is

$$\frac{\hat{T}(z,s)}{\hat{T}^{in}(s)} = \exp\left(-\frac{z}{v}s\right) \exp\left(-\frac{k_1\ z}{v}\right) \exp\left(\frac{k_1\ k_2\ z/v}{s + k_2}\right) \tag{3.24}$$

The steady-state value can be computed using (3.24)

$$\lim_{t\to\infty} T(z,t) = \overline{T^{in}} \tag{3.25}$$

where $\overline{T^{in}}$ is the steady-state value of T^{in}. The steady-state gain from inlet to outlet temperature is

$$G_{T^{in}} = 1 \tag{3.26}$$

which stresses that heat losses have been neglected. We now wish to compare the DOC responses to

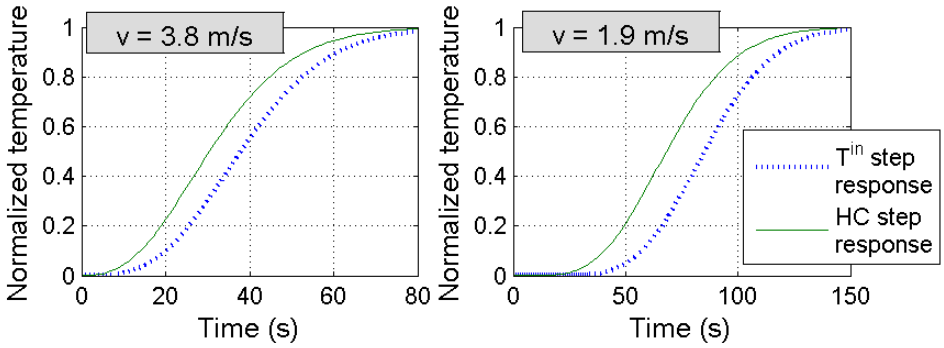

Figure 3.17: Comparison between HC step response and T^{in} step response (analytic data obtained from (3.15) and (3.22)). Inlet temperature response is slower than HC temperature response. This observation will be exploited for disturbance compensation. Simulation data.

T^{in} and HC variations. In practice, it is not possible with our experimental setup to fully decouple inlet temperature variations (see Appendix F), this is why the comparison is made based on the determined analytic form only. Analytic results derived from this model are presented in Fig. 3.17. For easier comparison, T^{in} and HC step responses are normalized using the steady-state values (3.25) and (3.13). *Results show that inlet temperature effects are slower than HC effects. It is then theoretically possible to compensate totally for these variations.* Extensive studies for various parameters give the same conclusions.

3.5.2 Rejection possibilities for the gas flow rate variations

Consider a change in gas flow rate (or v), taking place at constant T^{in}. Consider also that the HC flow rate u is adapted instantaneously with the steady-state gain G_u (given by 3.3) to keep the steady-state value T^{out} constant. In other words, the HC inlet concentration (scaled by η) is kept constant at the DOC inlet. The variation of v causes a variation in the reactive length L_c (see (3.6)). As is explained in 3.4.2.2, this variation transiently impacts on the DOC outlet temperature, causing the so-called overshoot and undershoot phenomena effect (see in particular Fig. 3.16). Although all conditions are met to keep T^{out} constant in the quasi-steady-state, in fact, T^{out} is disturbed. By abuse of terminology, it can be said that a "pure" (i.e. other variables are constant or adapted the quasi-steady-state conditions) variation of v causes T^{out} variations.

During a gas flow rise, the reactive zone lengthens and, in quasi-steady-state conditions, a zone is affected by heat release more than necessary. From a theoretical viewpoint, this local energy surplus can be compensated by reducing the HC supply. However, the combustion takes place from the DOC entry to this zone. Then, reducing the HC supply to compensate for a local surplus also affects the entry zone of the DOC, where HC supply is too small. If nothing is undertaken, this local lack of HC supply generates a delayed undershoot (because thermal phenomena evolve in the flow direction). A

new action is then necessary to compensate for it. So, from a theoretical viewpoint, it seems that an increase in v can be totally compensated by considering a highly-delayed oscillatory control, which is not suitable for real applications.

On the contrary, during a gas flow drop, the combustion zone shortens, leaving a zone unsupplied with heat release. This zone cannot be directly accessed by HC, because HC flow acts upstream of this zone. So, the only solution to make up for the coming undershoot is to heat the upstream local zone much more than necessary. This action compensates for the downstream-located lack of energy by thermal mixing effects similar to solid diffusion (phenomena will explained in § 4.2). Similarly to gas flow increase, this action has a consequence in the upstream zone, which will create a delayed temperature overshoot, and so on. Then, a compensating control requires more high-amplitude oscillations and more delays (see Appendix D for examples of control laws required to speed up DOC thermal responses).

As a conclusion, it seems difficult to get a realistic control law under unknown gas flow variations by solving this control problem. However, in both cases of gas flow rise and drop, the induced temperature variation can be attenuated. As will appear in Chapter 5, this conclusion is corroborated by experimental results.

3.6 Conclusions about the reduced model

In this chapter, a reduced model has been proposed and experimentally validated. It captures the main effects (even transient counter-intuitive ones) observed in practice, but it does not directly lead to control solutions. We need to go further into the analysis to determine appropriate control laws. To do so, we proceed in two steps. In Chapter 4, we focus on the propagation of thermal phenomena. We show that, under some assumptions, the reduced model is equivalent to a set of two parabolic equations (advection+diffusion) with inlet boundary conditions only. Their properties allow us to propose a mean to simply synchronize the inlet temperature and the control. It is used in the feedforward control law, dedicated to the rejection of the inlet temperature disturbances. This approach is also used to schedule the parameters of the feedback law, but it is not sufficient to cope with transient phenomena related to the variations of the gas flow rate. This issue is addressed in Chapter 5, where we show how the overshoot and undershoot can be partially compensated for. This provides guidelines for the design of a complementary feedforward control law, dedicated to the (partial) rejection of the effects due to the gas flow variations. The developments of Chapters 4 and 5 are gathered in Chapter 6, where the complete control law is proposed.

Chapter 4

Parameterized advection diffusion model

In the previous chapter, a reduced model describing all the main physical observations (see § 3.1), has been proposed. In this chapter, a parameterized model is inferred from this reduced model. Our goal is to get some further insight into the thermal propagation phenomenon, to be able to design a control law and to schedule its parameters according to the current value of the gas flow rate. Interesting properties resulting from this study will be exploited in the control strategy in Chapter 6: first in a part of the feedforward control law, to synchronize the disturbance T^{in} with the control u; second, to schedule the parameters of the feedback law. The approach developed in this chapter is not sufficient to describe the overshoot and undershoot phenomena presented in the previous chapter (see § 3.3.2 and § 3.4.2.2). Ways to compensate for these effects are studied in Chapter 5, which grounds a complementary part of the feedforward control law proposed in Chapter 6.

The study presented in this chapter is organized as follows. First, adaptations are made to transform the distributed control input of the reduced model into a boundary input. To proceed, we aggregate the distributed reactive zone as an entry point for a propagation zone described by two hyperbolic equations without any source terms except at the (inlet) boundary. The length of this propagation zone is determined to account for the variable length of the distributed reactive length and of the DOC length. Then, the resulting hyperbolic model is shown to be well-approximated by a parabolic advection-diffusion model. Finally, the model, which accounts for both the inlet temperature and the control variable u (HC inlet flow rate), is presented.

4.1 From distributed control to boundary control

Consider the reduced model (3.4)-(3.5)-(3.6)-(3.7), in which the source term Ψ is set to zero. This model describes propagation of the inlet temperature. In this section, it is shown how the HC response, previously modeled using a distributed input Ψ, can be approximated using an equivalent boundary input T_{eq}^{in}. This approximation only requires the adaptation of the considered propagation length.

4.1.1 Fitting the reduced model with an equivalent model

We aim at using the boundary input response to describe the response to distributed control input of the reduced model.

In Fig. 4.1a, the reduced model is used. It is shown that the overall shape of the HC step response, corresponding to a distributed input (computed with (3.15)), is very similar to the inlet temperature step response, corresponding to a boundary input (computed using (3.22) with $z = L$). This similarity suggests that it is possible to approximate HC step response by boundary input step response at the

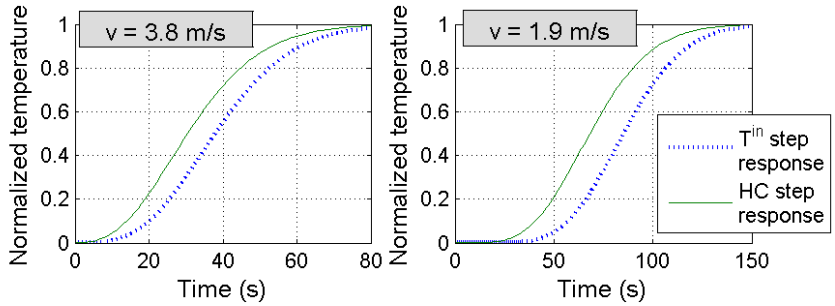

(a) Comparison between HC step response (distributed input of the reduced model) and T^{in} step response (boundary input of the reduced model). Analytic results obtained respectively from (3.15) and (3.22) with $z = L$. Results identical to those in Fig. 3.17.

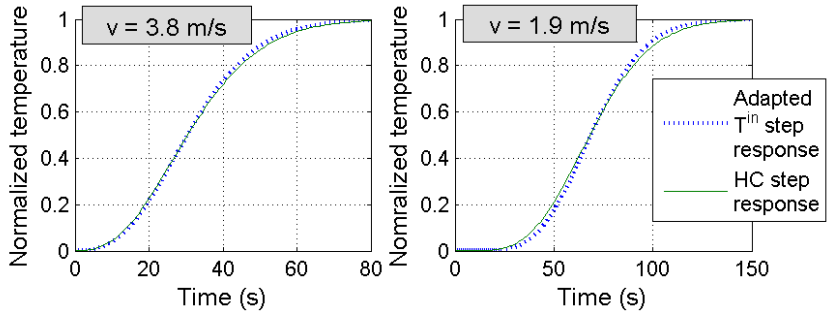

(b) Comparison between HC step response (distributed input of the reduced model) using the real DOC length ($z = L$) and T^{in} step response (boundary input of the reduced model) using an adapted value of the length. Analytic results obtained respectively from (3.15) and (3.22) with an adapted value of the length.

Figure 4.1: HC step response approximation in various operating conditions. Formulas (3.12) and (3.25) are used for normalization. Simulation data.

expense of an alternative identification procedure. Note that, for easier comparisons, responses are normalized using (3.13) and (3.25).

It is shown in Fig. 4.1b that it suffices to adapt the DOC length in the reduced model (3.4) and to use its boundary input, to get responses very similar to the ones obtained with the reduced model (3.4) using its distributed input and its full length L. *In other words, generating heat with HC is quite equivalent to propagating T^{in} through a DOC having a shorter length L_u.* This idea, that focuses on the propagation along the DOC rather than on the way heat is generated, is pictured in Fig. 4.2.

Remark. Note that this fictitious "transport" length L_u does not equal the "non-reactive" length of § 3.4.2.2 (i.e. $L - L_c$). In typical cases, everything behaves as if the source were located at about half the reactive length L_c. To precisely get in accordance the two viewpoints, a numeric identification is performed.

Equivalence between Ψ and the boundary input, noted T^{in}_{eq} for clarity, has a particular interest for the control because T^{in}_{eq} can be seen as a control variable on the length-adapted model with no source term.

This principle will ground a control design based on a synchronization technique in § 6.2. Before we experimentally validate this principle, we now make a precise presentation of the obtained model.

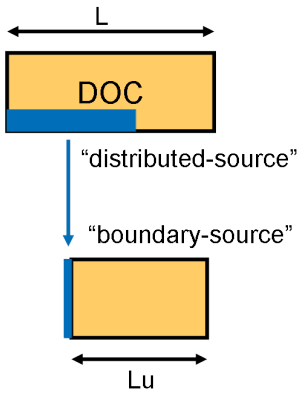

Figure 4.2: Schematic description of transformation of the control variable in the reduced model into the control variable of the model (4.1). The distributed input is transformed into a boundary input provided a length adaptation.

4.1.2 “Boundary-source” model presentation

This model can be viewed as a particular case of the reduced model (3.4)-(3.5)-(3.6)-(3.7), in which the source term is null: $\Psi = 0$. It is referred to as “boundary-source model” and writes, *at constant* v,

$$\left\{ \begin{array}{rcl} \dfrac{\partial T}{\partial t}(z,t) + v\dfrac{\partial T}{\partial z}(z,t) & = & -k_1\left(T(z,t) - T_s(z,t)\right) \\ \dfrac{\partial T_s}{\partial t}(z,t) & = & k_2\left(T(z,t) - T_s(z,t)\right) \end{array} \right. \tag{4.1}$$

Note T_{eq}^{in} the boundary condition (the boundary condition is noted T^{in} in the reduced model)

$$T_{eq}^{in}(t) \triangleq T(z=0,t) \tag{4.2}$$

Here, T_{eq}^{in} is the control variable. It plays a role similar to the one played by the distributed control variable u in the reduced model. It is related to u by

$$T_{eq}^{in} = G_u\, u \tag{4.3}$$

The system output T_{eq}^{out} corresponds to the temperature at the previously-introduced transport length L_u

$$T_{eq}^{out}(t) \triangleq T(z=L_u,t) \tag{4.4}$$

The length L_u is defined by

$$L_u(v) = \max(L - a_u\, v - b_u, \quad 0) \tag{4.5}$$

where a_u and b_u are positive constants. These constants are identified and are not equal to the constants a and b of the reduced model.

In the Laplace domain, the transfer function from input $\hat{T}_{eq}^{in}(s)$ to output $\hat{T}(z,s)$ is

$$\frac{\hat{T}(z,s)}{\hat{T}_{eq}^{in}(s)} = \exp\left(-\frac{z}{v}s\right)\exp\left(-\frac{k_1\, z}{v}\right)\exp\left(\frac{k_1\, k_2\, z/v}{s+k_2}\right) \tag{4.6}$$

4.1.3 Experimental validation of the model (4.1) with HC step responses

As stressed in the previous paragraph, considering a tuning of the parameters a_u and b_u, model (4.1) and model (3.4) yield similar results. In Fig. 4.3, experimental HC step responses under various operating conditions are presented. These responses are well fitted by the T_{eq}^{in} step response, given by, for $z = L_u$:

$$T_h(z,t) = \Upsilon(t - \frac{z}{v}) \exp\left(-\frac{k_1 z}{v}\right) \times \left[1 + \int_0^{t-z/v} \exp\left(-k_2\tau\right) \sqrt{\frac{m(z)}{\tau}} \mathrm{I}_1(2\sqrt{m(z)\tau}) d\tau\right] \quad (4.7)$$

corresponding to the model (4.1). Again (as in § 3.5.1), for efficient numeric evaluation of the above expression, the following power series expansion can be used, for $z = L_u$,

$$T_h(z,t) = \exp\left(-\frac{k_1 z}{v}\right) \Upsilon(t - z/v) \times \left[1 + \sum_{r=1}^{\infty} \frac{\Gamma_{\mathrm{inc}}(k_2(t - z/v), r)}{r!(k_2/m(z))^r}\right] \quad (4.8)$$

As illustrated in Fig. 4.3 this formula fits well experimental data formally described using a source term (as was illustrated in Fig. 3.10).

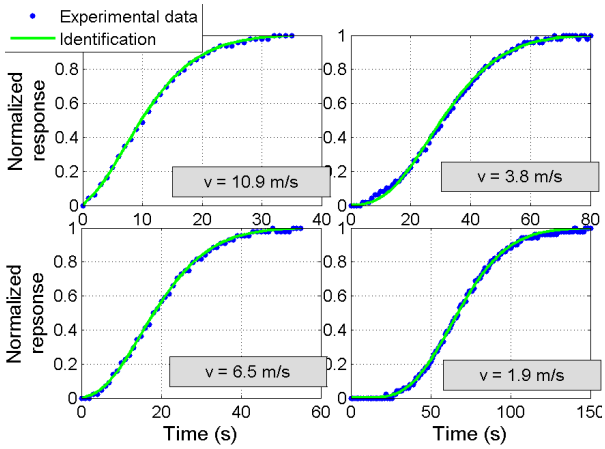

Figure 4.3: Experimental HC step response identified to model (4.1) under various operating conditions

4.1.4 Experimental validation of the model (4.1) with warm-up strategy

A first interesting feature of the proposed "boundary-source" model (4.1) is that it gives a very simple input-output view of the problem. This view can be exploited to solve an inverse problem, e.g. a motion planning problem. The employed methodology is presented in Appendix D.1, and we only reproduce here the experimental results that stress the relevance of this model. Further results are given in Appendix D. The theoretical approach was proposed in Lepreux et al. (2008), and experimental results and extensions appeared in Lepreux et al. (2009*c*).

In order to validate further the model (4.1) equivalence to the reduced model (T^{in} and v remain constant in the following experiments), we formulate the problem of the motion planning for the model (4.1) and validate it experimentally with HC flow control (corresponding to the reduced model).

Summary of motion planning results It is shown in Appendix D.1 how to derive an open-loop control law corresponding to a desired finite-time transition of the outlet temperature from one steady state to another. It results in high-frequency, large-amplitude and long-delayed control variations. This control is beyond actuation possibilities, safe DOC conditions of use, and model validity domain, but is insightful to develop numerical methods which can deal with explicit constraints. Two such methods are proposed in Appendix D.2. Eventually, it is shown that a pulse input signal is simple to implement and produces efficient solutions. Proposed solution consists of two pulses ($n = 2$) for the input signal before setting it to its steady-state value (Fig. 4.4 at abscissa 0%). Such a control profile is found to provide good performance (see Appendix D.3). Moreover, the pulse magnitude is set twice as high as the final step value ($M = 2$), or three times as high as the final step value ($M = 3$), in order not to affect the conversion efficiency.

Optimization results provide a theoretical temperature distribution as reported in Fig. 4.4: the pulse input generates temperature oscillations along the catalyst, and, finally, results in a temperature rise which is faster than the step response.

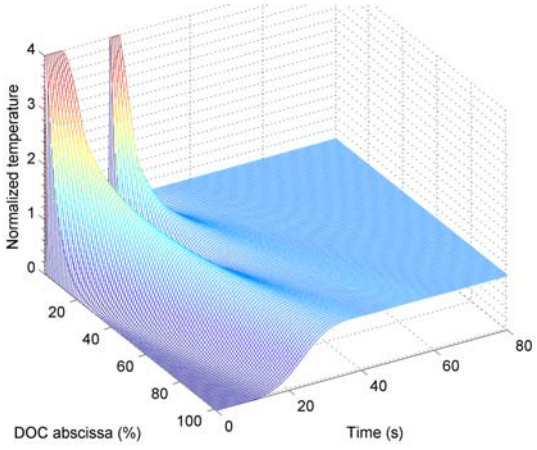

Figure 4.4: Optimized spatially-distributed temperature evolution. Pulse control input (abscissa 0%) leads to a fast transient output response (abscissa 100%). Simulation data.

Outlet temperature Two optimized control laws and corresponding experimental responses are presented in Fig. 4.5. The first pulse occurs at $t = 0$. For comparison, the step response is plotted. It clearly appears that the proposed strategies significantly shorten the rise time while keeping oscillations about final values very small. It is shown how oscillations appear when pulses get more spaced. This stresses that the choice of pulse switch times allows any potential oscillation to be canceled. Also, it stresses the robustness regarding the pulse switch times. In this last case, the 95%-rise time (time from 0% of the step size to 95% of the step size) is reduced by a factor of 37%.

Intra-catalyst temperature As detailed in Appendix F, the intra-catalyst temperature has also been measured. It is not a control objective, but it is instructive to examine how its variations are captured by the model. This shows how sounded is the simplifying assumption about the oxidation kinetics. A typical example of obtained experimental results is reported in Fig. 4.6 for both cases $M = 2$ and $M = 3$. Oscillations are clearly visible and give a representation of spatial evolution of boundary pulses: they produce oscillations near the inlet that gradually fade out at the outlet, as expected from the theoretical results given in simulation in Fig. 4.4. This phenomenon is well captured by our models. For validation, an experimental result is selected and the corresponding boundary control,

originally computed through (4.1), is applied to the reduced model (3.4). In Fig. 4.7, we present results of simulation and experimental data for both intra-catalyst temperature (at $z = L/2$) and outlet temperature (at $z = L$). Again, intra-catalyst and outlet temperatures are normalized for easier comparisons. We notice that simulated intra-catalyst temperature oscillations match closely the experimental data, although simulated temperature shows more pronounced oscillations. Globally, the dynamics are well-captured for both the intra-catalyst temperature and the outlet temperature. Although all phenomena are not included in this model (diffusion, thermal losses, ...), the essential feature of the DOC thermal dynamics appears to be well represented. This point stresses, at constant v, the relevance of the proposed reduced model (3.4) and the accuracy of its approximation by the "boundary-source" model (4.1) that we are going to use for the control design.

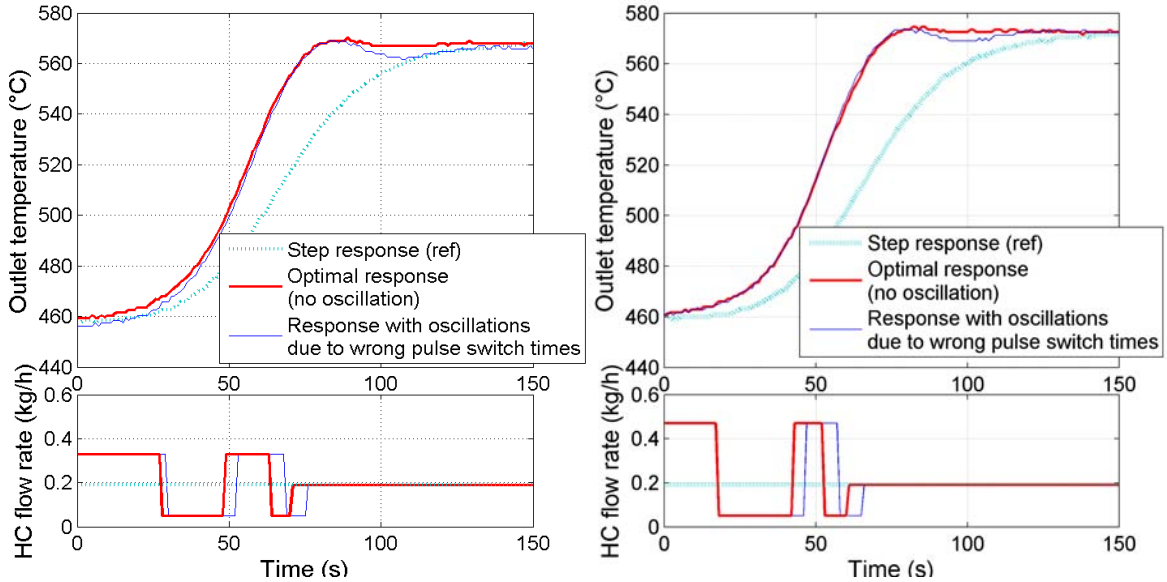

(a) M=2 (b) M=3

Figure 4.5: Outlet temperatures and controls. Experimental data.

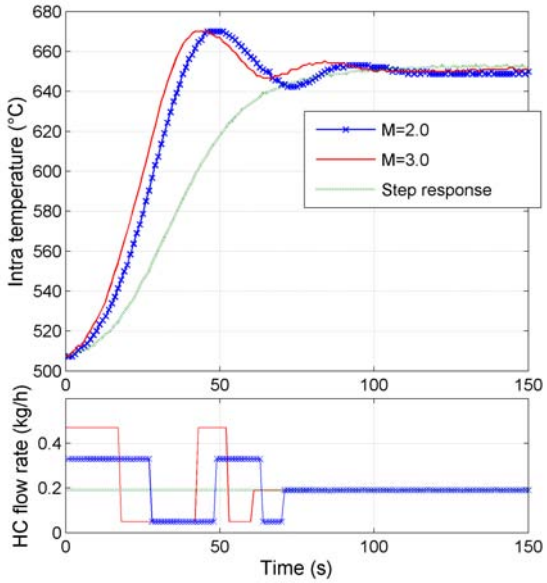

Figure 4.6: Intra-catalyst temperature. Experimental data.

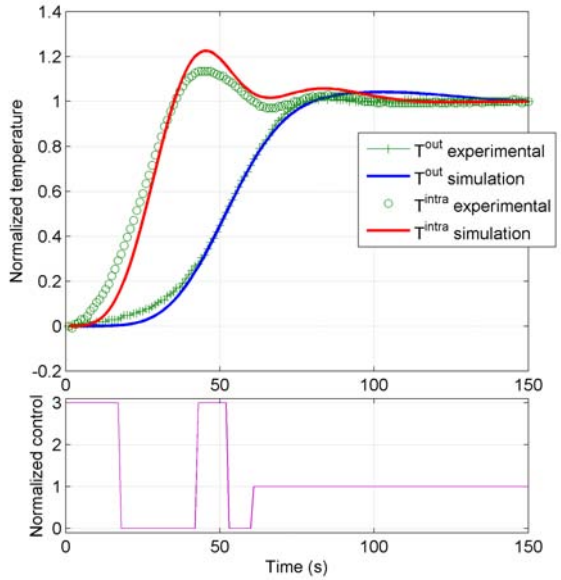

Figure 4.7: Pulse control signals responses (intra-catalyst and outlet temperatures) applied to the reduced model. Simulation and experimental data.

4.2 Equivalent advection-diffusion model

In this section, we now show that the model (4.1) describing two phases exchanging energy through two hyperbolic equations can be approximated by a parabolic advection-diffusion model in which the temperature evolves at a speed lower than v. To obtain this model, we perform a low-order series expansion of the partial derivatives equation. Finally, the obtained model is experimentally validated. Also, its properties that will be useful in the control design are discussed.

4.2.1 Advection-diffusion equation approximation

Introduction

In this part, it is shown that the system (4.1) (recalled below)

$$\begin{cases} \dfrac{\partial T}{\partial t}(z,t) + v\dfrac{\partial T}{\partial z}(z,t) &= -k_1\left(T(z,t) - T_s(z,t)\right) \\ \dfrac{\partial T_s}{\partial t}(z,t) &= k_2\left(T(z,t) - T_s(z,t)\right) \end{cases}$$

can be approximated by the following advection-diffusion equation[1] when v/k_1 is small

$$\frac{\partial T(z,t)}{\partial t} + \vartheta\frac{\partial T(z,t)}{\partial z} = \lambda\frac{\partial^2 T(z,t)}{\partial z^2} \tag{4.9}$$

with

$$\begin{cases} \vartheta = \dfrac{k_2 v}{k_1} \\ \lambda = \dfrac{k_2 v^2}{k_1^2} \end{cases} \tag{4.10}$$

Neglecting gas thermal storage

As will now appear, it is possible to neglect the gas thermal storage term of (4.1). Gas has a very small storage capacity compared to monolith ($(\rho_g Cp)/(\rho_s Cp_s) \ll 1$). For practical cases, neglecting the gas thermal storage term is thus a reasonable assumption. It has been considered in the past by numerous authors for modeling similar chemical processes with no further justification. In particular Depcik & Assanis (2005) conclude that this assumption holds for the vast majority of operating conditions.

As an illustration, we show how small the influence of this storage term on the transfer function (4.6) is. Consider the system (4.1) for a constant value of the gas speed v (in the case of a variable gas flow rate, the transfer can not be calculated as simply) in which the term $\partial T/\partial t$ has been neglected

$$\begin{cases} \dfrac{v}{k_1}\dfrac{\partial T}{\partial z}(z,t) &= -\left(T(z,t) - T_s(z,t)\right) \\ \dfrac{\partial T_s(z,t)}{\partial t} &= k_2(T(z,t) - T_s(z,t)) \end{cases} \tag{4.11}$$

[1] It is interesting to note that T_s follows exactly the same equation (boundary conditions are different)

$$\frac{\partial T_s(z,t)}{\partial t} + \vartheta\frac{\partial T_s(z,t)}{\partial z} = \lambda\frac{\partial^2 T_s(z,t)}{\partial z^2}$$

This approximation corresponds to neglecting gas storage. In the Laplace domain, let us now calculate the transfer function $\hat{T}/\hat{T}_{eq}^{in}$ of the new system (4.11) and compare it to the original transfer function (4.6). Some operational calculus leads to

$$\begin{cases} \dfrac{v}{k_1}\dfrac{\partial \hat{T}}{\partial z}(z,s) &= -(\hat{T}(z,s) - \hat{T}_s(z,s)) \\ s\,\hat{T}_s(z,s) &= k_2\,(\hat{T}(z,s) - \hat{T}_s(z,s)) \end{cases}$$

and so, to

$$\frac{\partial \hat{T}}{\partial z}(z,s) = \left(\frac{k_2}{s+k_2} - 1\right)\frac{k_1}{v}\hat{T}(z,s) \tag{4.12}$$

Finally

$$\frac{\hat{T}(z,s)}{\hat{T}_{eq}^{in}(s)} = \exp\left(-\frac{k_1 z}{v}\right)\exp\left(\frac{k_1 k_2 z/v}{s+k_2}\right) \tag{4.13}$$

It can be noticed that this result is the same as equation (4.6) without the z/v-delay. This delay is very small (a fraction of a second) when compared to DOC response time (typically 10^2 s). This guarantees the validity of the approximation.

Considering this approximation, the system of equations (4.11) leads, after a substitution of the second equation in the first equation, to the following PDE

$$\frac{\partial T(z,t)}{\partial t} + \frac{k_2 v}{k_1}\frac{\partial T(z,t)}{\partial z} + \frac{v}{k_1}\frac{\partial^2 T(z,t)}{\partial t \partial z} = 0 \tag{4.14}$$

Let us denote

$$\begin{aligned} \vartheta &= \frac{k_2 v}{k_1} \\ \lambda &= \frac{k_2 v^2}{k_1^2} \end{aligned} \tag{4.15}$$

Equation (4.14) can be rewritten as

$$\frac{\partial T(z,t)}{\partial t} + \vartheta\frac{\partial T(z,t)}{\partial z} + \frac{\lambda}{\vartheta}\frac{\partial^2 T(z,t)}{\partial t \partial z} = 0 \tag{4.16}$$

Series expansion of equation (4.16)

On one hand, we consider equation (4.16). Noting $\varepsilon \triangleq \dfrac{\lambda}{\vartheta} = \dfrac{v}{k_1}$, one has

$$\frac{\partial T(z,t)}{\partial t} + \vartheta\frac{\partial T(z,t)}{\partial z} + \varepsilon\frac{\partial^2 T(z,t)}{\partial t \partial z} = 0. \tag{4.17}$$

We wish to simplify this equation when ε is small. Following Il'in (1998), we expand T in the following series

$$T = T_0 + \varepsilon T_\varepsilon + \varepsilon^2 T_{\varepsilon^2} + \ldots \tag{4.18}$$

where T_0 is the solution of the following advection equation (i.e. (4.17) for $\varepsilon = 0$)

$$\frac{\partial T_0(z,t)}{\partial t} + \vartheta\frac{\partial T_0(z,t)}{\partial z} = 0 \tag{4.19}$$

A substitution of (4.18) into (4.17) gives the expansion

$$\varepsilon\frac{\partial^2 T_0}{\partial t\partial z}+\varepsilon\frac{\partial T_\varepsilon}{\partial t}+\vartheta\varepsilon\frac{\partial T_\varepsilon}{\partial z}+\varepsilon^2\frac{\partial^2 T_\varepsilon}{\partial t\partial z}+\ldots=0 \tag{4.20}$$

Matching ε-terms, we obtain

$$\varepsilon\frac{\partial^2 T_0}{\partial t\partial z}+\varepsilon\frac{\partial T_\varepsilon}{\partial t}+\vartheta\varepsilon\frac{\partial T_\varepsilon}{\partial z}=0 \tag{4.21}$$

Expansion of a simpler advection-diffusion equation

On the other hand, we consider the advection-diffusion equation (4.9)

$$\frac{\partial T(z,t)}{\partial t}+\vartheta\frac{\partial T(z,t)}{\partial z}=\lambda\frac{\partial^2 T(z,t)}{\partial z^2}$$

rewritten as

$$\frac{\partial T(z,t)}{\partial t}+\vartheta\frac{\partial T(z,t)}{\partial z}=\varepsilon\vartheta\frac{\partial^2 T(z,t)}{\partial z^2}. \tag{4.22}$$

Expanding (4.22) with (4.18) leads to (4.19) and

$$-\varepsilon\vartheta\frac{\partial^2 T_0}{\partial z^2}+\varepsilon\frac{\partial T_\varepsilon}{\partial t}+\vartheta\varepsilon\frac{\partial T_\varepsilon}{\partial z}-\varepsilon^2\vartheta\frac{\partial^2 T_\varepsilon}{\partial z^2}+\ldots=0 \tag{4.23}$$

Equation (4.19) yields

$$-\varepsilon\vartheta\frac{\partial^2 T_0}{\partial z^2}=\varepsilon\frac{\partial^2 T_0}{\partial t\partial z} \tag{4.24}$$

So, (4.23) can be rewritten as

$$\varepsilon\frac{\partial^2 T_0}{\partial t\partial z}+\varepsilon\frac{\partial T_\varepsilon}{\partial t}+\vartheta\varepsilon\frac{\partial T_\varepsilon}{\partial z}-\varepsilon^2\vartheta\frac{\partial^2 T_\varepsilon}{\partial z^2}+\ldots=0 \tag{4.25}$$

Matching ε-terms, we obtain

$$\varepsilon\frac{\partial^2 T_0}{\partial t\partial z}+\varepsilon\frac{\partial T_\varepsilon}{\partial t}+\vartheta\varepsilon\frac{\partial T_\varepsilon}{\partial z}=0 \tag{4.26}$$

Expanding solutions of T in ε for (4.16) and (4.9) lead to the same equations (4.21) and (4.26) up to order 1 in ε, i.e. T_0 and T_ε are the same in both cases. In this way, (4.16) and (4.9) are similar: their asymptotic expansions are equal up to order 1 (included) (see Il'in (1998)). From now on, we will work with (4.9).

4.2.2 Advection-diffusion model validation

Advection-diffusion models are frequently used to describe the behavior of temperatures or concentrations of a fluid (Danckwerts 1953). Considering the nature of the DOC, which is very similar to a tubular reactor, this is not a real surprise to see such a model (4.9) here. The model includes two parameters ϑ and λ. λ represents a diffusion in (m^2/s) and ϑ is a speed in (m/s). Interestingly, the parameter ϑ differs from the actual fluid speed v. In the DOC, ϑ represents an *apparent speed* for the temperature, which is significantly scaled down from the fluid speed. λ represents an *apparent diffusion* due to mixing effects by heat storage in the monolith.

In the following, the model is compared against experimentally measured HC step response. It is shown in Danckwerts (1953) that, when diffusion λ is small relatively to the speed ϑ, (4.9) with boundary condition

$$T(z=0,t)=\Upsilon(t) \tag{4.27}$$

can be accurately approximated using the following *initial condition* instead of the *boundary condition* (4.27)

$$T(z, t = 0) = \Upsilon(-z) \tag{4.28}$$

Then, it follows that the step response evolution is simply given by

$$T(z, t) = \frac{1}{2}\text{erfc}\left(\frac{z - \vartheta \cdot t}{2\sqrt{\lambda \cdot t}}\right) \tag{4.29}$$

One can report to Barraud (2006) for the details on the resolution.

In Fig. 4.8 temperature profiles for the two equations (4.29) and (4.7) are plotted at different times. It appears that the temperature profiles given by model (4.7) are approximated well by (4.29). The

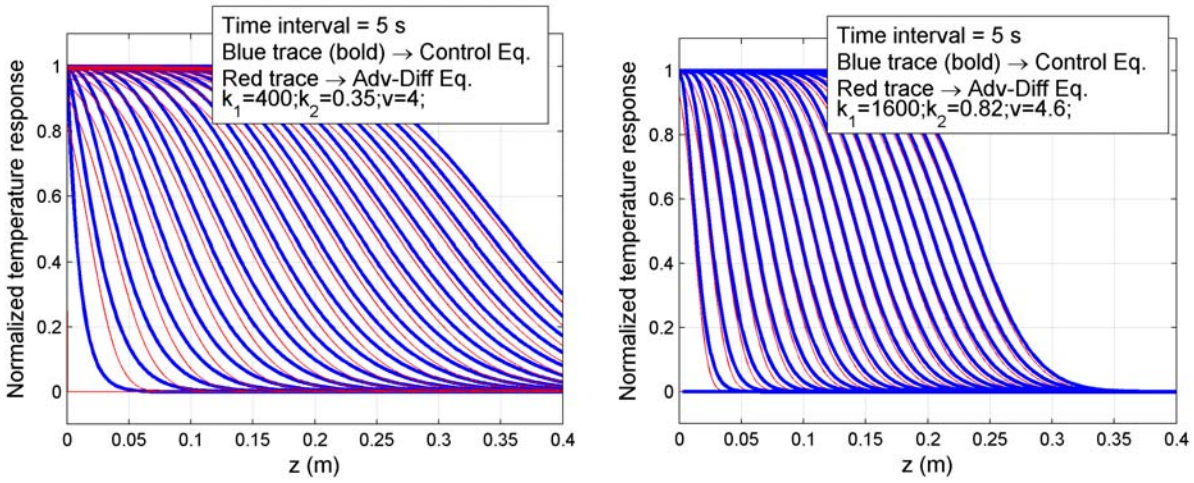

(a) Case A - Temperature profiles in response to a step input at times $0s, 5s, 10s, \ldots$

(b) Case B - Temperature profiles in response to a step input at times $0s, 5s, 10s, \ldots$

Figure 4.8: Comparison between the DOC and the advection diffusion responses to step input

approximation is particularly accurate where the diffusion effect is not important.

Fig. 4.9 shows parameters ϑ and λ resulting from an identification of model (4.29) to experimental results. It clearly validates the determined linear dependence of ϑ on the gas flow rate and the parabolic dependence of λ (see (4.10)). Fig. 4.9 presents mean values over multiple points. It must be specified that, at high gas flow rates, dispersion is important for the λ parameter. In this flow range, temperature response is very fast, and the approximations made do not remain very accurate. In particular, the change of boundary condition to initial condition, is wrong. Simply speaking, the overall shape for the temperature response in a high flow range differs from the advection-diffusion model step response. However the lack of accuracy in this zone is not problematic at all, because it is indeed the zone where the delay is small, and, thus, where the temperature control is easy.

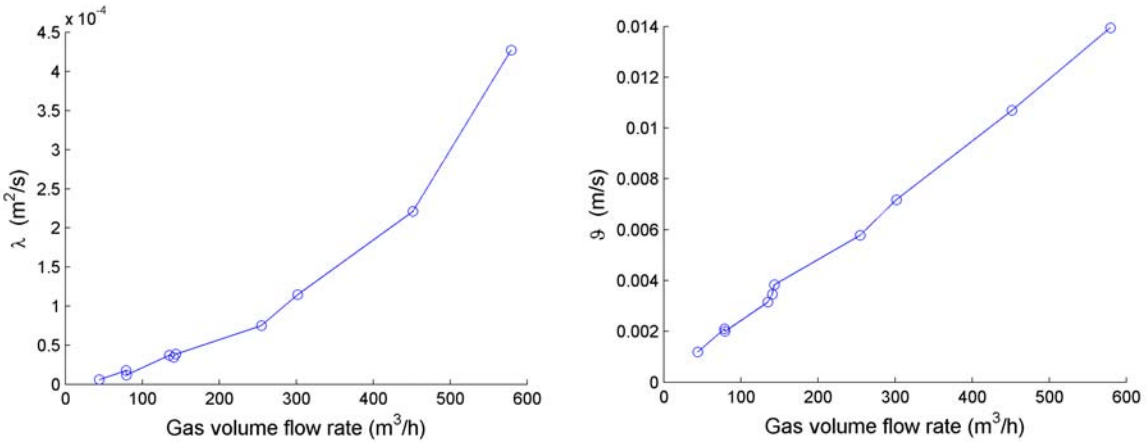

(a) Parameter λ (b) Parameter ϑ

Figure 4.9: Results of advection-diffusion model (4.9) identification to control HC experimental step responses. Experimental data.

4.2.3 Delay evolution under variable gas flow conditions

We must account for varying gas flow rate (v). Our goal is to compute a time that is characteristic of the thermal propagation phenomena described by the equation (4.1). This time will be used for model scheduling.

Previously, it has been shown that (4.1) can be approximated by the advection-diffusion equation (4.9). Although calculus have been carried out in v-pseudo-steady state conditions, *we assume that this approximation also holds when v depends on the time.* We now consider

$$\vartheta(t) = \frac{k_2 v(t)}{k_1}$$
$$\lambda(t) = \frac{k_2 v(t)^2}{k_1^2}$$

The advection-diffusion equation (4.9) allows, under some conditions, the separation of the propagation from the diffusion phenomena. Following along several calculus given in Cannon (1984), this separation is clearly made visible by using the following change of variables $w(\zeta, \tau) = T(z, t)$,

$$\begin{cases} \zeta = z - \displaystyle\int_0^t \vartheta(s) ds \\ \tau = \displaystyle\int_0^t \lambda(s) ds \end{cases} \tag{4.30}$$

Then, equation (4.9) simply leads to the heat equation

$$\frac{\partial w}{\partial \tau} = \frac{\partial^2 w}{\partial \zeta^2} \tag{4.31}$$

The reader can report to Appendix E.4 for more details. It is worth noticing that this transformation can be easily performed under variable conditions because the advection-diffusion equation (4.9) resulting from approximation of (4.1) leads to coefficients λ and ϑ depending only on the time variable t.

Consider now the following initial conditions for (4.9)

$$T(z,0) = \Upsilon(-z)$$

In the (ζ,τ)-coordinates, it is transformed into

$$w(\zeta,0) = \Upsilon(-\zeta)$$

Implicitly, by writing this initial condition, temperature propagation is studied on a system having an infinite length. In this infinite-length system, the boundary conditions are located at $\zeta = \pm\infty$ in the (ζ,τ)-coordinates or at $z = \pm\infty$ in the (z,t)-coordinates. In other words, it is considered that the boundaries are "far" from the phenomena studied (relatively to diffusion effects).

Referring to the heat equation For the infinite-length system, the well-known solution for (4.31), is

$$w(\zeta,\tau) = \frac{1}{2}\operatorname{erfc}\left(\frac{\zeta}{2\sqrt{\tau}}\right)$$

This formula represents a symmetric propagation of w, relatively to the point of abscissa $\zeta = 0$. This point of abscissa $\zeta = 0$, for which $w = 0.5$, is invariant, and represents a *reference point* in the current development. For this point, everything is as if the system were not diffusive.

Referring to the advection diffusion equation In the infinite-length system, and the (z,t)-coordinates (i.e. for the advection diffusion equation (4.9)), the initial condition is similar to the case of the heat equation, i.e. $T(z,0) = \Upsilon(-z)$. The temperature T behaves in the following way. Everything is as in the case of the heat equation, i.e. diffusion symmetrically takes place relatively to the invariant reference point defined above. This point corresponds to the point of abscissa $\zeta = 0$, i.e. $z = \int_0^t \vartheta(s)\,ds$. For this point, as in the previous case, normalized temperature is $T = 0.5$. This is what expresses the solution

$$T(z,t) = \frac{1}{2}\operatorname{erfc}\left(\frac{z - \int_0^t \vartheta(s)\,ds}{2\sqrt{\int_0^t \lambda(s)\,ds}}\right) \tag{4.32}$$

This is also expressed, at constant (λ,ϑ), in the solution (4.29) given e.g. in Danckwerts (1953).

Referring to equation (4.1) What expresses Danckwerts (1953), by changing boundary conditions to initial conditions, is that diffusion is not too fast compared to advection. From the coordinates of the reference point (defined above), transported at the speed of advection equation, the system rapidly becomes similar to the infinite-length system, since it is "quickly" far away from the boundaries effects. Generating an initial condition signal is then an approximation of generating a boundary condition signal.

Remark. Response to a discrete signal can be generated by considering a series of initial conditions taking place in parallel systems. This is exactly what is done in the online-computable model presented in Appendix E.4.

Furthermore, the performed transformation of equation (4.1) into advection-diffusion equation is particularly accurate in zones that are not influenced by the boundary conditions (this is explicitly mentioned in Il'in (1998)). Then, in the series of approximations leading to equation (4.31), it seems relevant to assume that the properties regarding evolution of the reference point (defined above) remain valid. In particular, the propagation of this point verifies the same equation as in (4.31) with initial conditions.

As a summary, a series of approximations, series expansion and a change of variables has transformed equation (4.1) into equation (4.31). The property finally extracted from the advection equation (see below), concerns the reference point, for which every performed approximation is the "most" valid.

As an illustration, one can refer to Fig. 4.8 to see that the approximation is "more" valid around the reference points (around $T = 0.5$ for each trace) than at places where diffusion and boundaries effects are large (around $T = 1$ and $T = 0$).

Relation with advection equation The advection equation (see below (4.34)) expresses the conveyance of its boundary condition. In this transformation, the value of the boundary condition has not a direct influence on the state of the system. Because of this, in an infinite-length system such as considered above, temperature T evolution is exactly the same as in a finite-length system. The initial condition is strictly equivalent to the boundary condition.

Remark. This explains why these conditions are useless to get the relation (4.35) below.

Then, the transformation of the reference point of the advection-diffusion system in the infinite-length system, can be described using the advection equation.

Delay evolution Consider the delay $\delta(t)$ defined by

$$T(z_p, t) = T(z - z_p, t - \delta(t)) \tag{4.33}$$

where z_p represents the considered length of propagation. It is shown in Appendix E.2 that the delay evolution for the following advection equation

$$\frac{\partial T}{\partial t} + \vartheta(t)\frac{\partial T}{\partial z} = 0 \tag{4.34}$$

verifies the following implicit equation, in which $\delta(t)$ is unknown

$$z_p = \int_{t-\delta(t)}^{t} \vartheta(w)dw \tag{4.35}$$

Reference points will be computed in the controller using (4.35) as a basis for the synchronization control strategy. This implicit equation will be used in the control design to describe the evolution of thermal phenomena and, in particular, to synchronize the control action with the disturbance effect.

4.3 Summary of the proposed model

As explained in § 3.2, the linearity of the reduced model allows the inlet temperature T^{in} effects and the HC effects to be decoupled. We have carefully studied the HC effect, and we now have to account for the T^{in} effects.

On one hand, as shown in § 4.1 the control variable of the reduced model can be transformed into a boundary condition, provided model identification is performed. Then, the obtained system can be approximated by an advection-diffusion system (§ 4.2).

On the other hand, in the reduced model, the inlet temperature is taken into account by using the inlet temperature as boundary condition and the source term equal to zero. This corresponds to the model (4.1) using T^{in} as boundary condition. Then, the approximation to an advection-diffusion system developed in the previous section remains valid (with T^{in} instead of T^{in}_{eq}). The inlet temperature propagation is described by an advection-diffusion system having a length $z = L$ and T^{in} as boundary condition. The temperature propagation time will be used in the control strategy (see § 6) using the general equation (4.35) (see § 6.2).

In summary, a schematic view of the T^{in} effects and the HC effects is presented in Fig. 4.10. The

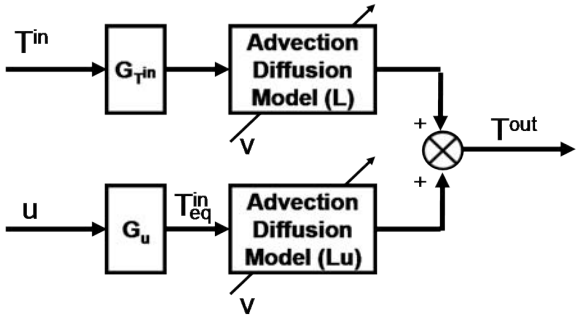

Figure 4.10: Proposed model. The HC effects can be assimilated to a front of temperature T^{in}_{eq} propagating on a fictitious length L_u. On the contrary, the T^{in} effect is propagating over the whole DOC length L.

HC flow rate u effects can be assimilated to a temperature T^{in}_{eq} propagating on a fictitious length L_u, which is shorter than the DOC real length. Besides, T^{in} is propagating over the whole DOC length L. Both sub-subsystems use the advection-diffusion equation to describe propagation. Although variable, v is identical in both sub-systems, and in particular, does not depends on z. This interesting property allows us to exploit the linearity of the model (4.1) to decouple the T^{in} effects and the HC effects. In both sub-systems, propagation coefficients (ϑ and λ) are identical (they depend on v). Altogether, the parameterized model consists of the two sub-models, the outputs of which are summed to yield the model output.

4.4 Conclusions

In this chapter, a parameterized model has been presented. It focuses on the thermal phenomena propagation in the DOC. It has been stressed that the reduced model used for inlet temperature response (i.e. $\Psi = 0$) could also be used as model for HC response, provided a boundary input equivalent to the source term and an adapted propagation length. This modeling suggests a part of the control solution consisting of synchronizing the control u to the disturbance T^{in}. Also, it allows the computation of the propagation times that will be used in the feedback control law. However, this model, which aggregates the distributed control as a boundary control, is unable to describe effects related to variations of reactive length. These effects were well-described by the reduced model presented in Chapter 3. Hence, in the next chapter, compensation possibilities for these disturbances (related to v) are investigated.

Chapter 5

Investigations on overshoot and undershoot phenomena

In this chapter, we first use in § 5.1 a simple advection model with a distributed source term. It is helpful to understand the origin of the overshoot and undershoot, that are observed in the experiments when the total gas flow rate varies, and the control HC u is adapted accordingly to keep the same output temperature value at equilibrium (these effect have already been discussed in § 3.5.2). For this advection model, we also propose a control approach to limit the overshoot. In summary, for an overshoot, after a gas flow increase, this method consists of zeroing the control, and then ramping it to its final value. This allows the overshoot magnitude to be limited, at the expense of a subsequent undershoot. In § 5.2, open loop experiments are reported[1], that apply control HC trajectories derived from the conclusions of § 5.1. It is shown that these trajectories indeed limit the magnitude of overshoot (resp. undershoot), but imply delayed undershoot (overshoot). In this sense, the disturbances related to the variations of the gas flow rate cannot be totally compensated for. We discuss the issue of practically achievable performance and suggest first to partly compensate for overshoots, second to limit the -risky- compensation of the undershoots.

The approach presented in this chapter is implemented in a specific feedforward control law, which, complemented with a feedforward law to reject T^{in} disturbances and a feedback law (both designed from results of Chapter 4), forms the actual controller presented in Chapter 6.

5.1 Explanation of overshoot on a simple model

In this section, we first present a simple model deduced from the reduced model. We give the formal expression of the output response to a step change in $L_c(t)$, for an arbitrary trajectory $\alpha(t)$, related to the actual control and forced to be uniform over the length $L_c(t)$. We show that, if $\alpha(t)L_c(t)$ is kept constant (the control being instantaneously changed to keep the same equilibrium output value), then the output response is subject to an overshoot. Then, we propose a trajectory that limits the overshoot magnitude, but induces an undershoot.

[1] This experimental approach is proposed in Lepreux et al. (2009*b*).

5.1.1 A simple model to understand the origin of overshoot

From the study of § 4.2, it can be verified that the model

$$\left\{\begin{array}{rcl} \dfrac{\partial T}{\partial t}(z,t) & + & v(t)\dfrac{\partial T}{\partial z}(z,t) = -k_1\left(T(z,t)-T_s(z,t)\right) \\ \dfrac{\partial T_s}{\partial t}(z,t) & = & k_2\left(T(z,t)-T_s(z,t)\right)+\Psi(z,u(t),v(t)) \end{array}\right.$$

is equivalent, at constant speed $v(t)=v$ and at order 0 in $\varepsilon = v/k_1$, with $\vartheta = k_1\, v/k_2$, to

$$\frac{\partial T(z,t)}{\partial t} + \vartheta \frac{\partial T(z,t)}{\partial z} = \Psi(z,u(t),v) \tag{5.1}$$

Now, consider a length $L=1$, $\vartheta = 1$ and $\Psi(z,u(t),v) = A(t)$ with

$$\left\{\begin{array}{ll} A(t)=\alpha(t), & 0 \le z \le L_c(t) \\ A(t)=0, & L_c(t) < z \le 1 \end{array}\right. \tag{5.2}$$

To summarize, focusing on the advection effect, we analyze step changes of L_c on the following system

$$\frac{\partial T(z,t)}{\partial t} + \frac{\partial T(z,t)}{\partial z} = A(t) \tag{5.3}$$

5.1.2 Existence of overshoot. Means to limit its magnitude

For $T(0,t)=0$, $L_c(t)=L_{c,1}$, and $\alpha(t)=\alpha_1$, the equilibrium is given by:

$$T(z,t) = \left\{\begin{array}{ll} \alpha_1 z & 0 \le z \le L_{c,1} \\ \alpha_1 L_{c,1} & L_{c,1} \le z \le 1 \end{array}\right.$$

From this equilibrium, assuming that $\alpha(t)$ follows a trajectory such that

$$d\Gamma(t)/dt = \alpha(t)$$

we have, as $L_c(t)$ is stepped from $L_{c,1}$ to $L_{c,2}$ ($L_{c,2} > L_{c,1}$) at $t=0$:

$$T(1,t) = \left\{\begin{array}{ll} \alpha_1 L_{c,1} & 0 \le t \le 1-L_{c,2} \\ \alpha_1 L_{c,1} - \Gamma(0) + \Gamma(t-1+L_{c,2}) & 1-L_{c,2} \le t \le 1-L_{c,1} \\ \alpha_1(1-t) - \Gamma(0) + \Gamma(t-1+L_{c,2}) & 1-L_{c,1} \le t \le 1 \\ \Gamma(t-1+L_{c,2}) - \Gamma(t-1) & t \ge 1 \end{array}\right.$$

The reader can refer to Appendix E.3 for details of computations.

Simultaneous step change in $L_c(t)$ and $\alpha(t)$: overshoot We assume that, as $L_c(t)$ changes from $L_{c,1}$ to $L_{c,2}$ ($L_{c,2} \ge L_{c,1}$), $\alpha(t)$ simultaneously changes from α_1 to α_2. To keep the same equilibrium value for $T(1,t)$, α_2 is chosen such that

$$\alpha_1 L_{c,1} = \alpha_2 L_{c,2}$$

Then, $\alpha_1 \ge \alpha_2$. In this case, $\Gamma(t) = \alpha_2 t$ and (see Fig. 5.1)

$$T(1,t) = \left\{\begin{array}{ll} \alpha_1 L_{c,1} & 0 \le t \le 1-L_{c,2} \\ \alpha_1 L_{c,1} + \alpha_2(t-1+L_{c,2}) & 1-L_{c,2} \le t \le 1-L_{c,1} \\ \alpha_1(1-t) + \alpha_2(t-1+L_{c,2}) & 1-L_{c,1} \le t \le 1 \\ \alpha_2 L_{c,2} & t \ge 1 \end{array}\right.$$

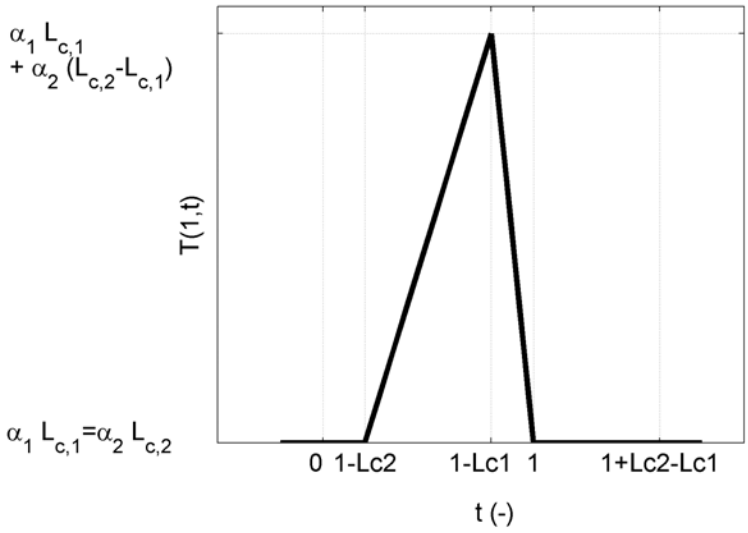

Figure 5.1: Plot of $T(1,t)$ to illustrate the existence of an overshoot when applying quasi-steady-state conditions

For t from 0 to $1 - L_{c,2}$, the output is constant to its previous value $\alpha_1 L_{c,1}$. At $t = 1 - L_{c,2}$, it begins to increase to reach its maximum $\alpha_1 L_{c,1} + \alpha_2(L_{c,2} - L_{c,1})$ at $t = 1 - L_{c,1}$. From that time, it decreases to reach its final value $\alpha_2 L_{c,2}$ at $t = 1$. There is an overshoot of duration $L_{c,2}$.

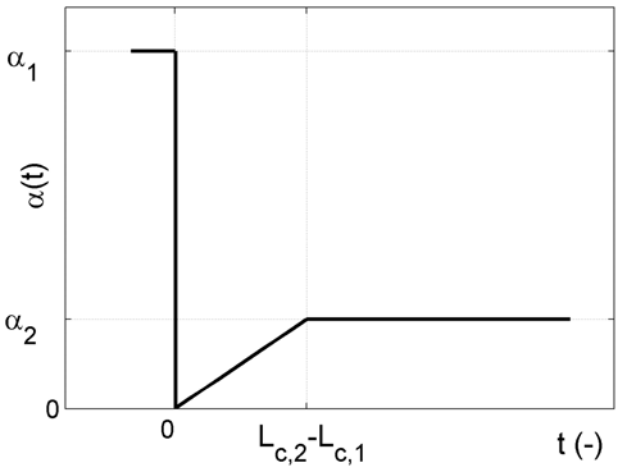

Figure 5.2: Profile of $\alpha(t)$ is plotted to illustrate the proposed compensation profile. Here, the length is changed from one constant value to another and the source term is updated to keep the same equilibrium point. Yet, during a period of time, an overshoot is observed at the outlet of the system

Limiting the overshoot Now, consider that $\alpha(t)$ (plotted in Fig. 5.2) follows a ramp, from 0 at time 0 to α_2 reached at $t = L_{c,2} - L_{c,1}$. From that time, $\alpha(t) = \alpha_2$:

$$\alpha(t) = \begin{cases} \dfrac{\alpha_2}{L_{c,2} - L_{c,1}} t & 0 \leq t \leq L_{c,2} - L_{c,1} \\ \alpha_2 & t \geq L_{c,2} - L_{c,1} \end{cases}$$

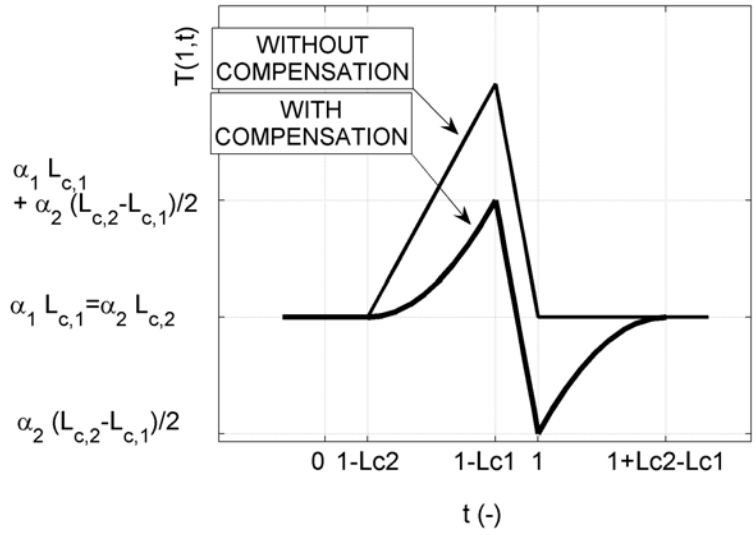

Figure 5.3: Profile of $T(1,T)$ is plotted to illustrate a partial overshoot compensation and the creation of a delayed undershoot. Compared to the result of Fig. 5.1, the overshoot has been divided by two.

Then, following computations details in Appendix E.3,

$$\Gamma(t) = \begin{cases} \dfrac{\alpha_2}{2(L_{c,2}-L_{c,1})}t^2 & 0 \le t \le L_{c,2}-L_{c,1} \\ \alpha_2 t - \dfrac{\alpha_2(L_{c,2}-L_{c,1})}{2} & t \ge L_{c,2}-L_{c,1} \end{cases}$$

and

$$T(1,t) = \begin{cases} \alpha_1 L_{c,1} & 0 \le t \le 1-L_{c,2} \\ \alpha_1 L_{c,1} + \dfrac{\alpha_2}{2(L_{c,2}-L_{c,1})}(t-1+L_{c,2})^2 & 1-L_{c,2} \le t \le 1-L_{c,1} \\ \alpha_1(1-t) + \alpha_2(t-1+L_{c,2}) - \dfrac{\alpha_2(L_{c,2}-L_{c,1})}{2} & 1-L_{c,1} \le t \le 1 \\ -\dfrac{\alpha_2}{2(L_{c,2}-L_{c,1})}(t-1)^2 + \alpha_2(t-1) + \dfrac{\alpha_2(L_{c,1}+L_{c,2})}{2} & 1 \le t \le 1+L_{c,2}-L_{c,1} \\ \alpha_2 L_{c,2} & t \ge 1+L_{c,2}-L_{c,1} \end{cases}$$

For t from 0 to $1-L_{c,2}$, the output is constant to its previous value $\alpha_1 L_{c,1}$. At $t = 1-L_{c,2}$, it begins to increase to reach its maximum $\alpha_1 L_{c,1} + \alpha_2(L_{c,2}-L_{c,1})/2$ at at $t = 1-L_{c,1}$. From that time, it decreases to reach the value $\alpha_2(L_{c,1}+L_{c,2})/2 = \alpha_1 L_{c,1} - \alpha_2(L_{c,2}-L_{c,1})/2$ at $t = 1$. From $t = 1$ it increases to reach its final value $\alpha_2 L_{c,2}$ at $t = 1+L_{c,2}-L_{c,1}$. Refer to Fig. 5.3. There is still an overshoot, but its maximum is *divided by two*. The counterpart is an undershoot that has the same magnitude than the overshoot. The total duration of the disturbance is increased by $L_{c,2}-L_{c,1}$.

5.2 Practical compensation of overshoot and undershoot

5.2.1 Compensation of overshoot

The overshoot phenomenon is caused by an increase in the gas flow rate[2]. This overshoot is problematic for the DPF regeneration because it increases the risk of DPF runaway. We want to sketch here how it can be compensated for.

As has been shown, the overshoot appears almost synchronously to the gas flow variation. Under driving conditions, the future values of the gas flow rate are unknown to the engine control system. So, as shown in § 5.1 an intuitive way to compensate for the overshoot is to reduce injection as soon as the gas flow increase is detected. In the experimental case presented in Fig. 5.4, one can see that this reduction is indeed effective. The consequence of this action is a delayed temperature

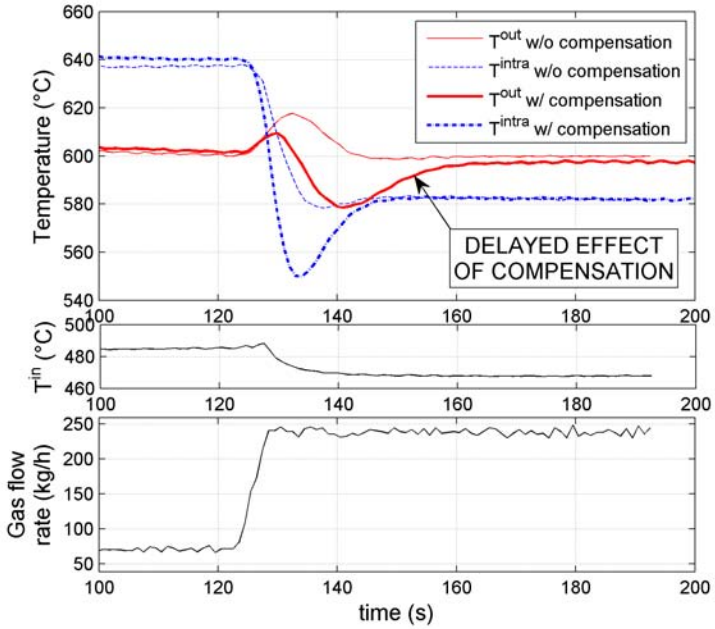

Figure 5.4: Catalyst undergoes a large increase in gas flow rate at $t \approx 125$ s. Without compensation, HC flow is adapted to keep a constant inlet HC concentration. With compensation, HC flow is temporarily reduced when the gas flow variation is detected. With compensation, the overshoot is attenuated but still present. Moreover, when compensating, a delayed undershoot appears consequently to the transient drop in heat supply. T^{in} is plotted for information but has no consequence on the describe phenomenon. Experimental data.

undershoot (as underlined in Fig. 5.4), which could be expected from the results of § 5.1. This is an important result for control application since undershooting does not increase the risks of DPF runaway. However, overshoot compensation is limited. First, because compensating totally for it creates a large delayed undershoot. It is usually better to allow a small overshoot in order to prevent large delayed undershooting. Second, because the gas flow rate increase corresponds to a fast increase in engine power request. Then, a significant quantity of disturbance reductants may be present in the engine exhaust gas. When this is the case, the overshoot cannot be avoided. In the scenario presented

[2]To properly analyze the experimental results, it should be noticed that the phenomena of "undershoot" and "overshoot" appear irrespective of whether the inlet temperature is rising or falling. As presented in § 3.5.1, T^{in} effects are highly delayed (because of the one-dimensional distributed state nature discussed in § 1.5). This is corroborated by experimental observations (see Fig. 5.6 for an example of a rising inlet temperature while the outlet temperature is undershooting).

in Fig. 5.5, it is shown that stopping late post-injection, for a rather long period, at the time of the gas flow rate detection "only" attenuates the overshoot. For robustness regarding unknown coming gas flow rate variations, late post-injection is stopped shortly after the beginning of the gas flow rate detection. The drop in heat supply, corresponding to stopping the late post-injection, is, in this case, not sufficient to completely compensate for this overshoot.

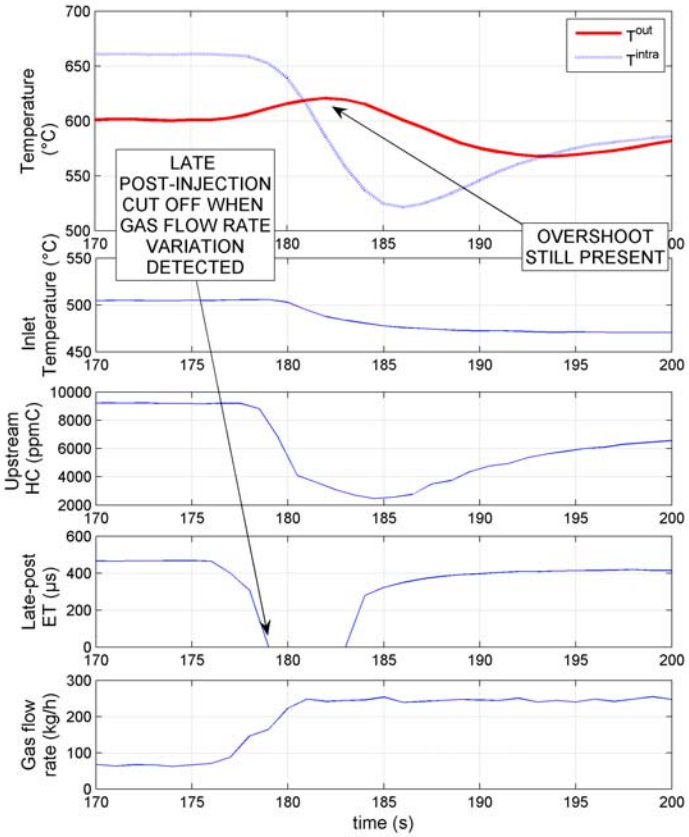

Figure 5.5: In this practical case, despite control HC flow rate of zero, overshoot is not totally compensated. The actuator (late post-injection) is stopped when the gas flow rate variation is detected. The detection is based on an algorithm using the filtered derivative of the gas flow rate. To ensure the algorithm robustness, the actuator energizing time (ET), which is the low-level control variable for u (see Appendix F), is "only" reduced at the beginning of the gas flow rate variation, and finally totally cut off (ET=0) "only" about 2 s after gas flow rate starts varying. Upstream HC is measured using a slow gas analyzer, and its time constant must be accounted for. Also, disturbance reductants flow rate may be significant during the increase in engine power (producing the increase in the gas flow rate). This is why HC measurement decreases slowly. Experimental data.

5.2.2 Compensation of undershoot: a risky strategy

The undershoot phenomenon, which was introduced in § 3.1.2.2, is caused by a decrease in the gas flow rate. Although it generates no particular risk of DPF damage, this variation is problematic for DPF regeneration. It increases the time required to oxidize the trapped soot and, in turn, also increases the fuel consumption. However, we want to show that it cannot be compensated without side effects.

To compensate for this undershoot, the HC flow rate can be increased. Two cases are worth discussions. First, under normal operating conditions, it is shown in Fig. 5.6 that the undershoot is not totally compensated by the above mentioned strategy. It is only reduced. It is worth noticing

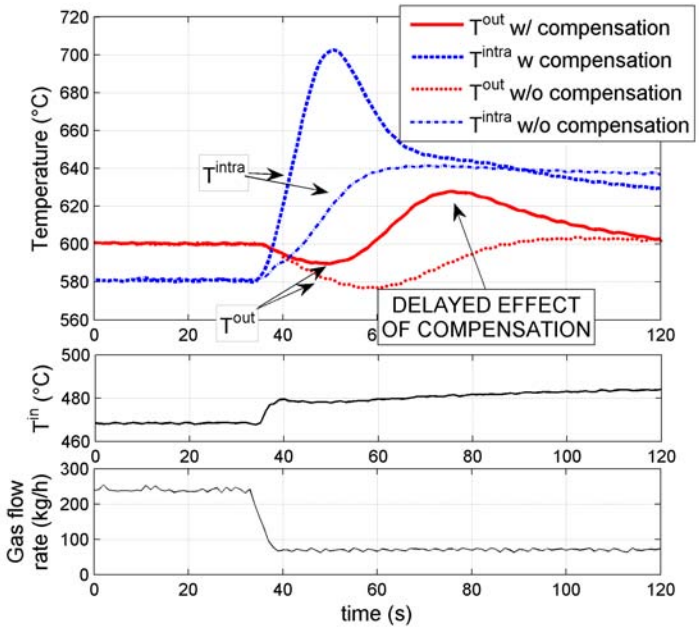

Figure 5.6: Catalyst undergoes a large decrease in gas flow rate at $t \approx 35$ s. When compensating the undershoot by a more-than-steady-state HC flow, a delayed overshoot appears consequently to the transient excess in heat supply. T^{in} is plotted for information but has no consequence on the described phenomenon. Experimental data.

that this action causes a delayed temperature overshoot (as can be noticed in Fig. 5.6). This delayed overshoot is caused by a pulse of injected HC during the gas flow drop. The larger the pulse is, the better the correction of the first undershoot is, but the larger the delayed overshoot is. Time between the pulse (and the gas flow variation) and the delayed overshoot is related to one-dimensional effects described in § 1.5. Referring to the scheme in Fig. 3.16b, the pulse acts in a distributed way on the reactive length L_c during the transient state. On the contrary, the undershoot is related to the gap between the reactive length and the transport length. Therefore, the pulse has no direct action on this gap: it acts always upstream. In fact, considering the involved time scales, the pulse effects and the supply gap effects are combined together and smoothed by diffusion effects. This explains why the undershoot is attenuated by the pulse. For the reasons mentioned previously, from a practical viewpoint, this delayed overshoot is not suitable. It is not easy to "re-compensate" for it, as this would imply an oscillatory highly-delayed control. Consequently, the undershoot must be carefully compensated for.

A second case is presented in Fig. 5.7. Compared to the latter case, the HC quantity is increased further. This allows the complete compensation of the undershoot. Nevertheless, it must be noticed that the amount of HC required at the inlet is very large. Moreover, as shown in Fig. 5.7, the amount of HC slipping to the outlet is also substantial. Hence, the DOC is saturated and the conversion efficiency plummets. It is interesting to note that the intra-catalyst temperature rises less in the second case than in the first one. This is because, in the second case, catalyst efficiency has dropped and more HC are oxidized close to the DOC outlet. In fact, by saturating the DOC, we forced the access to the L_c variable, which is, under normal operation, given by the external conditions (by the gas flow rate in

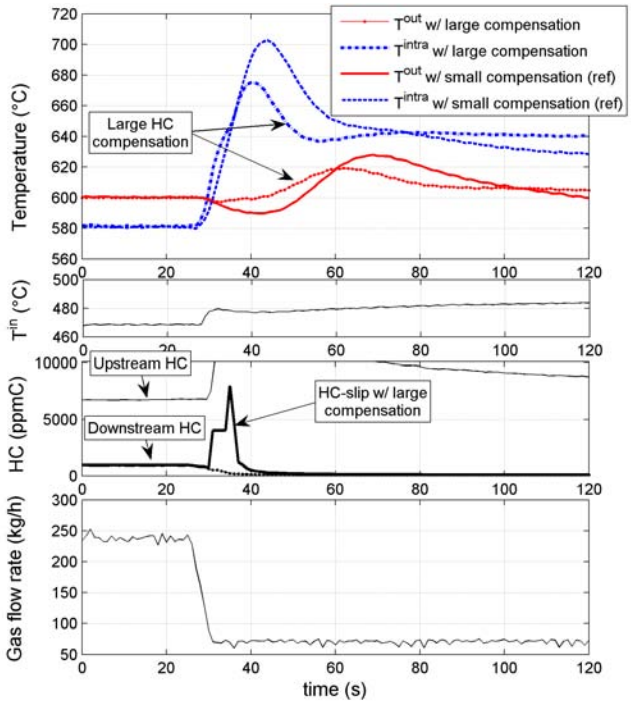

Figure 5.7: Large compensation for the undershoot (experimental data)

our modeling, see remark § 3.4.2.2). By this way, it is possible to compensate for the L_c decrease that would induce the decrease in gas flow rate. In other words, in the very special case of a huge level of inlet HC, in spite of the decrease in gas flow rate, the phenomena must be described as pictured in Fig. 5.8. Such phenomenon could be easily included in the model presented in § 3.4.2.2

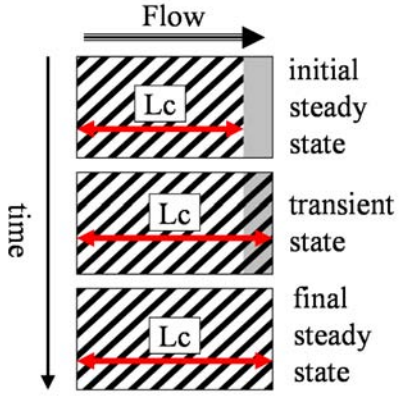

Figure 5.8: Phenomena involved in the special case of DOC saturation

by considering a growing L_c length versus HC concentration. However, it is not useful to complicate the modeling, because this "flooding" phenomenon must not be used in real applications. Saturations on the actuators must be implemented to prevent it.

We have shown that, although the compensation is physically possible, it clearly makes no sense to use it. As a conclusion, the undershoot phenomenon cannot be totally compensated for under normal operating conditions.

5.3 Conclusions

The simple advection model studied in § 5.1 helps to understand the overshoot phenomenon. The key aspect is the combination of heat storage and under-actuation, on a reactive length that is set by a disturbance, namely the gas flow rate. Means to limit the overshoot magnitude are also sketched in this section. Unfortunately, this overshoot compensation induces an undershoot. Section 5.2 illustrates the conclusions of § 5.1. Two scenarios of gas flow increase and gas flow decrease are analyzed through experimental observations. Practically, the temperature overshoot, which is caused by an increase in the gas flow rate, can most often be experimentally compensated for. The temperature undershoot, which is caused by a decrease in the gas flow rate, can be experimentally compensated for, but this causes high-level HC-slip, so it is advised not to try to totally compensate for it in practice. As a consequence, the achievable performance for the DOC outlet temperature control is limited. Depending on the tested DOC device, the expected range of performance would commonly not be better than $\pm 10°C$ to $\pm 20°C$ (or even worse). In chapter 6, following the lines of the approach described in § 5.1.2, a feedforward law is proposed, to limit the overshoot and undershoot effects due to gas flow rate variations. With the other feedforward control law design to reject the inlet temperature disturbances, and the feedback control law, both based on results of Chapter 4, this law forms the actual controller, presented in the next chapter.

Chapter 6

Proposed control strategy

6.1 Introduction

6.1.1 Control problem summary

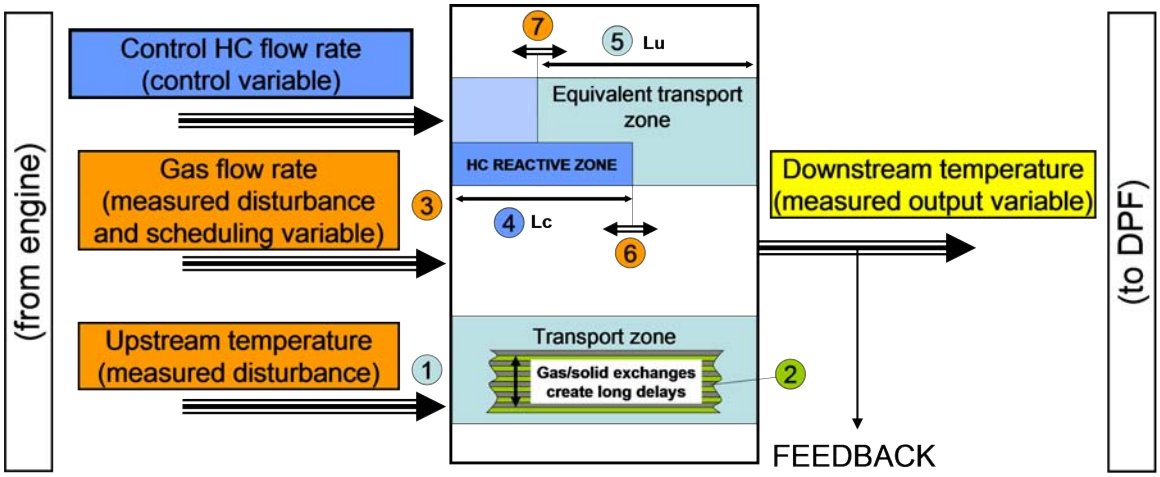

Figure 6.1: Control problem viewpoint after analysis of the thermal phenomena. Downstream temperature is the output variable. Control HC flow rate is the control variable. Inlet temperature variations (1) are propagating through the DOC, creating long delays due to gas/solid heat exchange (2). Inlet temperature is regarded as a disturbance. Delays value are strongly related to the gas flow rate (3). For the delays, gas flow rate (3) is regarded as a scheduling variable. Control HC flow is oxidized on a reactive length L_c (4). Control HC flow rate is regarded as a distributed control variable. Alternatively, it can be regarded as a boundary control variable equivalent to a temperature variation for a catalyst having an equivalent transport length L_u (5). Temperature rise corresponding to the control HC flow is strongly related to the gas flow rate (3), which is, once again, regarded as a scheduling variable. Gas flow rate (3) is not only a scheduling variable. When varying, it makes the reactive length - and the equivalent transport zone - vary (6 and 7). Then, it creates temperature disturbances inside the DOC. This is why it is also regarded as a disturbance.

Let us start by summarizing the physical analysis and simplified modeling of the thermal phenomena detailed in the previous chapters. Following along these lines, the control problem can be specified in the scheme presented in Fig. 6.1. In theory, the system is modeled by the proposed reduced model (3.4)-(3.5)-(3.6)-(3.7) as described in § 3.2. The conversion efficiency is taken into

account explicitly in the injection calculation of control input by (3.7). The output variable is the DOC outlet temperature, which must be controlled to a setpoint. Input variables are the control HC flow rate (u) and the disturbances: the inlet temperature (T^{in}), and the gas flow rate (so the speed v). Steady state value of the temperature response to the control HC is strongly related to the gas flow rate. The gas flow rate also governs the temperature dynamics response. For the inlet temperature and the control HC flow, the gas flow rate is regarded as a scheduling variable. Further, the gas flow must also be considered as a disturbance, because it has been shown that its variations (even under constant inlet temperature and constant oxidized reductants concentration) also create temperature effects at the DOC outlet due to variations of the reactive length.

6.1.2 Proposed control solution overview

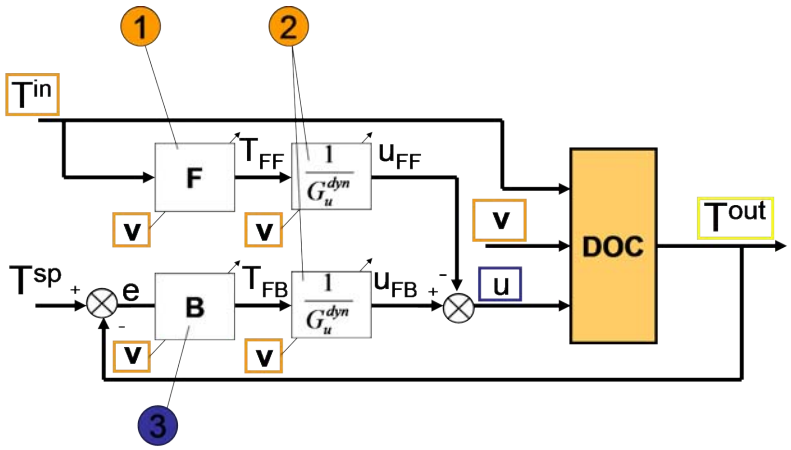

Figure 6.2: Advanced controller overview. Part (1) corresponds to feedforward control related to inlet temperature. Part (2) corresponds to feedforward control related to gas flow. Part (3) corresponds to feedback control.

From the previous description, a control strategy can be proposed. Our proposed strategy is implemented in three parts as schematized in Fig. 6.2. We will now detail these parts. First, a feedforward control law designed to handle inlet temperature disturbances is presented (block (1) in Fig. 6.2). Then, a feedforward solution accounting for the gas flow rate disturbance is detailed. It will appear that the actual solution consists of modifying gains (block (2) in Fig. 6.2). Finally, a simple feedback action is introduced (block (3) in Fig. 6.2).

Necessary adaptations to deal with disturbance reductants are detailed in Appendix A.

6.2 Feedforward treatment of inlet temperature

It has been shown in § 4.1.1 that a HC response can be approximated by an equivalent T^{in} response provided that an adaptation of the catalyst length is performed. Hence, *it is possible to compensate for effects of T^{in} by synchronizing them with delayed effects of HC*. As has been noted before, these delays are highly varying and have to be scheduled online. Thanks to the approximation to the advection-diffusion model, evaluation of the delay can be based on the implicit relation (4.35).

This section presents such an approach. The synchronizing method is based on the model from § 4.3. The analysis developed in § 4.2 allows us to schedule the controller parameters during gas flow transients.

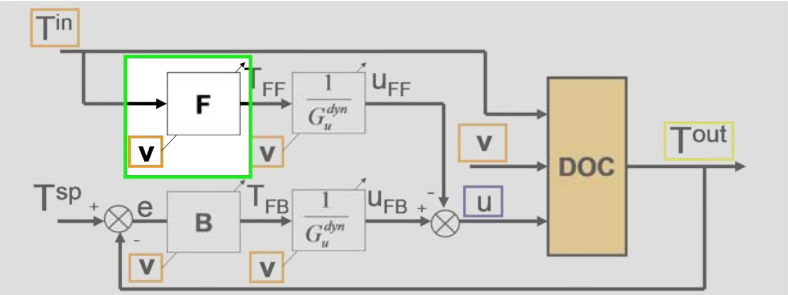

Figure 6.3: In this part, we focus on the feedforward treatment of T^{in}

In Fig. 6.4, a schematic view of the T^{in} effects and HC effects is presented. HC effects are

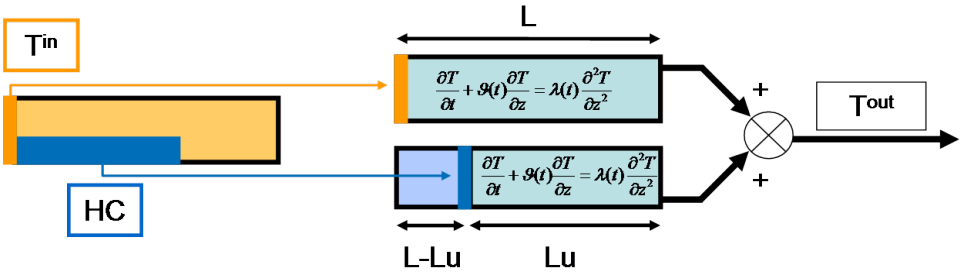

Figure 6.4: Temperature propagation from the advection diffusion modeling viewpoint. It grounds principles for T^{in} compensation. Propagation coefficients (ϑ and λ) are identical for T^{in} effects and HC effects. Hence, the difference in propagation length ($L - L_u$) plays a keyrole for T^{in} compensation.

assimilated to a front of temperature propagating on a fictitious length L_u, which is shorter than the DOC real length L. On the contrary, the T^{in} effect is propagating over the whole DOC length L. variable v is identical in both models, and in particular does not depends on z. In both sub-systems, propagation coefficients (ϑ and λ) are identical for T^{in} effects and HC effects. In the controller, these effects can be represented by two partial states. As pictured in Fig. 6.4, the synchronization between T^{in} and control HC must be considered on the first part of the DOC for the length difference $L - L_u$. Hence, from the advection-diffusion model viewpoint, the delay $\delta(t)$ to synchronize the inlet temperature variations with the control HC variations is simply given by the implicit equation, in which $\delta(t)$ is unknown and ϑ represents an apparent propagation speed.

$$L - L_u = \int_{t-\delta(t)}^{t} \vartheta(w)dw \tag{6.1}$$

Finally, the "F" block of the controller is simply a delay operator applying a delay value of $\delta(t)$

$$T_{FF}(t) = T^{in}(t - \delta(t))$$

Simulation Results : random inputs

Simulations are carried out with the reduced model (3.4)-(3.5)-(3.6)-(3.7) with a *constant* reactive length, so that the T^{in} compensation is isolated, as done in Appendix C.2.3 for a simpler control law based on first order plus delay models. The presented controller includes only the feedforward

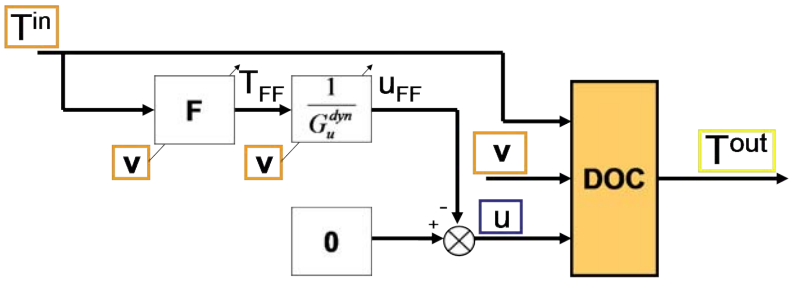

Figure 6.5: Test controller for feedforward treatment of T^{in}

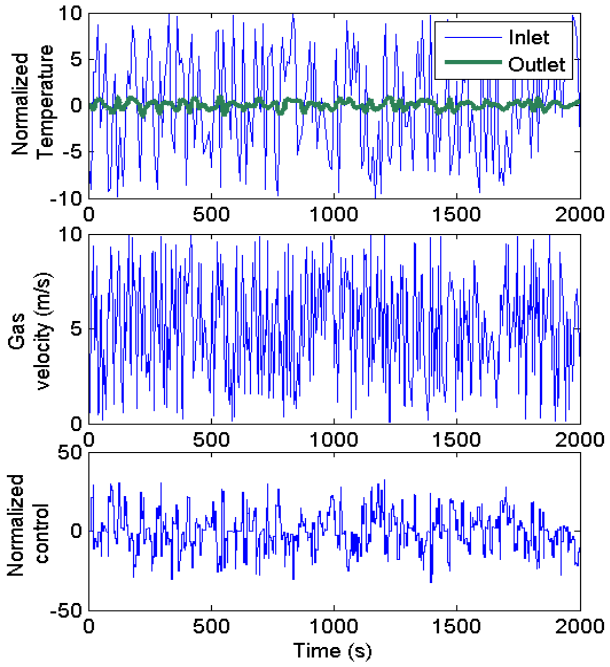

Figure 6.6: Results obtained by feedforward treatment of T^{in} on model (3.4). Inlet temperature variations are attenuated by a factor of 10 at the outlet even under high-amplitude gas velocity variations. Simulation data.

treatment of T^{in} as presented in Fig. 6.5. In this method, the adaptive gain G_u^{dyn} noted in Fig. 6.5 is chosen equal to the steady-state gain calculated with (3.3). The gain G_u^{dyn} will be adapted dynamically for feedforward gas flow rate compensation in the next part (see § 6.3).

In the simulation, the inlet temperature varies every 10 s randomly between -10 and 10. These variations should be compared to the outlet temperature variations. The channel gas speed varies every 5 s randomly between 0.1 m s^{-1} and 10 m s^{-1}. These represent indeed large gas speed variations in the sensitive zone of low gas speed values (corresponding to high delays). As a result of the controller, at the DOC outlet, temperature variations are attenuated between -1 and 1. Obtained results are reported in Fig. 6.6. The frequency of the variations are representative of those of a driving cycle, whereas the magnitude of the variations are greater than those taking place in a driving cycle. This situation is unfacilitating for the DOC controller.

6.3 Feedforward treatment of gas flow rate

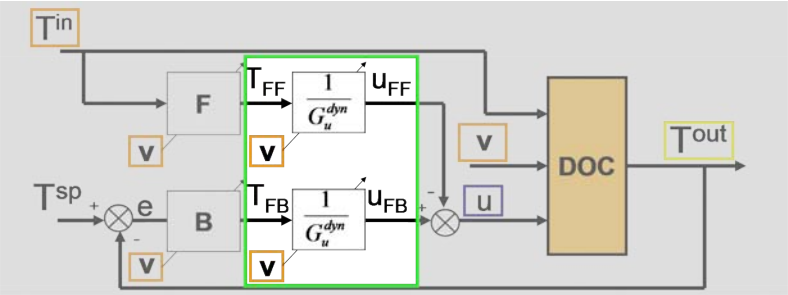

Figure 6.7: In this part, we focus on the feedforward treatment of gas flow rate. This is done by using the "adaptive" gain G_u^{dyn}.

It has been established in § 3.3.2 that gas flow variations cause undesired outlet temperature evolutions. In this section, we present an approach to compensate for this disturbance, according to considerations discussed in Chapter 5. An easy-to-implement dynamic gain adaptation is used, based on the time derivative of the gas flow rate. Such an approach is pictured in Fig. 6.7. Its behavior is illustrated by a simulation, carried out with model (3.4)-(3.5)-(3.6)-(3.7). The actual method mimics

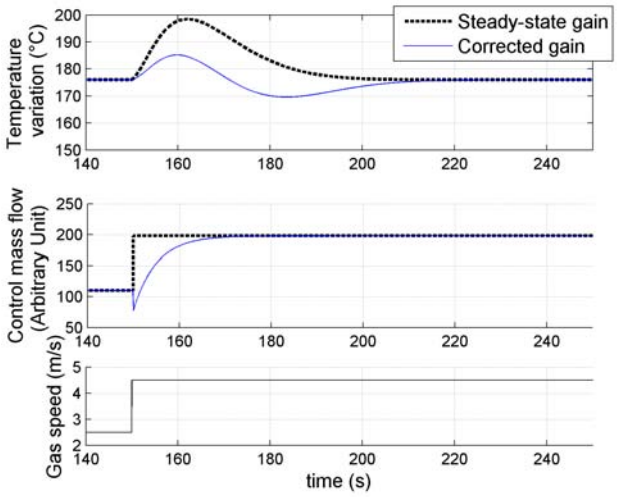

Figure 6.8: Overshoot compensation based on gas flow derivative. Simulation data.

the ramp variation described in § 5.1.2. It consists of a transient modification of the gain. A filtered derivative of the speed $v(t)$ is computed. The filter is a first order filter with time constant τ_B. The filtered derivative is normalized with the current value of the gas flow rate, and multiplied by a gain K_B to give a correction term X. The gain eventually G_u^{dyn} used is given by $G_u^{dyn} = G_u/(1-X)$. According to this relation, a rise (resp. decrease) of $v(t)$ induces a rise (resp. decrease) of X: the value G_u^{dyn} of the gain is then smaller (resp. larger) than the values of the static gain G_u. Accordingly, the control HC u is less than what is required to keep T^{out} constant. While $v(t)$ stabilizes to a new constant value, its derivative tends to 0. Then, X tends toward 0 and, as G_u^{dyn} tends toward G_u, the control HC u takes the value that is required to reach T^{out} setpoint. In details,

$$\frac{1}{G_u^{dyn}(t)} = \frac{1-X(t)}{G_u(t)} \tag{6.2}$$

where $X(t)$ is given by $Y(t)/v(t)$, $Y(t)$ corresponds to the inverse Laplace transform of $\hat{Y}(s)$ given by

$$\hat{Y}(s) = \frac{K_B s}{1 + \tau_B s} \hat{v}^{sat}$$

and v^{sat} is the saturated value of the current gas flow rate. This saturation corresponds to the saturation of the length L_c in (3.6).

K_B is a tuning parameter corresponding to compensation strength. The greater K_B is, the more the control HC flow is adapted during gas flow transients. If set too high, this parameter will favor side effects described in Chapter 5. Besides, τ_B is a tuning parameter corresponding to a time during which the compensation acts after a gas flow variation. Referring to § 5.1.2, it should be theoretically adapted to the current variation of L_c. However, in practice, this extra tuning is not needed since the correction is already quite efficient with constant parameter values.

A drawback of this method is that it may lead to HC peaks during gas flow drops. However, as the effects of gas flow drops are temperature undershoots, compensation is not critical, and the strategy can be less aggressive than during gas flow rises. Setting a small value of K_B during this phase is a good solution.

Another implementation detail is that, depending on the controller sample time, and because of the strictly causal filtering, a significant delay can be undergone before the detection of the gas flow variation becomes significant in the gain dynamic effect while the gain steady-state effect (G_u of (6.2)) has a direct transfer. This can be easily circumvented by delaying in turn the static gain G_u. This limits large temperature overshoots during gas flow increases.

The main advantage of this method is that it is extremely fast to compute. It is also interesting to notice that the use of a filtered derivative ensures a high stability regarding the noisy gas flow sensor.

6.4 Feedback control

As has been detailed before, control HC effects for a catalyst length of L are equivalent to boundary temperature effects for a catalyst length L_u. A variation of HC is interpreted as a boundary condition $T(z = 0, t) = T_{eq}^{in}(t)$ of system (4.9) over a propagation length L_u. Applying results of § 4.2.3, HC response time calculation can be based on the evaluation of the following implicit equation in which δ_{L_u} is unknown

$$L_u = \int_{t-\delta_{L_u}(t)}^{t} \vartheta(\tau) d\tau \tag{6.3}$$

For an HC step input, δ_{L_u} is the time at which the outlet temperature reaches about half its steady-state value.

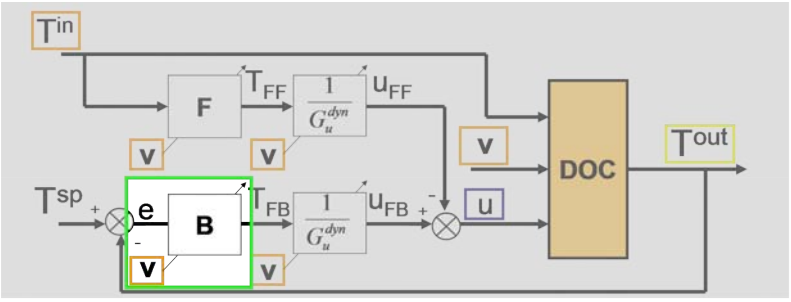

Figure 6.9: In this part, we focus on the feedback control

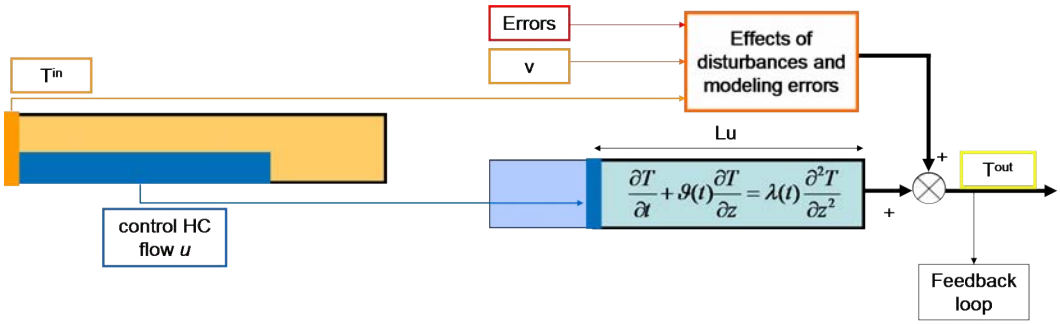

Figure 6.10: Phenomena governing control HC dynamic effects. Effects are propagating over the "transport" length L_u. Corresponding response time is used in feedback control design.

6.4.1 Actual feedback control

It has been shown in § 3.5 that, in practice, DOC outlet temperature cannot be perfectly controlled due to changes of reactive zone during gas flow variations. Typically, for a 4-inch long DOC, practical achievable performance is about ± 15°C. This observation is a big concern because this result is close to the performance requested for real applications. Therefore, the feedback control in this zone cannot be totally turned off (as would be done for example by a deadzone management) but it has to be very "slow". Typically, in this zone, it is not possible to use a classic feedback control law (as proposed for example in Appendix B and enhanced in § 6.4.2) because error to setpoint is related to non-compensable (weakly-compensable) disturbance effects.

To compensate for steady-state errors, an integral action is used. For the experiments presented in Chapter 7, integral time is set to $\tau_i = 2 \cdot \delta_{L_u}$. It means that, for a given gas flow rate, integral time is set equal to the duration of the "whole" HC effect. Finally, typical feedback action would set in Fig. 6.9 the "B" block of the controller to a simple integral term

$$T_{FB} = \int_0^t \frac{1}{\tau_i(w)} \left(T^{sp}(w) - T^{out}(w)\right) dw$$

6.4.2 Other feedback control possibilities

Scheduling classic feedback control for changes of setpoint

In the previous section (§ 6.4.1), the proposed feedback control law is designed to stay unaffected by non-compensable disturbance effects. These disturbances affect only a limited temperature zone. Hence, they become dominant when the error between the temperature setpoint and the measure ($T^{sp} - T^{out}$) is within the order of magnitude of the size of this small zone (typically ± 15°C for our device).

Using this feedback control law for large values of $|T^{sp} - T^{out}|$ is not sufficient, because the integral action is not strong enough. This situation happens (for example) when the regeneration controller is started. At that time, the DOC outlet temperature is around 450°C whereas the temperature setpoint is around 600°C.

In these situations, classical laws can be used. An attractive solution is to ground these laws on a first-order plus delay model such as the one presented in Appendix C. This control design was the work of Lepreux et al. (2009*a*). These laws require little calibration effort because the first-order plus delay model parameters τ_c and δ_c can be computed from the model of Chapter 4.

A drawback of the method is that the parameter adaptation is designed at a constant gas flow rate, and adapting directly the parameters value to the gas flow rate value may not be efficient.

To circumvent this, a method to schedule the parameters upon the gas flow rate is developed. On one hand, in Appendix C, the HC step response of model (4.1) is studied at constant gas flow rate. On the other hand, in § 4.2, equation (4.1) is approximated by equation (4.9) especially well for a reference point, which, furthermore, corresponds to the inflexion point of the response (4.32). We relate results of Appendix C to results of § 4.2 by matching the inflexion point t_I of the HC step response to the reference point of (4.1)

$$\delta_{L_u} = t_I \tag{6.4}$$

It leads to

$$\frac{k_1 L_u}{v} = k_2 \, \delta_{L_u} \tag{6.5}$$

Then, we get from (B.16)

$$\begin{cases} \tau_c = \dfrac{1 - T_h(z, \delta_{L_u})}{\exp(-2k_2\delta_{L_u}) k_2 \mathrm{I}_1(2k_2\delta_{L_u})} \\ \delta_c = \delta_{L_u} - \dfrac{1 - T_h(z, \delta_{L_u})}{\exp(-2k_2\delta_{L_u}) k_2 \mathrm{I}_1(2k_2\delta_{L_u})} \end{cases} \tag{6.6}$$

Parameters τ_c and δ_c of the first order plus delay model can be calculated online. Using this method easily allows an accurate description of the HC response and, further, to schedule the parameter adaptation during gas flow variations. The first order plus delay model is straightforwardly accounted for in the feedback control laws presented in Appendix C (these are PI, PID, and, Smith predictor).

Remark. Internal model represents an interesting option to remove the non-compensable effects from the feedback signal. If developed, such a model could allow more reactive strategies in the weakly-compensable error zone.

6.5 Conclusions

In this chapter, a control strategy derived from analyses of the previous chapters is presented. It is divided into three parts. The disturbance T^{in} is compensated by a feedforward strategy based on the application of a delay between the disturbance detection and the control HC action. The gas flow rate disturbance is treated by a gain adaptation. Its action attenuates the overshoot and undershoot phenomena caused by gas flow rate variations while limiting side effects. Finally, a simple feedback law is proposed. It is chosen weakly reactive so that it is undisturbed by non-compensable disturbance effects. The proposed control strategy is experimentally validated in the next chapter.

Chapter 7

Experimental results

In the previous chapter, we have presented different possible solutions for the controller subsystems: T^{in} feedforward control, gas flow rate feedforward control, and feedback control. From these, one complete controller scheme was constituted. We now present it along with obtained experimental results. We detail our implementation methodology, with a particular focus on the required calibration effort. General calibration principles for the engine during regeneration phases are explained in a dedicated part in Appendix G. In the second part of this chapter, experimental results obtained on the engine testbench are presented. The reader can refer to Appendix F for details on the experimental setup.

7.1 Controller used for experimental results

7.1.1 Controller

The control problem is pictured in Fig. 7.1. Input and output variables are:

- DOC downstream temperature is the output variable;
- control HC flow rate is the control variable;
- inlet temperature and gas flow rate are measured disturbances;
- disturbance reductants flow rate (undesired gas composition) is an unmeasured disturbance.

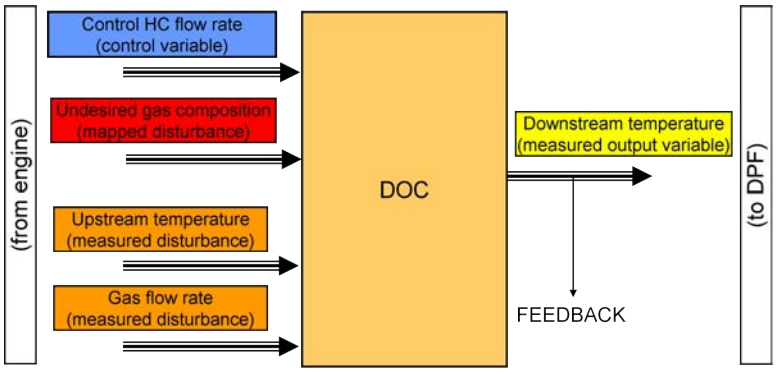

Figure 7.1: Input-to-output control problem.

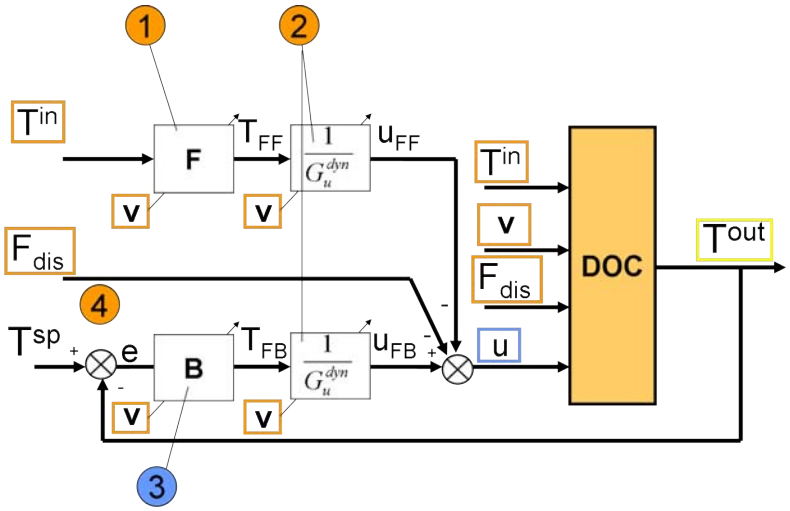

Figure 7.2: Advanced controller overview.

Controller overview is pictured in Fig. 7.2. Its design is divided into four parts:

(1) a feedforward control law for T^{in}

(2) an adaptation law for the gain G_u^{dyn} that handles gas flow rate disturbances

(3) a feedback control law

(4) a correction to account for disturbance reductants F_{dis}

(1) T^{in} feedforward control law

The "FF" block applies a delay $\delta(t)$,

$$T_{FF}(t) = T^{in}(t - \delta(t))$$

where $\delta(t)$ is obtained by solving the following implicit equation

$$L - L_u = \int_{t-\delta(t)}^{t} \vartheta(w)dw$$

(2) G_u^{dyn} adaptation law

$$\frac{1}{G_u^{dyn}(t)} = \frac{1 - X(t)}{G_u(t)}$$

where $X(t)$ is given by $Y(t)/v(t)$, $Y(t)$ corresponds to the inverse Laplace transform of $\hat{Y}(s)$ given by

$$\hat{Y}(s) = \frac{K_B s}{1 + \tau_B s}\hat{v}^{sat}$$

(3) Feedback control law

We use a feedback action u_{FB} defined by

$$u_{FB}(t) = \frac{1}{G_u^{dyn}(t)} \int_0^t \frac{1}{2 \cdot \delta_{L_u}(w)} \left(T^{sp}(w) - T^{out}(w) \right) dw$$

where $\delta_{L_u}(t)$ is obtained by solving the following implicit equation

$$L_u = \int_{t-\delta_{L_u}(t)}^{t} \vartheta(w) dw$$

Remark. In practice, integral time is saturated for low values.

(4) Accounting for F_{dis}

Here, the late post-injection is used as actuator, response to the disturbance reductants (corresponding to undesired engine exhaust gas composition) are similar to those to the control HC. Hence, the control HC flow rate u is computed by a simple subtraction of the estimated disturbance reductants flow rate F_{dis}. The reader can refer to Appendix A for further explanations.

7.1.2 Methodology and calibration effort for the DOC controller

Generally, the low to medium gas flow rate zone is the most difficult to control. By contrast, almost no time should be spent for calibration of the high gas flow rate zone. The calibration of the controller is divided into 3 steps. We now detail these.

Step 1 - HC dynamics

Experiments Engine operating points are chosen inversely spaced with the gas flow rate. Typically, five or six operating points are selected. For each chosen engine operating point corresponding to a gas flow rate value, open-loop control HC step responses are obtained. A typical response to control HC step profile for calibration results in T^{out} is pictured in Fig. 7.3. To get T^{out} steps close to

Figure 7.3: Illustration of a typical $T^{out} - T^{in}$ profile caused by control HC u step increases and decreases. T^{in} remains roughly constant during the test.

pre-defined values (for example 50°C), control HC flow rate can be easily pre-evaluated using the following approximate relation: 100°C increase corresponds to 5000ppmC of HC. This corresponds to the static gain detailed in (3.3).

Computations DOC geometric and material data are known. Then, k_2 is computed using these data and (3.18). The set of parameters (k_1, L_u) is identified to HC step responses using (4.8). Finally, k_1 is chosen constant to minimize the variability of constants a_u and b_u.

On-line calibration time Few days (typically four days).

Step 2 - Build steady-state gain and efficiency look-up tables

Experiments Results of previous experiments are used.

Computations Because of the lack of reliability in the absolute value given by the gas analyzers (for the presented controller settings), it is preferred to account for the gain and the HC conversion efficiency together. Results are analyzed in terms of temperature variations upon gas flow rate and control HC flow rate, in order to directly get the look-up table of $\eta\,\Delta H_u$ upon v (or F). This leads to a gain such as presented in Fig. 3.3 of § 3.1.1. This approach is relevant because the final objective is to control a temperature. We try to skip intermediate mappings.

Then, this global approach does not give the conversion efficiency map such as presented in Fig. 3.5. This information is also, to a minor degree, useful. First, it allows the consistency with the previous global method to be checked (drift must be checked in particular). Also, it is necessary to roughly estimate the conversion efficiency in order to evaluate HC flow rate at the DOC outlet. This HC quantity is oxidized on the DPF (which is usually catalyzed), causing direct heat supply in the DPF. At very large gas flow rates, this quantity may be significantly high, and it may be useful to decrease the DOC outlet temperature setpoint consequently. For these purposes, efficiency need not be known precisely and can be computed using the gas analyzers. The reader can refer to Appendix G.4 for a coarse identification method of the conversion efficiency.

Step 3 - v-transients

Experiments Fast drop-to-idle transient tests are performed.

On-line tuning Constant τ_B is set to $1/k_2$. Open-loop control is used during the transients, i.e. feedback control **(4)** of the controller presented in § 7.1.1 is not active. Parameter K_B is tuned so that no overshoot is obtained and HC-slip are prevented ($K_B \approx 4$).

On-line calibration time Typically two days.

Verification of model parameters Experimental transient data are matched against simulation data using the reduced model. Values of k_1 and k_2 for the model may be slightly tuned if necessary. This verification procedure usually takes one day.

Total calibration time

On overall, the controller calibration time is six or seven days of testbench experiments and a couple of days of offline analysis.

7.2 Experimental results

In this section, three practical cases using the temperature controller are presented. The first experimental result corresponds to a large drop in the gas flow rate, which is a difficult situation to handle. The second result illustrates the controller ability to deal with large and dynamic gas flow transients. The third experimental result is a European urban driving cycle, which is the most difficult part of the NEDC cycle in terms of control application (lowest flow rates, largest delays).

7.2.1 Scenario 1: large gas flow rate variations

Application interest This situation is close to a drop-to-idle situation. It corresponds to a realistic and problematic case of interest. This situation happens typically when a vehicle switches from motorway driving to urban driving. Once the regeneration process has started, in order to save fuel, regeneration time and catalyst wear, it is better to continue the regeneration process.

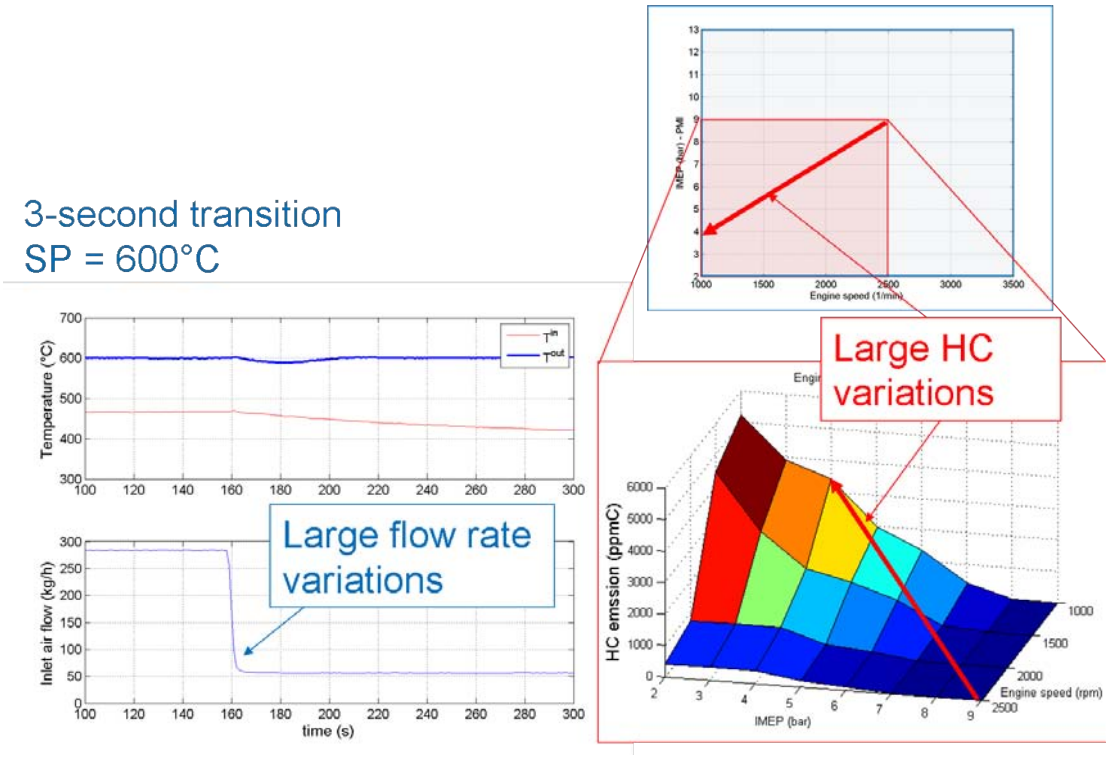

Figure 7.4: Results of T^{out} control during drop in gas flowrate. The DOC outlet temperature error remains within ± 11°C. Experimental data obtained with a 3-inch long DOC.

Control difficulties Drop-to-idle tests are among the most difficult situations to control. Control difficulties in this kind of situations are that

1. large drop in gas flow rate implies large non-compensable temperature effects (undershoot);
2. large drop in gas flow rate implies large delay variation. Also, final delay (i.e. the delay after the variation) is very large;
3. disturbance reductants flow is varying to a large extent.

Note that the presented case does not exactly correspond to an "idle" point. This is because it is difficult to keep a reasonable DOC inlet temperature level (see T_{min} in the engine calibration constraints of § G.2). Corresponding level of disturbance reductants is high, and it varies so that there is a real need to estimate them. Theoretical estimation is beyond the scope of this work. Empirical estimation is difficult because of the emissions variability. On low-load low-speed engine operating points, disturbance reductants cause inlet-to-outlet steady-state temperature rise as high as 100°C with high variability. A little time has been spent on this point with this setup. It has been preferred to focus on another setup to obtain the results presented in § 7.2.3.

In Fig. 7.4, inlet gas flow rate sensor measurement is represented. At $t \approx 160$ s, the engine operating point is changed in a 3-second transition from 2500 rpm - 9 b (IMEP) to 1000 rpm - 4 b (IMEP). From this time the inlet temperature continuously decreases in a medium range. One can report to Fig. 7.4 to get the corresponding steady-state disturbance HC emissions levels.

Remark. Large gas flow increase cause temperature overshoot, which must be compensated by feedforward control. Using filter derivative-based detection is not fast enough to totally compensate for it. Adding a small delay in the gain adaptation looks promising to further reduce the overshoot (method has not been tested experimentally). However, more generally, and regardless of the gas flow rate feedforward control strategy achievable performance, dealing with large gas flow increase is easier than dealing with gas flow decrease because the final delays (delays after the variation) are small. Small-delay situations can be efficiently treated by feedback control. Also, disturbance reductants flow rate is zero in this situation.

7.2.2 Scenario 2: experimental full range cycle

Application interest The situation presented in Fig. 7.5 corresponds to large and dynamic gas flow transients. It corresponds to an aggressive driving situation.

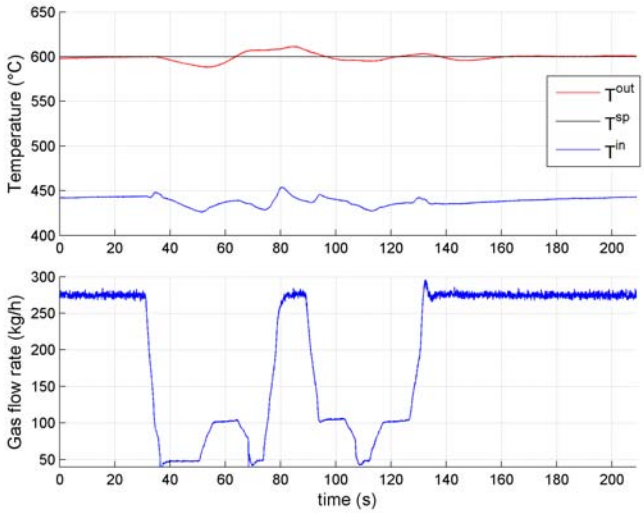

Figure 7.5: Results of T^{out} control during large gas flowrate variations. The DOC outlet temperature error remains within $\pm 10°$C. Experimental data obtained with a 4-inch long DOC.

Control difficulties This test stresses the controller ability to deal with large and frequent gas flow rate variations. These variations are higher and more frequent than those taking place during a normalized driving cycle (such as the one presented § 7.2.3). Then, this situation might seem more difficult to control. However, this is not the case, because, in this situation gas flow rate often increases to high values. When these values are reached, the delay gets very small and the presented feedback control is very efficient. Hence, these high gas flow rate values regularly "reset" the history in the DOC, which can be viewed as a finite memory system, as well as feedforward correction errors. This is described by the general formula

$$z_p = \int_{t-\delta(t)}^{t} \vartheta(w) dw$$

in which δ is small when ϑ is high.

7.2.3 Scenario 3: experimental urban cycle

Application interest The test presented in this section corresponds to the urban part of the NEDC European driving cycle. It is composed of four ECE driving cycles. NEDC cycle is normalized and is used in European countries for regulation tests. It is usually run when the engine is cold to test engine pollutant emission levels. However, DPF regeneration phases are started with warm engine. So, the presented test is run when the engine is already warm.

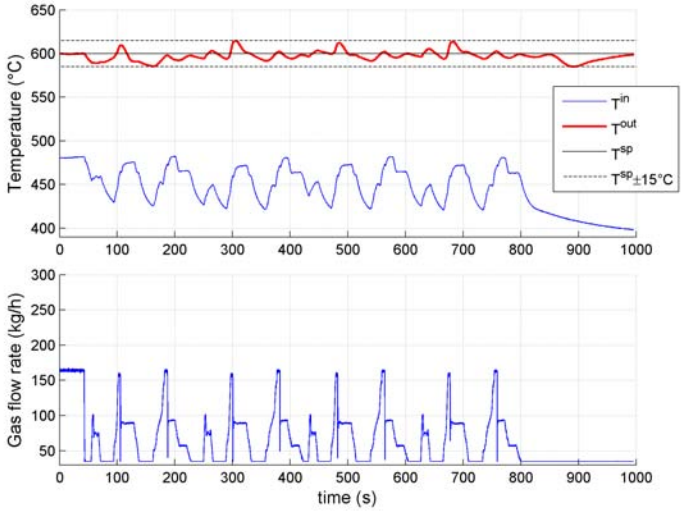

Figure 7.6: Results of T^{out} control for the urban part of the NEDC driving cycle. The DOC outlet temperature error remains within ± 15°C. Experimental data obtained with a 4-inch long DOC.

Control difficulties Although this test (presented in Fig. 7.6) is less aggressive than the full range cycle presented in the previous section (§ 7.2.2) for example, it represents one of the most difficult situation to control, together with the drop-to-idle test. In fact, operating points are continuously in difficult to control zones, which gather the four following difficulties:

- zones where delays vary on the sensitive part of the "hyperbolic" curve as pictured in Fig. 7.7;
- zones where the length of combustion is strongly impacted, leading to large and frequent non-compensable disturbance effects;
- zones where the inlet temperature largely varies;
- zones where the disturbance reductants flow rate largely varies.

Hence, testing larger and more frequent variations are not more difficult to control. Then, this experiment is considered particularly relevant to test the controller performance.

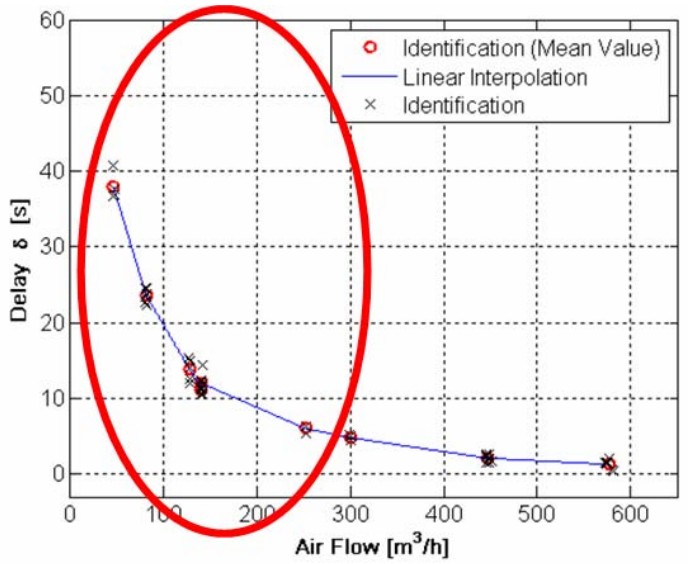

Figure 7.7: Illustration of delays involved during a urban cycle. Experimental data are identified to a first order plus delay model using a least mean-square algorithm.

7.3 Conclusions

Advanced control strategy has been tested on an engine testbench. The controller, which requires about eight days of calibration, has been detailed, as well as the calibration procedure. Experimental results are close to the best achievable performance (see Chapter 5) in the worst case situations: urban driving cycle and large gas flow rate transients. In particular, performance on the urban part of the normalized NEDC cycle obtained with a 4-inch long DOC is $\pm 15°$C about the setpoint value.

Conclusion and perspectives

In this manuscript, the problem of the thermal control of a DOC (Diesel Oxidation Catalyst) as used in aftertreatment systems of diesel vehicles has been studied. It has been stressed that the one-dimensional distributed nature of the DOC causes long and largely varying time responses of the outlet temperature (measured output variable) to HC flow (control variable). Besides, the DOC is subject to large and frequent disturbances. It is shown that a model-based approach successfully addresses the problem of DOC outlet temperature control. The proposed controller has few parameters and requires light calibration effort. It describes the main physical observations that can affect the control performance. The proposed strategy synchronizes the inlet temperature (measured disturbance) to the HC flow (control variable). Further, an additional feedforward control strategy partially compensates for effects related to gas flow rate variations (measured disturbance). The feedback control law is based on the delay evaluation from a parameterized model, which is derived from a proposed reduced model. Altogether, the solution proves to be efficient on an engine testbench. It leads to a control performance among the best practically achievable results: for the tested 4-inch long DOC, ± 15°C on the urban part of the urban part of a NEDC cycle.

For practical implementation The reader can report to Chapter 7 for a detailed presentation of the proposed control solution and experimental results.

Perspectives An important perspective would be to account for the catalyst ageing, which causes a decrease in the catalyst activity. In this situation, it is erroneous to assume that the combustion zone starts at the catalyst inlet. To account for this, our idea is to shift the reactive zone towards the catalyst outlet simply as is pictured in Fig. 7.8.

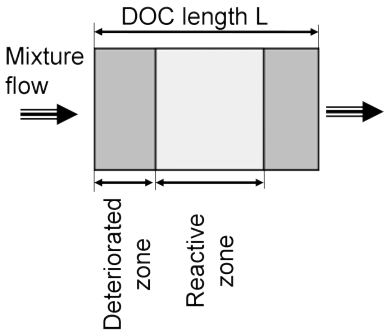

Figure 7.8: Model reactive zone

In term of control design, this would simply require the addition of a drift law for the beginning of reactive length over the time. Certainly, the study of this law would require investigations. Also, more complex combustion profiles could be considered. It is important to remark that the structure

of the proposed control law is not impacted by such model modifications. The oxidation of control HC would simply take place closer to the DOC outlet, yielding faster temperature responses. On the other hand, the inlet temperature disturbance still acts at inlet boundary. Therefore, the delay between the inlet temperature disturbance and the control HC flow rate in the synchronization technique is increased.

Bibliography

Abramowitz, M. & Stegun, I. A. (1965), *Handbook of mathematical functions*, Dover Publications.

ACEA (2009), 'Diesel - Historical series by country in Western Europe 1990-2009', Available online: http://www.acea.be/. European Automobile Manufacturers' Association.

Achour, L. (2001), Dynamique et contrôle de la régénération d'un filtre à particules Diesel, PhD thesis, École des Mines de Paris.

AECC (2007), 'Association for emissions control by catalyst', Available online: http://www.aecc.eu/.

Auto-innovations EURL (2007), 'Auto-innovations', Available online: http://www.auto-innovations.com/.

Barraud, J. (2006), Commande de procédés à paramètres variables, PhD thesis, École des Mines de Paris.

Benjamin, S. F. & Roberts, C. A. (2004), 'Automotive catalyst warm-up to light-off by pulsating engine exhaust', *Int. J. Eng. Res.* **5**, 125–147.

Bianchi, G. M., Falfari, S., Brusiani, F., Pelloni, P., Osbat, G. & Parotto, M. (2005), 'Numerical investigation of critical issues in multiple-injection strategy operated by a new c.r. fast-actuation solenoid injector'. SAE paper 2005-01-1236.

Bisset, E. (1984), 'Mathematical model of the thermal regeneration of a wall-flow monolith diesel particulate filter', *Chem. Eng. Sci.* **39**, 1232–1244.

Cannon, J. R. (1984), *The one-dimensional heat equation*, Vol. 23 of *Encyclopedia of Mathematics and its applications*, Addison-Wesley Publishing Company.

Chen, D. K. S., Bisset, E. J., Oh, S. H. & Ostrom, D. L. V. (1988), 'A three-dimensional model for the analysis of transient thermal and conversion characteristics of monolithic catalytic converters'. SAE paper 880282.

Corriou, J.-P. (2004), *Process control: theory and applications*, Springer.

Danckwerts, P. (1953), 'Continuous flow systems. Distribution of residence times', *Chem. Eng. Sci.* **2**, 1–13.

Depcik, C. (2003), Modeling reacting gases and aftertreatment devices for internal combustion engines, PhD thesis, Ann Arbor, Michiganr: The University of Michigan.

Depcik, C. & Assanis, D. (2005), 'One-dimensional automotive catalyst modeling', *Prog. Energy Combust. Sci.* **31**, 308–369.

Dubien, C., Schweich, D., Mabilon, G., Martin, B. & Prigent, M. (1998), 'Three-way catalytic converter modelling: fast- and slow-oxidizing hydrocarbons, inhibiting species, and steam-reforming reaction', *Chemical Engineering Science* **53**(3), 471–481.

Ecopoint Inc. (2008), 'DieselNet', Available online: http://www.dieselnet.com/.

Frobert, A., Creff, Y., Lepreux, O., Schmidt, L. & Raux, S. (2009), 'Generating Thermal Conditions to Regenerate a DPF: Impact of the Reductant on the Performances of Diesel Oxidation Catalysts'. SAE Paper 2009-01-1085.

Frobert, A., Creff, Y., Raux, S., Charial, C., Audouin, A. & Gagnepain, L. (2009), 'Model-based compensation of the injector dynamics for multiple-injection combustion patterns'. SAE paper 2009-01-1929.

Grossale, A., Nova, I., Tronconi, E., Chatterjee, D. & Weibel, M. (2008), 'The chemistry of the NO/NO_2-NH_3 "fast" SCR reaction over Fe-ZSM5 investigated by transient reaction analysis', *Journal of Catalysis* **256**, 312–322.

Harned, J. L. (1972), 'Analytical evaluation of a catalytic converter system', *SAE Transactions* **81**.

Herz, R. K. & Sell, J. A. (1985), 'Dynamic behavior of automotive catalysts - iii. transient enhancement of water-gas shift over rhodium', *J. Catal.* **94**, 166–174.

Il'in, A. M. (1998), The exponential boundary layer, *in* M. V. Fedoryuk, ed., 'Partial Differential Equations V: Asymptotic Methods for Partial Differential Equations', Springer-Verlag, section V.1.

Keith, J. M., Chang, H.-C. & Leighton, D. T. (2001), 'Designing a fast-igniting catalytic converter system', *AIChE Journal* **47**, 650–663.

Kuo, J. C. W., Morgan, C. R. & Lassen, H. G. (1971), 'Mathematical modeling of CO and HC catalytic converter systems', *SAE Trans.* **80**, 1098–1125.

Laroche, B., Martin, P. & Rouchon, P. (2000), 'Motion planning for the heat equation', *Int. J. Rob. Nonlinear Control* **10**, 629–643.

Leighton, D. & Chang, H. (1995), 'A theory for fast-igniting catalytic converters', *AIChE Journal* **41**, 1898–1914.

Lepreux, O., Creff, Y. & Petit, N. (2008), Motion planning for a Diesel Oxidation Catalyst, *in* 'Proc. of American Control Conference 2008', Seattle, USA.

Lepreux, O., Creff, Y. & Petit, N. (2009*a*), Model-based control design of a diesel oxidation catalyst, *in* 'Proc. of ADCHEM 2009, International Symposium on Advanced Control of Chemical Processes', Istanbul, Turkey.

Lepreux, O., Creff, Y. & Petit, N. (2009*b*), Practical achievable performance in diesel oxidation catalyst temperature control, *in* '2009 IFAC Workshop on Engine and Powertrain Control, Simulation and Modeling (E-COSM)', Rueil-Malmaison, France.

Lepreux, O., Creff, Y. & Petit, N. (2009*c*), Warm-up strategy for a diesel oxidation catalyst, *in* 'Proc. of European Control Conference 2009', Budapest, Hungary.

Levine, W. S. (1996), *The Control Handbook*, CRC Press and IEEE Press", sections 10.8-10.9.

Mercuri, D. (2007), GMPT approach to after-treatment calibration control, *in* 'Proc. of Optimizing Powertrain: Future Improvements through Control Symposium 2007', Turin.

Oh, S. & Cavendish, J. (1982), 'Transients of monolithic catalytic converters: response to step changes in feedstream temperature as related to controlling automobile emissions', *Ind. Eng. Chem.* **21**, 29–37.

Olsson, L. & Andersson, B. (2004), 'Kinetic modelling in automotive catalysis', *Topics in Catalysis* **28**(1-4), 89–98.

Olsson, L., Blint, R. J. & Fridell, E. (2005), 'Global kinetic for lean NOx traps', *Ind. Eng. Chem. Res.* **44**, 3021–3032.

Osizik, M. N. (1977), *Basic heat transfer*, McGraw-Hill.

Pattas, K. N., Stamatelos, A. M., Pistikopoulos, P. K., Koltsakis, G. C., Konstandinidis, P. A., Volpi, E. & Leveroni, E. (1994), 'Transient modeling of 3-way catalytic converters'. SAE paper 940934.

Please, C., Hagan, P. & Schwendeman, D. (1994), 'Light-off behavior of catalytic converters', *SIAM Journal on Applied Mathematics* **54**, 72–92.

Ramanathan, K., West, D. H. & Balakotaiah, V. (2004), 'Optimal design of catalytic converters for minimizing cold-start emissions', *Catalysis Today* **98**, 357–373.

Sciarretta, A. & Corde, G. (2007), 'Model-based compensation of the injector dynamics for multiple-injection combustion patterns'. SAE paper 2007-24-0071.

Shamim, T., Shen, H., Sengupta, S., Son, S. & Adamczyk, A. A. (2002), 'A comprehensive model to predict three-way catalytic converter performance', *J. Eng. Gas Turbines Power* **124**, 421–428.

Silva, G. J., Datta, A. & Bhattacharyya, S. P. (2005), *PID controllers for time-delay systems*, Birkhäuser.

Tavakoli, S. & Fleming, P. (2003), Optimal tuning of PI controllers for first order plus dead time/long dead time models using dimensional analysis, *in* 'Proc. of the 7th European Control Conference'.

Tavakoli, S. & Tavakoli, M. (2003), Optimal tuning of PID controllers for first order plus time delay models using dimensional analysis, *in* 'Proc. of the 4th International Conference on Decision and Automation (ICCA'03)', Montreal, Canada.

Tischer, S., Correa, C., & Deutschmann, O. (2001), 'Transient three-dimensional simulation of a catalytic combustion monolith using detailed models for heterogeneous and homogeneous reactions and transport phenomena', *Catalysis Today* **69**, 57–62.

Van Nieuwstadt, M. & Tennison, P. (2006), 'Control method and system for diesel particulate filter regeneration', US Patent 7047729.

Vardi, J. & Biller, W. (1968), 'Thermal behavior of an exhaust gas catalytic converter', *Ind. Eng. Chem.-Process Des. Dev.* **7**, 83–90.

Windmann, J., Braun, J., Zacke, P., Tischer, S., Deutschmann, O. & Warnatz, J. (2003), 'Impact of inlet flow distribution on the light-off behavior of a 3-way catalytic converter'. SAE paper 2003-01-0937.

Wolfram Research Inc. (2006), 'The Wolfram functions site', Available online: http://functions.wolfram.com/.

Yamauchi, T., Kubo, S. & Yamazaki, S. (2005), 'Detailed surface reaction model for three-way catalyst and nox storage reduction catalyst'. SAE paper 2005-01-1112.

Young, L. C. & Finlayson, B. A. (1974), 'Mathematical modeling of the monolith converter', *Advances in Chemistry Series* **13**, 629–643.

Appendix A

Accounting for disturbance reductants flow

For sake of clarity, the control problem detailed in Chapter 3 omits several disturbances. In particular, the reductants referred to as *disturbance reductants* were omitted. In details, the actual reductants flow at the DOC inlet is composed of disturbance reductants flow and control HC flow. The disturbance reductants flow rate is a disturbance variable. It is mainly produced by unburnt reductants of the coupled post-injection, which are used to increase the exhaust line temperature, and, in turn, ensure the DOC oxidation capacity. The control HC flow rate is the control variable. It is mainly produced by late-post injection or by exhaust injection.

In this appendix, an extension of results presented in the thesis to the case of disturbance reductants is detailed. This extension is required for real experimentations.

A.1 Modeling objectives

A.1.1 Distinguishing between disturbance reductants and control HC

The total reductants flow rate F_{red} at the DOC inlet is composed of control HC flow rate u and disturbance reductants flow rate F_{dis}

$$F_{red} = u + F_{dis}$$

Disturbance reductants flow rate may result in a catalyst inlet-to-outlet temperature rise as high as 100°C[1]. It has to be considered in the controller. Obviously, variables u and F_{dis} need to be separated because one is the control variable and the other is a disturbance variable. Further, it will be shown below that these variables may generate different temperature responses. Similarly, disturbance reductants flow rate F_{dis} can be decomposed into disturbance HC flow rate $F_{dis,HC}$ and disturbance CO flow rate $F_{dis,CO}$, HC and CO being the main reductants in the flow composition

$$F_{dis} = F_{dis,HC} + F_{dis,CO}$$

Because CO is easier to oxidize than HC, this distinction could, in theory, be worth mentioning. However, in the following, we do not get into this level of details and consider only one disturbance variable F_{dis} that includes all the kinds of disturbance reductants. Then, the scheme considered for control is given in Fig. A.1. The four inputs are the control variable u, the measured disturbances v,

[1] During DPF regeneration, engine is used in a particular mode leading to high HC emissions (refer to § G for more information)

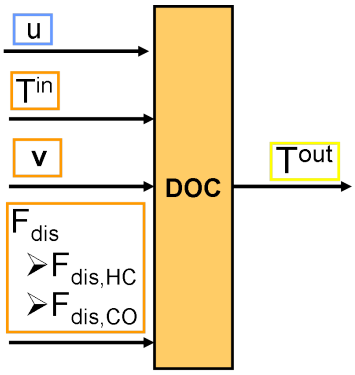

Figure A.1: In the "real picture", the model includes one (or more) disturbance reductants flow

T^{in}, and F_{dis}. The measured output is T^{out}. Note that F_{dis} is not measured online. It is estimated by look-up tables. In a rigorous approach, variables u and F_{dis} refer to actual flow rates at the DOC inlet. Control HC flow rate and disturbance reductants flow rate may interact before reaching the DOC inlet. However, in practice, it is considered that they are independent. Obviously, steady-state effects presented in § 3.1.1 relate to all kinds of reductants. Therefore, in the following we focus on the dynamic effects.

A.1.2 Preliminary observation: temperature response to different injection methods

It is experimentally observed that different HC speciation or injection method may lead to different DOC temperature responses. In particular, one can observe different responses to HC injected by late post-injection and to HC injected by exhaust injector, respectively. The different methods of injection (see Appendix F) lead to different HC speciation at the DOC inlet (Frobert, Creff, Lepreux, Schmidt & Raux 2009).

Remark. The different methods of injection and fuel speciation also lead to different DOC conversion efficiencies (see Fig. G.2 in § G.4).

Fig. A.2 clearly shows different response delays[2] for these two different types of injection. Results were obtained through an experimental study. In spite of several investigations (Kuo et al. 1971) (Dubien et al. 1998), such differences remain insufficiently understood from a chemical modeling viewpoint. In theory, coupled post-injection and late post-injection could potentially lead to different results, but *we assume that their effects are similar*. These injections are referred to as *in-cylinder* post-injection. To summarize:

- When the exhaust injector is used as actuator, the flow rate of HCs injected by exhaust injection is the control variable whereas the flow rate of "in-cylinder" reductants is the disturbance variable.
- When the late post-injection system is used as actuator, the flow rate of late post-injection is the control variable and the flow rate of the reductants resulting from other injections is a disturbance variable.

Consequences from a control viewpoint When using an exhaust injector as actuator, the effects of the disturbance reductants must be compensated in a specific way. When using the late post-injection as actuator, the reductants flow rate F_{dis} can simply be subtracted.

[2]Experimental step responses are identified to a first order plus delay model step response using a least squares algorithm

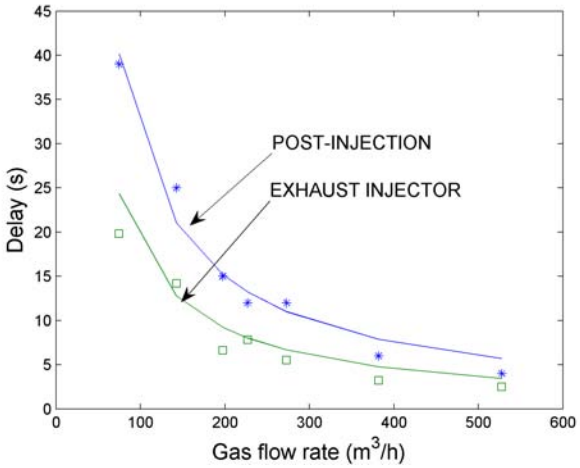

Figure A.2: Comparison of delay values for different injection methods of HC versus gas flow rate (step responses are identified to a first order plus delay model). Responses to HC injected by late post-injection are slower than responses to HC injected by the exhaust injector.

A.2 Model

In this section, adaptations of the reduced model presented in Chapter 3 and of the control model derived in Chapter 4 are presented.

A.2.1 Reduced model

The proposed reduced model is given by

$$\begin{cases} \dfrac{\partial T}{\partial t}(z,t) + v(t)\dfrac{\partial T}{\partial z}(z,t) = -k_1\left(T(z,t) - T_s(z,t)\right) \\ \dfrac{\partial T_s}{\partial t}(z,t) = k_2\left(T(z,t) - T_s(z,t)\right) + \Psi(z,u(t),v(t)) + \Psi_{dis}(z,u(t),v(t)) \end{cases} \tag{A.1}$$

where Ψ_{dis} is a distributed input variable related to the disturbance variable F_{dis}. This source term is different from Ψ, which refers to control HC. Ψ_{dis} is a distributed source term. It is constant over some spatial interval

$$\begin{cases} \Psi_{dis}(z,u,v) = \psi_{dis}(u,v), & 0 \le z \le L_{c,dis}(v) \\ \Psi_{dis}(z,u,v) = 0, & L_{c,dis}(v) < z \le L \end{cases} \tag{A.2}$$

where $L_{c,dis}$ is a piecewise affine function of the channel gas speed v,

$$L_{c,dis}(v) = \min(L, \quad a_{dis} \cdot v + b_{dis}) \tag{A.3}$$

a_{dis} and b_{dis} are two positive constants. The source term ψ_{dis} is related to the length $L_{c,dis}$, and F_{dis} the disturbance reductants flow rate through the following relation

$$\psi_{dis}(u,v) = \frac{1}{L_{c,dis}(v)}\, G_{dis}(v)\, \frac{k_2\, v}{k_1}\, F_{dis} \tag{A.4}$$

where G_{dis} is given by

$$G_{dis} = \eta_{dis} \frac{\Delta H_{dis}}{F\, Cp} \tag{A.5}$$

In the controller, the disturbance reductants conversion efficiency η_{dis} is assumed to equal the in-cylinder conversion efficiency (see Fig. G.2 in § G.4). Similarly, the heat of combustion ΔH_{dis} of disturbance reductants is assumed to be equal to ΔH_u.

A.2.2 Model validation

The presented reduced model allows the comparison of temperature responses to late post-injection input (which is assumed similar to response to disturbance reductants) to responses to exhaust injection input (exhaust injection flow rate is the control variable when this configuration is used). Further, as has been introduced in A.1.2, these responses differ when different injection methods are used. We show here how it is captured by our model. Interestingly, these differences can be explained by a variation of reactive length, as is evidenced by simulation results presented in Fig. A.3b. These

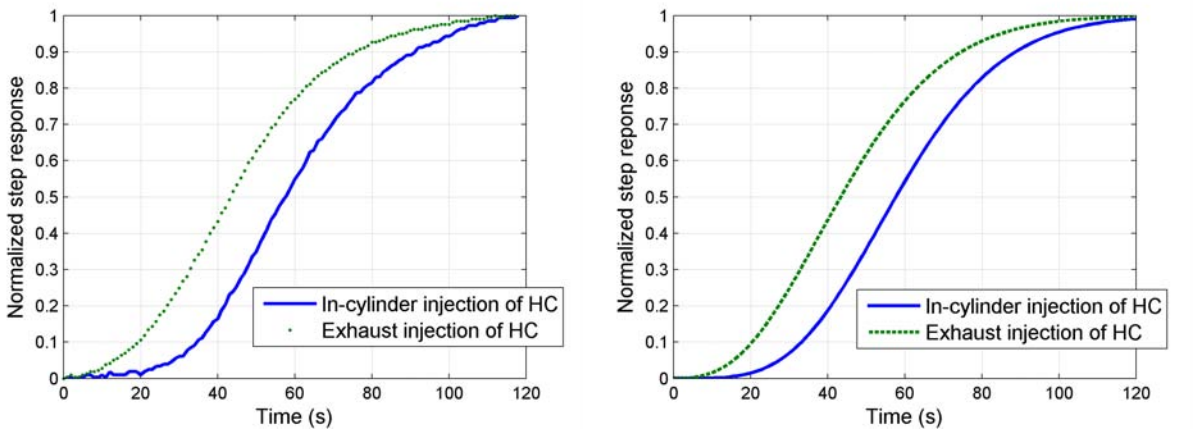

(a) Experimental data

(b) Simulation for 2 different reactive lengths (obtained from (3.15))

Figure A.3: Different reactive lengths are used to model responses of different kinds of HC. Temperature response of in-cylinder injection HC is slower than response of exhaust injection HC. Reactive length corresponding to exhaust injection is longer.

macroscopic results roughly encompass all the chemical phenomena. They describe that in-cylinder reductants (resulting from in-cylinder injections) are oxidized in a short entry part of the DOC. Then, the thermal response, which propagates along the catalyst, is highly delayed. By contrast, HCs resulting of the exhaust injection are oxidized on a longer part of the DOC. Therefore, this kind of HCs acts closer to the catalyst outlet and its temperature response is faster.[3] Finally, these observations allow the integration of different dynamics for the two kinds of HCs in the control strategy.

[3] "In-cylinder" HCs correspond to a short carbon chain and "exhaust" HCs correspond to a longer carbon chain (Dubien et al. 1998). Then, respective oxidation properties and access possibilities to catalytic surface are different. These differences may be intuitively related to the proposed different macroscopic reactive lengths.

A.2.3 Disturbance reductants "boundary-source" sub-model

Following § 4.1, disturbance reductants "boundary-source" sub-model corresponds to a particular case of the reduced model, in which the source terms are null. Here, system (A.1) yields

$$\left\{\begin{array}{rcl} \dfrac{\partial T}{\partial t}(z,t)+v(t)\dfrac{\partial T}{\partial z}(z,t) & = & -k_1\left(T(z,t)-T_s(z,t)\right) \\ \dfrac{\partial T_s}{\partial t}(z,t) & = & k_2\left(T(z,t)-T_s(z,t)\right) \end{array}\right. \tag{A.6}$$

Note $T^{in}_{eq,dis}$ the boundary condition of this sub-model

$$T^{in}_{eq,dis}(t) \triangleq T(z=0,t) \tag{A.7}$$

In this sub-model, $T^{in}_{eq,dis}$ is the input variable, which represents the disturbance flow rate F_{dis}. It plays a role similar to the one of the distributed disturbance variable Ψ_{dis} in the reduced model. It is related to F_{dis} by

$$T^{in}_{eq,dis} = G_{dis}\, F_{dis} \tag{A.8}$$

The system output $T^{out}_{eq,dis}$ corresponds to the temperature at the equivalent transport length $L_{u,dis}$

$$T^{out}_{eq,dis}(t) \triangleq T(z=L_{u,dis},t) \tag{A.9}$$

where the length $L_{u,dis}$ is defined by

$$L_{u,dis}(v) = \max(L - a_{u,dis}\, v - b_{u,dis}, \quad 0) \tag{A.10}$$

where $a_{u,dis}$ and $b_{u,dis}$ are constants. In this conception, the constants $a_{u,dis}$ and $b_{u,dis}$ are identified instead of the constants a_{dis} and b_{dis} of the reduced model.

A.2.4 Control model

In the same manner as for the development of the control model in § 4.3, the inlet temperature effects, the control HC effects, and the disturbance reductants effects are decoupled. As shown in § A.2.3 the disturbance reductants flow rate of the reduced model is transformed into a boundary condition, provided model adaptations. Following results of § 4.2, the obtained system can be approximated by an advection-diffusion system. Considering results of § 4.3, this leads to a model as pictured in Fig. A.4. The HC effects can be assimilated to a front of temperature T^{in}_{eq} propagating on a fictitious length L_u. The T^{in} effects are propagating over the whole DOC length L. The disturbance reductants are assimilated to a front of temperature $T^{in}_{eq,dis}$ propagating on the length $L_{u,dis}$. The three sub-subsystems use the advection-diffusion equation to describe propagation. Propagation coefficients (ϑ and λ) are identical (they depend on v). Altogether, the control model consists of the sub-models, the outputs of which are added up to yield the control model output.

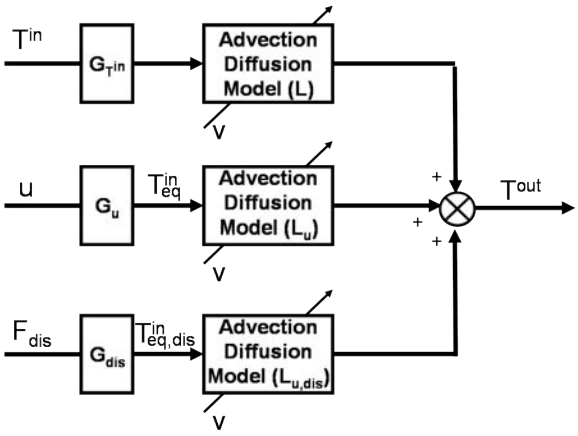

Figure A.4: Control model. The HC effects can be assimilated to a front of temperature T_{eq}^{in} propagating on a fictitious length L_u. The T^{in} effect is propagating over the whole DOC length L. The disturbance reductants are assimilated to the boundary condition $T_{eq,dis}^{in}$ over the length $L_{u,dis}$.

A.2.5 Rejection possibilities of the disturbance reductants effects

It has been mentioned in § A.2.2 that responses to "in-cylinder" reductants are faster than responses to "exhaust" HCs. Then, by using exhaust injection as actuator, it is theoretically possible to compensate for this disturbance.

When using late-post injection as actuator, both disturbance reductants and control HC are considered to be "in-cylinder" reductant and to have similar effects. Then, in this case, it is also theoretically possible to compensate for this disturbance reductants.

A.3 Accounting for undesired gas composition disturbance in the advanced control law

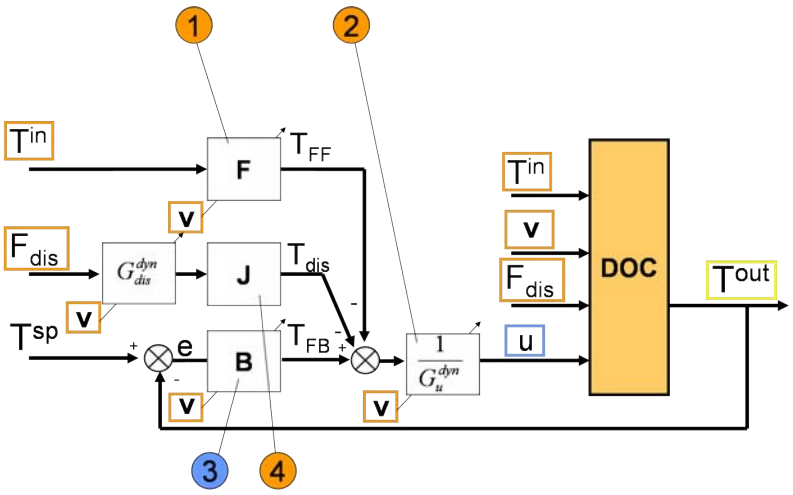

Figure A.5: Advanced controller overview.

The difference between "in-cylinder" reductants and "exhaust" HCs can be accounted for in an additional "J" block **(4)** as pictured in Fig. A.5. When using late post-injection system as actuator,

the two flow dynamics are considered similar, i.e. the "J" block is equal to 1. When using the exhaust injector as actuator, the two flow dynamics must be differentiated. Following the design of the "F" block presented in § 4.3, the delay $\delta_{dis}(t)$ to synchronize the disturbance reductants variations with the control HC variations is given by the following implicit equation, in which $\delta_{dis}(t)$ is unknown

$$L_{u,dis} - L_u = \int_{t-\delta_{dis}(t)}^{t} \vartheta(w)dw \tag{A.11}$$

The "J" block of the controller is simply a delay operator with the delay value $\delta_{dis}(t)$

$$T_{dis}(t) = T^{in}_{eq,dis}(t - \delta_{dis}(t))$$

Similarly to G_u^{dyn}, G_{dis}^{dyn} is the "dynamic" gain for F_{dis}. In practice, $G_{dis}^{dyn} = G_u^{dyn}$.

Appendix B

Approximating the DOC "boundary-source" model by a first-order plus delay model

This appendix details the (approximate) reduction of the "boundary-source" control sub-model equation (4.1) to a simple (finite dimensional) first order plus delay model

$$\begin{cases} \dfrac{\partial T}{\partial t}(z,t) + v(t)\dfrac{\partial T}{\partial z}(z,t) &= -k_1\left(T(z,t) - T_s(z,t)\right) \\ \dfrac{\partial T_s}{\partial t}(z,t) &= k_2\left(T(z,t) - T_s(z,t)\right) \end{cases}$$

This approximation is used in the control design in Chapter 6 and Appendix C. The desired representation of this equation is, for a constant v, a first order plus delay model, which belongs to a class of models relatively easy to design a controller for (Silva et al. 2005). The corresponding transfer function from boundary input $T_{eq}^{in}(t)$ to output $T(z,t)$ is (see § E.1.3 for calculation details)

$$\frac{\hat{T}(z,s)}{\hat{T}_{eq}^{in}(s)} = \exp\left(-\frac{z}{v}s\right)\exp\left(-\frac{k_1\, z}{v}\right)\exp\left(\frac{k_1\, k_2\, z/v}{s+k_2}\right) \tag{B.1}$$

where T_{eq}^{in} represents an input equivalent to HC, and the length of the DOC is L_u. One can refer to Chapter 4 for details. Alternatively, this transfer function represents the inlet temperature effects (see Eq. (3.24)). In this case, the boundary condition is noted T^{in} the length of the DOC is L. It is shown in this appendix that the transfer function (B.1) can be approximated by a first order plus delay model of the general form

$$\frac{\hat{T}(z,s)}{\hat{T}_{eq}^{in}(s)} = \frac{\exp\left(-\delta s\right)}{1+\tau s}$$

with

$$\begin{cases} \tau = \dfrac{1 - T_h(z,t_I)}{\exp\left(-2k_1 z/v\right)k_2 \mathrm{I}_1(2k_1 z/v)} \\ \delta = \dfrac{z}{v} + \dfrac{k_1 z}{k_2 v} - \dfrac{1 - T_h(z,t_I)}{\exp\left(-2k_1 z/v\right)k_2 \mathrm{I}_1(2k_1 z/v)} \end{cases}$$

and where T_h is the step response of (4.1) given by

$$T_h(z,t) = \exp\left(-\frac{k_1 z}{v}\right)\Upsilon(t - z/v) \times \left[1 + \sum_{r=1}^{\infty} \frac{\Gamma_{\text{inc}}(k_2(t-z/v), r)}{r!(k_2/m(z))^r}\right]$$

Low frequency approximation

It is explained in Appendix D that a DOC is a very low-pass system and that it is in fact almost insensitive to the high frequency content of the input signal. For this reason, the following approximation from the transfer function (B.1) can be made for small values of $|s|$ (i.e. the range of low frequencies)

$$\begin{aligned}
&\frac{\hat{T}(z,s)}{\hat{T}_{eq}^{in}(s)}\exp\left(\frac{z}{v}s\right)\exp\left(\frac{k_1\,z}{v}\right)=\exp\left(\frac{k_1\,k_2\,z/v}{s+k_2}\right)\\
&=\exp\left(-(1-\nu)\tfrac{k_1 z}{k_2 v}s\right)\exp\left(\tfrac{k_1 z}{v}\left((1-\nu)s/k_2+\tfrac{1}{1+s/k_2}\right)\right)\\
&\approx\exp\left(-(1-\nu)\tfrac{k_1 z}{k_2 v}s\right)\exp\left((1-\nu)s/k_2+1-s/k_2\right)^{\frac{k_1 z}{v}}\\
&\approx\exp\left(-(1-\nu)\tfrac{k_1 z}{k_2 v}s\right)\exp\left(\tfrac{k_1 z}{v}\right)\exp\left(-\nu s/k_2\right)^{\frac{k_1 z}{v}}\\
&\approx\exp\left(-(1-\nu)\tfrac{k_1 z}{k_2 v}s\right)\exp\left(\tfrac{k_1 z}{v}\right)\frac{1}{1+\nu\frac{k_1 z}{k_2 v}s}
\end{aligned}\tag{B.2}$$

for every $\nu\in]0,1[$. In fact ν can be seen as a weighting variable which will be discussed later on. This computation leads to the following transfer function which stands as an approximation of (B.1)

$$\frac{\hat{T}(z,s)}{\hat{T}_{eq}^{in}(s)}\approx\exp\left(-\underbrace{\left(\frac{z}{v}+(1-\nu)\frac{k_1 z}{k_2 v}\right)}_{\delta}s\right)\frac{1}{1+\underbrace{\nu\frac{k_1 z}{k_2 v}}_{\tau}s}\tag{B.3}$$

As a result, one obtains a delayed first-order transfer function $\dfrac{\exp\left(-\delta s\right)}{1+\tau s}$ where

$$\begin{cases}\tau=\nu\dfrac{k_1 z}{k_2 v}\\ \delta=\dfrac{z}{v}+(1-\nu)\dfrac{k_1 z}{k_2 v}\end{cases}\tag{B.4}$$

The weighting variable ν relates τ and δ. Explicitly, we get

$$\delta=\frac{z}{v}+\frac{k_1 z}{k_2 v}-\tau\tag{B.5}$$

From a parameter identification standpoint, the next step is to formulate a constraint to determine the value of τ, which, in turn, sets the value of δ and ν.

Inflexion point

The control model step response (3.22) is recalled here

$$T_h(z,t)=\Upsilon(t-\frac{z}{v})\exp\left(-\frac{k_1 z}{v}\right)\times\left[1+\int_0^{t-z/v}\exp\left(-k_2\tau\right)\sqrt{\frac{m(z)}{\tau}}\mathrm{I}_1(2\sqrt{m(z)\tau})d\tau\right]$$

with $m(z)=k_1 k_2 z/v$. One can calculate the abscissa of its inflexion point. It will be used to set the values of the weighting variable ν. The second-order derivative of the step response with respect to

the time variable is

$$\frac{\partial^2}{\partial t^2}T(z,t+\frac{z}{v}) = -\Upsilon(t)\exp\left(-\frac{k_1 z}{v}\right)\exp\left(-k_2 t\right)\times \left[\left(k_2+\frac{1}{t}\right)\sqrt{\frac{m(z)}{t}}\mathrm{I}_1\left(2\sqrt{m(z)t}\right)-\frac{m(z)}{t}\mathrm{I}_0\left(2\sqrt{m(z)t}\right)\right] \tag{B.6}$$

Using the following asymptotic expansion of the Bessel function I_ν (see Abramowitz & Stegun (1965))

$$\begin{cases} \mathrm{I}_\nu(z) \approx \dfrac{\mathrm{e}^z}{\sqrt{2\pi z}}\left(1-\dfrac{\mu-1}{8z}+\dfrac{(\mu-1)(\mu-9)}{2!(8z)^2}-\dots\right) \\ \mu = 4\nu^2 \end{cases} \tag{B.7}$$

at first-order, we get, for $\dfrac{3}{16\sqrt{m(z)t}} \ll 1$,

$$\frac{\partial^2}{\partial t^2}T(z,t+\frac{z}{v}) \approx -\Upsilon(t)\exp\left(-\frac{k_1 z}{v}\right)\exp\left(-k_2 t\right)\times \left[\left(k_2+\frac{1}{t}\right)\sqrt{\frac{m(z)}{t}}\frac{\mathrm{e}^{2\sqrt{m(z)t}}}{\sqrt{4\pi\sqrt{m(z)t}}}-\frac{m(z)}{t}\frac{\mathrm{e}^{2\sqrt{m(z)t}}}{\sqrt{4\pi\sqrt{m(z)t}}}\right] \tag{B.8}$$

The equation of the inflexion point, of which t_I is the unknown abscissa, is given by

$$\frac{\partial^2}{\partial t^2}T_h(z,t_I) = 0 \tag{B.9}$$

Denoting $t_{I'} = t_I - z/v$, this leads to

$$k_2 + \frac{1}{t_{I'}} - \sqrt{\frac{m(z)}{t_{I'}}} = 0 \tag{B.10}$$

Then,

$$t_{I'} \approx \frac{k_1 z}{k_2 v}\left(\frac{1}{2}+\frac{1}{2}\sqrt{1-\frac{4v}{k_1 z}}\right)-\frac{1}{k_2} \tag{B.11}$$

and assuming $\dfrac{4v}{k_1 z} \ll 1$ (strong assumption), we finally obtain

$$t_I \approx \frac{k_1 z}{k_2 v}+\frac{z}{v} \tag{B.12}$$

Parameters τ and δ

Note f the delayed first order model step response

$$f(t) = 1-\exp\left(-\frac{t-\delta}{\tau}\right)$$

Let t_E be the solution of

$$f(t_E) = T_h(z,t_I) \tag{B.13}$$

We request the slope of f at abscissa t_E to equal the slope of the T_h at t_I, i.e.

$$\frac{d}{dt}f(t_E) = \frac{\partial}{\partial t}T_h(z, t_I) \tag{B.14}$$

Then, we get

$$\tau = \frac{1 - T_h(z, t_I)}{\exp(-2k_1 z/v)k_2 \mathrm{I}_1(2k_1 z/v)} \tag{B.15}$$

To sum up, with the additional requirement (B.13)-(B.14), it is possible to write explicit values of τ and δ as a function of model parameters and the input disturbance v. This gives

$$\begin{cases} \tau = \dfrac{1 - T_h(z, t_I)}{\exp(-2k_1 z/v)k_2 \mathrm{I}_1(2k_1 z/v)} \\ \delta = \dfrac{z}{v} + \dfrac{k_1 z}{k_2 v} - \dfrac{1 - T_h(z, t_I)}{\exp(-2k_1 z/v)k_2 \mathrm{I}_1(2k_1 z/v)} \end{cases} \tag{B.16}$$

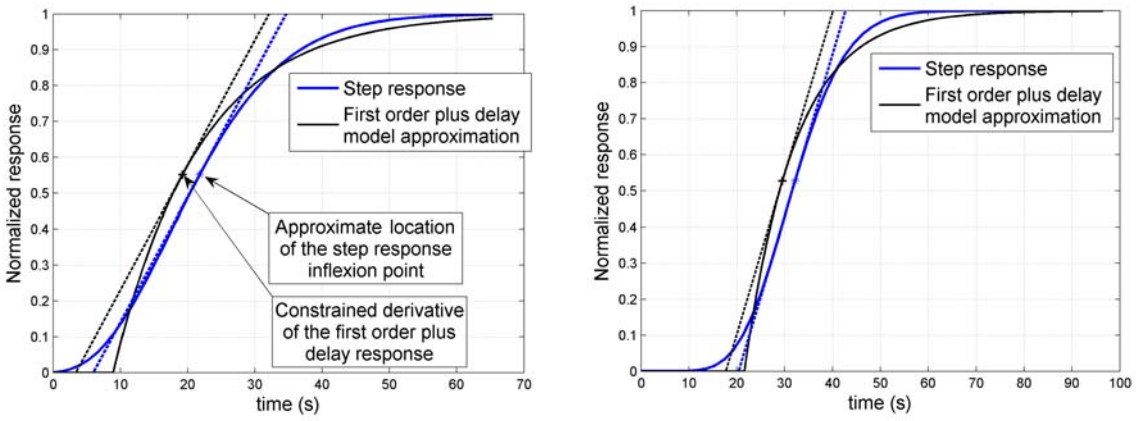

Figure B.1: Matching the DOC step response with a first order plus delay model. k_1=400, k_2=0.35, v=4 (left). k_1=1591.09, k_2=0.82, v=4.597 (right). Simulation data.

Two different cases that are representative of real DOC parameter values, are reported in Fig. B.1. It is shown that the choice of the constraint (B.13)-(B.14) leads to good matching of responses. Values of τ and δ for control HC step responses[1] at different flow rates are shown in Fig. B.2. Corresponding analytical values of (B.16) with $z = L_u$, are obtained using constant parameters k_1 and k_2, and L_u function of v (as mentioned in Chapter 4).

For easy online computation of τ and δ, $T_h(z, t_I)$ is computed offline and assumed constant. Exact computation of $T_h(z, t_I)$ has minor consequences on the control because it slightly affects the weighting variable ν (see above Eq. (B.5)), i.e. a small error on τ is compensated by δ. Further, a look-up table is built offline for the Bessel function I_1. If necessary, further approximation can be used to remove the need for an exact evaluation of the Bessel function. They are presented in the following.

[1]Experimental step responses are identified to a first order plus delay model step response using a least mean-square algorithm

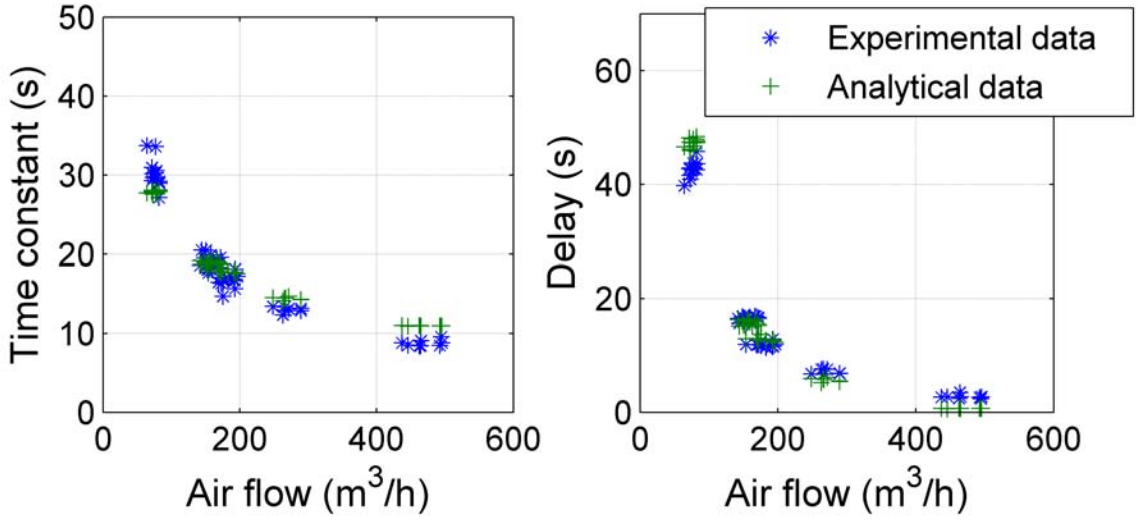

Figure B.2: Comparison of δ and τ evolution obtained by (B.16) (with $z = L_u$) or by experimental control HC step responses identification.

Further approximation of τ and δ

It has been shown that the choice of the constraint (B.13)-(B.14) leads to good matching of responses results. Further approximation can be made to prevent evaluation of the Bessel function. In experiment of Fig. B.1, we get $\frac{3}{8}\frac{1}{2k_1 z/v} \ll 1$ for the two presented cases. Referring to expansion (B.7), this validates the use of an asymptotic expansion of I_1. We can make the approximation $\mathrm{I}_1(2k_1 z/v) \approx \frac{\exp(2k_1 z/v)}{\sqrt{2\pi 2k_1 z/v}}$. Then, we get the following expressions

$$\begin{cases} \tau = \frac{1}{k_2}\left(1 - T_h(z, t_I)\right) \cdot 2 \cdot \sqrt{\pi} \cdot \sqrt{\dfrac{k_1 z}{v}} \\ \delta = \dfrac{z}{v} + \dfrac{1}{k_2}\dfrac{k_1 z}{v} - \dfrac{1}{k_2}\left(1 - T_h(z, t_I)\right) \cdot 2 \cdot \sqrt{\pi} \cdot \sqrt{\dfrac{k_1 z}{v}} \end{cases} \tag{B.17}$$

It is interesting to note that, considering requirement (B.13)-(B.14), δ does not have an hyperbolic behavior with respect to v.

Appendix C

DOC classic control design: an alternative (inefficient) control law

In this appendix, classic control design approach is followed to treat the problem of DOC outlet temperature control is presented. It corresponds to the derivation of a simple model (using two first-order plus delay models in parallel) straightforwardly leading to a control solution. The model, derived from the model (4.1), has its few parameters related to the original physical parameters. Obtained controllers require little tuning effort.

This appendix is organized as follows. First, the control model, alternative control model of Chapter 4, is developed. Then, derived control structures (adaptive PI, PID, Smith predictor) as well as simulation results are presented. Conclusions stress the need of the advanced control approach presented in Chapter 6.

Note that, adaptations of the results of advanced control (Chapter 6) to the case of disturbance reductants (undesired gas composition from engine) are presented in Appendix A. For the clarity of the presentation, this disturbance is not treated in this appendix. However, following the method presented for compensation of the inlet temperature (and presentation of Appendix A), extension to the case of disturbance reductants for the model and the controller developed in this appendix is straightforward.

C.1 First order plus delay model

On one hand, it has been shown in § 4.1 that the response of the DOC to the inlet temperature (which is regarded as a disturbance) could be described using the "boundary-source" model (4.1). On the other hand, it has been shown that the response to the control HC (u control variable) could be described using the same model considering a fictitious adaptation of the DOC length. This equation can be accurately approximated by a first order plus delay model (see Appendix B). Finally, the linearity of the reduced model allows T^{in} effects and u effects to be treated in separated states. As

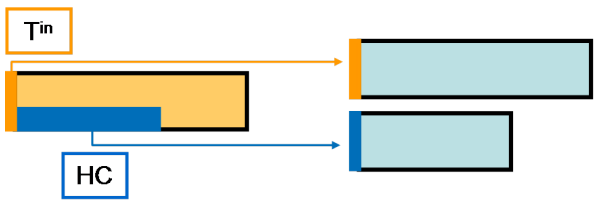

Figure C.1: Scheme of the first order plus delay model

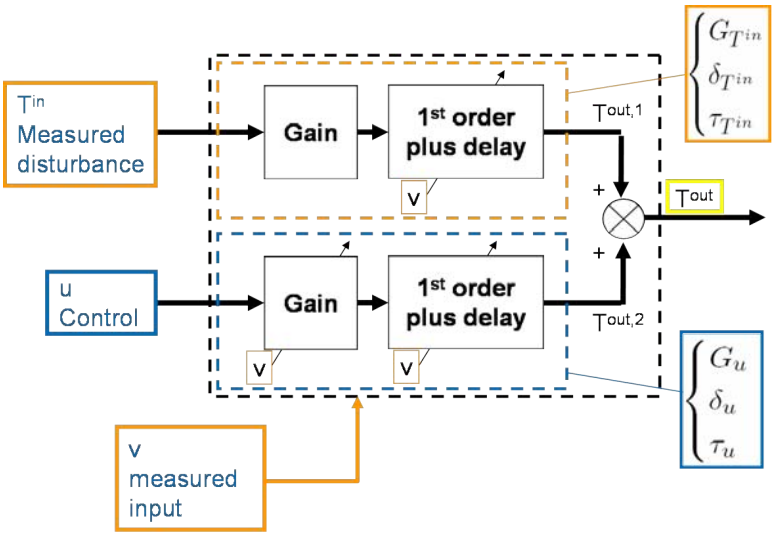

Figure C.2: Scheme of the first order plus delay model

a result, the DOC is decomposed into two sub-systems, one having the disturbance T^{in} as input and the other having the control variable u as input as is pictured in Fig. C.1. The obtained model is a combination of two first order plus delay models as is detailed in Fig. C.2. The first one uses T^{in} as input and $\tau_{T^{in}}$ and $\delta_{T^{in}}$ as parameters. These are evaluated using the general formula (B.16) and the whole DOC length L. The steady-state gain of this sub-system is evaluated using (3.26). Explicitly, the sub-system governing differential equation is

$$\begin{cases} \tau_{T^{in}}(t)\ \dot{x}_T(t) = -x_T(t) + G_{T^{in}}(t)\ T^{in}(t) \\ T^{out,1}(t) = x_T(t - \delta_{T^{in}}(t)) \end{cases} \tag{C.1}$$

with

$$\begin{cases} \tau_{T^{in}} = \dfrac{1 - T_h(L, t_I)}{\exp\left(-2k_1 L/v\right) k_2 \mathrm{I}_1(2k_1 L/v)} \\ \delta_{T^{in}} = \dfrac{L}{v} + \dfrac{k_1 L}{k_2 v} - \dfrac{1 - T_h(L, t_I)}{\exp\left(-2k_1 L/v\right) k_2 \mathrm{I}_1(2k_1 L/v)} \\ G_{T^{in}} = 1 \end{cases} \tag{C.2}$$

The second sub-system uses u as input, and corresponding parameters τ_u and δ_u which are evaluated by the same formula (B.16) using a part L_u of the DOC length as explained in § 4.1. The steady-state gain of this sub-system (from the control HC to the outlet temperature) is evaluated using (3.3). Explicitly, the second sub-system governing differential equation is

$$\begin{cases} \tau_u(t)\ \dot{x}_u(t) = -x_u(t) + G_u(t)\ u(t) \\ T^{out,2}(t) = x_u(t - \delta_u(t)) \end{cases} \tag{C.3}$$

with

$$\begin{cases} \tau_u = \dfrac{1 - T_h(L_u, t_I)}{\exp\left(-2k_1 L_u/v\right) k_2 \mathrm{I}_1(2k_1 L_u/v)} \\ \delta_u = \dfrac{L_u}{v} + \dfrac{k_1 L_u}{k_2 v} - \dfrac{1 - T_h(L_u, t_I)}{\exp\left(-2k_1 L_u/v\right) k_2 \mathrm{I}_1(2k_1 L_u/v)} \\ G_u = \eta \dfrac{\Delta H_u}{F\ Cp} \end{cases} \tag{C.4}$$

For both sub-systems, k_1 and k_2 are constant and equal. Finally, the two sub-systems are connected by the output equation

$$T^{out}(t) = T^{out,1}(t) + T^{out,2}(t) \tag{C.5}$$

In this section, the DOC model has been reduced to one of its simplest form. Such linear finite dimensional forms have been extensively studied in the literature before, and it is straightforward to design well-suited controllers for them with little tuning effort. We now present some of these solutions.

C.2 Controller presentation

C.2.1 Design motivations

Following the observations having led the alternative control model of the previous section, the following control design is proposed. First, the system is low-pass and has possibly large time constants, which suggests to look for a control design from the classic "toolboxes" of Corriou (2004) of process control methods. Second, the time constants are largely-varying and these variations (related to the disturbance v) require some adaptation. Third, decoupling T^{in} and u into partial states allows easy feedforward control for the disturbance. From this, it follows that good candidates control techniques are adaptive Smith controller or PI(D), including a feedforward term for T^{in}.

C.2.2 Control designs

We now consider the three mentioned classic controllers and evaluate their performance. The first two designs are simple PI and PID controllers with a feedforward term as presented in Fig. C.3. The third controller, presented in Fig. C.4, consists of a Smith controller (see e.g. Levine (1996)).

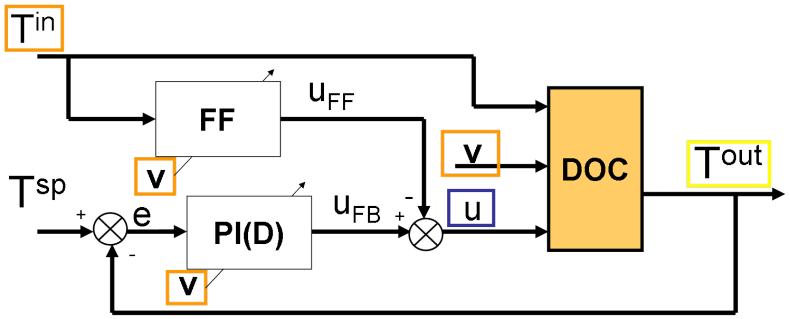

Figure C.3: Control scheme for the adaptive PI(D) controller

The feedforward "FF" block (of input T^{in} and output u_{FF}) is dedicated to treating the T^{in} disturbance. As has been shown in § 3.5.1, the T^{in} response are slower than the u response. For this reason it is possible, theoretically speaking, to compensate for the T^{in} disturbance. In the last section, these responses were approximated by two first order plus delay functions. Considering this fact, it is possible to use a standard feedforward strategy based on the *exact inverse control* computation for the disturbance compensation. Computation steps are briefly recalled here assuming that v has a steady-state value.

Consider that the disturbance delay is greater than the process delay ($\delta_{T^{in}} > \delta_u$), such as illustrated in Fig. C.2. The desired output histories T^{out*} are

$$T^{out*} = 0 \tag{C.6}$$

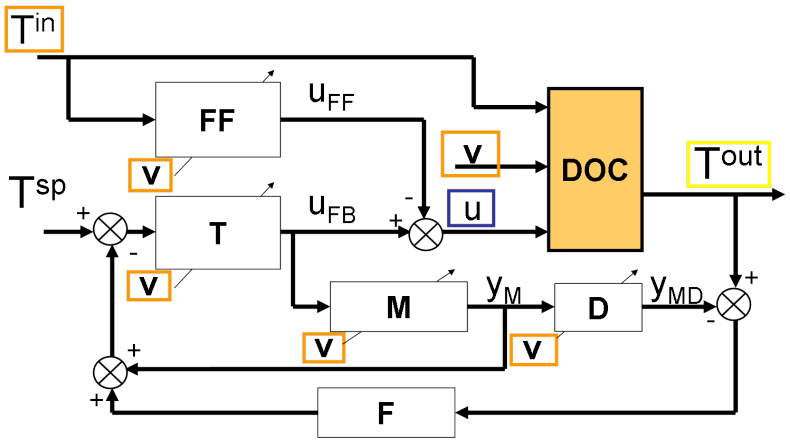

Figure C.4: Control scheme for the adaptive Smith controller

which leads to the equation verified by the desired feedforward transfer function FF^*

$$T^{in}(s)\ FF^*(s)\ G_u \frac{\exp\left(-\delta_u\ s\right)}{\tau_u\ s+1} + T^{in}(s)\ G_{T^{in}} \frac{\exp\left(-\left(\delta_{T^{in}}-\delta_u\right)\ s\right)\exp\left(\delta_u\ s\right)}{\tau_{T^{in}}\ s+1} = 0 \tag{C.7}$$

Finally,

$$FF^*(s) = -\frac{G_{T^{in}}}{G_u}\frac{\tau_u s+1}{\tau_{T^{in}} s+1}\exp\left(-\left(\delta_{T^{in}}-\delta_u\right)s\right) \tag{C.8}$$

To compute a similar solution in a time-varying case, the following equations are solved

$$\begin{cases} u_{FF}(t) = y\left(t-\left(\delta_{T^{in}}(t)-\delta_u(t)\right)\right) \\ y(t) = \dfrac{G_{T^{in}}(t)}{G_u(t)}\ \dfrac{1}{\tau_{T^{in}}(t)}\ \left(T^{in}(t)\ \tau_u(t) + \left(\tau_{T^{in}}(t)-\tau_u(t)\right)\ x(t)\right) \\ \tau_{T^{in}}(t)\ \dot{x}(t) = -x(t) + T^{in}(t) \\ x(0) = 0 \end{cases} \tag{C.9}$$

where parameters τ_u, δ_u, G_u, $\tau_{T^{in}}$, $\delta_{T^{in}}$ and $G_{T^{in}}$ and are evaluated using (C.2) and (C.4) respectively. This "FF" block is used in the three cases of the PI, the PID and the Smith predictor controllers.

Regarding the feedback control design for the PI and the PID controllers, we use respectively Tavakoli & Fleming (2003) and Tavakoli & Tavakoli (2003) parameters tuning rules. The PI controller of input $e(t)$ and output $u_{FB}(t)$ is given by

$$\begin{aligned} u_{FB}(t) = & \frac{1}{G_u(t)}\left(0.3047 + \left(0.4849\frac{\tau_u(t)}{\delta_u(t)}\right)\right) \times \\ & \left(e(t) + \int_0^t \frac{1}{\left(0.4262\ \delta_u(\mu) + 0.9581\ \tau_u(\mu)\right)} e(\mu)\ d\mu\right) \end{aligned} \tag{C.10}$$

while the PID controller is given by

$$\begin{aligned} u_{FB}(t) = & \frac{1}{G_u(t)}\left(\frac{1}{0.2+\dfrac{\delta_u(t)}{\tau_u(t)}}\right) \times \\ & \left(e(t) + \int_0^t e(\mu)\frac{0.08+\dfrac{\delta_u(\mu)}{\tau_u(\mu)}}{\left(1.2+0.3\dfrac{\delta_u(\mu)}{\tau_u(\mu)}\right)\delta_u(\mu)}d\mu + \frac{d}{dt}\left(e(t)\ \frac{\tau_u(t)}{90}\right)\right) \end{aligned} \tag{C.11}$$

Transfer functions for the Smith predictor controller (Fig. C.4) are detailed in the following. For the "T" block, of input $e(t)$ and output $u_{FB}(t)$, we choose

$$u_{FB}(t) = \frac{1}{G_u(t)} \left(1 + \int_0^t \frac{1}{\tau_u(t)} e(t) \right) \tag{C.12}$$

which corresponds to non-conservative settings. For the "M" block, of input $u_{FB}(t)$ and output $y_M(t)$, we have

$$\tau_u(t)\dot{y}_M(t) = y_M(t) + G_u(t)u_{FB}(t) \tag{C.13}$$

Finally, the "D" block operator, of input $y_M(t)$ and output $y_{MD}(t)$, applies a delay of $\delta_u(t)$

$$T(t) = y_M\left(t - \delta_u(t)\right) \tag{C.14}$$

The robustness filter "F" in the feedback loop is a first order filter which time constant set to 1 s. Classically, its role is to robustify the controller when the delay is not well-known. It is not strictly required here because, thanks to the presented detailed analysis of the DOC equations, delays are well approximated.

C.2.3 Simulation results

First, we study the influence of a disturbance step variation. Then, we present control performance obtained for a NEDC driving cycle. Simulation results are shown on the reduced model (3.4) with representative values $k_1 = 870$ s^{-1}, $k_2 = 0.45$ s^{-1}, $L_c = 0.0305$ m, $L = 0.0762$ m. Note that the L_c parameter has been chosen constant in these simulations so that the performance of the presented inlet feedforward strategy is not impacted by gas flow rate variations. These results are then the best achievable a priori. Also, they can easily be compared to results of advanced T^{in} feedforward control strategies that have been presented in § 6.2.

Basic performance

Fig. C.5 compares performance of the three controllers for a setpoint change. Setpoint is risen from 0 to 50 at $t = 200$. At the end of the transient, the system is disturbed by an important gas speed variation. These variations are directly caused by the driver's torque request. They are very fast and cannot be avoided. Although both controllers show similar tracking performance, the Smith controller has much better disturbance rejection capabilities. Similar results are presented in Fig. C.6

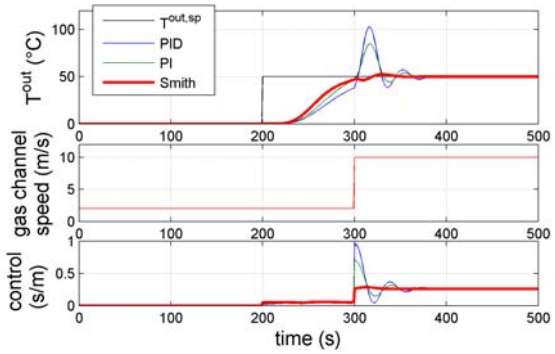

Figure C.5: Step setpoint transition and step v variation for PI, PID, and Smith controllers. $T^{in} = 0$. Simulation data.

with a 20% error on the k_1 parameter, which implies important delay misestimations. All three proposed controllers are quite robust with respect to this error.

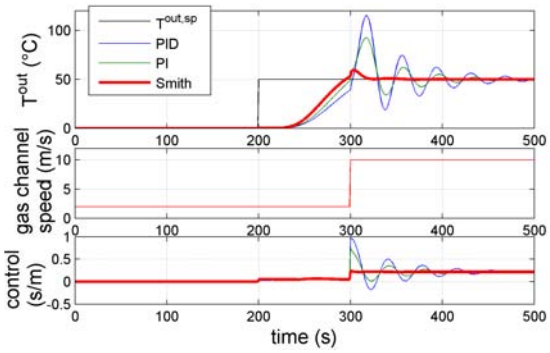

Figure C.6: Step setpoint transition and step v variation for PI, PID, and Smith controllers with a 20%-error on k_1. $T^{in} = 0$. Simulation data.

Performance on the NEDC cycle

Here, the three controllers are tested on a simulated NEDC cycle. Results are presented in Fig. C.7. In this case of a constantly-varying gas flow rate, the differences between the controllers are very small. Similar results are presented in Fig. C.8 with a 20% error on the k_1 parameter. Once again,

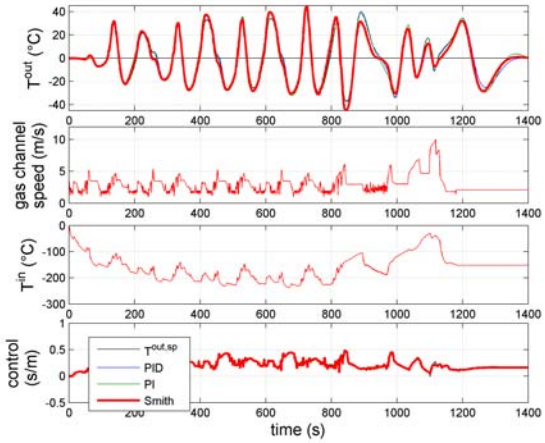

Figure C.7: PI, PID, and Smith controllers on NEDC cycle. Simulation data.

the presented controllers show good results of robustness with respect to this fundamental parameter.

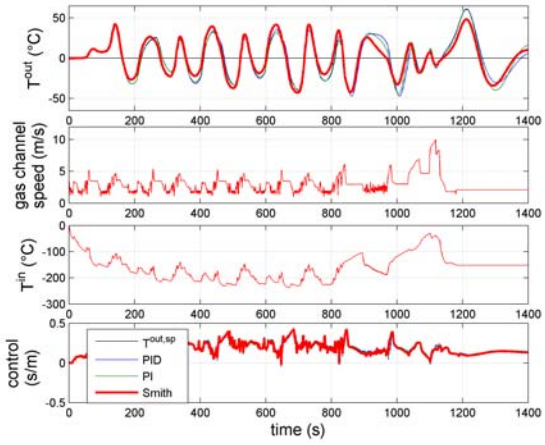

Figure C.8: PI, PID, and Smith controllers on NEDC cycle with a 20%-error on k_1. Simulation data.

Robustness on gain error on NEDC cycle

All three presented controllers need an estimate of the system steady-state gain G_u (see (C.4)). In real applications, the gain can be impacted, for example, by thermal losses or by the catalyst efficiency. Yet, they are usually relatively easy to evaluate. To limit overshoot, setpoint transition must be slowed down (ramp...), which results in a loss of time and energy, especially when starting a DPF regeneration. Indeed, a change of setpoint happens every time a DPF new regeneration phase is started, and, to a minor degree, during DPF regeneration process. Hence, this fact appears as an important issue. Results with a 20% error on G_u are shown in Fig. C.9 and in Fig. C.10.

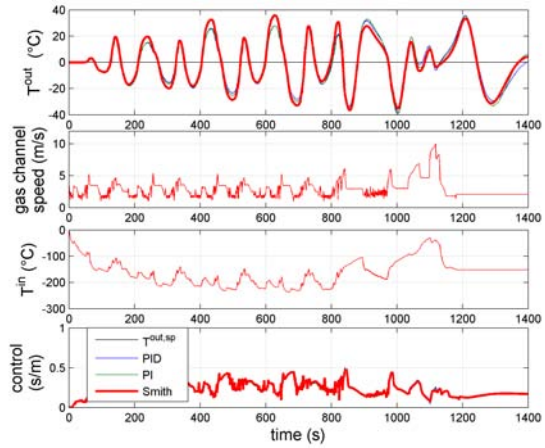

Figure C.9: Control results with a 20%-error on k_1 ($k_1' = 1.2 \cdot k_1$) and a 20%-error on G_u ($G_u' = 0.8 \cdot G_u$). Simulation data.

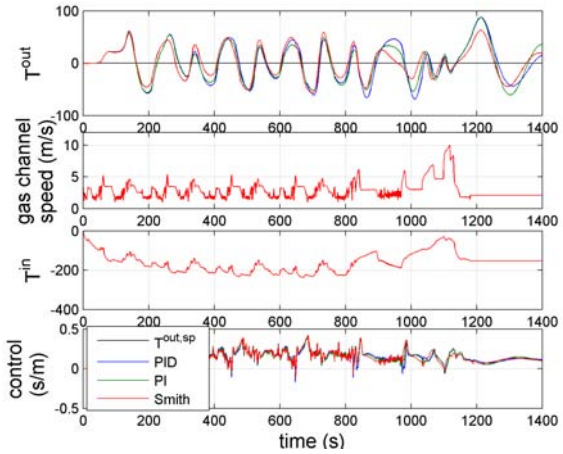

Figure C.10: Control results with a 20%-error on k_1 ($k_1' = 1.2 \cdot k_1$) and a 20%-error on G_u ($G_u' = 1.2 \cdot G_u$). Simulation data.

C.2.4 Conclusion

The presented Smith controller requires more computational effort than the presented PI(D) controllers and shows some advantages in specific cases (setpoint transition, large gas flow rate variation). It should be discussed if it is necessary to use it or not for every specific cases of application. It should be noted that its major drawback (lack of robustness toward a misestimation of the delay) has been circumvented thanks to the presented detailed analysis of the DOC equations and the relatively accurate estimate of the delays involved.

C.3 Conclusion

In this appendix, a simple model using two first-order plus delay sub-systems has been presented. It straightforwardly leads to control solutions. The obtained controllers require little tuning effort since the controller parameters are related to the model physical parameters.

Three classic control structures have been compared. Unfortunately, despite care taken for modeling, and although the controllers have all the inlet temperature (T^{in}) and control HC (u) dynamic information available, they lead to average performance (probably around $\pm 40°$ in practice) due to the not-perfectly-suited classic control structures. This stresses the relevance of the advanced control approach presented in Chapter 6.

Appendix D

Speeding up temperature response

In this appendix, several methods to speed up the DOC step response are explored. This study is used for the experimental validation of the model and gives insight into the DOC thermal behavior, which motivates the control model development (such as low-order order reduction or conclusions about practical disturbance rejection possibilities). It is based on the control sub-model (4.1) (recalled below)

$$\begin{cases} \dfrac{\partial T}{\partial t}(z,t) + v(t)\dfrac{\partial T}{\partial z}(z,t) &= -k_1\left(T(z,t) - T_s(z,t)\right) \\ \dfrac{\partial T_s}{\partial t}(z,t) &= k_2\left(T(z,t) - T_s(z,t)\right) \end{cases}$$

with T_{eq}^{in} as boundary condition

$$T_{eq}^{in}(t) \triangleq T(z=0,t)$$

D.1 Inversion-based open-loop control

To solve the motion planning problem, i.e. to a compute control law providing some desired output trajectories, we propose an open-loop control law based on a formal inversion of the input-output transfer function.

D.1.1 Inverse control

It is straightforward to invert (4.6) and formulate the input $\hat{T}_{eq}^{in}(s)$ as a function of the output $\hat{y}(s)$ (for all values of z)

$$\hat{T}_{eq}^{in}(s) = \exp\left(\frac{z}{v}s + \frac{k_1 z}{v} - \frac{m}{s+k_2}\right)\hat{y}(s) \tag{D.1}$$

The output $y(t)$ can be any delayed function of time. This delay equals z/v. Let $f(t)$ denote this function. We can write

$$\hat{y}(s) = \exp\left(-\frac{z}{v}s\right)\hat{f}(s) \tag{D.2}$$

Combining (D.1) and (D.2), we get

$$\hat{T}_{eq}^{in}(s) = \exp\left(\frac{k_1 z}{v} - \frac{m}{s+k_2}\right)\hat{f}(s)$$

The inverse Laplace calculus leads to

$$\begin{cases} T_{eq}^{in}(t) = e^{\frac{k_1 z}{v}} \Upsilon(t) \times \left[f(t) - \int_0^t \sqrt{\frac{m}{\tau}} J_1(2\sqrt{m\tau}) \exp(-k_2\tau) f(t-\tau) d\tau \right] \\ y(t) = f(t - z/v) \end{cases} \tag{D.3}$$

This result stems from the inverse Laplace transform of the following transfer function (from input $\hat{f}$ to output $\hat{T}_{eq}^{in}$):

$$\hat{T}_{eq}^{in}(s) = \exp\left(\frac{k_1 z}{v} - \frac{m}{s+k_2}\right) \hat{f}(s)$$

It gives

$$\begin{aligned} &\mathcal{L}^{-1}\left(\hat{T}_{eq}^{in}(s) \exp\left(-\frac{k_1 z}{v}\right)\right) \\ &= \mathcal{L}^{-1}\left(\exp\left(-\frac{m}{s+k_2}\right)\hat{f}(s)\right) \\ &= \left(\exp(-k_2 t)\mathcal{L}^{-1}\left(\exp\left(-\frac{m}{s}\right)\right)\right) * \mathcal{L}^{-1}\left(\hat{f}(s)\right) \\ &= \left(\exp(-k_2 t)\left(\delta(t) - \sqrt{\frac{m}{t}} J_1(2\sqrt{mt})\right)\right) * f(t) \\ &= (\exp(-k_2 t)\delta(t)) * f(t) - \left(\exp(-k_2 t)\sqrt{m/t} J_1(2\sqrt{mt})\right) * f(t) \end{aligned}$$

where δ denotes the Dirac delta function and $*$ the convolution. This yields

$$T_{eq}^{in}(t) = \exp\left(\frac{k_1 z}{v}\right) \Upsilon(t) \left[f(t) - \int_0^t \sqrt{\frac{m}{\tau}} J_1(2\sqrt{m\tau}) \exp(-k_2\tau) f(t-\tau) d\tau \right]$$

which is the first formula in (D.3).

In our application, the dead time z/v (typically 10^{-2} s) is very small when compared to the response time of the system (typically 10^2 s), so that $f(t)$ can be almost regarded as $y(t)$.

D.1.2 Simulation results

In this section, we consider two numeric scenarios that stress general problems that are encountered when controlling the DOC. In case A, we use $k_1 = 400$ s^{-1}, $k_2 = 0.35$ s^{-1}, $v = 4$ m.s^{-1} and $L = 7.62$ cm. In case B, we use $k_1 = 1600$ s^{-1}, $k_2 = 0.82$ s^{-1}, $v = 4.6$ m.s^{-1} and $L = 7.62$ cm. These two different cases (corresponding to two different geometries) correspond to long response times, which are in practice the most problematic to control. Because the system is linear and the steady-state gain is 1, figures are plotted with normalized temperature responses. The choice of the trajectory is *a priori* free, but several tries of usual transition functions have shown us it has important consequences. In order to obtain a smooth transition we choose the following C^∞ Gevrey function of order $1 + \frac{1}{\gamma}$ (see Laroche et al. (2000) for the mathematical properties of this function, and the smoothness of its derivative)

$$\begin{cases} f\left(\frac{t}{t_f}\right) = 0 \text{ if } \frac{t}{t_f} \leq 0 \\ f\left(\frac{t}{t_f}\right) = \dfrac{\displaystyle\int_0^{\frac{t}{t_f}} \exp\left(-\left(\frac{1}{u(1-u)}\right)^\gamma\right) du}{\displaystyle\int_0^1 \exp\left(-\left(\frac{1}{u(1-u)}\right)^\gamma\right) du} \text{ if } \frac{t}{t_f} \in]0,1[\\ f\left(\frac{t}{t_f}\right) = 1 \text{ if } \frac{t}{t_f} \geq 1 \end{cases}$$

Transition times t_f chosen in this section are inspired from results that will be obtained in § D.2. They are realistic. We use $t_f = 21.5$ s for case A and $t_f = 38.5$ s for case B, and $\gamma = 0.6$ for both cases. Depending on the values of parameters (k_1, k_2, v, L), we can get drastically different types of control trajectories. Although not intuitive, the control presented for case A in Fig. D.1a is quite simple. For case B, on the other hand, the control presented in Fig. D.1b is unrealistic because of its frequency and its amplitude. Further, in this case (actually probably in both cases) the control obtained by model inversion goes beyond the model validity region (non negligible conduction, non constants coefficients and non negligible heat losses ...). However, the computed control stresses interesting problems, related to the high-capacity energy storage of the solid phase. This partly explains why a DOC is a difficult system to control.

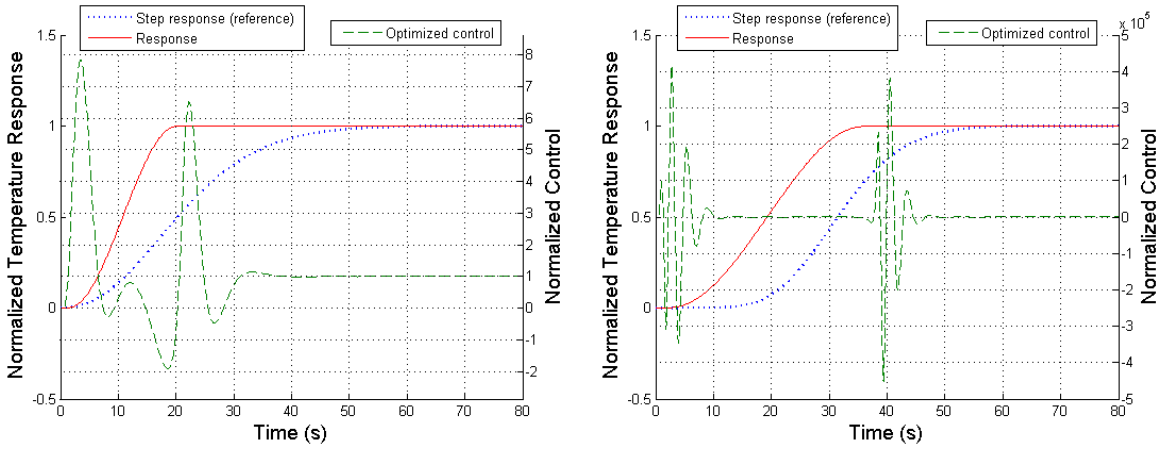

(a) Case A

(b) Case B

Figure D.1: Control corresponding to a smooth finite-time transition. Simulation data.

D.2 Trajectory optimization for constrained input

As seen in § D.1, inversion of the model can lead to a "shaking" control. Actually, this does not mean that such a system cannot be accelerated, but attention must be paid to the control bounds. In this section, to address this issue, we generate output trajectories under input constraints. First, we use a classic optimization approach, then we formulate the problem in a different way: we impose a limited number of possible values for the control, and a limited number of switches between these values. This drastically reduces the number of optimization variables, whereas the loss of performance appears negligible.

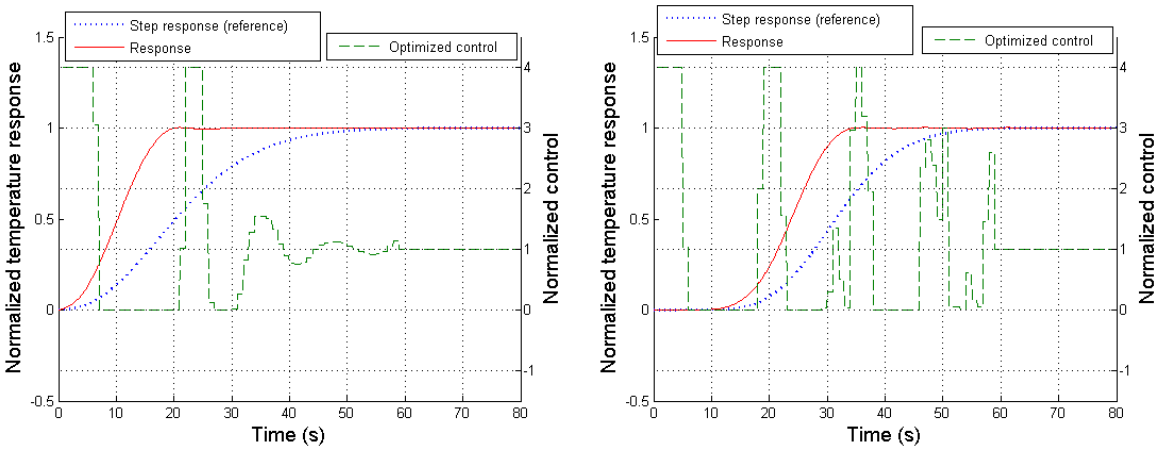

(a) Case A (b) Case B

Figure D.2: Optimized control with method 1. Simulation data.

D.2.1 Problem formulation 1 and simulation results

In this first formulation, we want to compute a piecewise constant control, subject to lower and upper bounds. This problem can be formally written under the form

$$\min_{(u_0,\ldots,u_n)} \int_0^H (T^{sp} - y(\tau))^2 d\tau$$

$$\begin{cases} T^{in}_{eq,min} \leq u_i = T^{in}_{eq}(iT_s) \leq T^{in}_{eq,max} & \forall i \in \{0,\ldots,n\} \\ y(t) \leq T^{sp} + \varepsilon & \forall t \in [0, H] \\ y(t) \geq T^{sp} - \varepsilon & \forall t \in [G, H] \end{cases} \tag{D.4}$$

where T^{sp} is the setpoint, ε is a small positive constant, T_s is the control sampling period, $n\ T_s$ is the control horizon, and H is the prediction horizon. G corresponds to the minimum time for which problem (D.4) is feasible. It is found iteratively, for example by dichotomy. Enforcing this minimum constraint avoids oscillations after the rise time. For numeric evaluation, we use $T^{sp} = 1$, $n = 60$, $T_s = 1$ s, $H = 200$ s, $T^{in}_{eq,min} = 0$, $T^{in}_{eq,max} = 4$, and $\varepsilon = 0.003$. Since the model is linear, for numerical experiments, its response to a given piecewise constant input can be quickly evaluated by a linear combination of time-delayed step responses. Step response T_h is evaluated by (4.8) and y is given by

$$y(t) = u_0\, T_h(t) + \sum_{i=1}^{n} (u_i - u_{i-1})\, T_h(t - iT_s)$$

Fig. D.2 shows that, in both cases, the system is accelerated as in § D.1, but, now, input constraints are satisfied. The transitions are not achieved in finite-time but, from the end time used in § D.1, the output remains within a tight range around the final value.

D.2.2 Problem formulation 2 and simulation results

The second method presented allows further simplification of the control with minor consequences on performance. We can notice in § D.2.1 that the control presents numerous pulses before

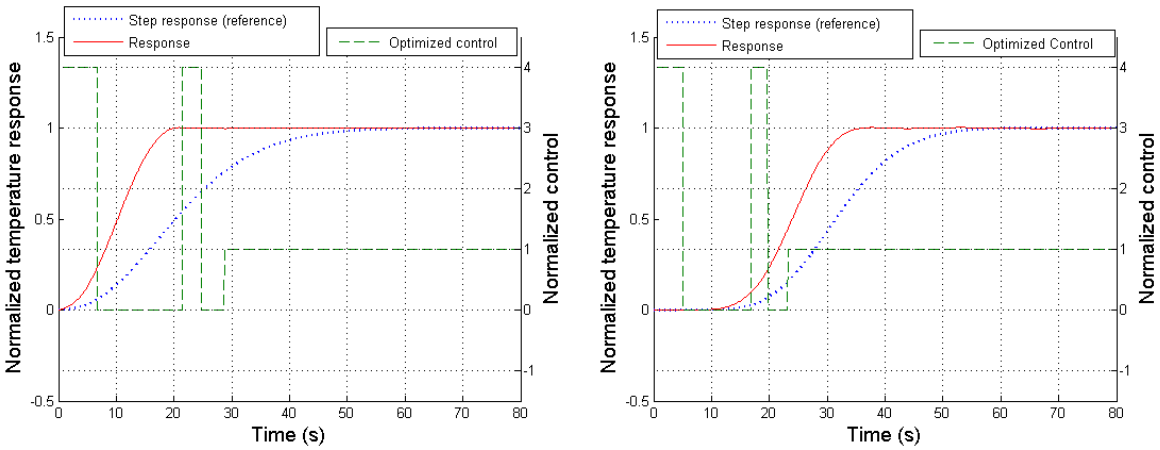

(a) Case A (b) Case B

Figure D.3: Optimized control with method 2. Simulation data.

finally setting to 1. In other words, once the output has almost reached its final value, the control still acts over a long period. We would like to shorten this period for an easier implementation of the control. To this end, we consider only a limited number of pulses n, before the final control value is kept constant. The n pulses share the same magnitude (equal to the allowed maximum $T^{in}_{eq,max}$), while their switch times have to be optimized. The optimizer also computes the time when the control is set to its final value. The constraints on y, as well as the objective function, are kept from problem (D.4). It seems clear that this problem has a solution for any n: shortening enough the pulses durations will generate a response close to the step response which satisfies the constraints.

We denote t_i the successive rise and fall times of the pulses, we choose $n = 2$ (i.e. $i \in \{0, .., 4\}$ with $t_0 = 0$ and t_4 representing the time of final step change) and $T^{in}_{eq,max} = 4$. The problem is formulated as

$$\min_{(t_1,\ldots,t_{2n})} \int_0^H (T^{sp} - y(\tau))^2 d\tau$$

$$\begin{cases} t_i \leq t_{i+1} \leq H & \forall i \in \{1, \ldots, 2n-1\} \\ y(t) \leq T^{sp} + \varepsilon & \forall t \in [0, H] \\ y(t) \geq T^{sp} - \varepsilon & \forall t \in [G, H] \end{cases} \tag{D.5}$$

In the same way as in § D.2.1 the response can be quickly evaluated by

$$y(t) = T^{in}_{eq,max} \sum_{i=0}^{N-1} (T_h(t - t_{2i}) - T_h(t - t_{2i+1})) + T_h(t - t_N)$$

Results of optimizations for cases A and B are presented in Fig. D.3. Control is simpler and time duration after which the control has reached its final value has been reduced. As shown in Table D.1, performance in terms of output variation has remained very close to the previous case. Moreover, the number of variables in the optimization problem has been considerably reduced, allowing a substantial reduction of the computational effort. Also, an energy expense index is obtained simply by integrating the absolute control value over the whole time range of the simulations (the integration time is equal for all scenarios, and the control value is 1 at the end of the integration time). It stresses the difficulty to follow precisely a given trajectory by the inversion method.

	Method	Rise time (s)	Energy expense index	Computational effort index
Case A	Inversion	19.77	86.18	12.53
	Optimization 1	19.70	71.73	18.54
	Optimization 2	19.74	71.73	1.000

	Method	Rise time (s)	Energy expense index	Computational effort index
Case B	Inversion	35.40	2.19×10^6	4881
	Optimization 1	34.28	68.59	42.93
	Optimization 2	35.30	68.93	1.000

Table D.1: Performance & Cost

D.2.3 Inversion of the resulting trajectory

We can notice that the trajectory resulting from optimization in § D.2 "takes off" much slower than the trajectory used for inverse control in § D.1. We can wonder if the "shaking" inverse control is caused by a wrongly chosen trajectory. In order to check this point, we inverse the trajectory obtained with optimization in § D.2. Fig. D.4 presents the inversion-based control corresponding to the trajectory obtained in Fig. D.3a. We notice a close matching between the two controls despite inaccuracy which is certainly due to difficulties in evaluating (D.3). This logically points out the fact that the trajectory should not be chosen as a simple transition function.

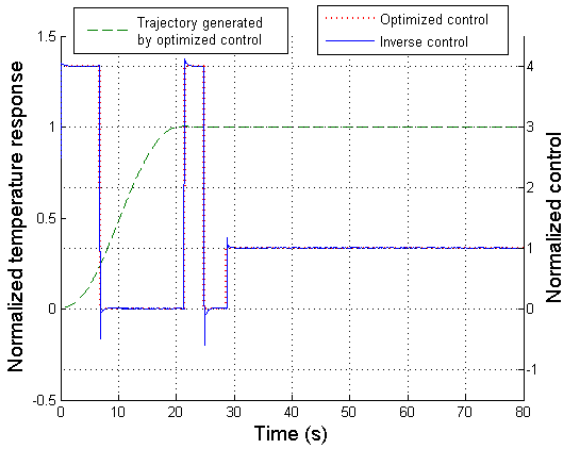

Figure D.4: Inverse control for optimized trajectory - case A. Simulation data.

D.3 Choice of step inputs parameters for problem formulation 2

It is previously found in § D.2 that two different control strategies can lead to very similar responses. Further, it is found that the problem formulation 2 (§ D.2.2) efficiently leads to a realistic control signal. In this section, choices of parameters of problem formulation 2 are examined. These are the number of pulses n and the pulse magnitude M.

D.3.1 Choice of the number of pulses

The first parameter to tune is the number of pulses n. Using a small number of pulses reduces computational efforts. It is shown in Fig. D.5 that, compared to step response, performance is much

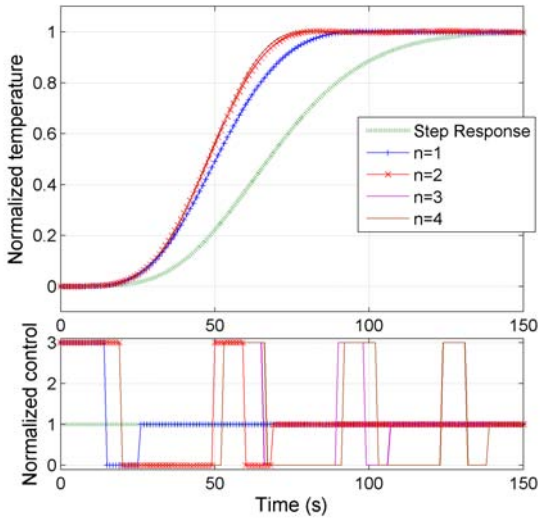

Figure D.5: Influence of pulse number n. Simulation data.

improved when using 1 pulse, slightly more when using 2 pulses, and that it is almost useless to consider more than 2 pulses. Results are identical for other pulse magnitudes. Hence, we choose to use 2 pulses.

D.3.2 Choice of pulse magnitude M

We compare here the two control laws obtained for different pulse magnitudes M. Once again, the obtained temperature responses are very similar whereas control laws are largely different. This effect is clearly shown in Fig. D.6 where experimental cases for $M = 2$ and $M = 3$ are reported. Temperatures are normalized for direct comparison. Temperature response in the case $M = 3$ is a bit faster than in the case $M = 2$. In simulations presented in Fig. D.7, we validate this fact for higher pulse magnitudes. Using $M = 3, 4, 5, 6...$ instead of $M = 2$ does not increase performance much. This fact is explained because a DOC is a very low-pass system. Using a constantly varying high frequency control yields almost no performance improvement. Indeed, *the system is mainly sensible to the low-pass content of the control*. Choosing a high pulse magnitude allows the next pulse to take place sooner. Nevertheless, consequences on the response are only minor. To obtain good results, the critical point is, for a given maximum magnitude, to compute switch times accurately.

So, increasing pulse magnitude does not increase performance much. In real application, the choice of M is limited by the decrease of the DOC efficiency when a very large amount of reductants is injected during pulses. Moreover, increasing pulse magnitude - that is enthalpy flow - obviously implies shortening pulse durations and, consequently, requires the accurate determination of the pulse switch times. The model may also fail to provide such accuracy. For all of these reasons, it is relevant to limit the pulse magnitude to about $M = 2$ to $M = 3$, depending on the application case.

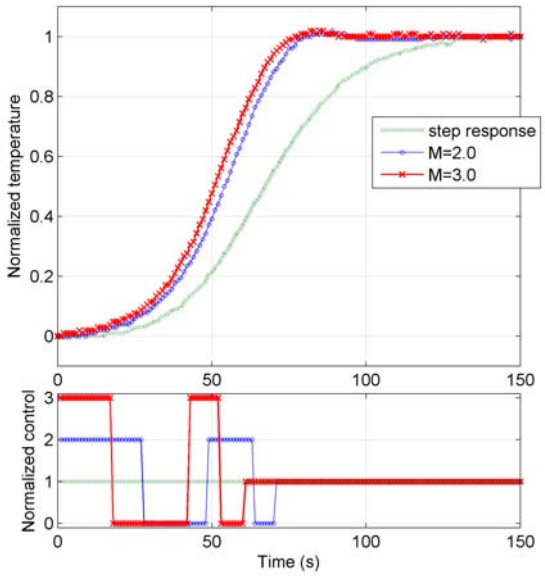

Figure D.6: Influence of pulse magnitude. Experimental data.

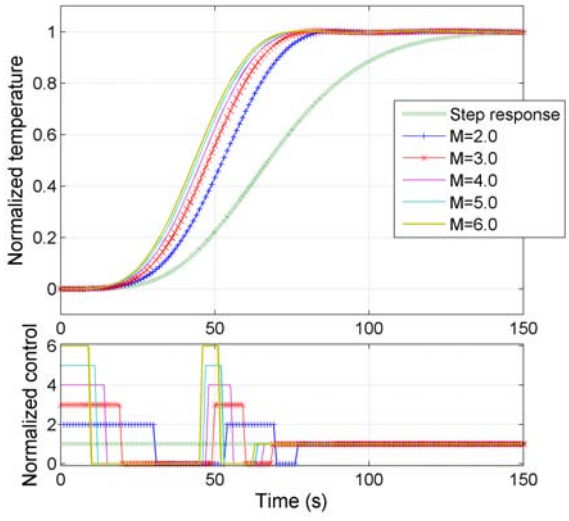

Figure D.7: Influence of pulse magnitude. Simulation.

D.4 Conclusion

Three different methods leading to control laws that speed up DOC temperature response have been presented. They have led to successful experimental results.

In practice, developed strategies are not used in the controller, because the rise time is only a small part of the regeneration process. However, this gives precious hints on the system behavior.

First, the different methods lead to very different control histories. However, the output histories are very similar. The system is mainly sensitive to the low-pass content of the control. This motivates low-order reduction of the model.

Accelerating the system responses requires a high control effort. Forcing the response to exact desired transient histories leads to unrealistic results. This hints at limited rejection possibilities for gas flow rate disturbances, which take place in the vicinity of the outlet.

Finally, optimizations are carried out using a boundary control in the control sub-model (4.1). On the contrary, experimental results correspond to a distributed input (reduced model). Presented strategies are used in Chapter 4 for experimental validation of the equivalence between these two models.

Appendix E

Details of computations

In this appendix, we detail several computations yielding formulas used in Chapters 3 and 4.

E.1 DOC temperature response

Denote $\mathcal{L}$ the Laplace operator, s the Laplace variable, $\hat{x}(s) = \mathcal{L}(x(t))$, and Υ the Heaviside function. Consider the following form for the source term Ψ

$$\Psi(z, u(t), v) = \Upsilon(t)\ \alpha\ \phi(\beta z)$$

with α and β real positive constants. Equations (3.4) and (3.8) lead to

$$\begin{cases} s\hat{T} + v\dfrac{\partial \hat{T}}{\partial z} = -k_1(\hat{T} - \hat{T}_s) \\ s\hat{T}_s = k_2(\hat{T} - \hat{T}_s) + \dfrac{\alpha\ \phi(\beta z)}{s} \end{cases}$$

and the boundary condition is written as

$$\hat{T}(0, s) = \hat{T}^{in}(s).$$

This gives the following first order linear differential equation

$$\frac{\partial \hat{T}}{\partial z} + \underbrace{\frac{1}{v}\left(s + k_1 - \frac{k_1 k_2}{s + k_2}\right)}_{\hat{A}(s)}\hat{T} = \underbrace{\frac{k_1}{v}\frac{\alpha}{s(s + k_2)}}_{\hat{B}(s)}\phi(\beta z) \tag{E.1}$$

In the following different profiles for the source term are considered.

E.1.1 Response to an exponentially decaying source term

In this subsection, the case $\phi(\beta z) = \exp(-\beta z)$ is considered. Equation (E.1) leads to

$$\hat{T} = \hat{T}^{in}\exp\left(-\hat{A}z\right) + \frac{\hat{B}}{\hat{A} - \beta}\left(\exp(-\beta z) - \exp\left(-\hat{A}z\right)\right) \tag{E.2}$$

First, let us invert the following expression

$$\hat{f}_{01}(s) = \frac{\hat{B}}{\hat{A} - \beta} = k_1\alpha\frac{1}{s\left(s^2 + (k_1 + k_2 - \beta v)s - \beta k_2 v\right)} \tag{E.3}$$

This yields, through the inverse Laplace transform $\mathcal{L}^{-1}$

$$f_{01}(t) = \mathcal{L}^{-1}\left(\hat{f}_{01}(s)\right) = \frac{2k_1\alpha}{\sqrt{\Delta}}\left(\frac{1-\exp\left(T_1 t\right)}{b-\sqrt{\Delta}} - \frac{1-\exp\left(T_2 t\right)}{b+\sqrt{\Delta}}\right) \tag{E.4}$$

where

$$\begin{cases} b & = k_1 + k_2 - \beta v \\ c & = -\beta k_2 v \\ \Delta & = b^2 - 4c \\ T_1 & = -(b-\sqrt{\Delta})/2 \\ T_2 & = -(b+\sqrt{\Delta})/2 \end{cases} \tag{E.5}$$

Now, let us invert $\dfrac{\hat{B}}{\hat{A}-\beta}\exp\left(-Az\right)$. For this, we compute the following intermediate result, where δ denotes the Dirac delta function and $*$ the convolution

$$\begin{aligned} &\mathcal{L}^{-1}\left(\hat{f}(s)\exp\left(\frac{m}{s+k_2}\right)\right) \\ &= \left(\exp\left(-k_2 t\right)\mathcal{L}^{-1}\left(\exp\left(\frac{m}{s}\right)\right)\right) * \mathcal{L}^{-1}\left(\hat{f}(s)\right) \\ &= \left(\exp\left(-k_2 t\right)\left(\delta(t) + \sqrt{\frac{m}{t}}\mathrm{I}_1(2\sqrt{mt})\right)\right) * f(t) \\ &= \left(\exp\left(-k_2 t\right)\delta(t)\right) * f(t) + e^{-k_2 t}\sqrt{\frac{m}{t}}\mathrm{I}_1(2\sqrt{mt}) * f(t) \\ &= f(t) + \int_0^t e^{-k_2\tau}\sqrt{\frac{m}{\tau}}\mathrm{I}_1(2\sqrt{m\tau})f(t-\tau)d\tau \end{aligned} \tag{E.6}$$

where I_1 is the modified Bessel function of the first kind. Using (E.6), we get

$$\begin{aligned} &\mathcal{L}^{-1}\left(\frac{\hat{B}}{\hat{A}-\beta}\exp\left(-Az\right)\exp\left(\frac{z}{v}s\right)\right) \\ &= \exp\left(-\frac{k_1 z}{v}\right)\mathcal{L}^{-1}\left(\exp\left(\frac{m}{s+k_2}\right)\hat{f}_{01}\right) \\ &= \exp\left(-\frac{k_1 z}{v}\right)\left(f_{01}(t) + \int_0^t \exp\left(-k_2\tau\right)\sqrt{\frac{m}{\tau}}\mathrm{I}_1(2\sqrt{m\tau})f_{01}(t-\tau)d\tau\right) \end{aligned} \tag{E.7}$$

with

$$m = \frac{k_1 k_2 z}{v} \tag{E.8}$$

and, then

$$\begin{aligned} &\mathcal{L}^{-1}\left(\frac{\hat{B}}{\hat{A}-\beta}\exp\left(-Az\right)\right) \\ &= \Upsilon\left(t-\frac{z}{v}\right)\exp\left(-\frac{k_1 z}{v}\right)\left(f_{01}(t-\frac{z}{v}) + \int_0^{t-\frac{z}{v}}\exp\left(-k_2\tau\right)\sqrt{\frac{m}{\tau}}\mathrm{I}_1(2\sqrt{m\tau})f_{01}(t-\tau)d\tau\right) \end{aligned} \tag{E.9}$$

To inverse $\hat{T}^{in}\exp(-Az)$, it is sufficient to replace f_{10} with T^{in} in (E.9). Finally, the result is written as

$$\begin{aligned}
T(z,t) &= \mathcal{L}^{-1}\left(\hat{T}\right) \\
&= \Upsilon\left(t-\frac{z}{v}\right)\exp\left(-\frac{k_1 z}{v}\right)\left(T^{in}(t-\frac{z}{v})+\int_0^{t-\frac{z}{v}}\exp(-k_2\tau)\sqrt{\frac{m}{\tau}}\mathrm{I}_1(2\sqrt{m\tau})T^{in}(t-\tau)d\tau\right) \\
&-\Upsilon\left(t-\frac{z}{v}\right)\exp\left(-\frac{k_1 z}{v}\right)\left(f_{01}(t-\frac{z}{v})+\int_0^{t-\frac{z}{v}}\exp(-k_2\tau)\sqrt{\frac{m}{\tau}}\mathrm{I}_1(2\sqrt{m\tau})f_{01}(t-\tau)d\tau\right) \\
&+f_{01}(t)\exp(-\beta z)
\end{aligned} \tag{E.10}$$

Final value According to the fact that a finite amount of energy is provided to the system, the final value of T exists and is given by

$$\lim_{t\to\infty}T(t)=\lim_{s\to 0}s\hat{T}(s)=\overline{T^{in}}+\frac{k_1\alpha}{\beta k_2 v}(1-\exp(-\beta z)) \tag{E.11}$$

where $\overline{T^{in}}$ is the steady-state value of T^{in}.

Relation with the control variable u The steady-state system analysis leads to the following relation between Ψ and u

$$u=\frac{1}{G_u}\int_0^z\Psi(\xi,u,v)d\xi \tag{E.12}$$

In particular,

$$u=\frac{1}{G_u}\int_0^z\alpha\,\phi(\beta\xi)d\xi \tag{E.13}$$

E.1.2 Response to a spatially uniform source term

We treat the following discontinuous case

$$\begin{cases}\Psi(z,u(t),v)=\psi(u(t),v), & 0\le z\le L_c(v)\\ \Psi(z,u(t),v)=0, & L_c(v)<z\le L\end{cases}$$

for a step input of $\psi(u(t),v)$

$$\psi(u(t),v)=\alpha\,\Upsilon(t)$$

This is a particular case of § E.1.1, in which $\beta=0$ for the DOC reactive length L_c, and $\alpha=0$ for the non-reactive length. We get

$$\hat{T}(L_c,s)=\hat{T}^{in}\exp\left(-\hat{A}L_c\right)+\frac{\hat{B}}{\hat{A}}\left(1-\exp\left(-\hat{A}L_c\right)\right) \tag{E.14}$$

Then, for $z>L_c$, solving equation (E.2) with $\alpha=0$ and $\hat{T}(L_c,s)$ as boundary condition

$$\hat{T}(z,s)=\hat{T}(L_c,s)\exp\left(-\hat{A}(z-L_c)\right) \tag{E.15}$$

yields

$$\hat{T}(z,s)=\hat{T}^{in}\exp\left(-\hat{A}z\right)-\frac{\hat{B}}{\hat{A}}\exp\left(-\hat{A}z\right)+\frac{\hat{B}}{\hat{A}}\exp\left(-\hat{A}(z-L_c)\right) \tag{E.16}$$

Now, we use (E.3) with $\beta = 0$. Then,

$$\hat{f}_{02} = \frac{\hat{B}}{\hat{A}} = k_1\alpha \frac{1}{s^2\,(s + k_1 + k_2)} \tag{E.17}$$

and

$$f_{02} = \frac{k_1\alpha}{k_1 + k_2} t - \frac{k_1\alpha}{(k_1 + k_2)^2}\,(1 - \exp\,(-(k_1 + k_2)t)) \tag{E.18}$$

Finally, an inverse Laplace transform on $\hat{T}$ yields

$$\begin{array}{rcl} T(z,t) & = & \Upsilon\,(t - z/v) \exp\left(-\dfrac{k_1 z}{v}\right) M(z, t - z/v) \\ & - & \Upsilon\,(t - z/v) \exp\left(-\dfrac{k_1 z}{v}\right) N(z, t - z/v) \\ & + & \Upsilon\,(t - z/v) \exp\left(-\dfrac{k_1 z}{v}\right) N(z - L_c, t - z/v) \end{array} \tag{E.19}$$

where

$$\left\{ \begin{array}{rcl} M(z,t) & = & T^{in}(t) + \displaystyle\int_0^t \exp\,(-k_2\tau) \sqrt{\frac{m(z)}{\tau}} \mathrm{I}_1(2\sqrt{m(z)\tau}) T^{in}(t - \tau) d\tau \\ N(z,t) & = & f_{02}(t) + \displaystyle\int_0^t \exp\,(-k_2\tau) \sqrt{\frac{m(z)}{\tau}} \mathrm{I}_1(2\sqrt{m(z)\tau}) f_{02}(t - \tau) d\tau \\ f_{02}(t) & = & \dfrac{k_1\alpha}{k_1 + k_2} t - \dfrac{k_1\alpha}{(k_1 + k_2)^2}\,(1 - \exp\,(-(k_1 + k_2)t)) \\ m(z) & = & k_1 k_2 z / v \end{array} \right.$$

Final value The final value for $\hat{T}^{in}(s) = \overline{T^{in}}/s$ and $\hat{\psi}(s) = \alpha/s$ can easily be computed. According to the fact that a finite amount of energy is provided to the system, the final value of T exists and is given by

$$\lim_{t\to\infty} T(t) = \lim_{s\to 0} s\hat{T}(s) = \overline{T^{in}} + \frac{k_1\alpha L_c}{k_2 v} \tag{E.20}$$

E.1.3 Response to boundary step input

We treat the case $\alpha = 0$ from § E.1.1. Consider $T^{in}(t) = \overline{T^{in}}\Upsilon(t)$. Let us invert $\hat{T}^{in} \exp\left(-\hat{A}z\right)$. To this end, the result (E.9) is used with $f_{01}(t) = \overline{T^{in}}\Upsilon(t)$. Then, we get

$$\begin{array}{l} \mathcal{L}^{-1}\left(\overline{T^{in}}\Upsilon(t) \exp\left(-\hat{A}z\right)\right) \\ \quad = \overline{T^{in}}\Upsilon\left(t - \dfrac{z}{v}\right) \exp\left(-\dfrac{k_1 z}{v}\right) \left(1 + \displaystyle\int_0^{t-\frac{z}{v}} \exp\,(-k_2\tau) \sqrt{\frac{m}{\tau}} \mathrm{I}_1(2\sqrt{m\tau}) d\tau\right) \end{array} \tag{E.21}$$

Series expansion of the integral term Denoting $w = 2\sqrt{m\tau}$, $dw = \sqrt{m/\tau} d\tau$ and $b = k_2/(4m)$, integral representation (E.21)

$$\int_0^{t - z/v} \exp\,(-k_2\tau) \sqrt{\frac{m}{\tau}} I_1(2\sqrt{m\tau}) d\tau \tag{E.22}$$

can be transformed into

$$\int_0^{2\sqrt{m(t-z/v)}} \exp(-bw^2) I_1(w) dw. \tag{E.23}$$

Besides, considering the following result (Wolfram Research Inc. 2006)

$$\int_0^t \exp(-mv^b) v^{\alpha-1} dv = \frac{m^{-\alpha/b}}{b} \Gamma(\alpha/b) \Gamma_{\text{inc}}(mt^b, \alpha/b), \tag{E.24}$$

where

$$\Gamma_{\text{inc}}(x, m) = \frac{1}{\Gamma(m)} \int_0^x t^{m-1} \exp(-t) dt$$

with the integral representation of the Bessel function I_1 (Abramowitz & Stegun 1965)

$$I_1(x) = \sum_{r=0}^{\infty} \frac{1}{r!(r+1)!} \left(\frac{x}{2}\right)^{2r+1} \tag{E.25}$$

it is possible to write integral (E.22) as an infinite sum of standards functions. We use the series representation (E.25) in integral term (E.23), and use property (E.24). Finally, this yields

$$\int_0^{t-z/v} \exp(-k_2\tau) \sqrt{\frac{m}{\tau}} I_1(2\sqrt{m\tau}) d\tau = \sum_{r=1}^{\infty} \frac{\Gamma_{\text{inc}}(k_2(t-z/v), r)}{r!(k_2/m)^r}$$

E.1.4 Response to a discrete source term

In § E.1.1 and § E.1.2, the responses to an exponentially decaying source term, and to spatially uniform source term have been computed. In order to get further insights into the source term spatial distribution in experimental responses, we now propose to compute the analytic response to a discrete source term. Several optimization procedures have been carried out with these results to analyze the distribution of the heat release. It has been concluded that most heat was released in the upstream part of the DOC, and that a spatially uniform source term was sufficient to handle the phenomena description well. However, computations details are reported here for information.

We divide the source term into N source terms of magnitude α_n, $n \in \{1, .., N\}$. We treat the following discontinuous case

$$\Psi = \alpha_n \Upsilon(t), \quad L_{n-1} \leq z \leq L_n, \quad n \in \{1, .., N\}$$

denoting $L_0 = 0$ and $L_N \leq L$. Following results of § E.1.2, it can be shown that the general solution is

$$\begin{aligned} \hat{T}(z \geq L_N, t) = &\left(\hat{T}_0 - \frac{\hat{B}_1}{\hat{A}}\right) \exp\left(-\hat{A}\, L_N\right) \\ &+ \sum_{i=1}^{n-1} \frac{\hat{B}_i - \hat{B}_{i+1}}{\hat{A}} \exp\left(-\hat{A}\,(z - L_i)\right) + \frac{\hat{B}_N}{\hat{A}} \exp\left(-\hat{A}\,(z - L_N)\right) \end{aligned}$$

where

$$\begin{cases} \hat{B}_i = \dfrac{k_1}{v\,(s+k_2)} \dfrac{\alpha_i}{s} \\ \hat{A} = \dfrac{1}{v}\left(s + k_1 - \dfrac{k_1\, k_2}{s+k_2}\right) \end{cases}$$

Denoting

$$g_i(t) = \mathcal{L}^{-1}\left(\frac{\hat{B}_i - \hat{B}_{i+1}}{\hat{A}}\right)$$

finally, this yields

$$\begin{cases} T_N(z,t) &= \sum_{i=0}^{N} \Upsilon\left(t - \frac{z-L_i}{v}\right) \exp\left(-k_1 \frac{z-L_i}{v}\right) f_i(z-L_i, t-\frac{z-L_i}{v}) \\ f_i(z,t) &= g_i(t) + \int_0^t \exp\left(-k_2\tau\right) \sqrt{\frac{m_i(z)}{\tau}} \mathrm{I}_1(2\sqrt{m_i(z)\tau}) g_i(t-\tau) d\tau \end{cases}$$

where

$$\begin{cases} g_i(t) &= \frac{k_1\left(\alpha_i - \alpha_{i+1}\right)}{k_1+k_2} t - \frac{k_1\left(\alpha_i - \alpha_{i+1}\right)}{\left(k_1+k_2\right)^2}\left(1 - \exp\left(-(k_1+k_2)t\right)\right) \\ m_i(z) &= k_1 k_2 z / v \\ L_0 &= 0 \\ \alpha_{N+1} &= 0 \\ \alpha_0 &= 0 \end{cases}$$

This result can be easily extended to the case $T^{in} \neq 0$.

Final value The final value for the source term considered above, and $\hat{T}^{in}(s) = \overline{T^{in}}/s$ can easily be computed. According to the fact that a finite amount of energy is provided to the system, the final value of T exists and is given by

$$\lim_{t\to\infty} T(t) = \lim_{s\to 0} s\hat{T}(s) = \overline{T^{in}} + \frac{k_1}{k_2 v}\left(\alpha_1 L_1 + \sum_{i=2}^{N} \alpha_i (L_i - L_{i-1})\right)$$

E.1.5 Selection of the z-profile

Here are some details on the process the have led us to select a uniform profile rather than other profiles.

During identification process to experimental results, a step of u is performed. As mentioned in § 3.4, it is supposed that the z-profile establishes very rapidly to its steady state value. Only HC are considered. Then, consider equations (2.4) and (2.5) at steady state, i.e. $dC_{u,g}/dt = 0$ and $dC_{u,s}/dt = 0$, where C_u refers to the control HC concentration. Then, $dC_u/dz = -K \cdot R$, where R is the reaction rate of control HC. Then, two hypotheses are considered:

- R is independent of concentration. This leads to $C_u = a - bz$, where a and b are constants. This hypothesis refers to the "uniform profile".
- R depends, at first order, on the concentration, i.e., $R = c \cdot C_u$ where c is constant. This leads to $C_u = a \cdot \exp\left(-\beta \cdot z\right)$. This hypothesis refers to the "exponentially decaying profile".

The following identification procedure has been used (refer to Appendix E.1.1 for details on computation of analytical responses):

- the steady state values of temperature are known, i.e. $\int \Psi(z)dz$ is constrained to match the difference between the steady-state temperature values (before and after the step change). Parameter a is computed from this integral;

- parameter k2 is fixed;
- the following sets of parameters are identified
  - (k_1, L_c) for the uniform profile
  - (k_1, β) for the exponentially decaying profile

At large gas flow rates both the uniform and the exponentially decaying profiles lead to a good description of the experimental data. Typical identification results are reported in Fig. E.1. However, we are particularly interested in describing responses at low gas flow rates. In this case, experimental responses are not well described by an exponentially decaying profile. In particular, it can be noticed in Fig. E.2 that the exponentially decaying profile poorly describes the "beginning" of the response compared to the uniform profile. We therefore use a uniform profile. Other profiles are left unused.

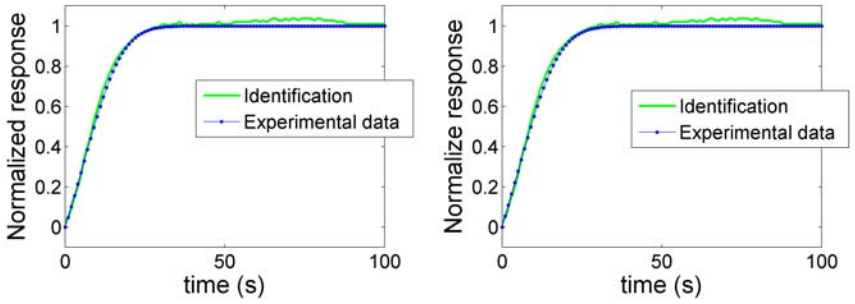

Figure E.1: At large gas flow rates, quality of identification results is identical for both the uniform profile (left) and the exponentially decaying profile (right). Experimental and analytical data.

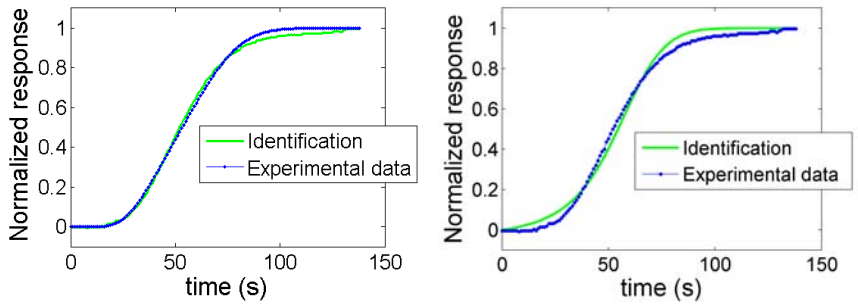

Figure E.2: At low gas flow rates, quality of identification results is better for the uniform profile (left) than for the exponentially decaying profile (right). Experimental and analytical data.

E.2 Delay evolution in the advection equation

Consider the advection equation

$$\frac{\partial x}{\partial t} + v(t)\frac{\partial x}{\partial z} = 0 \tag{E.26}$$

and the following change of variables

$$\begin{array}{l} x(z,t) = X(f(z,t), g(z,t)) \\ \left\{ \begin{array}{l} f(z,t) = t \\ g(z,t) = -z + \int_0^t v(s)ds, \quad v > 0 \end{array} \right. \end{array}$$

Equation (E.26) leads to

$$\begin{array}{l} \dfrac{\partial X}{\partial f} = 0 \\ X(f,g) = \Phi(g) \\ x(z,t) = \Phi(-z + \int_0^t v(s)ds) \end{array} \tag{E.27}$$

Define the delay $\delta(t)$ by

$$x(z,t) = x(z - z_p, t - \delta(t))$$

where z_p is the considered length of propagation. Equivalently, we have

$$\Phi\left(-z + \int_0^t v(s)ds\right) = \Phi\left(-z + z_p + \int_0^{t-\delta(t)} v(s)ds\right)$$

and the delay $\delta(t)$ verifies the following implicit equation

$$z_p = \int_{t-\delta(t)}^{t} v(\tau)d\tau$$

For a given value of $z_p > 0$, considering $v > 0$, $\delta(t)$ exists and is unique.

E.3 Computations on a simple advection model

Consider

$$\frac{\partial x}{\partial t} + \frac{\partial x}{\partial z} = \Psi(z,t)$$

with

- $x(z = 0, t) = 0 \quad \forall t \geq 0$
- $x(z, t = 0) = 0 \quad \forall t \in [0, 1]$
- $\Psi(z,t) = \left\{ \begin{array}{ll} \alpha(t) & 0 \leq z \leq l(t) \\ 0 & z \geq l(t) \end{array} \right.$

We study the response at the output, i.e. $x(1, t)$.

Remark. The solution of

$$\frac{\partial x}{\partial t} + \frac{\partial x}{\partial z} = \alpha(t)$$

for $\alpha(t) = d\Gamma(t)/dt$ has the form $x(z,t) = g(t - z) + \Gamma(t)$

E.3.1 Initial condition

Assume that, for $t \geq 0$, $\alpha(t) = \alpha_1$ and $l(t) = l_1$.
◦ For $z \in [l_1, 1]$,

$$\frac{\partial x}{\partial t} + \frac{\partial x}{\partial z} = 0$$

Then $x(z,t) = h(t-z)$. This yields, for $t = 0$, $x(z,0) = h(-z) = 0$, for $z \in [l_1, 1]$. Also $x(l_1,t) = h(t-l_1) = b(t)$ for $t \geq 0$, where $b(t)$ is a function to be determined. These two relations give

$$h(z) = \begin{cases} 0 & -1 \leq z \leq -l_1 \\ b(z+l_1) & z \geq -l_1 \end{cases}$$

◦ For $z \in [0, l_1]$,

$$\frac{\partial x}{\partial t} + \frac{\partial x}{\partial z} = \alpha_1$$

As $\alpha(t) = \alpha_1$, $\Gamma(t) = \alpha_1 t$, and, $x(z,t) = g(t-z) + \alpha_1 t$. Then, for $t = 0$, $x(z,0) = 0 = g(-z)$ for $z \in [0, l_1]$. Also $x(0,t) = 0 = g(t) + \alpha_1 t$, for $t \geq 0$. These two relations give

$$g(z) = \begin{cases} 0 & -l_1 \leq z \leq 0 \\ -\alpha_1 z & z \geq 0 \end{cases}$$

◦ We have $b(t) = x(l_1,t) = g(t-l_1) + \alpha_1 t$, with

$$g(t-l_1) = \begin{cases} 0 & 0 \leq t \leq l_1 \\ -\alpha_1(t-l_1) & t \geq l_1 \end{cases}$$

which yields

$$b(t) = \begin{cases} \alpha_1 t & 0 \leq t \leq l_1 \\ \alpha_1 l_1 & t \geq l_1 \end{cases}$$

◦ According to the previously established relations, given t_0 sufficiently large, we have

- for $z \in [0, l_1]$, $x(z, t_0) = \alpha_1 z$;
- for $z \in [l_1, 1]$, $x(z, t_0) = \alpha_1 l_1$.

These relations will serve as initial conditions $i(z)$ in the sequel:

$$i(z) = \begin{cases} \alpha_1 z & 0 \leq z \leq l_1 \\ \alpha_1 l_1 & l_1 \leq z \leq 1 \end{cases}$$

E.3.2 Step change in $l(t)$

At time $t = 0$, $l(t)$ is subject to a step change from l_1 to l_2, with $l_2 \geq l_1$, while $\alpha(t)$ becomes such that $\alpha(t) = d\Gamma(t)/dt$.
◦ For $z \in [0, l_2]$,

$$\frac{\partial x}{\partial t} + \frac{\partial x}{\partial z} = \alpha(t)$$

Then $x(z,t) = k(t-z) + \Gamma(t)$. For $t = 0$, $x(z,0) = i(z) = k(-z) + \Gamma(0)$ for $0 \leq z \leq l_2$. For $z = 0$, $x(0,t) = k(t) + \Gamma(t) = 0$ for $t \geq 0$, as it is assumed that $x(0,t)$ is always null. Then,

$$k(z) = \begin{cases} i(-z) - \Gamma(0) & -l_2 \leq z \leq 0 \\ -\Gamma(z) & z \geq 0 \end{cases}$$

which leads to

$$x(z,t) = \begin{cases} i(z-t) - \Gamma(0) + \Gamma(t) & z - l_2 \leq t \leq z \\ -\Gamma(t-z) + \Gamma(t) & t \geq z \end{cases}$$

In particular, we have

$$b_c(t) = x(l_2,t) = \begin{cases} i(l_2-t) - \Gamma(0) + \Gamma(t) & 0 \leq t \leq l_2 \\ -\Gamma(t-l_2) + \Gamma(t) & t \geq l_2 \end{cases}$$

∘ For $z \in [l_2, 1]$,

$$\frac{\partial x}{\partial t} + \frac{\partial x}{\partial z} = 0$$

Then $x(z,t) = p(t-z)$. We have $x(z,0) = i(z) = p(-z)$ for $l_2 \leq z \leq 1$, and $x(l_2,t) = b_c(t) = p(t-l_2)$ for $t \geq 0$, which leads to

$$p(z) = \begin{cases} i(-z) & -1 \leq z \leq -l_2 \\ b_c(z+l_2) & z \geq -l_2 \end{cases}$$

so

$$x(z,t) = \begin{cases} i(z-t) & z-1 \leq t \leq z-l_2 \\ b_c(t-z+l_2) & t \geq z-l_2 \end{cases}$$

∘ At the outlet $z = 1$, we then have

$$x(1,t) = \begin{cases} i(1-t) & 0 \leq t \leq 1-l_2 \\ b_c(t-1+l_2) & t \geq 1-l_2 \end{cases}$$

with

$$b_c(t-1+l_2) = \begin{cases} i(1-t) - \Gamma(0) + \Gamma(t-1+l_2) & 1-l_2 \leq t \leq 1 \\ -\Gamma(t-1) + \Gamma(t-1+l_2) & t \geq 1 \end{cases}$$

As $l_2 \geq l_1$, for $0 \leq t \leq 1-l_2$, $i(1-t) = \alpha_1 l_1$. But for $1-l_2 \leq t \leq 1$, two cases must be distinguished for $i(1-t)$, depending on the position of t with respect to $1-l_1$. Finally, we obtain

$$x(1,t) = \begin{cases} \alpha_1 l_1 & 0 \leq t \leq 1-l_2 \\ \alpha_1 l_1 - \Gamma(0) + \Gamma(t-1+l_2) & 1-l_2 \leq t \leq 1-l_1 \\ \alpha_1(1-t) - \Gamma(0) + \Gamma(t-1+l_2) & 1-l_1 \leq t \leq 1 \\ \Gamma(t-1+l_2) - \Gamma(t-1) & t \geq 1 \end{cases}$$

E.3.3 Simultaneous step change in $\alpha(t)$

We assume that, as $l(t)$ changes from l_1 to l_2 ($l_2 \geq l_1$), $\alpha(t)$ simultaneously changes from α_1 to α_2. To keep the same equilibrium value for $x(1,t)$, α_2 is chosen such that $\alpha_1 l_1 = \alpha_2 l_2$. Then, $\alpha_1 \geq \alpha_2$. In this case, $\Gamma(t) = \alpha_2 t$, and

$$x(1,t) = \begin{cases} \alpha_1 l_1 & 0 \leq t \leq 1-l_2 \\ \alpha_1 l_1 + \alpha_2(t-1+l_2) & 1-l_2 \leq t \leq 1-l_1 \\ \alpha_1(1-t) + \alpha_2(t-1+l_2) & 1-l_1 \leq t \leq 1 \\ \alpha_2 l_2 & t \geq 1 \end{cases}$$

For t from 0 to $1-l_2$, the output is constant and equals its previous value $\alpha_1 l_1$. At $t = 1-l_2$, it begins to increase to reach its maximum $\alpha_1 l_1 + \alpha_2(l_2 - l_1)$ at $t = 1-l_1$. From that time, it decreases to reach its final value $\alpha_2 l_2$ at $t = 1$. There is an overshoot of duration l_2.

E.3.4 Limiting the overshoot

Now, $\alpha(t)$ follows a ramp, from 0 at time 0 to α_2 reached at $t = l_2 - l_1$. From that time, $\alpha(t) = \alpha_2$

$$\alpha(t) = \begin{cases} \dfrac{\alpha_2}{l_2 - l_1} t & 0 \leq t \leq l_2 - l_1 \\ \alpha_2 & t \geq l_2 - l_1 \end{cases}$$

Then,

$$\Gamma(t) = \begin{cases} \dfrac{\alpha_2}{2(l_2 - l_1)} t^2 & 0 \leq t \leq l_2 - l_1 \\ \alpha_2 t - \dfrac{\alpha_2 (l_2 - l_1)}{2} & t \geq l_2 - l_1 \end{cases}$$

and

$$x(1,t) = \begin{cases} \alpha_1 l_1 & 0 \leq t \leq 1 - l_2 \\ \alpha_1 l_1 + \dfrac{\alpha_2}{2(l_2 - l_1)} (t - 1 + l_2)^2 & 1 - l_2 \leq t \leq 1 - l_1 \\ \alpha_1 (1 - t) + \alpha_2 (t - 1 + l_2) - \dfrac{\alpha_2 (l_2 - l_1)}{2} & 1 - l_1 \leq t \leq 1 \\ -\dfrac{\alpha_2}{2(l_2 - l_1)} (t - 1)^2 + \alpha_2 (t - 1) + \dfrac{\alpha_2 (l_1 + l_2)}{2} & 1 \geq t \geq 1 + l_2 - l_1 \\ \alpha_2 l_2 & t \geq 1 + l_2 - l_1 \end{cases}$$

For t from 0 to $1 - l_2$, the output is constant to its previous value $\alpha_1 l_1$. At $t = 1 - l_2$, it begins to increase to reach its maximum $\alpha_1 l_1 + \alpha_2 (l_2 - l_1)/2$ at at $t = 1 - l_1$. From that time, it decreases to reach the value $\alpha_2 (l_1 + l_2)/2 = \alpha_1 l_1 - \alpha_2 (l_2 - l_1)/2$ at $t = 1$. From $t = 1$ it increases to reach its final value $\alpha_2 l_2$ at $t = 1 + l_2 - l_1$. There is still an overshoot, but it maximum is divided by two. The counterpart is an undershoot that has the same magnitude than the overshoot.

E.4 A change of variables for the advection-diffusion equation

Let us consider the following advection-diffusion equation with variable coefficients $\lambda(t)$ and $\vartheta(t)$

$$\frac{\partial T(z,t)}{\partial t} + \vartheta(t) \frac{\partial T(z,t)}{\partial z} = \lambda(t) \frac{\partial^2 T(z,t)}{\partial z^2} \tag{E.28}$$

with initial condition

$$T(z,0) = \Upsilon(-z) \tag{E.29}$$

where Υ denote the Heaviside step function. Let us use the following change of variables

$$w(\zeta, \tau) = T(z,t)$$

with

$$\begin{cases} \zeta = z - \displaystyle\int_0^t \vartheta(s) ds \\ \tau = \displaystyle\int_0^t \lambda(s) ds \end{cases}$$

Equation (E.28) leads to

$$\begin{aligned}
\frac{\partial T}{\partial t} &= \frac{\partial w}{\partial \tau}\frac{\partial \tau}{\partial t} + \frac{\partial w}{\partial \zeta}\frac{\partial \zeta}{\partial t} = \frac{\partial w}{\partial \tau}\lambda(t) - \frac{\partial w}{\partial \zeta}\vartheta(t) \\
\frac{\partial T}{\partial z} &= \frac{\partial w}{\partial \tau}\frac{\partial \tau}{\partial z} + \frac{\partial w}{\partial \zeta}\frac{\partial \zeta}{\partial z} = \frac{\partial w}{\partial \zeta} \\
\frac{\partial^2 T}{\partial z^2} &= \frac{\partial}{\partial \tau}\left(\frac{\partial w}{\partial \zeta}\right)\frac{\partial \tau}{\partial z} + \frac{\partial}{\partial \zeta}\left(\frac{\partial w}{\partial \zeta}\right)\frac{\partial \zeta}{\partial z} = \frac{\partial^2 w}{\partial \zeta^2}
\end{aligned}$$

Finally, Eq. (E.28) leads to the heat equation

$$\frac{\partial w}{\partial \tau} = \frac{\partial^2 w}{\partial \zeta^2}$$

Because variable $v(t) > 0$, we have $\lambda(t) > 0$ and $\vartheta(t) > 0$, then

$$t = 0 \Longleftrightarrow \begin{cases} \tau = 0 \\ \zeta = z \end{cases}$$

Initial condition (E.29) is transformed into

$$w(\zeta, 0) = \Upsilon(-\zeta)$$

Appendix F

Experimental setup

The experiments reported in this thesis were conducted on an experimental setup that is described here. The DOC is installed inside a diesel engine exhaust line. The OEM Engine Control Unit (ECU) is fully bypassed. The engine is used to vary both the gas flow rate and the DOC inlet temperature. DOC inlet temperature T^{in} can be risen from 300°C to 500°C by means of a coupled post-injection taking place in addition to the pilot and the main injections. As is pictured in Fig. F.1, two distinct configurations can be used to control the reductants flow: either by an Exhaust Port Injector (EPI) located right upstream of the turbine, or by common-rail late post-injection. The reader can report to Appendix G.6 for details about EPI management and to Appendix G.5 for more information about the late-injection.

Experimental results presented in the thesis were all obtained with one of these two setups. Two 2.2L 4-cylinder engines were used. In all cases, mass air flow rate is measured at the engine intake (thanks to an embedded[1] sensor). Note that the gas flow rate is not measured in the exhaust line. The engine air path is actuated by an intake throttle, a Variable Geometry Turbine (VGT), an Exhaust Gas Recirculation (EGR) valve and an EGR bypass valve (not pictured in Fig. F.1). The engine fuel path is actuated by a high-pressure pump and common-rail injectors (up to 5 injections are possible).

The aftertreatment experimental setup is composed of a DOC and a DPF as presented in Fig. F.2. Both a 3-inch long and a 4-inch long platinum-based DOC were tested. Both monoliths are made of cordierite and have a cell density of 400 cpsi. Temperature is measured at three different locations: the DOC inlet (thanks to an embedded sensor), the DOC outlet (thanks to an embedded sensor), and at the center of the DOC (using a testbench-specific sensor[2]). An inlet pressure sensor (which is embedded) is used to compute the density, and then the gas speed. Note that the inlet temperature and pressure sensors are the turbine downstream sensors. They are present in most turbocharged engine commercial lines configurations. The DPF differential pressure (measured with an embedded sensor) is used to estimate particulate matter (PM) loading of the DPF. The gas composition can be analyzed either upstream or downstream of the DOC by a 5-gas analyzer (testbench sensor). *In some experiments, gas analyses are reported for both upstream and downstream locations. In fact, these experiments have been carried out twice, taking a particular care to verify that all external conditions, inputs and measurements were very close.* Thermocouples are mainly used for model fitting. In particular, the intra-catalyst thermocouple is used to understand some DOC thermal phenomena (see § 3.1), the corresponding simplified model descriptions (see § 3.4.2) and consequences on control performance (§ 3.5). It is also used for an extensive model validation (see § 4.1.4). Gas analyzer

[1] Sensor is needed and commonly available in embedded applications. It is used in the control strategies.

[2] Sensor is NOT available in embedded application. It is NOT used in the control strategies.

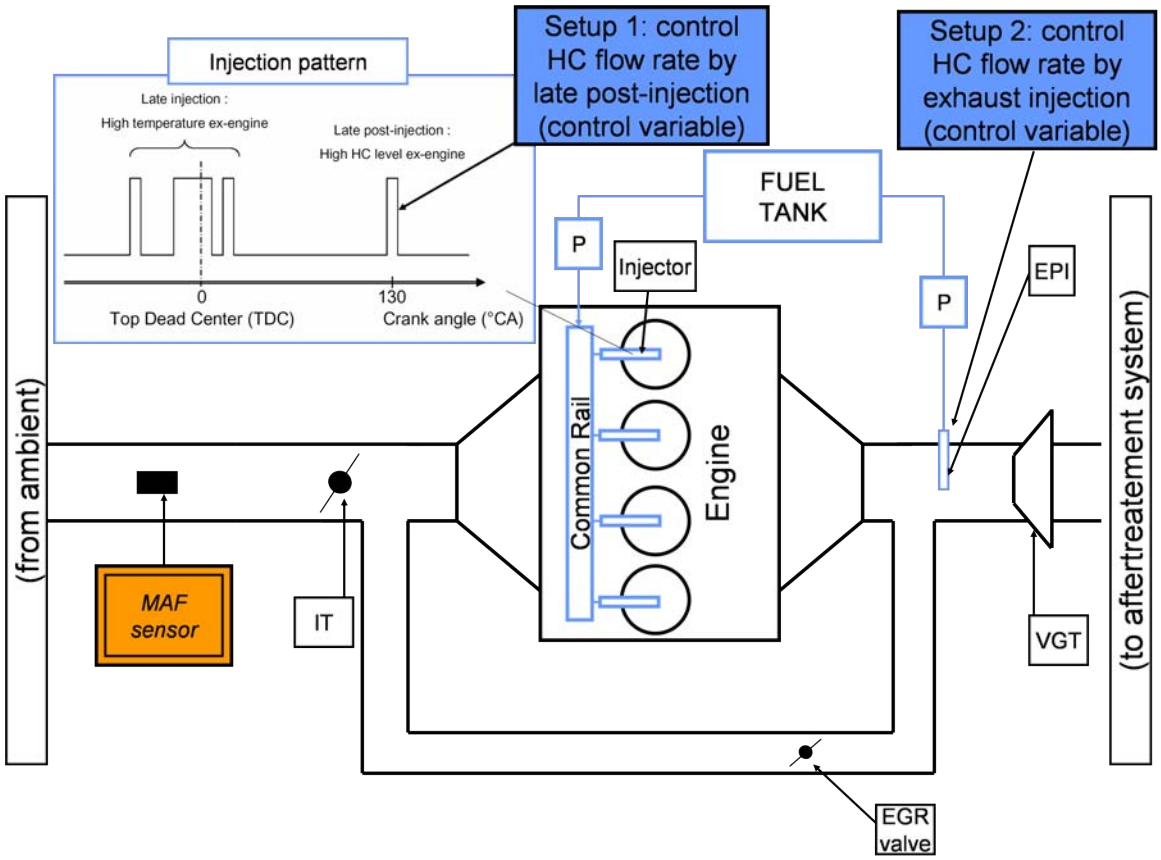

Figure F.1: Simplified scheme of the engine in the considered experimental setup (*not all devices are represented*). The mass air flow (MAF) sensor at the engine intake, is used to estimate the gas flow rate in the exhaust line. Intake throttle (IT), exhaust gas recirculation (EGR) valve, and variable geometry turbine (VGT) are the actuators used for air path control. In order to produce the control HC flow, late post-injection is used in the engine injection system. Alternatively, control HC flow rate can be supplied by a specific exhaust injection using the exhaust port injector (EPI). In both cases the fuel is supplied by pumps (P).

is used to measure the DOC conversion efficiency and to build up a model for engine unburnt HC (details are given in Appendix G.3).

On the considered experimental setup, generating an input signal (inlet temperature, gas flow rate, engine gas composition) independently from the others is not possible. This explains why they are not isolated in the results presented in the thesis.

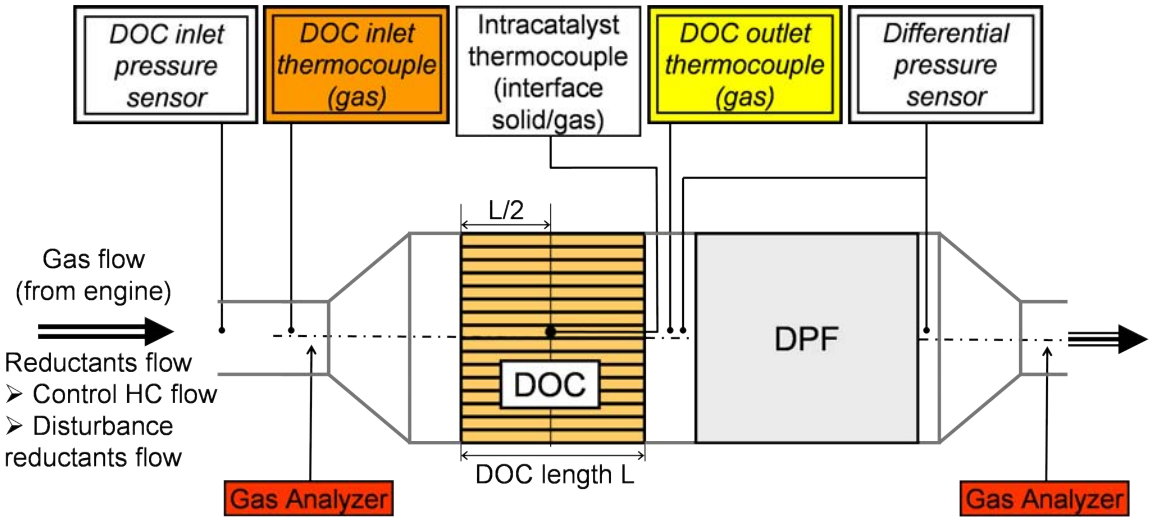

Figure F.2: Exhaust aftertreatment system of the considered experimental setup. Double borders refer to commonly available sensors in embedded applications. Thermocouples are mainly used for model fitting. Gas analyzer is used to measure the DOC conversion efficiency and to build up a model for engine unburnt HC. It can be switched to the upstream or the downstream location. Gas speed is computed from the engine intake mass air flow sensor and the DOC inlet pressure sensor. DPF differential pressure sensor is used to estimate particulate matter loading of the DPF.

Appendix G

Controller environment: engine calibration, actuators management & DOC calibration details

G.1 Introduction

In order to start an active regeneration process, an obvious requirement is that the DOC is activated (i.e. its temperature is above the light-off temperature of about 250°C). This is usually the case except during cold-start phases.

At high-load operating points, the exhaust gas temperature may be sufficient even to generate a partial regeneration process (called passive regeneration).

In general, the normal engine operation does not provide good conditions for the active regeneration process or for other aftertreatment operations requiring catalyst heating (e.g. LNT desulfations). For example, performing an active regeneration when the exhaust gas temperature is low (even if above the light-off temperature) would require a large control HC quantity to be injected in order to reach the regeneration temperature and would cause many issues. Especially, when using exhaust injection (EPI) as actuator, high exhaust HC quantity cause DOC efficiency drop. When using in-cylinder late post-injection as actuator, exhaust HC quantity must be carefully looked at because it severely increases oil dilution, which could be a cause of frequent servicing. Further, when the engine switches from low to high load operating points, this induces higher DOC inlet temperature variations and, thus, unnecessary disturbances.

In order to limit the HC flow in the exhaust line, and gas temperature variations at the DOC inlet, the engine is used in a sub-optimal mode (its power efficiency is decreased). At a constant power output (speed and torque), exhaust gas temperature is increased when compared to the normal operation mode.

This sub-optimal mode is called post-injection mode (PI mode), because a coupled post-injection is used. In the normal injection mode (NI mode), the injection pattern is usually composed of a pilot and a main injection. In PI mode, these injections are postponed in the engine cycle, and a third injection is added (referred to as coupled post-injection (coupled PI)). This mode requires a specific calibration, which, at least, doubles the engine calibration effort.

In this appendix, first, we stress the objectives for PI mode calibration. Then, a black-box model for engine reductants emissions (variable F_{dis}) is proposed. Also, some details are given about the conversion efficiency identification procedure. Finally, actuation issues related to late post-injection are addressed.

G.2 Engine optimization objectives

The calibration is performed in PI mode to reach the following objectives:

1. maximizing engine exhaust temperature;
2. minimizing HC & CO emissions;
3. minimizing HC & CO variability in the engine map;
4. minimizing temperature variability in the engine map;

with the following hard constraints :

$$T_{min} < T < T_{max}$$

Typically, $T_{min} = 300°C$ and $T_{max} = 480°C$. T_{min} value is chosen greater than the light-off temperature, taking into account a margin in case of particularly large heat losses (due to cold ambient temperature). Note that it is checked online that the exhaust gas temperature is higher than the light-off temperature before starting the regeneration. The T_{max} value is chosen significantly lower than PM oxidation temperature so that the active regeneration process does not start without control HC injection. Maximizing engine exhaust temperature and minimizing HC emissions (objectives 1 and 2) are opposite objectives, especially for the low-load, low-speed engine operating points. Minimizing HC and temperature variability in the engine map (objective 3) aims at yielding smooth maps. It is not an easy task because HC emissions are high at engine low-load, low-speed operating points and are almost zero at points of higher load. In a similar manner, minimizing temperature variability in the engine map (objective 4) is not easy to realize together with objective 3, because temperature is close to T_{min} at low-load, low-speed operating points and is rapidly increasing to T_{max} when load is increasing with small HC variability. Solving this optimization problem is usually carried out manually by engine engineering practitioners.

G.3 Disturbance reductants emissions (F_{dis})

As explained in § G.1, in PI mode, a coupled post-injection is used. Calibration objectives for this mode (see § G.2) are difficult and unavoidably lead to high HC emissions for low-load operating points. Resulting disturbance reductants flow rate F_{dis} is significant. It may result, in some cases, in a reductants flow rate causing a DOC temperature increase as high as 100°C. This quantity largely varies largely with the engine operating point. Then, an evaluation of a "real" HC flow rate at the catalyst inlet is necessary. Unlike the inlet gas temperature and the gas flow rate (disturbances T^{in} and F), HC flow rate is not measured online. Its evaluation would probably require a minimal (online-computable) model for engine emissions. Such a model is the subject of on-going research. To carry out the experiments, a simple black-box model was used instead. This model requires the measurement of the steady-state emissions, especially for the low-load operating points. These measures are usually available from the engine calibration process and do not require any specific calibration. Dynamic responses are obtained by performing fast transients between operating points. Typically, a few transients are performed between low-load points (where emissions are high) and higher load points (where emissions are negligible).

Benefits of including a disturbance reductants flow F_{dis} at the control inlet has been clearly made visible when using the exhaust injection, which does not influence the in-cylinder oxidation process. Obviously, using the late post-injection as actuator would ideally require finer analyses of influence of this additional injection. However, the same model was used.

We sketch here the black-box model used in the controller. This brief presentation is for information (and perspectives) only. A little time has been allowed for theory in this field, which is beyond the scope of this thesis.

An example of HC emissions caused by a fast change of engine operating point, is reported in Fig. G.1. It leads, in this case (decrease in engine load), to an important rise in HC emissions. We propose to identify this response to the response of a first order model using two different time

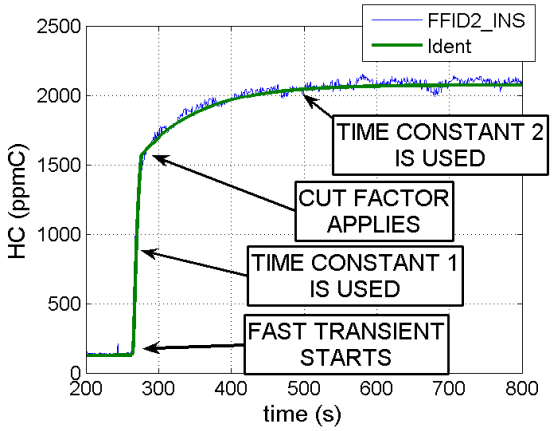

Figure G.1: A simple identification model is used to take into account unburnt HC emissions without late-injection.

constants. The ratio of HC variation to static variation, at which the time constant is switched is also identified. It is called "cut factor". In the model, two different modes are used: a "rise mode" and a "fall mode". The rise mode is used when the current emission value is below its static-mapped value given by current engine operating point. For each mode, two different time constants are proposed. These time constants are significantly different. When a change of mode is detected, e.g. current value increases and crosses the static-mapped value that decreases (according to the engine operating point), a reference value is stored. This reference is used in each mode to select the right time constant, according to the so-called cut factor. In summary, the model has 6 parameters: 2 time constants and 1 cut factor for each mode.

Note that many factors of influence may significantly shift the steady-state map value. In particular, emissions are strongly correlated to the gas temperature. An interesting perspective would be to infer the emissions from this measurement (and other variables).

G.4 Conversion efficiency identification

As presented in Fig. G.2, the conversion efficiency mostly depends on the gas flow rate (or gas speed), the HC speciation (fuel type), and the injection method. Once a setup has been selected (i.e. injection method (see § F) and fuel type), it is considered that the conversion efficiency depends only on the gas flow rate (or gas speed). Further details about this study can be found in Frobert, Creff, Lepreux, Schmidt & Raux (2009).

The conversion efficiency is identified to two affine decreasing functions, one for the low gas flow rate, and the other for the medium to high gas flow rate. It is assumed that $\lim_{F \to 0} \eta(F) = 1$. The identification model is written as

$$\eta(F) = \begin{cases} 1 - c_1 \, F(v), & 0 < F < F_L \\ 1 - c_1 \, F_L - c_2 \, F, & F_L < F \end{cases}$$

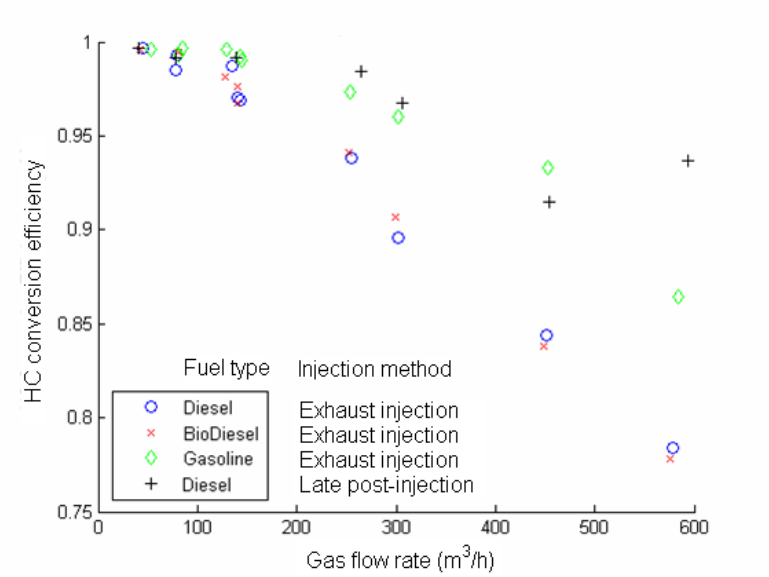

Figure G.2: DOC conversion efficiency η versus gas volumetric flow rate depends. Conversion efficiency on the experimental setup. Experimental data.

where $0 < c_1 < c_2$ and F_L are identified values.

G.5 Actuator management: common-rail late post-injection

An approach based on the torque analysis is presented here because it relates the problem directly to the use of the system in real conditions. Obviously the system should be more instrumented (pressure sensors, ...), and studied first on a dedicated testbench. This is a topic of on-going activities.

Description of phenomena

In this part, the common-rail late post-injection (late PI) is considered as actuator.

In the DOC control problem, the high-level control variable is HC control flow rate, which is provided by post-injection (PI). In fact, the low-level variable is the injector energizing time, i.e. the time during which current acts to open the injector. Each injector is open at each engine cycle, allowing HC to discharge from the injector pipe into the cylinder (discontinuous flow). Additionally to this energizing time, another degree of freedom is the phase of the injection, which is the time at which the injection begins in the combustion cycle.

In order to precisely master the control variable (exhaust HC flow rate), it is desired that this control is not intrusive for engine and aftertreatment strategies. From the engine control system viewpoint, a key requirement is that the output torque is not affected by the late-injection. From the aftertreatment control system viewpoint, a key requirement is that the HC flow reaching the DOC inlet closely matches the desired control variable flow rate (u).

To these ends, first, control HC are injected late in the engine combustion cycle (around -130°CA[1]). At this time of the engine cycle, HC are not (not much) oxidized while being in the cylinders. It is also commonly assumed that they produce no extra torque (this assumption will be verified in the following conclusions).

However, these requirements are difficult to satisfy. In fact, if no particular care is taken, it leads to important difficulties, which are described in the sequel.

First obvious observation, pictured in Fig. G.3, is that the phase of the late PI can strongly impact on the engine output torque (linear transform of BMEP[2]). For these experiments, a constant energizing time is used. However, the output torque is strongly affected by the phase of this injection. These torque variations are caused by variations of injected masses by the other injections. It is clearly made visible in Fig. G.3, that the flow rate of total supplied fuel significantly varies. Impact on the torque is a fundamental issue to provide acceptable driving conditions.

Further, in some cases, this injection impacts the combustion process differently from one cylinder to the other. Such an observation is pictured in Fig. G.4. It is shown in Fig. G.5 that the late PI can even cause global instabilities in the engine output torque. This leads to unusual balancing of the mechanical parts, and may reduce engine life expectancy.

These variations are also associated to significant variations of the exhaust temperature, and exhaust emissions, which raises important issues for actuation of aftertreatment control systems.

Although impact on torque, temperature, and HC emissions are usually correlated (e.g. torque is lower when HC is higher), it is possible to show that, even if the fuel supply is globally constant and the torque is constant, phasing the late PI can strongly impact on the temperature control possibilities. Two different late PI phases, for which the output torques are equal, are reported in Fig. G.6. As evidenced by the flow rate measurement, the HC flow rate in the exhaust line is decreased, while the exhaust temperature remains constant. Corresponding steady-state value of the DOC outlet temperature is decreased by about 50°C, which is beyond our temperature control objective. It stresses that the importance of the problem of actuation when considering aftertreatment control systems.

[1] Crankshaft Angle degrees

[2] Break Mean Effective Pressure

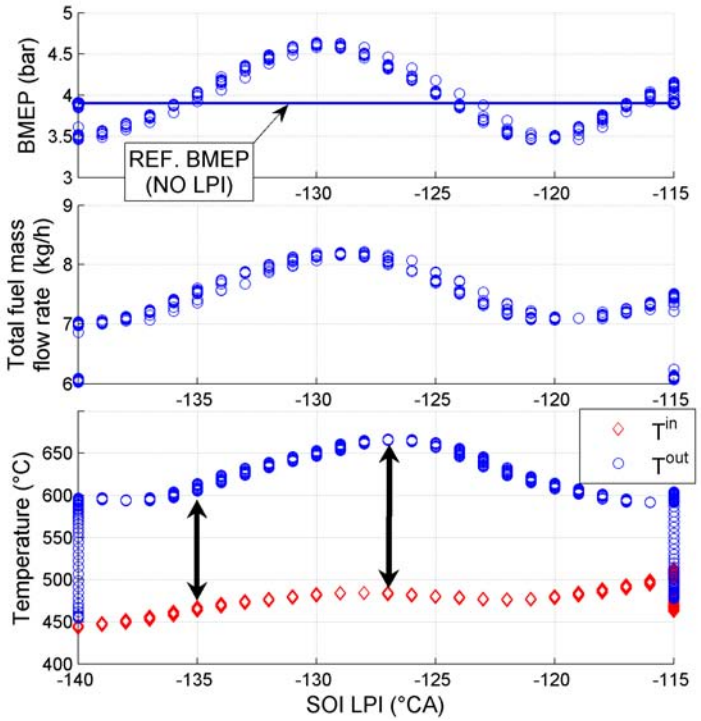

Figure G.3: BMEP (linear transform of torque), supplied fuel mass flow rate, and DOC inlet and outlet temperature *vs. the phase of the late post-injection* (SOI LPI). All injections energizing times (ETs), and in particular, the late post-injection ET stays constant during the experiment. The choice of the phase of the late post-injection (PI) heavily impacts on injected fuel masses, and, in turn, on torque, and on T^{in} and T^{out}. Reductants flow rate (not plotted) varies also (it is related to $T^{out} - T^{in}$ variations). Experimental data.

Modeling and controlling the injection systems, i.e. transforming the low-level variable (energizing time) into the high level variable (injected mass), is a critical issue in engine management. In particular, multi-pulse injection control has been the subject of numerous research works since the introduction of this actuator. However, most of the literature on the subject focuses on pressure waves oscillations inside the pipe connecting the rail to the injector (see e.g. Sciarretta & Corde (2007)). Although common-rail pressure wave oscillation have been reported in the literature, it is generally concluded that the impact of an injection on the consecutive injector is much smaller than the impact of multiple pulses of a given injector; because the dwell time to consecutive injector is large (see e.g. Bianchi et al. (2005)). Our experimental observations clearly evidence interactions between injectors. When a late PI is used, it seems that pressure waves are weakly damped in the common-rail. Then, they affects the pressure inside the next injector. In fact, the dwell time between the coupled PI and the late PI is smaller than the dwell time between the late PI and the injection of the consecutive injector.

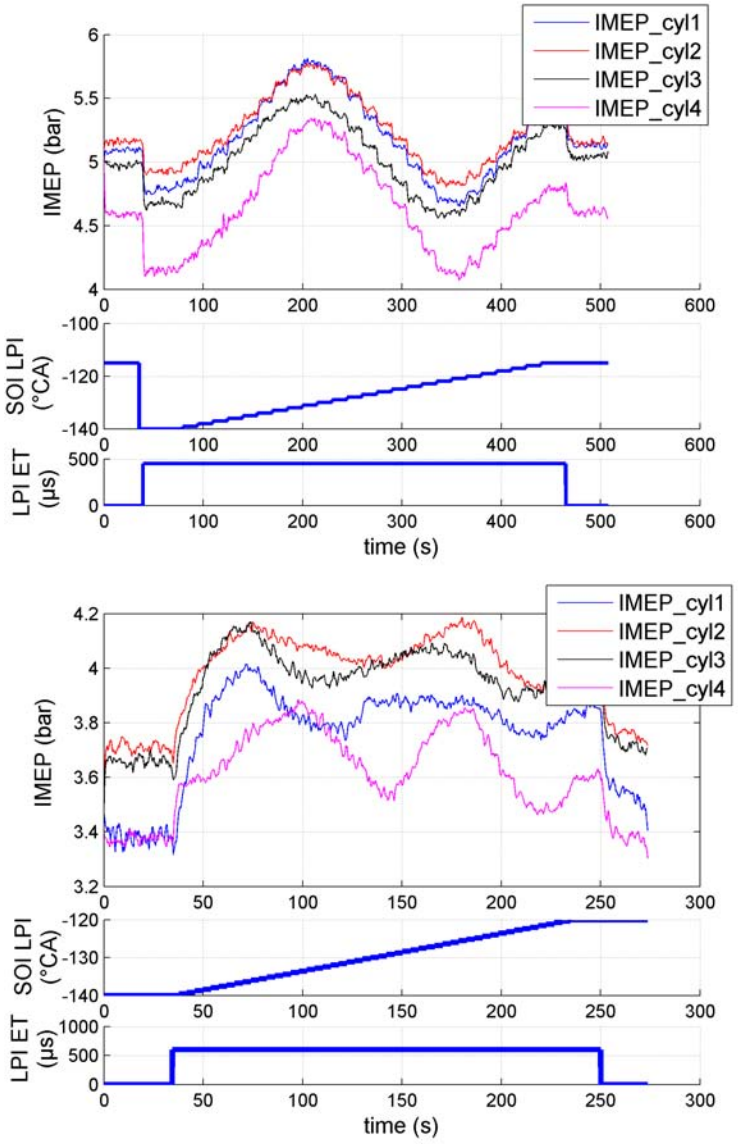

Figure G.4: The choice of the phase of late post-injection (SOI LPI) at constant energizing time (ET), can have different influences on IMEP (related to BMEP) in each cylinder (down) compared to a "normal" case (up). Experimental data.

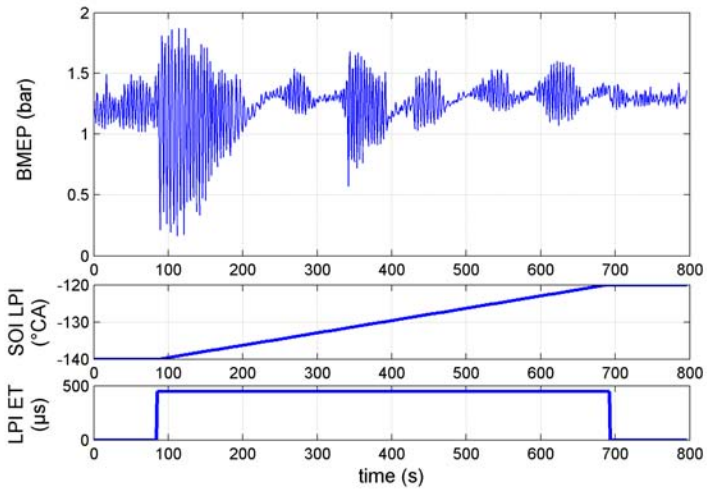

Figure G.5: The choice of the phase of late post-injection (SOI LPI) at constant energizing time, can cause global instabilities. BMEP is the image of the torque. Experimental data.

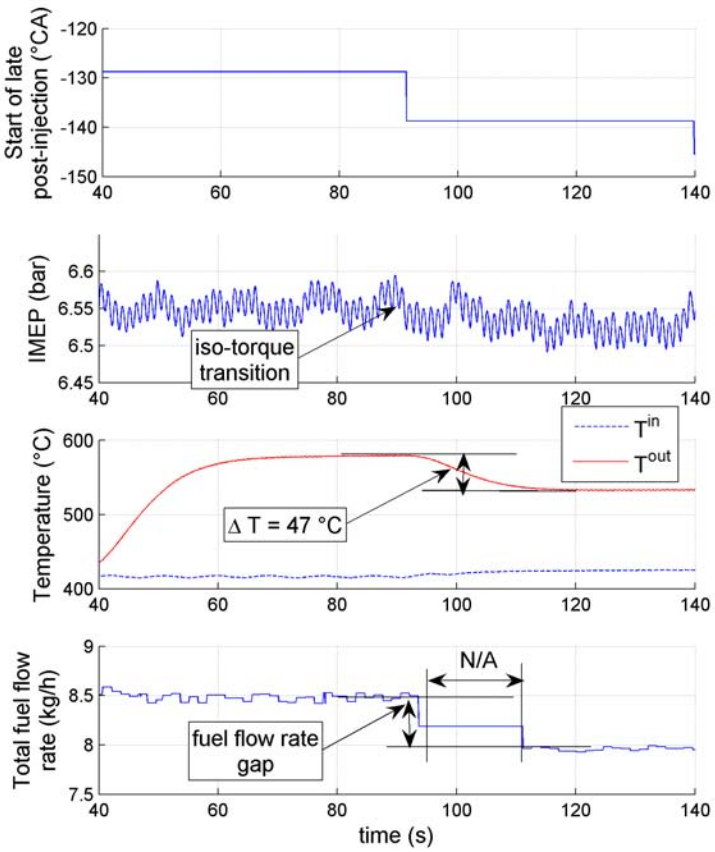

Figure G.6: The choice of the phase of the late post-injection (PI) impacts on the steady-state value of T^{out} by 47°C. In this experiment, energizing time (low-level variable) is constant (not plotted). The torque and the inlet temperature T^{in} roughly remain constant. However, the choice of the late PI impacts on the total fuel flow rate. Note that, on this experimental device, the mass flow rate measurements are unavailable during a period of time reported in the figure. This technical detail is not a big concern because one should focus on the steady-state values for this measurement. Experimental data.

Ideas for compensation

Different factors of influence (engine speed, rail pressure, injections (pilot, main, coupled PI, dwell times, ETs)) have been studied to get further insights into the selection of late PI phases. One first interesting observation is that the crank angle interval of the variations, such as pictured by arrows in Fig. G.7, is independent of all other factors but the engine speed. Further, it is found

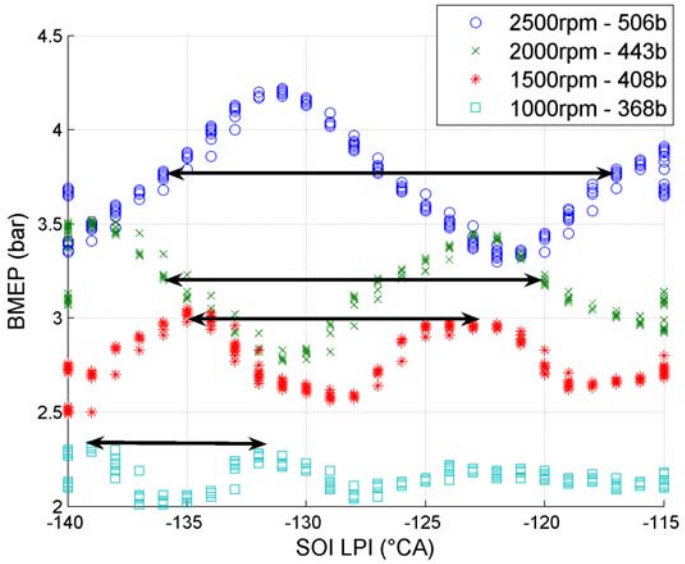

Figure G.7: BMEP *vs. the phase of the late post-injection* (SOI LPI). Late post-injection ET stays constant. Experimental data.

linearly dependent on the engine speed (see Fig. G.8). The length of the time interval (in seconds)

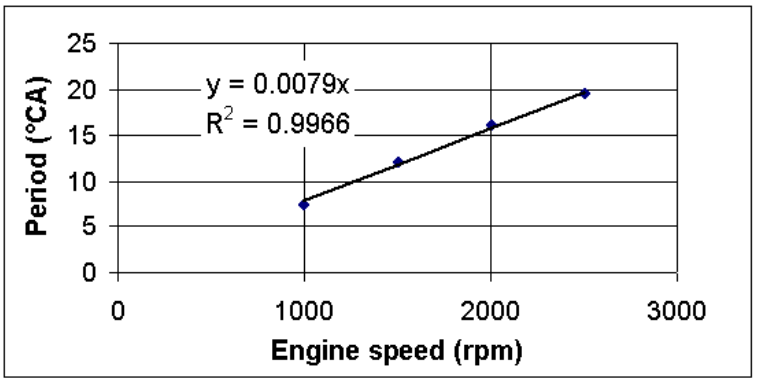

Figure G.8: Period of oscillations observed in Fig. G.7 are linearly dependent on the engine speed. Then, period of oscillations in time are constant, and it seems that they are independent of all parameters but the system (including pump) natural frequency. Experimental data.

is inversely proportional to engine speed and proportional to the period (in °CA). Then, the period (in time units) of the oscillations is independent of all other factors. It only depends on the system (including pumping device which is directly related to the engine speed) natural frequency.

Influence of the other factors is not so straightforward. A simplified approach for compensation would require more insight into modeling. In particular, it is important to note that the late post-

injection ET has an impact on the torque (see e.g. Fig. G.9). When late PI is active, it is desired

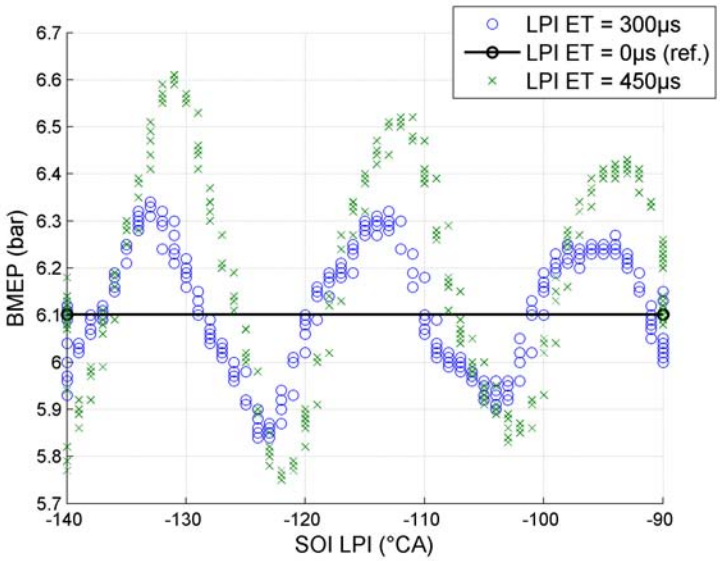

Figure G.9: Late post-injection energizing time (PI ET) impacts on the torque (and therefore BMEP). In order to be able to use a continuous value of late PI ET to control the exhaust HC flow, the late PI phase must be carefully selected. Experimental data.

that the torque remains constant. This must be verified, first, when the late PI is activated, and further, in operation, late post-injection influence should be decoupled from the other injections so that continuous late PI ET can be used. A simple way to meet this requirement, is to select the phase of the late PI such that the torque is equal to the torque when no late PI is present (see again Fig. G.9). At different ET values, the phase values can differ. Then, the phase of the late PI is implemented as a function of the injection time is. Using this mapping, the torque roughly remains constant whatever the ET value used by the controller.

Model-based modeling is a good candidate to reduce the calibration process.

G.6 Actuator management: exhaust injector

Exhaust injector is an optional device to replace late post-injection (late PI). It discharges HC directly into the exhaust line (see Chapter F). Its use has an extra cost, but it limits the discussed oil dilution problems. Also, it is easier to implement than late PI because it is totally independent of the other injections. This is because a dedicated low-pressure pumping system supplies the exhaust injector with fuel. However, a couple of specificities are worth mentioning:

- It is subject to pressure oscillations in the pumping system.
- DOC conversion efficiency can be reduced compared to PI HC's (see § G.4).
- It becomes clogged when not used.

The last two points are now briefly commented. First, it is noted in § G.4 that the DOC conversion efficiency is reduced when using EPI. To address this issue, an interesting option can be to use the late PI only for large gas flow rate values. Regarding the third point, a simple strategy consists of

injecting a small quantity of fuel with the exhaust injector at regularly-spaced periods of time (e.g. a pulse injection every few seconds).

It has been noticed that injected quantities largely vary depending on the separation between two pulses (dwell time). In order to meet the request for continuous rate and reduce the calibration process, the following procedure is used:

- Determine the minimum injection duration T_i to get repeatable injection mass m_1. The goal here is to maximize the DOC conversion efficiency.
- Determine pressure oscillations stabilization duration T_w.
- Calculate the maximum obtainable flow rate from m_1 and T_w. If too low, determine a 2-pulse injection pattern, and the corresponding injected mass m_2. All pulses have the minimal duration T_i determined above. Choose the separation to get a repeatable mass m_2.
- If necessary, determine a 3-pulse injection pattern and the corresponding mass m_3 and so on.

Then the following algorithm is used. Integrate flow rate u to get the mass to inject M. Inject the mass m_i so that $m_i < M < m_{i+1}$ by applying the corresponding injection pattern, and subtract the injected mass m_i from the mass to inject M. Formally, M is given by

$$M = \int_0^t u(\tau)d\tau - \int_0^t m_i(M(\tau))d\tau$$

About involved delays This method involves a delay between the control signal and the actuation (M can be seen as a buffer). This delay is not problematic. At high gas flow rates, injected quantities are high. Then, there is no risk of delay. At low gas flow rates, injected quantities are small. So, time between injection may be large. However, the DOC is a very low-pass system: the effects of this discrete strategy are completely smoothed out, and lead to results that are equivalent to strategies allowing continuous variations of the injection time, which requires heavier calibration effort.